High-Temperature Superfluidity in an Ultracold Fermi Gas

by

Martin W. Zwierlein

Submitted to the Department of Physics
in partial fulfillment of the requirements for the degree of

Doctor of Philosophy

at the

MASSACHUSETTS INSTITUTE OF TECHNOLOGY

October 2006

© Massachusetts Institute of Technology 2006. All rights reserved.

Author .....
Department of Physics
October 25, 2006

Certified by .....
Wolfgang Ketterle
John D. MacArthur Professor of Physics
Thesis Supervisor

Accepted by .....
Thomas J. Greytak
Professor of Physics, Associate Department Head for Education

MASSACHUSETTS INSTITUTE OF TECHNOLOGY
JUL 0 2 2007
LIBRARIES
ARCHIVES

High-Temperature Superfluidity in an Ultracold Fermi Gas

by

Martin W. Zwierlein

Submitted to the Department of Physics
on October 26, 2006, in partial fulfillment of the
requirements for the degree of
Doctor of Philosophy

Abstract

This thesis presents experiments in which a strongly interacting gas of fermions was brought into the superfluid regime. The strong interactions are induced by a Feshbach scattering resonance that allows to tune the interfermion scattering length via an external magnetic field. When a Fermi mixture was cooled on the molecular side of such a Feshbach resonance, Bose-Einstein condensation of up to 10^7 molecules was observed. Subsequently, the crossover region interpolating between such a Bose-Einstein condensate (BEC) of molecules and a Bardeen-Cooper-Schrieffer superfluid of long-range Cooper pairs was studied. Condensates of fermion pairs were detected in a regime where pairing is purely a many-body effect, the pairs being stabilized by the presence of the surrounding particles. Superfluidity and phase coherence in these systems was directly demonstrated throughout the crossover via the observation of long-lived, ordered vortex lattices in a rotating Fermi mixture. Finally, superfluidity in imbalanced Fermi mixtures was established, and its Clogston limit was observed for high imbalance. The gas was found to separate into a region of equal densities, surrounded by a shell at unequal densities.

Thesis Supervisor: Wolfgang Ketterle
Title: John D. MacArthur Professor of Physics

To my family,
Erika and Otto, Anne-Julia and Cornel

Acknowledgments

Over the years at MIT I had the good fortune to learn from and the pleasure to work with an exceptional group of people. These few lines can only be a knowing nod to all of them, while there is no way to fully express my gratitude in writing.

First of all, I would like to thank Wolfgang Ketterle for teaching me the ways of a physicist. His sparkling enthusiasm for science is well known to be infectious. The trust he had in every one of us to achieve our goals is what made us believe that we actually might. I treasure every discussion we had, be it about physics or general matters of life.

It is my pleasure to thank my fellow graduate students on the lithium project, its first members and initiators, Zoran Hadzibabic, Claudiu Stan and Subhadeep Gupta, the new crew around Christian Schunck and André Schirotzek, and special guest Jamil Abo-Shaeer. None of the work in this thesis would have been possible without them. I consider myself a lucky guy, as all of them have not only been the greatest colleagues, but have also become wonderful friends.

When I first came to MIT as a visiting student from Paris, Zoran took me under his wings. I immediately grew attached to his way of doing science, of figuring things out instead of taking them for granted, and having tremendous fun at it. He taught me invaluable lessons about physics and life, and he was a big reason for me to come back for my PhD. We shared a lot of habits, the bizarre schedule, the preference for Miracle burgers with extra chutney, later I copied his addiction to diet coke. Unfortunately I could not copy his wit, but maybe that simply means we need more time to work together.

From Claudiu I learned that what has to work well has to look good: His precision and care in building apparatus was the pillar for the reliability and success of our experiments. If you have any question about some unknown, weird-looking and potentially dangerous substance, Claudiu can tell you all about it. I was always amazed by his ability to keep his cool when everything around us seemed to fall apart. The only way you could tell that the problem he just fixed could have turned into a major catastrophe was by the number of cigarettes consumed afterwards.

When lithium atoms and light were ready for the upgrade of the sodium BEC machine, we teamed up with Deep Gupta, an exceptional scientist and a great teacher. He introduced me to the sodium BEC machine, the dye(t) laser, the subtleties of the sodium MOT, saddle points (sic) of magnetic trapping and evaporative cooling and to frequent punning. It was wonderful to watch Zoran and Deep bounce ideas off

each other during the optimization of the sympathetic cooling scheme, and see the atom number grow by the minute.

We, the youngens, were thrown into cold water when they both graduated a day from each other, but they had left a miraculous heritage, the brightest source of ultracold fermions in the world.

Christian first joined the crew as a diploma student, while I was back in Paris, and he must have experienced the same welcoming warmth I had felt, as he was able to cite the relevant puns even before having watched The Big Lebowski. He now makes the best White Russian in the Northern Hemisphere, as I can certify. He has been a dependable friend, office-mate and lab companion through countless days and nights. Not widely known are his superb musical skills: His harp play is simply outstanding. I wish him and his newly-wed wife Alessandra all the best for the future.

In a memorable night in February 2001, I heard a tremendous outcry coming from the BEC II lab. I jumped inside, fearing something terrible had happened, and saw a stunning image on the screen: Jamil Abo-Shaeer and Chandra Raman had just created a vortex lattice in a Bose-Einstein condensate containing about 100 vortices! The image stuck in my mind. Over the next years, Jamil had found in me, his poor office-mate, the ideal subject for his teases. He tricked me, embarrassingly more than once, into believing that I was really heavy (which I am not!), next, that his mouse has a life of its own and that he could solve the Rubik's cube in less than five minutes. Jamil was our star in soccer. He needed twelve sure chances to score one goal. At least he always scored. My biggest success in grad school was to convince Jamil to defect from BEC II, delay his thesis and "bring the vortices over" to the sodium condensates in BEC I. Which he did. In a day. Within the two months or so he had been a member of our lab I learned experimental skills for a lifetime. I pay this back by dedicating Fig. 6-9 to him.

André, from the same village in Germany and almost as well-built as me, had been a close friend from day one. His enthusiasm and fearlessness in the lab are by now legendary. When we were almost about to give up on vortices in Fermi gases, but had a beautiful gas cloud on our screen, he asked "should we try it once m...?", I interrupted saying "yes!", and the result was Fig. 6-8a. I will always cherish the times watching Friends in Clinton Street, eating entire cows, "making gym" and playing all sorts of existing or invented sports inside building 26. We were all happy to have André on our soccer defense, where he flattened the other team's players with grace. Next time we play squash, I might let him win once or twice.

I am grateful for all things I learned from our postdocs Axel Görlitz, Kai Dieck-

mann and Jamie Kerman, and the newest addition to the lithium lab, Yong-Il Shin. After seminal works on bosons in BEC III, Yong immediately jumped onto the hottest topic in fermion physics and made his lasting mark. His clear way of thinking is admirable, and I profited enormously from discussions with him.

Thanks also go to Sebastian Raupach, philosopher/physicist, who joined us for his diploma thesis in the heyday of fermion pair BEC. He competed with Christian for the title of the nicest guy on earth. Peter Zarth, another diploma student, and new PhD student Ye-yroung Lee impressed me with their enthusiasm and drive to get the first potassium MOT at MIT, working in the same little room where Zoran, Claudiu and myself produced our first laser cooled lithium atoms.

I owe a lot to the crew of BEC II. The past members Roberto Onofrio, Chandra Raman, Jamil, and Johnny Vogels for developing the robust technique of stirring ultracold atoms, and the new team Kaiwen Xu, Takashi Mukaiyama, Jit Kee Chin, Dan Miller, Yingmei Liu, Christian Sanner and Widagdo Setiawan for letting me steal Jamil for a while. Dan Miller must receive extra thanks for the many parties at his house that helped foster the group spirit, for buying excellent Dunkin' Donuts coffee, for having me park my belongings at his place and generally for being hilarious.

With BEC III we lithium guys are connected in a love-hate relationship, because of the illegal "trade" of optics and other equipment that is constantly going on. They should have put the wall back up a long time ago. Aaron Leanhardt provided the role model for everyone in our group with his work ethics and deep understanding of the most diverse areas of physics. I thank him for his excellent advice. Tom Pasquini I thank for improving my general behavior, especially related to coffee mugs. Michele Saba was not only an invaluable resource of knowledge and original thoughts but also the best soccer player we ever had and the best cook, and because of the latter I let him stay in my apartment during his final month. Thanks also go to Gyu-Boong Jo and Caleb Christensen, for letting me steal optics behind their backs. Sebastian Will, diploma student filling the role of a grad student, I thank for the fun we had out in the city, and I am looking forward to exploring Mainz with him.

I want to apologize to BEC IV for the many times we forgot to ask them to join us for lunch, but I thank Micah Boyd, Eric Steed, Gretchen Campbell, Dominik Schneble, Luis Marcassa, Patrick Medley, and Jongchul Mun for being good sports about it. Micah paid that back with a good tease towards me every now and then, being second only to Jamil in this profession. It was great having him around when we were attacked by a huge chunk of sodium, and generally when we needed a good time. Gretchen deserves two PhDs, one for physics and one for helping everyone out

with little and big things, holding up the group spirit and having us feel at home in a big family. I do not see how the gap she will leave behind in the group can be filled. I thank her for her company during countless coffee breaks I needed at the most abnormal hours, for convincing me that it's all ok when I laid on her couch and for handing in this thesis for me.

My thanks go to James Anglin for very useful discussions on vortex physics, to Dan Kleppner for advice and help at numerous occasions, and to Dave Pritchard for being a great academic advisor, in the fullest sense of the word.

The late Carol Costa has made our hallway in building 26 a warmer place. She warned me to never write acknowledgements at the end of writing a thesis. I should have listened. She is heavily missed. Ellenor Emery took her role and mothered us as Carol did. I am very happy for her that she has become a real mum. Joanna Keseberg is now the good heart of the hallway, and I thank her for all the help over the last year. Big thanks go to the RLE Support staff, especially Maxine Samuels and Al McGurl.

I owe many memorable matches to the entire intramural soccer team "The Ball-drivers", including the above-mentioned as well as Adam Black, Marko Cetina, Andrew Grier (the actual best player), Cort Johnson, Ian Leroux, Yu-ju Lin, Bonna Newman, Dave Palazzo, Monika Schleier-Smith, Jon Simon (the best player ever), Igor Teper, James Thompson (thanks also for great advice in diverse matters) and Mukund Vengalattore (the truly best player), and my room mate and friend from old times at the University of Bonn, Andreas Malmendier. When I told Andreas that I would come to MIT, he immediately offered that we could share an apartment. The rest is history. I loved cracking ancient math problems with him, watching the worst movies ever and holding parties that we will certainly never forget, guaranteed. With André we found our brother in crime, and these crimes should be left untold.

Finally, I would like to thank my parents, Otto and Erika, as well as my sister Anne-Julia (Anju) and my brother Cornel for providing me with inspiration. To them I dedicate this thesis.

Contents

List of Figures

Chapter 1

Introduction

> *Γίνεσθαι δὲ τοὺς κόσμους οὕτω· φέρεσθαι κατὰ ἀποτομὴν ἐκ τῆς ἀπείρου πολλὰ σώματα παντοῖα τοῖς σχήμασιν εἰς μέγα κενόν, ἅπερ ἀθροισθέντα δίνην ἀπεργάζεσθαι μίαν, καθ' ἣν προσκρούοντα ⟨ἀλλήλοις⟩ καὶ παντοδαπῶς κυκλούμενα διακρίνεσθαι χωρὶς τὰ ὅμοια πρὸς τὰ ὅμοια. ἰσορρόπων δὲ διὰ τὸ πλῆθος μηκέτι δυναμένων περιφέρεσθαι, τὰ μὲν λεπτὰ χωρεῖν εἰς τὸ ἔξω κενόν, ὥσπερ διαττώμενα· τὰ δὲ λοιπὰ συμμένειν καὶ περιπλεκόμενα συγκατατρέχειν ἀλλήλοις καὶ ποιεῖν πρῶτόν τι σύστημα σφαιροειδές.*
>
> *This is how the worlds are formed. In a given section many atoms of all manner of shapes are carried from the unlimited into the vast empty space. These collect together and form a single vortex, in which they jostle against each other and, circling round in every possible way, separate off, by like atoms joining like. And, the atoms being so numerous that they can no longer revolve in equilibrium, the light ones pass into the empty space outside, as if they were being winnowed; the remainder keep together and, becoming entangled, go on their circuit together, and form a primary spherical system.*
>
> Diogenes Laertius, *Lives of eminent Philosophers*, IX 31
> (LEUCIPPUS, fifth century B.C.)

Superfluidity, frictionless flow, is a most remarkable phenomenon that we come across in many different areas of physics. The most prominent examples are superconductors, charged superfluids, in which electrical current flows without resistance. Liquid helium forms a superfluid at low temperatures. Superfluid phenomena occur in nuclei and inside a neutron star, whose core is even believed to contain a superfluid of quark pairs, and particles are thought to owe their very *mass* to a process similar to a superfluid phase transition: The formation of a Higgs condensate. It is indeed tempting to identify the excitation spectrum of a superconductor, $\sqrt{\epsilon_p^2 + \Delta^2}$ (ϵ_p being the free

particle dispersion, and Δ the superfluid gap), with the relativistic expression for a particle's energy, $\sqrt{p^2 + m^2}$. This Higgs mechanism might be verified in the near future in experiments at the new Large Hadron Collider (LHC).

Evidently, superconductors are of great relevance for technology and the transport of energy. However, the record critical temperature below which materials would become superconducting had for many decades been fixed at 23 K, well below any easily accessible temperature. The discovery of high-temperature superconductors in cuprates by Bednorz and Müller [29] in 1986 started an entire new era of research. The record critical temperature quickly rose above liquid nitrogen temperatures, and is currently 138 K.

Clearly, the ultimate goal would be to find a room-temperature superconductor. Rather than following a trial and error approach in the discovery of new materials, one would like to fully understand the mechanism behind the phenomenon and *predict* materials with higher critical temperature. Unfortunately, the mechanism leading to High-T_C superconductivity is not fully understood. The superconducting state comes about in an intricate compromise between several competing states. Strong interactions between the electrons obscure our understanding of the normal state above T_C, that cannot be described as a simple collection of (quasi-)particles [147].

The success of ultracold atomic gases over the past 11 years gives new hope that some fundamental questions on superfluidity and strongly correlated systems might find an answer in the near future. Bose-Einstein condensates (BECs) of atoms provide the paradigm of the weakly-interacting Bose gas [67, 136]. Atomic gases confined in optical lattices allow the simulation of condensed matter systems, such as the study of the superfluid-to-Mott insulator transition [101]. The advent of superfluids of fermionic atom pairs, the topic of this dissertation, brings us in direct contact with the phenomenon of superconductivity. Fermi gases give us access to the crossover from a Bose-Einstein condensate of tightly bound molecules to a superfluid consisting of long-range Cooper pairs. The fermions are strongly interacting within this crossover. This allows them to form a superfluid state already at a high critical temperature.

In fact, scaling the density of the atomic gas up to the density of electrons in solids, the critical temperature for superfluidity lies far above room temperature. In the future, ultracold fermionic gases, confined in optical lattices with tunable interactions and variable spin imbalance, might provide us with a basic model system for High-T_C superconductivity.

In this dissertation I will describe our work on the creation and direct observation of fermionic superfluidity in strongly interacting atomic gases. In the following I will

briefly review the history of superfluids and superconductors, showing how ideas and discoveries in one field have always brought fruitful insight into the understanding of the other. Two seemingly distinct ideas, the condensation of point-like bosons and the condensation of long-range Cooper pairs, leading to vastly different predictions for the critical temperature, are found to be simply two extremes of the same underlying phenomenon.

1.1 Discovery of superfluidity and superconductivity — from BEC to BCS

In a remarkable "accident of history", the first superfluid was produced (without noticing its remarkable properties) by the same scientist who later used it as a coolant to discover superconductivity. Kamerlingh Onnes liquefied helium-4 in 1908, and lowered its temperature below the superfluid transition point (the λ-point) at $T_\lambda = 2.2$ K. He remarked in his Nobel lecture 1913 "that the density of the helium, which at first quickly drops with the temperature, reaches a maximum at 2.2 K approximately, and if one goes down further even drops again. Such an extreme could possibly be connected with the quantum theory" [177]. But he first focussed his studies on the behavior of metals at low temperatures. In 1911, Onnes used helium-4 to cool down mercury, finding that the resistivity of the metal suddenly dropped to non-measurable values at $T_C = 4.2$ K, it became "superconducting". Tin (at $T_C = 3.8$ K) and lead (at $T_C = 6$ K) showed the same remarkable phenomenon.

The special properties of helium-4 below T_λ went practically unnoticed until the 1930s, when Keesom and Clusius discovered the λ-shaped peak in the specific heat curve versus temperature at T_λ. In 1938, the vanishing viscosity of the substance was independently discovered by Kapitza [132] and Allen & Misener [8], suggesting the term "superfluid" in direct analogy with superconductivity. Obviously, the similar phenomena of resistance-less currents in metals and frictionless flow in helium-4 hint at a similar underlying mechanism. However, as we will see, the similarities in the two critical temperatures T_λ and T_C turned out to be a complete accident of Nature.

1.1.1 Bose-Einstein condensation

F. London suggested in 1935 that superconductivity was a quantum mechanical phenomenon occurring on a macroscopic scale, stemming from a certain rigidity of the particles' wave functions against perturbations [155]. The lowest quantum state of the

system should be "separated by a finite distance from the excited ones" and therefore be protected against the influence of a weak perturbation. This is the essence of what we now call the superconducting gap. In 1938, he proposed that quantum statistics might play an important part in the explanation of superfluid helium-4. He was the first to make a connection to Bose-Einstein condensation [34, 86], at that time only a theoretical concept, in which a collection of non-interacting, indistinguishable bosons condenses into one and the same macroscopic wave function. This occurs when the number of available quantum states becomes comparable to the number of particles N (a condition called "degeneracy"), and bosons start to condense into a single quantum state rather than being distributed over all possible states. As the extent of an average particle's wave function at temperature T is given by the de Broglie wavelength $\lambda = \sqrt{\frac{2\pi\hbar^2}{mk_BT}}$ (with m the particle mass), the number of available quantum states in a volume Ω is roughly equal to Ω/λ^3. Setting this equal to N we can deduce the characteristic temperature for reaching degeneracy and Bose-Einstein condensation, $T_{\mathrm{BEC}} \sim \frac{2\pi\hbar^2}{m}(N/\Omega)^{2/3} \approx 3$ K. For this estimate, we have inserted the mass $m_{^4\mathrm{He}}$ of a helium-4 atom and a typical density of $n = 10^{22}$ cm^{-3}. The similarity of this value to the observed critical temperature of 2.2K was intriguing. Furthermore, L. Tisza pointed out that for the Bose gas below T_{BEC}, one can make a natural distinction between the condensed part of the gas and the thermal, or excited fraction [244]. Only particles in the thermal fraction take part in dissipative processes. This idea of a *two-fluid model* is so fruitful that it applies quite generally to superfluids and conventional superconductors [22].

Of course, Einstein had considered a *non-interacting* Bose gas, a condition that should hardly be justified for the liquid helium-4. For this reason, L.D. Landau rejected the concept of Bose-Einstein condensation, and rather approached the problem of superfluidity with a highly successful *phenomenological* two-fluid model [144]. The important issue of how to combine the idea of BEC with interactions was dealt with at a later time starting with Bogoliubov's theory of the weakly-interacting Bose gas [150]. The fact that quantum statistics was crucial to the understanding of superfluid helium-4 was clarified beyond any doubt when liquid helium-3, a fermion, became available and did *not* show superfluid properties at temperatures on the scale of T_λ.

1.1.2 Fermionic superfluidity and Bardeen-Cooper-Schrieffer theory

How can the idea of Bose-Einstein condensation, the two-fluid model etc. be carried over to superconductors? What determines their critical temperature T_C? Clearly, the superfluid current must somehow be carried by electrons, but the degeneracy temperature of this Fermi gas lies a factor $m_{^4\mathrm{He}}/m_e > 7000$ above the condensation temperature for Helium-4 atoms, and cannot set the scale for T_C. Condensation of the electrons themselves is in any case not allowed. Electrons being fermions, they cannot occupy one and the same quantum state but instead must arrange themselves in *different* states. At zero temperature, a gas of N fermions will fill all available states one by one, starting with the ground state, up to the N^{th} state at the Fermi energy E_F. For an electron density $n \sim$ several $10^{22}\,\mathrm{cm}^{-3}$, a similar counting as above gives $E_F = \frac{\hbar^2}{2m}(6\pi^2 n)^{2/3} \sim 50\,000\mathrm{K}$. An obvious idea might be to form tightly bound pairs of electrons, which can act as bosons and would form a condensate. Apart from the problem that the condensation temperature would still be on the order of E_F/k_B, there is no known interaction which could be sufficient to overcome the strong Coulomb repulsion and form tightly bound electron pairs (Schafroth pairs [213]). Considering these problems, one can understand why it took more than four decades from the discovery to the explanation of the phenomenon of superconductivity. It turned out that the general idea of electrons forming pairs was after all correct.

In 1950, it became clear that there was indeed an effective attractive interaction between electrons, mediated by the crystal lattice vibrations (phonons), that was responsible for superconductivity. The lattice vibrations left their mark in the characteristic variation $T_C \propto 1/\sqrt{M}$ of the critical temperature T_C with the isotope mass M of the crystal ions, the isotope effect [206, 165] that had been predicted by H. Fröhlich [93]. Vibrational energies in the lattice are a factor $\sqrt{m_e/M}$ smaller than the typical electronic energy[1] E_F, on the order of $k_B\times$ several 100 K (the Debye temperature T_D of the metal). While the isotope effect strongly argues for T_C being proportional to T_D, the Debye temperature is still one or two orders of magnitude higher than the observed critical temperature. In addition, attempts to explain superconductivity by including electron-phonon interactions in a perturbative way failed.

[1]The average distance between electrons r_0 is on the order of atomic distances (several Bohr radii a_0), the Fermi energy $E_F \sim \hbar^2/m_e r_0^2$ is thus on the scale of typical Coulomb energies in an atom. Vibrational energies of the lattice ions are then on the order $\hbar\omega_D \approx \hbar\sqrt{\frac{\partial^2 U_{\mathrm{Coulomb}}}{\partial r^2}/M} \sim \hbar\sqrt{E_F/Mr_0^2} \sim \sqrt{m_e/M}E_F$.

A breakthrough came in 1956, when L. Cooper realized that fermions interacting via an arbitrarily weak attractive interaction on top of a filled Fermi sea can form a bound pair [66]. In other words, the Fermi sea is unstable towards pair formation. However, unlike the tightly bound pairs considered before, the "Cooper" pair is of a very large extent, much larger than the interparticle spacing. That is, a collection of these pairs necessarily needs to overlap very strongly in space. In this situation, it was initially far from obvious whether interactions between different pairs could be simply neglected. But this was what led to the final goal: Bardeen, Cooper and Schrieffer (BCS) developed a full theory of superconductivity starting from a new, stable ground state in which pair formation was included in a self-consistent way [23]. Using the effective electron-electron interaction V, attractive for energies smaller than $k_B T_D$ (and assumed constant in this regime), the pair binding energy was found to be $\Delta = 2k_B T_D\, e^{-1/N(0)|V|}$, with $N(0) = m_e k_F/2\pi^2\hbar^2$ the density of states at the Fermi energy and $N(0)|V|$ assumed small compared to 1. The bound state energy (or pairing gap) depended in the non-analytic fashion $e^{-1/N(0)|V|}$ on the electron-electron interaction V, explaining why the earlier attempts using perturbation theory had to fail. Also, this exponential factor can now account for the small critical temperatures $T_C \simeq 5$ K: Indeed, it is a result of BCS theory that $k_B T_C$ is simply proportional to $\Delta(0)$, the pair binding energy at zero temperature: $k_B T_C \approx 0.57\,\Delta(0)$. Hence, the critical temperature $T_C \sim T_D\, e^{-1/N(0)|V|}$ is proportional to the Debye temperature T_D, in accord with the isotope effect, but the exponential factor suppresses T_C by a factor that can easily be 100.

A remarkable example for such a BCS-type fermionic superfluid is helium-3, for which the superfluid transition had been observed in 1972 [183, 182] at $T_C \sim 3$ mK. Here the necessary attractive interaction between the helium-3 atoms occurs via (p-wave) collisions[2]. The low T_C can be compared to $T_\lambda = 2.2\,\mathrm{K}$ for the bosonic counterpart ^{4}He. Clearly, Cooper pairing is a fragile affair, strongly reducing T_C from the degeneracy temperature scale.

1.1.3 The BEC-BCS crossover

As F. London had already suspected in 1950 [156], the BCS state can be understood as a pair condensate in momentum space, in contrast to a BEC of tightly bound pairs in real space. The former will occur for the slightest attraction between fermions, while the latter appears to require a true two-body bound state to be available to a fermion

[2]Strong hard-core repulsion between the atoms renders s-wave pairing unfavorable.

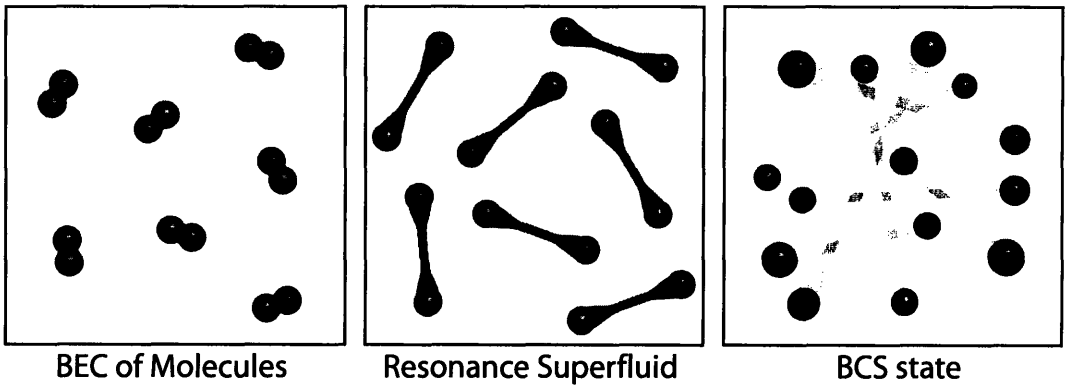

Figure 1-1: The BEC-BCS crossover. By tuning the interaction strength between the two fermionic spin states, one can smoothly cross over from a regime of tightly bound molecules to a regime of long-range Cooper pairs, whose characteristic size is much larger than the interparticle spacing. In between these two extremes, one encounters an intermediate regime where the pair size is comparable to the interparticle spacing. This strongly interacting "soup" of particles is a fascinating state of matter that might provide a model for the interior of neutron stars or the Quark-Gluon plasma of the early Universe.

pair. Eagles [85] noted in 1969 that, in the limit of very high density, the BCS state smoothly evolves into a condensate of pairs that are smaller than the interparticle distance (In the language of Fermi gases, he fixed the negative scattering length and varied the interparticle spacing). Using a generic two-body potential, Leggett showed in 1980 that the limits of tightly bound molecules and long-range Cooper pairs are connected in a smooth crossover [149] (here it was the interparticle distance that was fixed, while the scattering length was varied, which allowed the inclusion of a true two-body bound state). The size of the fermion pairs changes smoothly from being much larger than the interparticle spacing in the BCS-limit to the small size of a molecular bound state (see Fig. 1-1). Accordingly, the pair binding energy varies smoothly from its small BCS value (weak, fragile pairing) to the large binding energy of a molecule in the BEC limit (stable molecular pairing). The presence of a paired state is in sharp contrast to the case of two particles interacting in free (3D) space: For too weak an attraction, there is *no* bound state available to the particles. Only at a critical interaction strength does the molecular state become available and a bound pair can form. Leggett's result shows that in the many-body system, the physics changes smoothly with interaction strength, also at the point where the two-body bound state disappears. Nozières and Schmitt-Rink extended Leggett's model to finite temperatures and verified that the critical temperature to attain superfluidity

varies smoothly from the BCS limit, where it is exponentially small, to the BEC-limit where one recovers the value for Bose-Einstein condensation of tightly bound molecules [172]. These results are presented in chapter 2.

The importance of considering strongly interacting fermions became clear with the discovery of novel materials. Up to 1986, BCS theory (or more involved variations of it) was largely successful in explaining the properties of superconductors. The record critical temperature increased only slightly from 6 K in 1911 to 23 K in 1985. In 1986, however, Bednorz and Müller [29] discovered superconductivity at 35 K in the compound $La_{2-x}Ba_xCuO_4$, triggering a focussed search for even higher critical temperatures. Soon after, materials with transition temperatures above 100 K were found. Due to the strong interactions and quasi-2D structure, the exact mechanisms leading to High-T_C superconductivity are still not fully understood.

The physics of the BEC-BCS crossover in a gas of interacting fermions does not directly relate to the complicated phenomena observed in High-T_C materials. However, some features of the two problems are shared: In the crossover regime, the pair size is comparable to the interparticle distance. One therefore deals with a strongly correlated "soup" of particles, where interactions between different pairs can no longer be neglected. Also the normal state above the phase transition temperature is a highly non-trivial state. Even here, correlations are still large enough to form uncondensed pairs at finite momentum. This region is sometimes called the "Pseudo-Gap".

1.1.4 Universal regime at unitarity

One point in the BEC-BCS crossover is of special interest: When the interparticle potential is just about strong enough to bind two particles in free space, the bond length of this molecule tends to infinity (unitarity regime). In the medium, this bond length can thus not play any role anymore in the description of the many-body state. The only length scale of importance is then the interparticle distance $n^{-1/3}$, the corresponding energy scale is the Fermi energy E_F. In this case, physics is said to be universal [119]. The average energy content of the gas, the binding energy of a pair and (k_B times) the critical temperature must be related to the Fermi energy by universal numerical constants. The size of a fermion pair must be given by a universal constant times the interparticle distance. This means that results obtained with one system at unitarity will directly carry over to another system (sharing the same symmetry), even if their densities are vastly different. Results obtained in an ultracold gas at unitarity, at densities of $10^{12}\,\mathrm{cm}^{-3}$, might thus have relevance for the

physics inside a neutron star[3] at densities of $10^{38}\,\mathrm{cm}^{-3}$.

1.2 Ultracold atomic gases - model systems for bosonic and fermionic superfluids

When our understanding of a physical system is obscured by too many competing effects, it is a natural approach to consider simpler, well-defined problems and increase complexity in a controlled way. Instead of dealing with dense, strongly interacting liquids like for example helium-4, it would be of great advantage to have at one's disposition a *dilute gas*, in which one can enhance interactions starting from the well-understood limit of weak interactions - for bosons, Bogoliubov's weakly interacting Bose gas. But what are the requirements to reach the regime of degeneracy in a gas? They seem impossible to fulfill: Essentially all gases (helium being the exception) solidify at low temperatures.

The only way out can be to work at *ultralow* densities: It turns out that forming a solid takes a certain amount of time: Three atoms have to meet before a molecule can form, as the released energy and momentum has to be carried away by a third particle. At densities of $10^{15}\,\mathrm{cm}^{-3}$, one has a window of about 1 s before molecules and larger clusters can form in the gas. If this is long compared to the timescale needed to reach thermal equilibrium, one can hope to observe a gas in the degenerate regime before it collapses into its true solid ground state. Thermal equilibrium requires only *two-body* collisions, their rate is thus proportional to the density, whereas molecule formation requires *three-body* collisions, at a rate proportional to the *square* of the density. For low enough densities, the "good" collisions occur at a faster rate than the "bad" ones.

There is one major road block: *Ultralow* densities mean, given the condition for degeneracy we saw above, *ultracold* temperatures. For $n \sim 10^{14}\,\mathrm{cm}^{-3}$, the degeneracy temperature is on the order of μK! This seems already unrealistically low. But it appears completely hopeless to even think about observing a BCS-like superfluid in a gas of fermions: The exponential suppression we have seen above would render this phase transition unobservable.

Laser cooling and evaporative cooling were the key to achieve submicro-Kelvin temperatures in dilute atomic gases. In addition, in the seemingly hopeless case of

[3]The physics inside neutron stars is very intricate. This simple comparison rests on the observation that the neutron-neutron scattering length of about -18.8 fm is large in absolute terms compared to the distance between neutrons at these high densities, which is only a few fm.

fermions, a "magic knob" came to the rescue: Feshbach resonances.

1.2.1 Bosonic gases

The realization of Bose-Einstein condensation in ultracold atomic gases in 1995 has led to a revolution in atomic physics which is still on-going [67, 136]. These condensates represent the paradigm of Bogoliubov's weakly interacting Bose gas. As such, they are very well described by one macroscopic wave function that is the solution to a non-linear Schrödinger equation, the Gross-Pitaevskii-equation. Beautiful experiments for example on interference, on solitons and on vortices have directly demonstrated coherence, the wave-like nature of the gas and superfluid flow [133, 208, 15]. From a condensed matter perspective, these weakly interacting condensates represent the most fundamental, basic many-body wave functions.

The importance of interactions compared to the kinetic energy of the particles can be increased in (at least) two ways: The first is to impose a lattice potential via interfering laser beams and thereby localize particles onto lattice sites, quenching their kinetic energy. A prominent example is given by the superfluid-to-Mott insulator transition for bosons confined in a 3D lattice [101, 31]: As the repulsive interactions start to dominate over the tunneling between adjacent lattice sites, atoms are pinned to their respective site and long-range coherence and superfluidity is lost. This can be observed as a loss of coherence peaks in momentum space, revealed after expansion from the lattice, and more directly by measuring the insulator gap an atom needs to overcome in order to hop to an already occupied lattice site.

A second way to increase the role of interactions is to directly modify the interatomic scattering using a so-called Feshbach resonance [241, 243]. These resonances occur when the energy of two colliding atoms coincides with the energy of a bound molecular state in the interatomic potential, tunable via an applied magnetic field. On resonance, the scattering length describing the interatomic interactions diverges. Feshbach resonances were first observed in 1998 in a ^{23}Na Bose-Einstein condensate [126] and in a laser-cooled cloud of ^{85}Rb [68]. However, while it was shown in [126] that elastic scattering was indeed highly increased, unfortunately inelastic scattering due to molecule formation was also resonantly enhanced, leading to strong losses in the BEC. To the very fortunate surprise for the ultracold atom community, gases of *fermionic* atoms were found *not* to decay close to a Feshbach resonance, but instead to be very stable. This was the key fact that enabled all of the subsequent studies on fermionic superfluids.

1.2.2 Fermionic gases

The first degenerate Fermi gas of atoms was created in 1999 by B. DeMarco and D. Jin at JILA using fermionic ^{40}K [76]. Until the end of 2003, six more groups had succeeded in producing ultracold degenerate Fermi gases [247, 214, 100, 112, 207, 129], one more using ^{40}K (M. Inguscio's group in Florence, '02) and five using fermionic ^{6}Li (R. Hulet's group at Rice, C. Salomon's group at the ENS in Paris, J. Thomas' group at Duke, our group at MIT in 2001 and R. Grimm's group in Innsbruck in 2003). Already before the discovery of Feshbach resonances, the hopes to observe fermionic superfluidity in lithium were high due to the unusually large and negative triplet scattering length [3, 124]. Starting in 2002, experiments began to employ Feshbach resonances to induce strong interactions between the fermions [78, 154, 175, 175, 130, 204, 106, 36]. As the energy of the Feshbach molecular state was tuned below that of two free atoms ("molecular" or "BEC" side of the Feshbach resonance), molecules could be produced [205] that were surprisingly long-lived [69, 128, 239, 202]. Petrov, Shlyapnikov and Salomon [192] pointed out that this remarkable stability of the gas close to a Feshbach resonance is directly owed to the fermionic nature of the atoms: Inelastic three-body collisions, resonantly enhanced in a gas of bosons, are strongly Pauli suppressed for a two-state mixture of fermions, as the process would involve at least two fermions of the same spin state to be in close proximity. The surprising longevity of the (bosonic!) molecules spurred hopes of their Bose-Einstein condensation. Indeed, in November 2003 three groups reported the realization of Bose-Einstein condensation of molecules [102, 271, 129] (also see [26]). In retrospect, one can say that the binding of these "molecules" already had a strong many-body character, as their size was not very small compared to the interparticle spacing. Soon after, fermion pair condensates were observed via a rapid ramp from the "BCS" side of the Feshbach resonance, were no two-body bound state exists for isolated atom pairs [203, 272]. Here, pairing was necessarily purely a many-body effect. Tuning the magnetic field across the Feshbach resonance thus gave access to the physics of the BEC-BCS crossover described above.

Over the past two years, the properties of this "tunable" fermionic superfluid were studied in thermodynamic measurements [37, 139], experiments on collective excitations [138, 25], RF spectroscopy revealing the formation of pairs [59], analysis of the two-body part of the pair wave function [188], and finally, in April 2005, fermionic superfluidity and phase coherence was directly demonstrated at MIT through the observation of vortices [265] (chapter 6).

1.2.3 High critical temperature

This new type of fermionic superfluid differs from Helium-3, conventional and even High-T_C superconductors in its high critical temperature T_C when compared to the Fermi temperature T_F. Indeed, while T_C/T_F is about $10^{-5}\ldots10^{-4}$ for conventional superconductors, about 10^{-3} for Helium-3 and 10^{-2} for High-T_C superconductors, the strong interactions induced by the Feshbach resonance allow the fermionic gases to enter the superfluid state already at[4] $T_C/T_F \approx 0.2$. It is this large value which allows us to call this phenomenon *"high-temperature superfluidity"*. Scaled to the density of electrons in a metal, this form of superfluidity would already occur far above room temperature (actually, even above the melting temperature).

With gases of strongly interacting fermionic atoms we have a new "model material" at our disposition, which can serve as a test-bed for many-body theories. All the defining parameters of this material can be freely controlled, such as the density, temperature, dimensionality and interaction strength. Already at the present time, we are learning new facts about fermionic superfluidity in the presence of spin imbalance, which challenge current theories. For the future, one can expect that fermions confined in optical lattices will shed light on the workings of real materials, the most important class of which being High-T_C superconductors.

1.3 Outline

In the following chapters, I summarize the work by my colleagues and me on the observation of superfluidity in strongly interacting Fermi gases. This work was carried out in the research group of Professor Wolfgang Ketterle at MIT.

I will focus the discussion on fermionic superfluidity. The production of degenerate Fermi gases [112, 111] and strongly interacting Fermi mixtures [106] has been described in previous dissertations of our group [110, 104, 233] and will be briefly reviewed in chapter 4. The work on the absence of clock-shifts in an interacting Fermi mixture [266], important for the interpretation of RF spectroscopy experiments on fermionic superfluids [59], is included in appendix A. The observation of Feshbach resonances between two different atomic species [234], that might allow us to produce heteronuclear molecules in future experiments, is not included but may be found in the PhD Thesis of Claudiu Stan [233] who led the effort.

In chapter 2, we will introduce some of the theoretical tools necessary to treat

[4]Predictions for the homogeneous case vary between 0.15 and 0.25 [172, 74, 190, 231, 39, 42, 6].

strongly interacting Fermi gases with tunable interactions, namely the variational BCS approach due to Leggett, Nozières and Schmitt-Rink [149, 172]. Chapter 3 presents the phenomenon of Feshbach resonances, which has allowed to freely tune the scattering length in ultracold atom gas experiments.

Chapter 4 describes the apparatus which was used for our work, a double-species experiment that cools fermionic lithium atoms by sympathetic cooling with bosonic sodium.

In chapter 5, I present our observation of Bose-Einstein condensates of fermion pairs, both on the molecular side of the Feshbach resonance ([271], reproduced in Appendix B) and on the "BCS-side" ([272], Appendix C), where pairing is purely a many-body effect. It also discusses the relevant time scales for the growth of a fermion pair condensate, subject of the publication [270] reproduced in Appendix E. At the end of this chapter, I include unpublished data on the density profiles of an equal mixture on resonance that show a clear, direct signature of the condensate.

Chapter 6 discusses in its first part the experimental technique developed for setting optically trapped atomic gases into rotation. In its second part, the observation of vortices and ordered vortex lattices in strongly interacting Fermi gases is described, which provided the direct demonstration of superfluidity and phase coherence in these systems [265]. This work is reproduced in Appendix F. Vortex lattices enabled us to study the expansion of a rotating Fermi gas [216], Appendix G.

Finally, chapter 7 reviews our work on fermionic superfluidity with imbalanced spin populations. This has been subject of three publications, on imbalanced superfluidity and the Clogston limit [268] (Appendix H), the direct observation of the phase transition [269] (Appendix I) and the observation of phase separation between a superfluid core of equal densities and a shell of excess atoms at unequal densities [223].

Chapter 2

Superfluidity in bosonic and fermionic gases

This chapter will present some of the theory of superfluidity in bosonic and fermionic gases, relevant to our experiments on strongly interacting gases. We will first study the physics of the two "extremes" of the BEC-BCS crossover, the weakly interacting Bose gas on the one hand and the formation of Cooper pairs on the other. Finally, we will see how the variational BCS Ansatz is able to smoothly connect these two limits [85, 149, 172].

2.1 Quantum statistics at work - bosons vs fermions

We will start with a quick reminder of quantum statistics, second quantization notation and the grand canonical ensemble. For details we refer the reader to the many excellent books on many-body theory, for example by Fetter and Walecka [90] and by Abrikosov, Gorkov and Dzyaloshinski [5]. In section 2.1.1, we closely follow the presentation in [90].

2.1.1 Quantum statistics and second quantization

We consider a collection of N *indistinguishable* particles in a system described by single-particle states $\psi_{E_k}(x)$, with x denoting the collection of spatial and spin coordinates and E_k the appropriate set of quantum numbers. For example, for atoms with spin confined in a box, E_k denotes the definite momentum $\mathbf{k}$ and z-component

of spin σ. Let $A(E_1, \ldots, E_N)$ be the probability amplitude to find particle 1 in state E_1, particle 2 in E_2, etc. Since the particles are indistinguishable, the probability to find the a^{th} particle in state E_a and the b^{th} particle in state E_b must equal the one for which the particles a and b are exchanged:

$$|A(\ldots E_a \ldots E_b \ldots)|^2 = |A(\ldots E_b \ldots E_a \ldots)|^2 \tag{2.1}$$

This leaves two possibilities for the probability amplitudes under exchange:

$$A(\ldots E_a \ldots E_b \ldots) = \pm A(\ldots E_b \ldots E_a \ldots) \tag{2.2}$$

Thus, the concept of indistinguishability immediately leads to the grouping of all particles into two fundamental classes: bosons (upper sign here and in the following) and fermions (lower sign). Quantum field theory teaches us that particles with integer spin are bosons, particles with half-integer spin are fermions (Pauli's spin-statistics theorem [189, 238]).

Indistinguishability implies that we cannot decide which particle is in what quantum state. The only information which we can hope to measure is *how many* particles occupy a particular state. From Eq. 2.2 directly follows that two **fermions** can never occupy the same quantum state (Pauli's exclusion principle),

$$\begin{aligned} A(\ldots E_a \ldots E_a \ldots) &= -A(\ldots E_a \ldots E_a \ldots) \\ \Rightarrow A(\ldots E_a \ldots E_a \ldots) &= 0 \quad \text{for Fermions} \end{aligned} \tag{2.3}$$

For **bosons**, no such restriction applies. We can then fully specify a collection of N bosons by giving the particle numbers n_k occupying each quantum state E_k (with $\sum_i n_i = N$). For example, if we have two bosons, and we know that state E_1 and state E_2 is each occupied, the total wavefunction of the system is

$$\Phi_{1,1}(x_1, x_2) = \frac{1}{\sqrt{2}} \left(\psi_{E_1}(x_1)\psi_{E_2}(x_2) + \psi_{E_1}(x_2)\psi_{E_2}(x_1)\right) \tag{2.4}$$

However, if we know that only state E_1 is occupied ($n_1 = 2$), the wavefunction reads

$$\Phi_{2,0}(x_1, x_2) = \psi_{E_1}(x_1)\psi_{E_1}(x_2) \tag{2.5}$$

Note that for correct normalization, there is no factor $\frac{1}{\sqrt{2}}$ in front. For a general state of N bosons, the basis states specifying state E_1 occupied n_1 times, state E_2 occupied

n_2 times, etc., is

$$\Phi_{n_1 n_2 \ldots n_\infty}(x_1, \ldots, x_N) = \left(\frac{n_1! n_2! \ldots n_\infty}{N!}\right)^{1/2} \sum_{\substack{E_1 \ldots E_N \\ (n_1 n_2 \ldots n_\infty)}} \psi_{E_1}(x_1)\psi_{E_2}(x_2)\ldots\psi_{E_N}(x_N) \tag{2.6}$$

where the sum is over all different distributions of N particles over the states, with n_1 particles in state 1, n_2 in state 2 etc. There are $N!/n_1!n_2!\ldots n_\infty!$ such arrangements, which explains the normalization factor.

For **fermions**, the Pauli principle states we will never have more than 1 particle occupying a given state, $n_k = 0$ or 1. Two fermions in two distinct states E_1 and E_2 are described by the fully antisymmetric wavefunction

$$\Phi_{1,1} = \frac{1}{\sqrt{2}}\left(\psi_{E_1}(x_1)\psi_{E_2}(x_2) - \psi_{E_1}(x_2)\psi_{E_2}(x_1)\right) \tag{2.7}$$

For N fermions, the basis states can be conveniently written in terms of a *Slater* determinant,

$$\Phi_{n_1 n_2 \ldots n_\infty}(x_1, \ldots, x_N) = \frac{1}{\sqrt{N!}} \begin{vmatrix} \psi_{E_1}(x_1) & \psi_{E_1}(x_2) & \ldots & \psi_{E_1}(x_N) \\ \psi_{E_2}(x_1) & \psi_{E_2}(x_2) & \ldots & \psi_{E_2}(x_N) \\ \ldots & \ldots & \ldots & \ldots \\ \psi_{E_N}(x_1) & \psi_{E_N}(x_2) & \ldots & \psi_{E_N}(x_N) \end{vmatrix} \tag{2.8}$$

This ensures the required antisymmetry under exchange of any two particle coordinates.

Many-particle operators

Consider a typical operator $t_a(x_a)$ in standard "first" quantization (for example the kinetic energy or an external potential), that we constrain to act *only* on the coordinate x_a of the a^{th} particle. The fully symmetric operator with respect to all N particles is

$$T = \sum_{a=1}^{N} t_a \tag{2.9}$$

It is not hard to see that this operator only allows transitions of the many-body state for which the occupation numbers n_k are either unchanged or those in which the occupation of one state is reduced by one and that of another state is augmented by one (one particle has changed its state). It is a simple exercise to show that for

example for **bosons**, in the first case,

$$\langle \Phi_{n_1 n_2 \ldots n_\infty} | \, T \, | \Phi_{n_1 n_2 \ldots n_\infty} \rangle = \sum_k \langle k | \, t \, | k \rangle \, n_k \tag{2.10}$$

For the second case, one finds

$$\left\langle \Phi_{n_1 \ldots n_i \ldots n_j - 1 \ldots} \right| T \left| \Phi_{n_1 \ldots n_i - 1 \ldots n_j} \right\rangle = \langle i | \, t \, | j \rangle \, \sqrt{n_i n_j} \tag{2.11}$$

One can imagine that keeping track of all the factors $\sqrt{n_i}$ etc. in calculations can get extremely tedious, especially when two-particle operators are introduced that act on *two* particle coordinates. Second quantization provides a very elegant way of "book-keeping" for these combinatoric factors arising in calculations as well as ensuring the correct full (anti-)symmetry of the many-body state.

Second quantization

For this, a natural set of basis states is defined:

$$| n_1 n_2 \ldots n_\infty \rangle \equiv | n_1 \rangle \, | n_2 \rangle \ldots | n_\infty \rangle \tag{2.12}$$

which describes n_1 particles in state 1, n_2 in state 2 etc. For **bosons**, all occupation numbers are allowed. One associates particle "creation" and "annihilation" operators $a_k^\dagger$ and a_k to each *mode* $|n_k\rangle$ that satisfy the commutation rules

$$\begin{aligned} \left[a_k^\dagger, a_j^\dagger \right]_- &= 0 \\ [a_k, a_j]_- &= 0 \\ \left[a_k, a_j^\dagger \right]_- &= \delta_{ij} \qquad \text{for bosons} \end{aligned} \tag{2.13}$$

where $[A, B]_- = AB - BA$. These are the same commutation rules as for the creation and annihilation operator of a harmonic oscillator. Thus, they act just in the same way, namely by raising and lowering the number of particles in state E_k: $a_k^\dagger \, |n_k\rangle = \sqrt{n_k + 1} \, |n_k + 1\rangle$, $a_k \, |n_k\rangle = \sqrt{n_k} \, |n_k - 1\rangle$, and especially $a_k \, |0\rangle = 0$, where $|0\rangle$ is the vacuum state. $a_k^\dagger a_k$ is the number operator.

For fermions, the occupation numbers are necessarily $n_k = 0$ or 1. This is ensured if the following *anti*commutation rules are imposed on the *fermionic* operators $c_k^\dagger$, c_k:

$$\begin{aligned}\left[c_k^\dagger, c_j^\dagger\right]_+ &= 0 \\ \left[c_k, c_j\right]_+ &= 0 \\ \left[c_k, c_j^\dagger\right]_+ &= \delta_{ij} \qquad \text{for fermions}\end{aligned} \tag{2.14}$$

where $[A, B]_+ = AB + BA$. We see that for fermions, $c_k^\dagger c_k^\dagger = 0$, which is again Pauli's exclusion principle. It also follows $c_k^\dagger |0\rangle = |1\rangle$, $c_k^\dagger |1\rangle = 0$, $c_k |1\rangle = |0\rangle$ and $c_k |0\rangle = 0$.

As an example, for N non-interacting (and spinless) bosons confined in a box, the (unnormalized) ground state will simply be

$$\Psi_N^{\text{bosons}} = (a_{\mathbf{0}}^\dagger)^N |0, 0, 0, \dots\rangle \propto |N, 0, 0, \dots\rangle \tag{2.15}$$

with $a_{\mathbf{0}}^\dagger$ the creation operator for the single-particle ground state with $\mathbf{k} = \mathbf{0}$. That is, all bosons occupy the same state: this is the Bose-Einstein condensate. Fermions, on the other hand, cannot occupy one and the same single-particle state and need to arrange themselves in different states. At zero temperature, N fermions will thus occupy the N lowest single-particle states:

$$\Psi_N^{\text{fermions}} = \prod_{k<k_F} c_{\mathbf{k}}^\dagger |0, 0, 0, \dots\rangle \quad \propto \quad |\underbrace{1, 1, \dots, 1}_{N \text{ times}}, 0, 0, \dots\rangle \tag{2.16}$$

with k_F defined such that $\sum_{k<k_F} = N$.

Many-particle operators in second quantization

With these definitions, it turns out that we can now represent the operator T from above by the second quantized operator

$$\hat{T} = \sum_{i,j} \langle i| t |j\rangle \, a_i^\dagger a_j \tag{2.17}$$

Indeed, the matrix elements of $\hat{T}$ in the states $|n_1 n_2 \dots n_\infty\rangle$ are identical to the ones of the first quantized operator T in Eqs. 2.10 and 2.11, as is easy to check. A many-body hamiltonian involving the kinetic energy operator $t(x)$ and a potential $V(x_a, x_b)$

can thus be written as

$$\hat{H} = \sum_{i,j} \langle i| t |j\rangle \, a_i^\dagger a_j + \sum_{i,j,k,l} a_i^\dagger a_j^\dagger \langle ij| V |kl\rangle \, a_l a_k \tag{2.18}$$

where the ordering in the last term is important if we deal with fermions (replacing the bosonic operators a_k with the fermionic ones c_k).

Introducing the field operators $\hat{\Psi}(x) = \sum_k \psi_k(x) a_k$ and $\hat{\Psi}^\dagger(x) = \sum_k \psi_k(x)^\dagger a_k^\dagger$ one can rewrite $\hat{H}$ as[1]

$$\hat{H} = \int d^3x \hat{\Psi}^\dagger(x) t(x) \hat{\Psi}(x) + \frac{1}{2} \int d^3x d^3x' \hat{\Psi}^\dagger(x) \hat{\Psi}^\dagger(x') V(x,x') \hat{\Psi}(x') \hat{\Psi}(x) \tag{2.19}$$

In this form, the origin of the name "second quantization" is apparent: The hamiltonian is "disguised" as the expectation value of operators $t(x)$ and $V(x,x')$ in a state described by a wavefunction $\hat{\Psi}(x)$. However, here, $\hat{\Psi}(x)$ and $\hat{\Psi}^\dagger(x)$ are operators, not wave functions, and $t(x)$ and $V(x,x')$ are complex *numbers*, not operators.

2.1.2 Bose-Einstein versus Fermi-Dirac distribution

The postulate of statistical mechanics states that an isolated system in equilibrium is equally likely to be found in any of its accessible states. Accessible states are those that are consistent with the specified number N and total energy E_{tot} of the system (micro-canonical ensemble). However, it is often convenient to consider a system in contact with a reservoir, with which it can exchange particles and energy (grand canonical ensemble). The probability that the system is in *any* state with particle number N and energy E_{tot} is then given by the Boltzmann factor $e^{-(E_{\text{tot}} - \mu N)/k_B T}$, where the temperature T and the chemical potential μ are imposed by the large reservoir.

For non-interacting particles with single-particle spectrum E_i, E_{tot} for the many-particle state $|n_1 n_2 \ldots n_\infty\rangle$ is thus simply given by $\sum_i n_i E_i$. The grand canonical partition function Z is then

$$Z = \sum_{\{n_i\}} e^{-\left(\sum_i E_i n_i - \mu n_i\right)/k_B T} \tag{2.20}$$

$$= \sum_{\{n_i\}} \prod_i e^{-n_i (E_i - \mu)/k_B T} \tag{2.21}$$

[1] To simplify the notation, we assume here that x denotes a spatial coordinate.

For bosons, all n_i run from 0 to ∞, so that

$$Z_B = \prod_i \frac{1}{1 - e^{-(E_i - \mu)/k_B T}} \tag{2.22}$$

For fermions, the only possible values for n_i are 0 and 1, so that

$$Z_F = \prod_i (1 + e^{-(E_i - \mu)/k_B T}) \tag{2.23}$$

The average occupation of state i is then

$$\langle n_i \rangle = k_B T \frac{\partial \ln Z}{\partial \mu} = \frac{1}{e^{(E_i - \mu)/k_B T} \mp 1} \tag{2.24}$$

again with the upper sign corresponding to bosons, the lower sign to fermions. These are the Bose-Einstein and Fermi-Dirac distributions, respectively. Typically, the number of particles is fixed, which can be achieved by choosing μ such that $N = \sum_i \langle n_i \rangle$.

2.1.3 Ideal Bose and Fermi gases in a harmonic trap

Let us now consider particles confined in a harmonic trap, with trapping potential

$$V(\mathbf{r}) = \frac{1}{2} m(\omega_x^2 x^2 + \omega_y^2 y^2 + \omega_z^2 z^2) \tag{2.25}$$

Typical values in our experiment are $\omega_z = 2\pi \cdot 20\,\mathrm{Hz}$ and $\omega_x = \omega_y = 2\pi \cdot 100\,\mathrm{Hz}$. The single particle spectrum is

$$E_{n_x,n_y,n_z} = \hbar \left[\left(n_x + \frac{1}{2} \right) \omega_x + \left(n_y + \frac{1}{2} \right) \omega_y + \left(n_z + \frac{1}{2} \right) \omega_z \right] \tag{2.26}$$

We will assume that the thermal energy $k_B T$ is much larger than the level spacings $\hbar\omega_{x,y,z}$. In this case, sums over discrete states can be replaced by integrals over phase space, which is divided in cells of size h. The occupation of phase space cell $\{\mathbf{r}, \mathbf{p}\}$ is then given by the semi-classical distribution

$$f(\mathbf{r}, \mathbf{p}) = \frac{1}{e^{\left(\frac{\mathbf{p}^2}{2m} + V(\mathbf{r}) - \mu \right)/k_B T} \mp 1} \tag{2.27}$$

The density distribution of the gas (for bosons: not including the condensate) is

$$\begin{aligned} n(\mathbf{r}) &= \int \frac{\mathrm{d}^3 p}{(2\pi\hbar)^3} f(\mathbf{r},\mathbf{p}) \\ &= \pm\frac{1}{\lambda_{dB}^3}\,\mathrm{PolyLog}\left(3/2, \pm e^{(\mu - V(\mathbf{r}))/k_B T}\right) \end{aligned} \tag{2.28}$$

where $\sqrt{\frac{2\pi\hbar^2}{m k_B T}}$ is the de Broglie wavelength and $\mathrm{PolyLog}(n,\lambda)$ is the n^{th}-order Polylogarithm, defined as

$$\mathrm{PolyLog}(n,\lambda) \equiv \frac{1}{\pi^n}\int \mathrm{d}^{2n} r \frac{1}{e^{\mathbf{r}^2}/\lambda - 1} \overset{n\neq 0}{=} \frac{1}{\Gamma(n)}\int_0^\infty \mathrm{d}q \frac{q^{n-1}}{e^q/\lambda - 1} \tag{2.29}$$

where the first integral is over $2n$ dimensions, $\mathbf{r}$ is the radius vector in $2n$ dimensions, n is any positive half-integer or zero and $\Gamma(n)$ is the Gamma-function[2]. Note that expression 2.28 is correct for any potential $V(\mathbf{r})$. However, we still need to relate the chemical potential to the given particle number

$$N = \int d^3 r\; n(\mathbf{r}) \tag{2.31}$$

For a harmonic potential 2.25, we obtain using Eq. 2.30 (see footnote below):

$$N = \pm\left(\frac{k_B T}{\hbar\bar{\omega}}\right)^3 \mathrm{PolyLog}(3, \pm\, e^{\mu/k_B T}) \tag{2.32}$$

with $\bar{\omega} = (\omega_x\omega_y\omega_z)^{1/3}$ the geometric mean of the trapping frequencies.

In the classical limit at high temperature, both density distributions go over to the Maxwell-Boltzmann result, that is

$$n_{cl}(\mathbf{r}) = \frac{N}{(2\pi)^{3/2}\sigma_x\sigma_y\sigma_z} e^{-\sum_i x_i^2/2\sigma_{x_i}^2} \qquad \text{with } \sigma_{x,y,z}^2 = \frac{k_B T}{m\omega_{x,y,z}^2} \tag{2.33}$$

so density is given by the number of particles times the classical probability to find a

[2]Special cases: $\mathrm{PolyLog}(0,\lambda) = \frac{1}{1/\lambda - 1}$, $\mathrm{PolyLog}(1,\lambda) = -\mathrm{Ln}(1-x)$, $\mathrm{PolyLog}(2,\lambda) = \mathrm{Li}_2(\lambda)$, the Dilogarithm. We see that $f(\mathbf{r},\mathbf{p})$ can be written as $\pm\mathrm{PolyLog}(0, \pm e^{(\mu - \frac{\mathbf{p}^2}{2m} - V(\mathbf{r}))/k_B T})$. A useful formula for integrals over Polylogarithms is

$$\int_{-\infty}^{\infty} dr\; \mathrm{PolyLog}(n, \lambda\, e^{-x^2}) = \sqrt{\pi}\;\mathrm{PolyLog}(n + \frac{1}{2}, \lambda) \tag{2.30}$$

which can be quite directly seen from the definition Eq. 2.29. Limiting values: $\mathrm{PolyLog}(n,\lambda) \to_{\lambda \ll 1} \lambda$ and $-\mathrm{PolyLog}(n,-\lambda) \to_{\lambda\to\infty} \frac{1}{\Gamma(n+1)}\,\ln^n(\lambda)$.

particle at point $\mathbf{r}$, which is simply a gaussian for a harmonic potential.

However, as the temperature decreases, the central density grows to the point where the de Broglie waves of different particles start to overlap and we enter the regime of quantum degeneracy. For **bosons**, it is at this point that the ground state becomes macroscopically occupied, the condensate forms. As the number of condensed atoms N_0 grows to be significantly larger than 1, from Eq. 2.24 we find the relation between N_0 and the chemical potential $\mu = -\frac{k_B T}{N_0}$. For N_0 large, μ will be much closer to the ground state energy than even the first excited harmonic oscillator state. We can thus set $\mu = 0$ in the expression for the non-condensed density n_{th} and number N_{th} and obtain

$$n_{th}(\mathbf{r}) = \frac{1}{\lambda_{dB}^3}\text{PolyLog}(3/2, e^{-V(\mathbf{r})/k_B T}) \tag{2.34}$$

$$N_{th} = N(T/T_C)^3 \tag{2.35}$$

with the critical temperature

$$T_C \equiv \hbar\bar{\omega}\,(N/\zeta(3))^{1/3} = 0.94\,\hbar\bar{\omega}N^{1/3} \tag{2.36}$$

where $\zeta(3) \approx 1.202$. The maximum density of the thermal cloud is capped at the critical value $n = 2.612/\lambda_{dB}^3$: The gas is a quantum saturated vapor. The density profile of the thermal cloud is a bit more peaked than a gaussian, a direct effect of bosonic stimulation at low momenta [232]. The condensate fraction is given by

$$N_0/N = 1 - (T/T_C)^3 \tag{2.37}$$

We note that for $T/T_C = 0.5$ the condensate fraction is already almost 90%. The density profile of the condensate is simply given by the square of the ground state wave function of the harmonic oscillator:

$$n_c(\mathbf{r}) = \frac{N_0}{\pi^{3/2} a_x a_y a_z} e^{-\sum_i \frac{x_i^2}{a_{x_i}^2}} \tag{2.38}$$

where $a_{x_i} = \sqrt{\frac{\hbar}{m\omega_{x_i}}}$ are the harmonic oscillator lengths. The width of the condensate profile is much smaller than that of the thermal cloud, $a_{x_i}/\sigma_{x_i} = \sqrt{\frac{\hbar\omega_i}{k_B T}} \ll 1$, and the central density of the condensate is much larger, $n_c(\mathbf{0})/n_{th}(\mathbf{0}) \propto \frac{N_0 \lambda_{dB}^3}{a_x a_y a_z} \propto \sqrt{N}(\frac{T_C}{T})^{3/2}(1-(T/T_C)^3)$. Condensation in a harmonic trap thus results in a dramatic change in the density profile of the bosonic gas, the condensate is clearly visible as a

central dense feature in the cloud. We will see below that this qualitative signature of condensation survives in the presence of weak interactions, but is no longer true in the case of strongly interacting gases (see chapter 5).

For **fermions**, nothing dramatic happens around the degeneracy temperature. The occupation of available phase space cells approaches 1 in a smooth fashion. Accordingly, the density profile smoothly changes from its gaussian form at high temperatures to its zero temperature shape given by

$$n_F(\mathbf{r}) = \frac{1}{6\pi^2} k_F^3 \left(1 - \sum_i \frac{x_i^2}{R_i^2}\right)^{3/2} \tag{2.39}$$

with the Thomas-Fermi radius $R_{x,y,z}^2 = \frac{2E_F}{m\omega_{x,y,z}^2}$, the Fermi wave vector $k_F = \sqrt{2mE_F/\hbar^2}$ and the Fermi energy defined by the number of fermions N,

$$N = \int d^3r \; n_F(\mathbf{r}) = \frac{1}{6}\left(\frac{E_F}{\hbar\bar{\omega}}\right)^3 \tag{2.40}$$

or $E_F = \hbar\bar{\omega}(6N)^{1/3}$. All these equations can be directly obtained from $n(\mathbf{r}) = \int_{k<k_F(\mathbf{r})} \frac{d^3k}{(2\pi\hbar)^3} = \frac{1}{6\pi^2} k_F(\mathbf{r})^3$ using the local Fermi energy at point $\mathbf{r}$, $\epsilon_F(\mathbf{r}) = \frac{\hbar^2 k_F(\mathbf{r})^2}{2m} = E_F - V(\mathbf{r})$.

2.2 Interacting gases

At low temperatures, the stable phase for practically all substances is the solid. The only exception to that rule is helium, which remains a liquid even at zero temperature, due to the large zero-point motion of the very light atoms. But even though the gas phase is only metastable, at the ultralow densities we deal with in our experiments it can take minutes until the gas solidifies. The reason is that three-body collisions are needed to form molecules and larger clusters, and these collisions are extremely rare at our densities[3] of $\sim 10^{12-15}$ cm^{-3}. However, two-body collisions are important even at these low densities. Elastic collisions between atoms redistribute momenta, allowing thermalization of the gas, and let particles experience attraction or repulsion from the surrounding gas. Inelastic collisions between two particles lead to a change in the internal state of one or both collision partners, leading to trap loss. These collisions are unwanted but can be eliminated by working with the lowest internal

[3]This is only true away from scattering resonances. If a weakly bound molecular state is available to the atoms, three-body collisions can populate this state efficiently, even at our low densities.

energy states of the atoms.

2.2.1 Elastic collisions

If we neglect the weak magnetic dipole interaction between the spins, the interatomic interaction is described by a central potential $V(r)$. At large distances from each other, atoms interact with the van der Waals-potential $-C_6/r^6$ as they experience each other's fluctuating electric dipole[4]. At short distances on the order of a few Bohr radii a_0, the two electron clouds strongly repel each other, leading to "hard-core" repulsion. If the spins of the two valence electrons (we are considering alkali atoms) are in a triplet configuration, there is an additional repulsion due Pauli's exclusion principle. Hence, the triplet potential $V_T(r)$ is shallower than the singlet one $V_S(r)$.

The exact inclusion of the interatomic potential in the description of the gas would be extremely complicated. However, the gases we are dealing with are ultradilute: The range of the interatomic potential r_0 (on the order of the van der Waals length $r_0 \sim (\mu C_6/\hbar^2) \sim 50\, a_0$ for ^{6}Li) is much smaller than the interparticle distance $n^{-1/3} \sim 5\,000{-}10\,000\, a_0$. Also, our samples are ultracold, that is, typical collisions occur at low relative momenta $k \ll 1/r_0$ with an associated de Broglie wavelength $\lambda = 2\pi/k \gg r_0$. The scattering particles thus never explore the fine details of the short-range scattering potential. The entire collision process can thus be described by a single quantity, the *scattering length.*

What follows is a quick reminder on scattering theory including the definition of the scattering length.

The scattering amplitude

The Schrödinger equation for the reduced one-particle problem in the center-of-mass frame of the colliding atoms (with reduced mass $m/2$ and distance vector r) is

$$(\nabla^2 + k^2)\Psi(\mathbf{r}) = v(r)\Psi(\mathbf{r}) \quad \text{with } k^2 = \frac{mE}{\hbar^2} \quad \text{and } v(r) = \frac{mV(r)}{\hbar^2} \tag{2.41}$$

Far away from the scattering potential, the wave function $\Psi(\mathbf{r})$ will be given by the sum of the incident plane wave $e^{i\mathbf{k}\cdot\mathbf{r}}$ and an outgoing scattered wave, which satisfies

[4]For distances on the order of or larger than the characteristic wavelength of radiation of the atom, $\lambda \gg r_0$, retardation effects change the potential to a $-1/r^7$ law.

$(\nabla^2 - k^2)\Psi_{out}(\mathbf{r}) = 0$:

$$\Psi(\mathbf{r}) = e^{i\mathbf{k}\cdot\mathbf{r}} + f(\mathbf{k},\mathbf{k}')\frac{e^{ikr}}{r} \tag{2.42}$$

$f(\mathbf{k},\mathbf{k}')$ is the scattering amplitude for scattering an incident plane wave with wave vector $\mathbf{k}$ into the direction $\mathbf{k}'$ (energy conservation implies $k' = k$). The probability per unit time for the scattered particle to traverse the surface element $dS = r^2 d\Omega$ is $v|f|^2/r^2 dS = v|f|^2 d\Omega$ (v is the incident - and final - velocity). Dividing by the incident particle flux we arrive at the *differential scattering cross section*

$$d\sigma = |f|^2 d\Omega \tag{2.43}$$

Since we deal with a central potential, the scattered wave must be axially symmetric with respect to the incident wave vector $\mathbf{k}$, that we choose to lie in z-direction (no azimuthal ϕ-dependence). We can thus expand $\Psi(\mathbf{r})$ into the basis of free spherical waves with angular momentum corresponding to quantum numbers l and zero z-projection [145]:

$$\Psi(\mathbf{r}) = \sum_{l=0}^{\infty} P_l(\cos\theta) R_{kl}(r) \tag{2.44}$$

The radial functions $R_{kl}(r)$ verify a radial Schrödinger equation containing the potential $V(r)$ and the centrifugal potential $\hbar^2 l(l+1)/mr^2$ that depends on the angular momentum quantum number l. Far way from the potential, the $R_{kl}(r)$ must behave like

$$R_{kl}(r) \propto \frac{1}{r}\sin(r - l\frac{\pi}{2} + \delta_l) \tag{2.45}$$

The incident plane wave can also be expanded like 2.44, but here $\delta_l = 0$. The entire effect of the potential $V(r)$ on the incoming wave is thus to add a phase shift δ_l to each spherical wave with angular momentum l. This quite remarkable result allows us to write the scattering amplitude entirely in terms of the δ_l:

$$f(\theta) = \frac{1}{2ik}\sum_{l=0}^{\infty}(2l+1)(e^{2i\delta_l} - 1)P_l(\cos\theta) \tag{2.46}$$

The total cross section is given by

$$\sigma = \frac{4\pi}{k^2}\sum_{l=0}^{\infty}(2l+1)\sin^2\delta_l \tag{2.47}$$

For our ultracold collisions, we are interested in describing the scattering process at

low momenta $k \ll 1/r_0$, where r_0 is the range of the interatomic potential. That is, the particles do not have enough energy to resolve the fine details of the potential (their de Broglie wavelength $\frac{2\pi}{k}$ being much larger than the size of these fine details). Using the radial Schrödinger equation one can show that for low momenta $\delta_l \sim k^{2l+1}$ and thus each *partial wave* $f_l = \frac{1}{2ik}(e^{2i\delta_l} - 1)$ appearing in 2.46 behaves like $f_l \approx \frac{\delta_l}{k} \sim k^{2l}$. In the absence of resonance phenomena for $l \neq 0$, *s-wave scattering* $l = 0$ is dominant over all other partial waves:

$$f \approx f_0 = \frac{1}{2ik}(e^{2i\delta_0} - 1) \tag{2.48}$$

We already know that at low momenta, $\delta_0 \sim k$. It is thus useful to define the *scattering length*

$$a = \lim_{k \ll 1/r_0} \frac{\tan \delta_0}{k} \tag{2.49}$$

with which we can rewrite f as

$$f = -\frac{a}{1 + ika} \tag{2.50}$$

In the limit $ka \ll 1$, f becomes independent on momentum and equals $-a$. For $ka \gg 1$, the scattering amplitude is limited by $f = -\frac{1}{ik}$ and the cross section $\sigma = \frac{4\pi}{k^2}$. This is the so-called unitarity limit.

Consequence of quantum statistics

If the colliding particles are identical, there are two scattering processes with the same outcome: *direct* and *exchange* scattering. In the case of bosons, the two-particle wave function needs to be symmetric and we have to add the corresponding scattering amplitudes. For fermions, the wave function needs to be antisymmetric, so we have to subtract the amplitudes. Partial waves of even angular momentum quantum number are symmetric under exchange, those with odd l are antisymmetric. It follows that the total scattering amplitude for bosons only contains (twice) the even terms in the partial wave expansion, whereas for fermions it only contains (twice) the odd terms. The total s-wave scattering cross section for two identical bosons is $\sigma = 8\pi a^2$, while for two identical fermions the s-wave scattering cross section is identically zero. This means that a polarized Fermi gas at ultracold temperatures is essentially non-interacting.

Pseudo-potentials

If the de Broglie wavelength $\frac{2\pi}{k}$ of the colliding particles is much larger than the fine details of the interatomic potential, $1/k \gg r_0$, we can "cheat" a bit and modify the potential in such a way that it is much easier to manipulate in the calculations, but still reproduces the correct s-wave scattering. An obvious candidate for such a "pseudo-potential" is a delta-potential $\delta(\mathbf{r})$. However, there is a subtlety involved which we will address in the following. The goal is to find an expression for the scattering amplitude $f(\mathbf{k}, \mathbf{k}')$ in terms of the potential $V(r) = \frac{\hbar^2 v(r)}{m}$, so that we can try out different pseudo-potentials, always ensuring that $f \to -a$ in the s-wave limit. For this, let us go back to the Schrödinger equation Eq. 2.41. If we knew the solution to the following equation:

$$(\nabla^2 + k^2)G(\mathbf{r}) = \delta(\mathbf{r}) \tag{2.51}$$

we could write an integral equation for the wavefunction $\Psi(\mathbf{r})$ as follows:

$$\Psi(\mathbf{r}) = e^{i\mathbf{k}\cdot\mathbf{r}} + \int d^3r' G(\mathbf{r} - \mathbf{r}')v(\mathbf{r}')\Psi(\mathbf{r}') \tag{2.52}$$

This can be simply checked by inserting this implicit solution for Ψ into Eq. 2.41. $G(\mathbf{r})$ can be easily obtained from the Fourier transform of Eq. 2.51, defining $G(\mathbf{p}) = \int d^3r e^{-i\mathbf{p}\cdot\mathbf{r}} G(\mathbf{r})$:

$$(-p^2 + k^2)G(\mathbf{p}) = 1 \tag{2.53}$$

The solution for $G(\mathbf{r})$ is

$$G_+(\mathbf{r}) = \int \frac{d^3p}{(2\pi)^3} \frac{e^{i\mathbf{p}\cdot\mathbf{r}}}{k^2 - p^2 + i\eta} = -\frac{1}{4\pi}\frac{e^{ikr}}{r} \tag{2.54}$$

where we have chosen (by adding the infinitesimal constant $i\eta$, with $\eta > 0$ in the denominator) the solution that corresponds to an outgoing spherical wave, which is what we need. $G_+(\mathbf{r})$ is the *Green's function* of the scattering problem. Far away from the origin, $|\mathbf{r} - \mathbf{r}'| \sim r - \mathbf{r}' \cdot \mathbf{u}$, with the unit vector $\mathbf{u} = \mathbf{r}/r$, and

$$\Psi_{\mathbf{k},+}(\mathbf{r}) \approx e^{i\mathbf{k}\cdot\mathbf{r}} - \frac{e^{ikr}}{4\pi r}\int d^3r' e^{-i\mathbf{k}'\cdot\mathbf{r}'} v(\mathbf{r}')\Psi_{\mathbf{k},+}(\mathbf{r}') \tag{2.55}$$

Now using the definition of the scattering amplitude in Eq. 2.42, this gives us a formula for $f(\mathbf{k}, \mathbf{k}')$:

$$f(\mathbf{k}, \mathbf{k}') = -\frac{1}{4\pi}\int d^3r' e^{-i\mathbf{k}'\cdot\mathbf{r}'} v(\mathbf{r}')\Psi_{\mathbf{k},+}(\mathbf{r}') \tag{2.56}$$

The fourier transform of the product $v(\mathbf{r}')\Psi_{\mathbf{k},+}(\mathbf{r}')$ equals the convolution of the fourier transforms of both factors, $v(\mathbf{q})$ and $\Psi_{\mathbf{k}}(\mathbf{q})$:

$$f(\mathbf{k},\mathbf{k}') = -\frac{1}{4\pi}\int \frac{d^3q}{(2\pi)^3} v(\mathbf{q})\Psi_{\mathbf{k}}(\mathbf{k}'-\mathbf{q}) \tag{2.57}$$

On the other hand, $\Psi_{\mathbf{k}}(\mathbf{q})$ satisfies the integral equation Eq. 2.52 written in momentum space:

$$\begin{aligned}\Psi_{\mathbf{k}}(\mathbf{p}) &= (2\pi)^3\delta(\mathbf{p}-\mathbf{k}) + \frac{1}{k^2-p^2+i\eta}\int \frac{d^3q}{(2\pi)^3} v(\mathbf{q})\Psi_{\mathbf{k}}(\mathbf{k}'-\mathbf{q}) &(2.58)\\ &= (2\pi)^3\delta(\mathbf{p}-\mathbf{k}) - \frac{4\pi f(\mathbf{k},\mathbf{k}')}{k^2-p^2+i\eta} &(2.59)\end{aligned}$$

Multiplying by $v(\mathbf{q}-\mathbf{p})$, integrating $\int \frac{d^3p}{(2\pi)^3}$ and relabelling yields

$$-4\pi f(\mathbf{p},\mathbf{k}) = v(\mathbf{p}-\mathbf{k}) - 4\pi\int \frac{d^3q}{(2\pi)^3}\frac{v(\mathbf{p}-\mathbf{q})f(\mathbf{q},\mathbf{k})}{k^2-q^2+i\eta} \tag{2.60}$$

This is an integral equation for f in terms of the potential v, useful to perform perturbation expansion. If we only keep the first order in v, we obtain the scattering amplitude in *Born approximation*:

$$f(\mathbf{p},\mathbf{k}) = -\frac{1}{4\pi}v(\mathbf{p}-\mathbf{k}) \tag{2.61}$$

which is simply given by the fourier transform of the potential, evaluated at the transferred momentum vector $\mathbf{p}-\mathbf{k}$. For a **delta-potential** $V(\mathbf{r}) = V_0\,\delta(\mathbf{r})$, we obtain as $f \to -a$

$$V_0 = \frac{4\pi\hbar^2 a}{m} \tag{2.62}$$

However, already the second order term in the expansion of 2.60 would not converge, as it involves the integral $\int \frac{d^3q}{(2\pi)^3}\frac{1}{q^2}$. The reason is of course that the δ-potential does not fall off at large momenta (ultra-violet divergence). Any physical potential *does* fall off at some large momentum, so this is not a "real" problem. We can formally work with the fourier transform V_0 of the delta-potential in the following, but if we are to calculate physical quantities, we should replace it in favor of the observable and meaningful quantity a using the formal prescription

$$\frac{1}{V_0} = \frac{m}{4\pi\hbar^2 a} - \frac{m}{\hbar^2}\int \frac{d^3q}{(2\pi)^3}\frac{1}{q^2} \tag{2.63}$$

(for this, use the limit $k = p = 0$ in Eq. 2.60 and replace $f \to -a$). We will always find that the diverging integral is exactly balanced by another diverging integral in the final expressions, so this is a "sane" procedure [74, 115].

2.2.2 The interacting Bose gas

We are now in the position to formulate the problem of an interacting Bose gas. The second-quantized hamiltonian reads

$$\hat{H} = \int d^3r \hat{\Psi}^\dagger(\mathbf{r})(-\frac{\hbar^2\nabla^2}{2m} + V_{\text{ext}}(\mathbf{r}))\hat{\Psi}(\mathbf{r}) + \frac{1}{2}\int d^3r\, d^3r' \hat{\Psi}^\dagger(\mathbf{r})\hat{\Psi}^\dagger(\mathbf{r}')V(\mathbf{r},\mathbf{r}')\hat{\Psi}(\mathbf{r}')\hat{\Psi}(\mathbf{r}) \tag{2.64}$$

where $V_{\text{ext}}(\mathbf{r})$ is the external trapping potential of Eq. 2.25 and $V(\mathbf{r}',\mathbf{r}) = V(\mathbf{r}-\mathbf{r}')$ is the interatomic potential, for which we can choose the Pseudo-potential $V(\mathbf{r}) = g\delta(\mathbf{r})$ of the preceding section. As long as we work in real space, we can safely set $g = \frac{4\pi\hbar^2 a}{m}$. We will limit our discussion to the case of repulsive interactions, relevant to our experiment. Let us assume that even in the interacting system, there still is a macroscopic occupation of a single-particle state $\psi(\mathbf{r})$. That is we set $\hat{\Psi}(\mathbf{r}) = \psi(\mathbf{r}) + \delta\hat{\Psi}(\mathbf{r})$, with $\psi(\mathbf{r})$ being the thermal average of $\hat{\Psi}(\mathbf{r})$ in the many-body state: $\psi(\mathbf{r}) = \left\langle \hat{\Psi}(\mathbf{r}) \right\rangle$, and $\delta\hat{\Psi}(\mathbf{r})$ represents the fluctuations around this "mean-field". Neglecting these fluctuations leads to the time-dependent *Gross-Pitaevskii* equation for $\psi(\mathbf{r},t)$:

$$i\hbar\frac{\partial}{\partial t}\psi(\mathbf{r},t) = \left(-\frac{\hbar^2\nabla^2}{2m} + V_{\text{ext}}(\mathbf{r}) + g\left|\psi(\mathbf{r},t)\right|^2\right)\psi(\mathbf{r},t) \tag{2.65}$$

Its validity is limited to *weakly interacting* gases, for which $na^3 \ll 1$. In typical experiments on alkali BECs, this condition is very well fulfilled. For a sodium BEC with $n \approx 10^{14}\,\text{cm}^{-3}$ and $a = 3.3\,\text{nm}$, we have $na^3 \approx 4 \cdot 10^{-6}$. However, for the molecular condensates produced in our experiment, the scattering length can be tuned at will, so this condition can be violated. We will see in section 2.3 how to approximately describe this regime.

The ground state wave function can be obtained from Eq. 2.65 by setting $\psi(\mathbf{r},t) = e^{-i\mu t/\hbar}\psi(\mathbf{r})$:

$$\left(-\frac{\hbar^2\nabla^2}{2m} + V_{\text{ext}}(\mathbf{r}) + g\left|\psi(\mathbf{r})\right|^2\right)\psi(\mathbf{r}) = \mu\psi(\mathbf{r}) \tag{2.66}$$

In the *Thomas-Fermi* approximation, it is assumed that the condensate wave function is only slowly varying in space such that one can neglect the kinetic energy term. This is valid as long as interactions $\sim gn$ dominate over the zero-point motion of the particles $\sim \hbar\omega$. Already for weakly interacting alkali gases, this condition is very

well fulfilled (not too close to the edge of the condensate), with typical interaction energies in our experiment of $gn \sim 150\,\mathrm{nK}$ and $\hbar\omega_r \approx 4\,\mathrm{nK}$. In this approximation we obtain the condensate density $n_c(\mathbf{r}) = |\psi(\mathbf{r})|^2$:

$$n_c(\mathbf{r}) = \max\left(\frac{\mu - V(\mathbf{r})}{g}, 0\right) \tag{2.67}$$

The chemical potential μ is constrained by the normalization condition on $n_c(\mathbf{r})$: $N = \int d^3r\, n_c(\mathbf{r})$. For the harmonic trapping potential of Eq. 2.25, we obtain (compare with the expression for a Fermi gas, Eq. 2.39)

$$n_c(\mathbf{r}) = n_{c0}\left(1 - \sum_i \frac{x_i^2}{R_i^2}\right) \tag{2.68}$$

with the central density $n_{c0} = \mu/g$, the *Thomas-Fermi radii* $R_i = \sqrt{\frac{2\mu}{m\omega_i^2}}$ and

$$\mu = \frac{1}{2}\hbar\bar{\omega}\left(\frac{15Na}{\bar{a}_{h.o.}}\right)^{2/5} \tag{2.69}$$

where $\bar{a}_{h.o.} = (a_x a_y a_z)^{1/3}$ is the geometric mean of the harmonic oscillator lengths.

Interactions thus have a major effect on the shape of the Bose-Einstein condensate. Instead of a gaussian, the density profile is now parabolic. The size of the condensate is no longer given by the harmonic oscillator length but by the much larger Thomas-Fermi radius $R_{x,y,z} = a_{x,y,z}\left(\frac{15Na}{\bar{a}_{h.o.}}\right)^{1/5}$. The parameter $\left(\frac{15Na}{\bar{a}_{h.o.}}\right)^{1/5} \sim 6$ for a typical sodium BEC. However, such weakly interacting condensates are still considerably smaller in size than a thermal cloud, as long as $T > \mu/k_B$, and more dense: At $T = 0$, the density of a typical sodium BEC is an order of magnitude higher than the density of a thermal cloud at T_C. We conclude that the condensate in weakly interacting, trapped Bose gases can still be detected as a dense, central feature emerging in the midst of a large thermal cloud. In the case of strong interactions, when μ becomes comparable to (k_B times) T_C, this direct signature will be considerably weaker (see chapter 5).

At finite temperatures, the question arises whether interactions in the thermal cloud, and between the thermal cloud and the condensate have to be taken into account. In alkali BECs, $gn_{th} \sim \frac{\hbar^2 a}{m}\frac{1}{\lambda_{dB}^3} \sim k_B T(n_{th}a^3)^{1/3} \ll k_B T$, so one can neglect interactions in the thermal cloud. The condensate is also practically unaffected by the thermal cloud. In turn, however, the condensate has quite a strong effect on the thermal atoms, as $gn_c = \mu$ can be on the order of $k_B T$. The thermal cloud

thus experiences the "mexican hat" potential $V_{\text{ext}}(\mathbf{r}) + 2gn_c(\mathbf{r})$, it is repelled by the condensate (the factor of two coming from the exchange term, see section 2.2.1). In more strongly interacting gases, a self-consistent mean-field approximation could be carried out by including the self-interaction of the thermal cloud and its effect on the condensate. For very strong interactions, the mutual repulsion can lead to an essentially complete separation of the thermal cloud and the condensate. Imbalanced Fermi mixtures allow to clearly demonstrate such a dramatic repulsion, see chapter 7.

Bogoliubov transformation for the interacting Bose gas

We will now turn to another point of view of the interacting Bose gas at zero temperature, given by Bogoliubov [32]. It allows the identification of the elementary excitations of the system, thereby giving a natural explanation for superfluidity. It also introduces the concept of quantum depletion, about which we will have more to say in the following chapters. Lastly, it will be interesting to compare this description to the BCS case in the following section.

The model hamiltonian considered by Bogoliubov describes a dilute Bose gas confined in a box of volume Ω:

$$\hat{H} = \sum_k \epsilon_k a_k^\dagger a_k + \frac{V_0}{2\Omega} \sum_{k,l,m} a_k^\dagger a_l^\dagger a_m a_{k+l-m} \tag{2.70}$$

where $\epsilon_k = \frac{\hbar^2 k^2}{2m}$ is the free particle spectrum and the notation V_0 for the Fourier transform of the pseudo-potential reminds us that we have to correctly renormalize the interaction according to Eq. 2.63 when calculating physical properties.

As we did before, we assume a macroscopic occupation of the ground state $k = 0$ and can thus replace

$$a_0, a_0^\dagger \to \sqrt{N_0} \tag{2.71}$$

with N_0 the ground state occupation number. It is supposed that $N_0 \approx N$, the total number of particles. With that assumption, and keeping only terms of order N or N^2, the hamiltonian becomes *quadratic* in the operators a_k, $a_k^\dagger$. Bogoliubov showed that this hamiltonian can be solved exactly by introducing a canonical transformation of the operators a_k, $a_k^\dagger$:

$$a_k = u_k \alpha_k - v_k \alpha_{-k}^\dagger \qquad a_k^\dagger = u_k \alpha_k^\dagger - v_k \alpha_{-k} \tag{2.72}$$

The new operators α_k, $\alpha_k^\dagger$ also obey the bosonic commutation relations $\left[\alpha_k, \alpha_{k'}^\dagger\right] =$

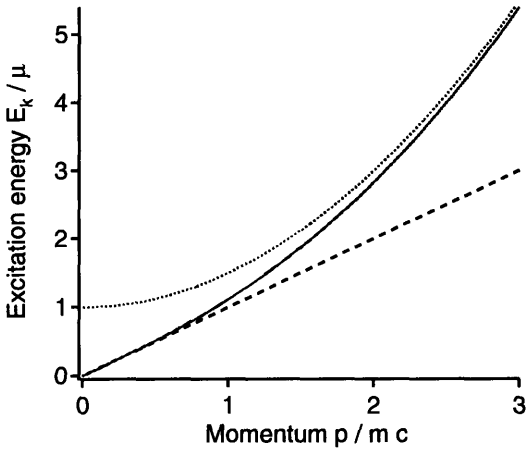

Figure 2-1: Excitation spectrum of the weakly interacting Bose gas. For low momenta $p < mc$, excitations are sound waves with linear dispersion $E_k = c\hbar k$ (dashed line). At large momentum transfer $p \gg mc$, excitations are free-particle like (dotted line), with energy offset μ.

$\delta_{kk'}$ and $[\alpha_k, \alpha_{k'}] = \left[\alpha_k^\dagger, \alpha_{k'}^\dagger\right] = 0$. For a judicious choice of the real parameters u_k and v_k the hamiltonian can be transformed into

$$\hat{H} = \frac{1}{2}\sum_k E_k \left(\alpha_k^\dagger \alpha_k + \alpha_{-k}^\dagger \alpha_{-k}\right) \tag{2.73}$$

The correct choice is $u_k = \cosh\phi_k$, $v_k = \sinh\phi_k$, with $\tanh 2\phi_k = \frac{\mu}{\epsilon_k + \mu}$ and $\mu = ng$ from the preceding section. From the commutation relations for α_k, $\alpha_k^\dagger$ immediately follows that $\alpha_k^\dagger \alpha_k$ has eigenvalues $0, 1, 2, \ldots$ and thus E_0 represents the ground state energy and E_k is the excitation spectrum of the hamiltonian. The ground state is defined by $\alpha_k |\mathbf{O}\rangle = 0$ for all $k \neq 0$ and can be thought of as the "quasi-particle vacuum". One finds for the average energy per particle, with the particle density $n = N/\Omega$,

$$\frac{E_0}{N} = \frac{2\pi\hbar^2 an}{m}\left(1 + \frac{128}{15}\sqrt{\frac{na^3}{\pi}}\right) \tag{2.74}$$

The first term in this expression is simply $\frac{1}{2}\mu$, which we could have obtained from the preceding perturbation treatment. The second term is the *Lee-Yang* correction [148], which is nonanalytic in the interaction parameter na^3 and thus cannot be obtained from perturbation theory.

The excitation spectrum E_k is given by (see Fig. 2-1)

$$E_k \equiv \left[(\epsilon_k + \mu)^2 - \mu^2\right]^{1/2} \tag{2.75}$$

which has the two limiting cases

$$E_k \approx \begin{cases} \sqrt{\frac{\mu}{m}}\,\hbar k, & k \to 0 \\ \epsilon_k + \mu, & k \to \infty \end{cases} \tag{2.76}$$

The long-wavelength excitations are thus sound waves with a *speed of sound* $c = \sqrt{\mu/m}$. At large momenta, the excitations correspond to free particles excited above the condensate mean-field μ.

Quantum depletion

Even in the ground state, the particles are *not* all condensed in the same single-particle state $k = 0$. Indeed, $a_k |\mathbf{O}\rangle = -v_k \alpha^\dagger_{-k} |\mathbf{O}\rangle \neq 0$ and thus the ground state contains particles in excited k-states. This number of excited particles is $\frac{N-N_0}{N} = \frac{8}{3}\sqrt{\frac{na^3}{\pi}}$. For a typical sodium BEC, it is less than 1%. Again, however, for our molecular condensates this number can in principle be large. Of course, once na^3 is no longer small compared to 1, the approximation of weak interactions is no longer allowed. Let us point out that the particles populating nonzero k-states are not to be confused with thermally excited particles. They are in fact perfectly correlated admixtures to the many-body wave function. One can show that these admixtures occur in pairs of opposite momenta $(k, -k)$, which one could probe by noise correlation experiments. If the range of available k-states is restricted, for example by imposing a weak lattice potential that singles out certain k-directions, the quantum depleted part of the many-body wavefunction should lead to a distinct structure in the interference pattern of expanding condensates[5] [96, 254].

Superfluidity in weakly interacting Bose gases

With the aid of the excitation spectrum we are now able to argue that weakly interacting Bose gases must show superfluidity. The well-known *Landau criterion* states that, given a dispersion relation E_k of the medium, an object moving at a velocity v *smaller* than $v_c = \min_k E_k/\hbar k$ cannot scatter from the medium. For free particles (hence also for the Bose-Einstein condensate in an ideal gas), $E_k \sim k^2$ and thus $v_c = 0$. However, for the weakly interacting Bose gas, we find $v_c = c > 0$, and thus for particle velocities smaller than v it is a frictionless superfluid. Indeed, superfluidity of weakly

[5]This structure should be distinguished from the Bragg peaks due to atoms in the macroscopically occupied single-particle state *and* from the incoherent (spherically symmetric gaussian) background due to atoms localized in single lattice sites

interacting Bose gases has been studied for example by creating a single vortex in a two-component BEC [164, 11], through impurity scattering [58, 179] and as a most spectacular demonstration via the creation of vortex lattices [160, 2, 120, 87]. The origin of quantized vortices will be discussed in chapter 6.

2.2.3 Fermi gases with attractive interaction: Cooper instability

The non-interacting Fermi gas did not show any phase transition down to zero temperature. One might assume that this qualitative fact should not change as interactions are introduced. This is true in the case of repulsive interactions. For attractive interactions, the situation is, however, dramatically different. By taking advantage of the attraction, the fermions regroup into pairs, which can then form a condensate.

The idea of pairing might be natural, as tightly bound pairs of fermions can be regarded as point-like bosons, which should condense according to the preceding section. However, for weak attractive interaction – as is the case for the electron-electron interaction in metals – it is not evident that a paired state exists. Indeed, we will see in the following that in three dimensions there is no bound state for two isolated particles and arbitrarily weak interaction.

Two-body bound states in 1D, 2D and 3D

Localizing a quantum-mechanical particle down to a certain range R leads to an increased momentum uncertainty of $p \sim \hbar/R$ at a kinetic energy cost of about $E_R = p^2/2m = \hbar^2/mR^2$. Clearly, a shallow potential well of size R and depth V with $V/E_R \equiv \epsilon \ll 1$ cannot confine the particle within its borders. But we can search for a bound state at energy $E_B \ll E_R$ of much larger size $r_B = 1/k \equiv \sqrt{\hbar^2/2mE_B} \gg R$.

- **In 1D**, the bound state wavefunction far away from the well necessarily behaves like $e^{\pm kx}$ for negative (positive) x (see Fig. 2-2a). As we traverse the well, the wavefunction has to change its slope by $2k$ over a range R. This costs kinetic energy $\hbar^2\psi''(x)/2m\bar{\psi} \approx \hbar^2 k/mR$ that has to be provided by the potential energy $-V$ (here, $\bar{\psi}$ is the average value of $\psi(x)$ in the well). We deduce that $k \approx mRV/\hbar^2 = \epsilon/R$, the size of the bound state $r_B \approx R/\epsilon$ is indeed much larger than the size of the well, and the bound state energy $E_B \approx -E_R\,\epsilon^2/2$ depends quadratically on the weak attraction $-V$. Importantly, we can *always* find a bound state even for arbitrarily weak (purely) attractive potentials.

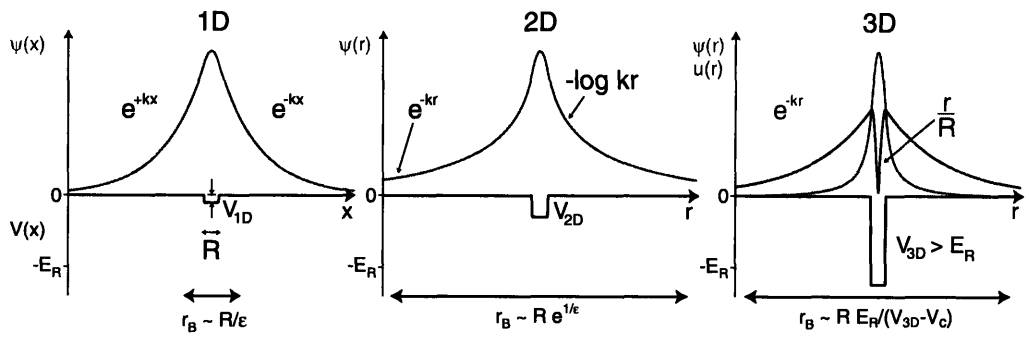

Figure 2-2: Bound state wavefunctions in 1D, 2D and 3D for a potential well of size R and depth V. In 1D and 2D, bound states exist for arbitrarily shallow wells. In terms of the small parameter $\epsilon = V/E_R$ with $E_R = \hbar^2/mR^2$, the size of the bound state in 1D is R/ϵ. In 2D, the bound state is exponentially large, of size $Re^{-1/\epsilon}$. In 3D, due to the steep slope in $u(r) = r\Psi(r)$, bound states can only exist for well depths V_{3D} larger than a certain threshold $V_c \approx E_R$. The size of the bound state diverges as $RE_R/(V_{3D} - V_c)$ for $V_{3D} > V_c$.

- **In 2D** and for a spherically symmetric well, the Schrödinger equation for the radial wavefunction $\psi(r)$ *outside* the well reads $\frac{1}{r}\partial_r(r\partial_r\psi) = k^2\psi$. The solution is the modified Bessel function which vanishes like e^{-kr} as $r \gg 1/k$ (see Fig. 2-2b). For $R \ll r \ll 1/k$, we can neglect the small bound state energy $E_B \propto k^2$ compared to the kinetic energy and have $\partial_r(r\psi') = 0$ or $\psi(r) \approx \log(kr)/\log(kR)$, where $1/k$ is the natural scale of evolution for $\psi(r)$ and we have normalized ψ to be of order 1. Note that in 2D, it is not the change in the slope ψ' of the wavefunction which costs kinetic energy, but the change in $r\psi'$. *Inside* the well, we can assume $\psi(r)$ to be practically constant as $V \ll E_R$. Thus, $r\psi'$ changes from $\approx 1/\log kR$ (outside) to ≈ 0 (inside) over a distance R. The corresponding kinetic energy cost is $\frac{\hbar^2}{2mr}\partial_r(r\psi') \approx \hbar^2/2mR^2\log(kR) = E_R/2\log(kR)$, which has to be provided by the potential energy $-V$. We deduce $k \approx \frac{1}{R}e^{-cE_R/2V}$ and $E_B \approx E_R e^{-cE_R/V}$ with a numerical constant c on the order of 1. The particle is extremely weakly bound, with its bound state energy depending exponentially on the shallow potential $-V$. Accordingly, the size of the bound state is exponentially large, $r_B \approx Re^{cE_R/2V}$. Nevertheless, we can *always* find this weakly bound state, for arbitrarily small attraction[6].

[6]Mathematically, the condition for the potential $V(r)$ to allow a bound state in 2D requires the integral $\int_0^\infty rV(r)dr$ to be finite [145].

	1D	2D	3D
V	$\ll E_R$	$\ll E_R$	$> V_c \approx E_R$
$\psi(r > R)$	e^{-r/r_B}	$K_0(\frac{r}{r_B}) = \begin{cases} -\log r/r_B, & R \ll r \ll r_B \\ e^{-r/r_B}, & r \gg r_B \end{cases}$	$\frac{e^{-r/r_B}}{r}$
r_B	$R\frac{E_R}{V}$	$Re^{-cE_R/2V}$	$R\frac{E_R}{V-V_c}$
$E_B = -\frac{\hbar^2}{mr_B^2}$	$-V^2/E_R$	$-E_R e^{-cE_R/V}$	$-(V-V_c)^2/E_R$

Table 2.1: Bound states in 1D, 2D and 3D for a potential well of size R and depth V. $\psi(r > R)$ is the wave function outside the well, r_B is the size of the bound state, and E_B its energy ($E_R = \hbar^2/mR^2$).

- **In 3D** and for a spherically symmetric well, the Schrödinger equation for the wavefunction ψ transforms into an effective one-dimensional problem for the wavefunction $u = r\psi$ (see Fig. 2-2c). We might now be tempted to think that there must always be a bound state in 3D, as we already found this to be the case in 1D. However, the boundary condition on $u(r)$ is now to vanish linearly at $r = 0$, in order for $\psi(0)$ to be finite. Outside the potential well, we still have $u \propto e^{-kr}$ for a bound state. Inside the well the wavefunction must fall off to zero at $r = 0$ and necessarily has to change its slope from $-k$ outside to $\sim 1/R$ inside the well over a distance R. This costs the large kinetic energy $\hbar^2 u''(r)/2m\bar{u} \approx \hbar^2/mR^2 = E_R$ (with $\bar{u}$ the average value of $u(r)$ in the well). If the well depth V is smaller than a *critical depth* V_c on the order of E_R, the particle cannot be bound. At $V = V_c$, the first bound state enters at $E = 0$. As $k = 0$, u is then constant outside the well. If the potential depth is further increased by a small amount $\Delta V \ll V_c$, u again falls off like e^{-kr} for $r > R$. This requires an additional change in slope by k over the distance R, provided by ΔV. So we find analogously to the 1D case $k \sim mR\Delta V/\hbar^2$. Hence, the bound state energy $E \approx -\Delta V^2/E_R$ is quadratic in the "detuning" $\Delta V = (V - V_C)$, and the size of the bound state diverges as $r_B \approx RE_R/(V - V_C)$. We will find exactly the same behavior for a weakly bound state when discussing Feshbach resonances in chapter 3.

The analysis holds for quite general shapes $V(r)$ of the potential well (in the formulas, we only need to replace V by its average over the well - if it exists -, $\frac{1}{R}\int_{-\infty}^{\infty} V(r)dr$ in 1D, $\frac{1}{R^2}\int_{-\infty}^{\infty} rV(r)dr$ in 2D etc.). Table 2.1 summarizes the different cases.

Applying these results to the equivalent problem of two interacting particles colliding in their center-of-mass frame, we see that in 1D and 2D, two isolated particles

	1D	2D	3D
$\frac{\hbar^2}{m\Omega}\rho(\epsilon)$	$\frac{1}{\pi}\sqrt{\frac{\hbar^2}{2m\epsilon}}$	$\frac{1}{2\pi}$	$\frac{1}{2\pi^2}\sqrt{\frac{2m\epsilon}{\hbar^2}}$
$\frac{1}{\lvert V_0\rvert} = \frac{1}{\Omega}\int_{\epsilon<E_R} d\epsilon \frac{\rho_n(\epsilon)}{2\epsilon+\lvert E\rvert}$	$\sqrt{\frac{m}{4\hbar^2\lvert E\rvert}}$	$\frac{m}{4\pi\hbar^2}\log\left(\frac{2E_R+\lvert E\rvert}{\lvert E\rvert}\right)$	$\frac{1}{2\pi^2}\left(\frac{m}{\hbar^2}\right)^{3/2}\left(\sqrt{2E_R}-\frac{\pi}{2}\sqrt{\lvert E\rvert}\right)$
$E = -\frac{\hbar^2k^2}{m}$	$-\frac{m}{4\hbar^2}V_0^2$	$-2E_R\, e^{-\frac{4\pi\hbar^2}{m\lvert V_0\rvert}}$	$-\frac{8}{\pi^2}E_R\left(\frac{\lvert V_0\rvert-V_{0c}}{\lvert V_0\rvert}\right)^2 = -\hbar^2/ma^2$

Table 2.2: Link between the density of states and the existence of a bound state for arbitrarily weak interaction. To compare with table 2.1 note that $V_0 \sim VR^n$. $V_{0c} = \frac{2\pi^2}{\sqrt{2E_R}}(\frac{\hbar^2}{m})^{3/2}$ is the threshold interaction for the 3D case. The formula for the 3D bound state energy as a function of scattering length a follows from the renormalization procedure outlined in section 2.2.1.

can bind for an arbitrarily weak purely attractive interaction. Hence in 1D and 2D, pairing of fermions and their subsequent condensation can in principle be understood already at the two-particle level. Indeed, one can show that the existence of a two-body bound state in 1D and 2D is a necessary and sufficient condition for a BCS instability [201]. In 3D, however, there is a threshold interaction below which two isolated particles are unbound. We conclude that if pairing and condensation occur for arbitrarily weak interactions in 3D, then this must entirely be due to many-body effects.

Density of states

What physical quantity decides whether there are bound states or not? To answer this question, we formulate the problem of two interacting particles of mass m in momentum space. This allows a particularly transparent treatment for all three cases at once, and identifies the *density of states* in the different dimensions as the decisive factor for the existence of bound states.

Searching for a shallow bound state of energy $E = -\frac{\hbar^2k^2}{m}$ ($m/2$ is the reduced mass), we start by writing the Schrödinger equation for the relative wavefunction $\frac{\hbar^2}{m}(\nabla^2 - k^2)\psi = V\psi$ in (n-dimensional) momentum space:

$$\psi_{\mathbf{k}}(\mathbf{q}) = -\frac{m}{\hbar^2}\frac{1}{q^2+k^2}\int\frac{d^nq'}{(2\pi)^n}V(\mathbf{q}-\mathbf{q}')\psi_{\mathbf{k}}(\mathbf{q}') \tag{2.77}$$

For a short-range potential of range $R \ll 1/k$, $V(\mathbf{q})$ is practically constant, $V(\mathbf{q}) \approx V_0$, for all relevant q, and falls off to zero on a large q-scale of $\approx 1/R$. For example,

for a potential well of depth V and size R, we have $V_0 \sim VR^n$. Thus,

$$\psi_{\mathbf{k}}(\mathbf{q}) = -\frac{mV_0}{\hbar^2}\frac{1}{q^2+k^2}\int_{q'<\frac{1}{R}}\frac{d^nq'}{(2\pi)^n}\psi_{\mathbf{k}}(\mathbf{q}') \tag{2.78}$$

We integrate once more over $\mathbf{q}$, applying the same cut-off $1/R$, and can then divide by the common factor $\int_{q<\frac{1}{R}}\frac{d^nq}{(2\pi)^n}\psi_{\mathbf{k}}(\mathbf{q})$. We obtain the following equation for the bound state energy E:

$$-\frac{1}{V_0} = \frac{m}{\hbar^2}\int_{q<\frac{1}{R}}\frac{d^nq}{(2\pi)^n}\frac{1}{q^2+k^2} = \frac{1}{\Omega}\int_{\epsilon<E_R}d\epsilon\frac{\rho_n(\epsilon)}{2\epsilon+|E|} \tag{2.79}$$

with the density of states in n dimensions $\rho_n(\epsilon)$, the energy cut-off $E_R = \hbar^2/mR^2$ and the volume Ω of the system (note that V_0 has units of energy times volume). The question on the existence of bound states for arbitrarily weak interaction has now been reformulated: As $|V_0| \to 0$, the left hand side of Eq. 2.79 diverges. If this equation is to have a solution for any small $|V_0|$, the right hand side needs to diverge as well as the bound state energy $|E| \to 0$. The question is thus whether the integral over the density of states in Eq. 2.79 can take on any large value - or whether it is bound from above. Table 2.2 presents the different cases in 1D, 2D, 3D. In 1D, the integral diverges as $1/\sqrt{|E|}$, so one can always find a bound state solution. The binding energy depends quadratically on the interaction, as we had found before. In 2D, where the density of states $\rho_{2\mathrm{D}}$ is *constant*, the integral still diverges logarithmically as $|E| \to 0$, so that again one can find a solution $|E|$ for any small $|V_0|$. The binding energy now depends exponentially on the interaction and $\rho_{2\mathrm{D}}$:

$$E_{2\mathrm{D}} = -2E_R\, e^{-\frac{2\Omega}{\rho_{2\mathrm{D}}|V_0|}} \tag{2.80}$$

However, in 3D the integral is finite for vanishing $|E|$, and one needs to overcome a minimum threshold interaction in order to bind the two particles.

These results might give us a hint why there might be a paired state for two fermions immersed in a medium, even for arbitrarily weak interactions: It must be that, somehow, the free 3D density of states for the fermions is altered due to the presence of the surrounding atoms. This is exactly what happens, as will be discussed in the next section.

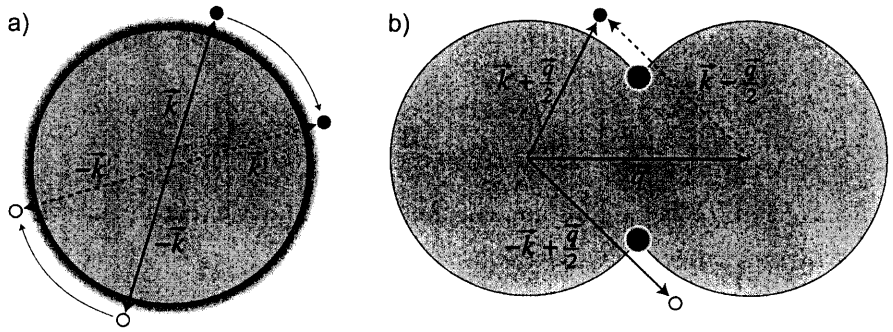

Figure 2-3: Cooper problem: Two particles scattering on top of a Fermi sea. a) Particles with equal and opposite momenta can scatter as shown. The Fermi sea (grey shaded) blocks possible final momentum states. b) Here, the total momentum of the two particles $\mathbf{q}$ is nonzero. Possible scattering states $\mathbf{k} + \mathbf{q}/2$ and $-\mathbf{k} + \mathbf{q}/2$ (or, equivalently, $\mathbf{k} - \mathbf{q}/2$, see construction) must lie outside the Fermi sea. Only in the small shaded region (a circle in 3D) can both particles be close to their respective Fermi surface. In contrast, pairs at rest in a) can take advantage of the entire Fermi surface.

Pairing of fermions - The Cooper problem

Consider now two weakly interacting spin 1/2 fermions not in vacuum, but on top of a (non-interacting) filled Fermi sea, the Cooper problem [66]. Momentum states below the Fermi surface are not available to the two scattering particles due to Pauli blocking (Fig. 2-3a). For weak interactions, the particles' momenta are essentially confined to a narrow shell above the Fermi surface. We thus realize that the problem is *effectively 2D*, and we should find a *bound state* for the two-particle system *for arbitrarily weak attractive interaction.* The effective "2D" density of states should be $\rho_{3D}(E_F)$, the density of states at the Fermi surface.

In principle, the two fermions could form a pair at any finite momentum. However, considering the discussion in the previous section, the largest binding energy can be expected for the pairs with the largest "2D" density of scattering states. For zero-momentum pairs, the entire Fermi surface is available for scattering, as we can see from Fig. 2-3a. If the pairs have finite center-of-mass momentum $\mathbf{q}$, the number of contributing states is strongly reduced, as they are confined to a circle (see Fig. 2-3b). Consequently, pairs at rest experience the strongest binding. In the following we will calculate this energy.

We can write down the Schrödinger equation for the two interacting particles as before, but now we need to search for a small binding energy $E_B = E - 2E_F < 0$ on

top of the large Fermi energy $2E_F$ of the two particles. The equation for E_B is

$$-\frac{1}{V_0} = \frac{1}{\Omega}\int_{E_F<\epsilon<E_F+E_R} d\epsilon \frac{\rho_{3D}(\epsilon)}{2(\epsilon - E_F) + |E_B|} \tag{2.81}$$

The effect of Pauli blocking of momentum states below the Fermi surface is explicitly included by only integrating over energies $\epsilon > E_F$.

In superconductors, the natural cut-off E_R is given by the Debye frequency ω_D, $E_R = \hbar\omega_D$, corresponding to the highest frequency at which ions in the crystal lattice can respond to a bypassing electron. Since we have $\hbar\omega_D \ll E_F$, we can approximate $\rho_{3D}(\epsilon) \approx \rho_{3D}(E_F)$ (a constant just like in two dimensions!) and find:

$$E_B = -2\hbar\omega_D e^{-2\Omega/\rho_{3D}(E_F)|V_0|} \tag{2.82}$$

In the case of an interacting Fermi gas, we should replace $1/V_0$ by the physically relevant scattering length $a < 0$ using the prescription in Eq. 2.63. The equation for the bound state becomes

$$-\frac{m}{4\pi\hbar^2 a} = \frac{1}{\Omega}\int_{E_F}^{E_F+E_R} d\epsilon \frac{\rho_{3D}(\epsilon)}{2(\epsilon - E_F) + |E_B|} - \frac{1}{\Omega}\int_0^{E_F+E_R} d\epsilon \frac{\rho_{3D}(\epsilon)}{2\epsilon} \tag{2.83}$$

The right hand expression is now finite as we let the cut-off $E_R \to \infty$, the result being (one assumes $|E_B| \ll E_F$)

$$-\frac{m}{4\pi\hbar^2 a} = \frac{\rho_{3D}(E_F)}{2\Omega}\left(-\log\left(\frac{|E_B|}{8E_F}\right) - 2\right) \tag{2.84}$$

Inserting $\rho_{3D}(E_F) = \frac{\Omega m k_F}{2\pi^2\hbar^2}$ with the Fermi wave vector $k_F = \sqrt{2mE_F/\hbar^2}$, one arrives at

$$E_B = -\frac{8}{e^2} E_F \, e^{-\pi/k_F|a|} \tag{2.85}$$

The binding energies Eqs. 2.82 and 2.85 can be compared with the result for the bound state of two particles in 2D, Eq. 2.80. The role of the constant density of states ρ_{2D} is here played by the 3D density of states at the Fermi surface, $\rho_{3D}(E_F)$. As this is largest for zero-momentum pairing (see Fig. 2-3), Cooper pairs at rest have the largest binding energy.

The result is remarkable: Two weakly interacting fermions on top of a Fermi sea form a bound state due to Pauli blocking. However, in this artificial problem we neglected the interactions between particles *in* the Fermi sea. As we "switch on" the interactions for all particles from top to the bottom of the Fermi sea, the preceding

discussion shows that the gas will reorder itself into a completely new, paired state. The Fermi sea is thus unstable towards pairing. The full many-body description of such a paired state, including the necessary anti-symmetrization of the full wave function, was achieved by Bardeen, Cooper and Schrieffer (BCS) in 1957 [23]. As we will see in the next section, the self-consistent inclusion of all fermion pairs leads to more available momentum space for pairing. The effective density of states is then twice as large, giving a superfluid gap Δ that is exponentially larger than $|E_B|$ from Eq. 2.85:

$$\Delta = \frac{8}{e^2} E_F \, e^{-\pi/2k_F|a|} \tag{2.86}$$

2.3 The BEC-BCS crossover

The preceding section has shown that in the many-body problem we can expect pairing for an arbitrarily weak interaction between fermions. The ground state of the gas will be a condensate of Cooper pairs as described by BCS theory. For strong interactions, a true two-body bound state between fermions exists even in vacuum. Here, we expect a Bose-Einstein condensate of these tightly bound fermion pairs or molecules to be the ground state of the system. It was realized by Leggett [149], building upon work by Eagles [85], that the crossover from the BCS- to the BEC-regime is smooth. This might surprise, as we know from before that two-body physics shows a threshold behavior at a critical interaction strength, below which there is no bound state for two particles. In the medium, however, we simply cross over from a regime of tightly bound pairs to a regime where the pairs are of much larger size than the interparticle spacing. Closely following the work of [149, 172, 74], we will describe the BEC-BCS crossover in a simple "one-channel" model, where the scattering length a is the parameter which "tunes" the interaction. For positive $a > 0$, there is a two-body bound state available at $E_B = -\hbar^2/ma^2$ (see table 2.2), while for $a < 0$, corresponding to attractive interaction, pairing is purely a many-body effect. In either case, for s-wave scattering the orbital part of the pair wavefunction $\varphi(\mathbf{r}_1, \mathbf{r}_2)$ will be symmetric under exchange of the paired particles' coordinates and will only depend on their distance $|\mathbf{r}_1 - \mathbf{r}_2|$. We will attempt to find a many-body wavefunction

$$\Psi(\mathbf{r}_1, \ldots, \mathbf{r}_N) = \mathcal{A}\varphi(|\mathbf{r}_1 - \mathbf{r}_2|)\chi_{12} \ldots \varphi(|\mathbf{r}_{N-1} - \mathbf{r}_N|)\chi_{N-1,N} \tag{2.87}$$

that describes a condensate of such fermion pairs, with the operator $\mathcal{A}$ denoting the correct antisymmetrization of all fermion coordinates, and the spin function

$\chi_{ij} = \uparrow(i)\downarrow(j)$.

In second quantization notation we write

$$|\Psi\rangle_N = \int \prod_i d^3r_i \, \varphi(\mathbf{r}_1-\mathbf{r}_2)\Psi_\uparrow^\dagger(\mathbf{r}_1)\Psi_\downarrow^\dagger(\mathbf{r}_2)\ldots\varphi(\mathbf{r}_{N-1}-\mathbf{r}_N)\Psi_\uparrow^\dagger(\mathbf{r}_{N-1})\Psi_\downarrow^\dagger(\mathbf{r}_N)\,|0\rangle \quad (2.88)$$

where the fields $\Psi_\sigma^\dagger(\mathbf{r}) = \sum_k c_{k\sigma}^\dagger e^{i\mathbf{k}\cdot\mathbf{r}}$. With the Fourier transform $\varphi(\mathbf{r}_1 - \mathbf{r}_2) = \sum_k \varphi_k e^{i\mathbf{k}\cdot\mathbf{r}_1}e^{-i\mathbf{k}\cdot\mathbf{r}_2}$ we can introduce the pair creation operator

$$b^\dagger = \sum_k \varphi_k c_{k\uparrow}^\dagger c_{-k\downarrow}^\dagger \quad (2.89)$$

and write

$$|\Psi\rangle_N = b^{\dagger N/2}\,|0\rangle \quad (2.90)$$

In this way, $|\Psi\rangle_N$ looks very suggestive, reminding of a condensate of bosonic particles. However, it is important to realize that the operators $b^\dagger$ do not obey the Bose-Einstein commutation relations and thus do not describe bosons. In fact, we can calculate

$$\left[b^\dagger, b^\dagger\right]_- = \sum_{kk'} \varphi_k\varphi_{k'} \left[c_{k\uparrow}^\dagger c_{-k\downarrow}^\dagger, c_{k'\uparrow}^\dagger c_{-k'\downarrow}^\dagger\right]_- = 0 \quad (2.91)$$

$$[b, b]_- = \sum_{kk'} \varphi_k\varphi_{k'} \left[c_{-k\downarrow}c_{k\uparrow}, c_{-k'\downarrow}c_{k'\uparrow}\right]_- = 0 \quad (2.92)$$

$$\left[b, b^\dagger\right]_- = \sum_{kk'} \varphi_k\varphi_{k'} \left[c_{-k\downarrow}c_{k\uparrow}, c_{k'\uparrow}^\dagger c_{-k'\downarrow}^\dagger\right]_- = \sum_k \varphi_k^2(1 - n_{k\uparrow} - n_{k\downarrow}) \quad (2.93)$$

The first two relations are fine, but the third one spoils Bose-Einstein statistics for the b-particles. Only in the limit where the pairs are tightly bound do the b-particles correspond to point-like bosons: Here, the pairs occupy a wide region in momentum space and the occupation n_k of any momentum state k is very small (see section 2.3.2 below). Thus, $\left[b, b^\dagger\right]_- \approx \sum_k \varphi_k^2 = 1$.

Working with the N-particle state $|\Psi\rangle_N$ is inconvenient, as one would face a complicated combinatoric problem in manipulating the sum over all the $c_k^\dagger$'s (as one chooses a certain k for the first fermion the choices for the second depend on this k, etc.). Rather, one passes over to the grand canonical formalism, not fixing the number of atoms but the chemical potential μ, and defines the many-body state:

$$\begin{aligned} \mathcal{N}\,|\Psi\rangle &= \sum_N \tfrac{1}{(N/2)!}\,|\Psi\rangle_N &&= \sum_N \frac{1}{(N/2)!} b^{\dagger N/2}\,|0\rangle = e^{b^\dagger}\,|0\rangle \\ &= \prod_k e^{\varphi_k c_{k\uparrow}^\dagger c_{-k\downarrow}^\dagger}\,|0\rangle &&= \prod_k (1 + \varphi_k c_{k\uparrow}^\dagger c_{-k\downarrow}^\dagger)\,|0\rangle \end{aligned} \quad (2.94)$$

where the last equation follows from $c_k^{\dagger 2} = 0$. If we choose the constant $\mathcal{N} = \prod_k \frac{1}{u_k} = \prod_k (1 + \varphi_k^2)^{1/2}$, then $|\Psi\rangle$ becomes a properly normalized state

$$|\Psi_{BCS}\rangle = \prod_k (u_k + v_k c_{k\uparrow}^\dagger c_{-k\downarrow}^\dagger) |0\rangle \tag{2.95}$$

with $v_k = u_k \varphi_k$ and $|u_k|^2 + |v_k|^2 = 1$. This is the BCS variational wavefunction, first introduced by BCS to describe condensation of Cooper pairs in momentum space. From the above derivation, however, it is clear that its applicability encompasses the entire regime of pairing, all the way towards the limit of small molecules.

2.3.1 Gap and number equation

The variational parameters u_k and v_k are derived in the standard way by minimizing the free energy $E - \mu N = \left\langle \hat{H} - \mu \hat{N} \right\rangle$. The many-body hamiltonian for the system is

$$\hat{H} = \sum_{k,\sigma} \epsilon_k c_{k\sigma}^\dagger c_{k\sigma} + \frac{V_0}{\Omega} \sum_{k,k',q} c_{k+\frac{q}{2}\uparrow}^\dagger c_{-k+\frac{q}{2}\downarrow}^\dagger c_{k'+\frac{q}{2}\downarrow} c_{k'-\frac{q}{2}\uparrow} \tag{2.96}$$

The approach taken by BCS consists in finding the wave function $|\Psi\rangle$ that describes a condensate of pairs at rest. As we have seen in section 2.2.3, such Cooper pairs have the largest binding energy. Neglecting interactions between pairs at finite momentum, we only keep the term for $\mathbf{q} = 0$. The free energy becomes

$$\begin{aligned} \left\langle \hat{H} - \mu \hat{N} \right\rangle &= \sum_k 2\xi_k v_k^2 + \frac{V_0}{\Omega} \sum_{k,k'} u_k v_k u_{k'} v_{k'} \\ \text{with } \xi_k &= \epsilon_k - \mu \end{aligned} \tag{2.97}$$

Minimizing $E - \mu N$ leads to

$$\begin{aligned} v_k^2 &= \frac{1}{2}\left(1 - \frac{\xi_k}{E_k}\right) \\ u_k^2 &= \frac{1}{2}\left(1 + \frac{\xi_k}{E_k}\right) \\ \text{with } E_k &= \sqrt{\xi_k^2 + \Delta^2} \end{aligned} \tag{2.98}$$

combined with the *gap equation* $\Delta \equiv -\frac{V_0}{\Omega} \sum_k \langle c_{k\uparrow} c_{-k\downarrow} \rangle = -\frac{V_0}{\Omega} \sum_k u_k v_k = -\frac{V_0}{\Omega} \sum_k \frac{\Delta}{2E_k}$ or

$$-\frac{1}{V_0} = \int \frac{d^3k}{(2\pi)^3} \frac{1}{2E_k} \tag{2.99}$$

(compare with the analogous equation in free space Eq. 2.79 and for the simplified Cooper problem Eq. 2.81) and the *number equation* for the total particle density $n = N/\Omega$

$$n = 2\int \frac{d^3k}{(2\pi)^3}\, v_k^2 \tag{2.100}$$

which have to be solved simultaneously to yield the two unknowns μ and Δ. We will once more replace V_0 by the scattering length a using prescription Eq. 2.63, so that the gap equation becomes (compare Eq. 2.83)

$$-\frac{m}{4\pi\hbar^2 a} = \int \frac{d^3k}{(2\pi)^3}\left(\frac{1}{2E_k} - \frac{1}{2\epsilon_k}\right) \tag{2.101}$$

where the integral is now well-defined. The equations can be rewritten in dimensionless form with the Fermi energy $E_F = \hbar^2 k_F^2/2m$ and wave vector $k_F = (3\pi^2 n)^{1/3}$

$$-\frac{1}{k_F a} = \frac{2}{\pi}\sqrt{\frac{\Delta}{E_F}}\, I_1\left(\frac{\mu}{\Delta}\right) \tag{2.102}$$

$$1 = \frac{3}{2}\left(\frac{\Delta}{E_F}\right)^{3/2} I_2\left(\frac{\mu}{\Delta}\right) \tag{2.103}$$

$$\text{with } I_1(z) = \int_0^\infty dx\, x^2\left(\frac{1}{\sqrt{(x^2-z)^2+1}} - \frac{1}{x^2}\right) \tag{2.104}$$

$$\text{and } I_2(z) = \int_0^\infty dx\, x^2\left(1 - \frac{x^2-z}{\sqrt{(x^2-z)^2+1}}\right) \tag{2.105}$$

This gives

$$-\frac{1}{k_F a} = \frac{2}{\pi}\left(\frac{2}{3I_2\left(\mu/\Delta\right)}\right)^{1/3} I_1\left(\frac{\mu}{\Delta}\right) \tag{2.106}$$

$$\frac{\Delta}{E_F} = \left(\frac{2}{3I_2\left(\frac{\mu}{\Delta}\right)}\right)^{2/3} \tag{2.107}$$

The first equation can be inverted to obtain μ/Δ as a function of the *interaction parameter* $1/k_F a$, which can then be inserted in the second equation to yield the gap Δ. The result for μ and Δ as a function of $1/k_F a$ is shown in Fig. 2-4. Marini, Pistolesi and Strinati have shown that one can even obtain analytic expressions for the above in terms of complete elliptic integrals [163].

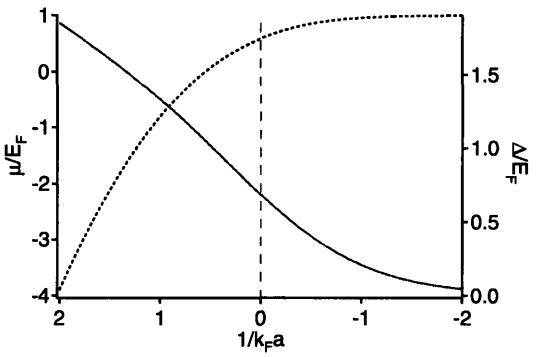

Figure 2-4: Chemical potential (dotted line) and gap (straight line, red) in the BEC-BCS crossover as a function of the interaction parameter $1/k_F a$. The BCS-limit of negative $1/k_F a$ is to the right on the graph. The resonance where $1/k_F a = 0$ is shown by the dashed line.

BCS limit

In the BCS-limit of weak attractive interaction, $k_F a \to 0_-$, we have[7]

$$\mu \approx E_F \tag{2.108}$$

$$\Delta \approx \frac{8}{e^2} e^{-\pi/2k_F|a|} \tag{2.109}$$

The first equation tells us that adding a spin up and spin down particle to the system costs a Fermi energy per particle [8]: In the weakly interacting BCS limit Pauli blocking still dominates over interactions, and hence the particles can only be added at the Fermi surface. The second equation is the classic result of BCS theory for the superfluid gap[9]. Compared to the bound state energy for a single Cooper pair on top of a non-interacting Fermi sea, Eq. 2.85, the gap is exponentially larger (a factor $e^{\pi/2k_F|a|}$), as the entire collection of particles now takes part in the pairing[10].

[7]This follows by substituting $\xi = x^2 - z$ in the integrals and taking the limit $z \to \infty$. One has $I_1(z) \approx \sqrt{z}\,(\log(8z) - 2)$ and $I_2(z) = \frac{2}{3} z^{3/2}$.

[8]BCS theory implicitly assumes an equal number of spin up and spin down atoms. The chemical potential is thus the energy cost for adding a spin up atom *if at the same time* a spin down particle is added.

[9]The present mean-field treatment does not include density fluctuations, which modify the prefactor in the expression for the gap Δ [98].

[10]In the self-consistent BCS solution, not only the momentum states above the Fermi surface contribute to pairing, but also those *below* it, in a symmetric shell around the Fermi momentum. In the Cooper problem the states below the Fermi surface were excluded, reducing the effective density of states by a factor of two. The pairing energy depends exponentially on the density of states, which explains the difference between the binding energy in the Cooper problem and the gap energy of BCS theory.

However, the gap is still exponentially small compared to the Fermi energy: Cooper pairing is fragile.

To give a sense of scale, Fermi energies in our dilute lithium gas are on the order of a μK, corresponding to $1/k_F \sim 4\,000\,a_0$. A "typical" scattering length for lithium, in the absence of scattering resonances, will be about $50 - 100\ a_0$ (on the order of the van der Waals-range). The gap is thus vanishingly small, $\Delta/k_B \approx 10^{-30} \ldots 10^{-60}\,\mathrm{K}$. With that number in mind, it seems simply hopeless to achieve superfluidity in Fermi gases. However, Feshbach resonances allow tuning of the scattering length, bringing the gas into the strongly interacting regime where $k_F\,|a| > 1$ (see chapter 3). In this case, there is a good chance to reach superfluidity: The above mean-field theory predicts $\Delta = 0.22 E_F$ or $\Delta/k_B \approx 200\,\mathrm{nK}$ for $k_F\,|a| = 1$. Such temperatures are now routinely achieved in experiments on ultracold gases.

BEC limit

In the BEC limit of tightly bound pairs, for $k_F a \to 0_+$, one finds[11]

$$\mu = -\frac{\hbar^2}{2ma^2} + \frac{\pi\hbar^2 an}{m} \tag{2.110}$$

$$\Delta \approx \sqrt{\frac{16}{3\pi}} \frac{E_F}{\sqrt{k_F a}} \tag{2.111}$$

The first term in the expression for the chemical potential is the binding energy per fermion in a tightly bound molecule (see table 2.2). Naturally, this energy is only available if we add *two* fermions of opposite spin at the same time to the system (we have assumed an *equal* mixture of spin-up and spin-down fermions when writing down the wave-function in Eq. 2.87). Adding only one spin-up fermion to the system does not give or cost any energy to first approximation: The tightly bound fermions occupy a large region in momentum space, hence the Fermi gas is not degenerate and Pauli blocking not relevant anymore[12]. The second term is a mean-field contribution describing the repulsive interaction between molecules in the gas. Indeed, a condensate of molecules of mass $m_M = 2m$, density $n_M = n/2$ and a molecule-molecule scattering length a_M will have a chemical potential $\mu_M = \frac{4\pi\hbar^2 a_M n_M}{m_M}$ (see section 2.2.2). Since μ_M is twice the chemical potential for each fermion, we obtain from the above expression

[11] This result follows from the expansion of the integrals for $z < 0$ and $|z| \to \infty$. One finds $I_1(z) = -\frac{\pi}{2}\sqrt{|z|} - \frac{\pi}{32}\frac{1}{|z|^{3/2}}$ and $I_2(z) = \frac{\pi}{8}\frac{1}{\sqrt{|z|}}$.

[12] To the next order of approximation, the single fermion feels a repulsive mean-field interaction from the gas of molecules, so it costs an energy to add this particle. This is discussed in detail in chapter 7.

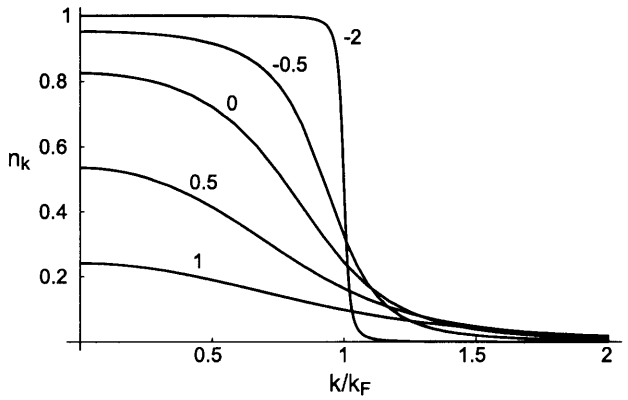

Figure 2-5: Occupation n_k of momentum states k in the BEC-BCS crossover. The numbers give the interaction parameter $1/k_F a$.

the molecule-molecule scattering length $a_M = 2a$. However, this result is not exact. Petrov, Shlyapnikov and Salomon [193] have performed an exact calculation for the interaction between four fermions and shown that $a_M = 0.6a$. The present mean-field approach neglects correlations between different pairs, or between one fermion and a pair. If those are included, the correct few-body physics is recovered [195, 123].

2.3.2 Evolution from BCS to BEC

Our variational approach smoothly interpolates between the two known regimes of a BCS-type superfluid and a BEC of molecules. The transition, which occurs approximately between $1/k_F a = -1$ and $+1$, appears fully continuous. The occupation of momentum states $n_k = v_k^2$ evolves smoothly from the step-function $\Theta(k_F - k)$ of a degenerate Fermi gas, broadened over a width $\Delta \ll E_F$ due to pairing, to n times the square of the molecular wave-function $\varphi_k \propto \frac{1}{1+k^2a^2}$ (see Fig. 2-5). It is also interesting to follow the evolution of the "Cooper pair" wavefunction[13] in k-space, where it is given by $\langle \Psi_{BCS} | \, c^\dagger_{k\uparrow} c^\dagger_{-k\downarrow} \, | \Psi_{BCS} \rangle = u_k v_k$, and in real space, where it is

$$\phi(\mathbf{r}_1 - \mathbf{r}_2) = \langle \Psi_{BCS} | \, \Psi^\dagger_\uparrow(\mathbf{r}_1) \Psi^\dagger_\downarrow(\mathbf{r}_2) \, | \Psi_{BCS} \rangle = \int \frac{d^3k}{(2\pi)^3} u_k v_k e^{i\mathbf{k}\cdot(\mathbf{r}_1 - \mathbf{r}_2)} \quad (2.112)$$

$$= \frac{1}{2} \int \frac{d^3k}{(2\pi)^3} \frac{\Delta}{\sqrt{\xi_k^2 + \Delta^2}} e^{i\mathbf{k}\cdot(\mathbf{r}_1 - \mathbf{r}_2)} \quad (2.113)$$

[13]Note that this definition is not equal to the Fourier transform of the pair wavefunction $\varphi(\mathbf{r})$ introduced in Eq. 2.87, which would be v_k/u_k. The definition given here is the two-point correlation function. Both definitions for the Cooper pair wavefunction show a sharp feature, either a peak or an edge at the Fermi surface, of width $\sim \delta k$, thus giving similar behavior for the real space wavefunction.

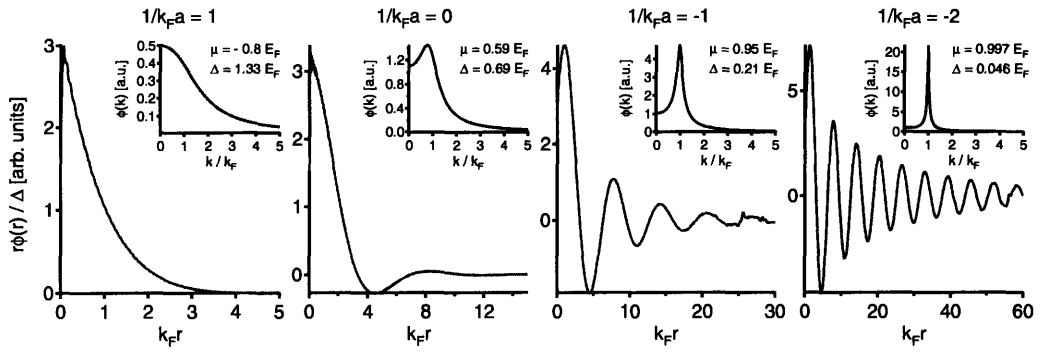

Figure 2-6: Evolution of the spatial pair wavefunction $\phi(r)$ in the BEC-BCS crossover. The inset shows the Fourier transform $\phi(k)$, showing clearly that in the BCS-limit, momentum states around the Fermi surface make the dominant contribution to the wavefunction. In the crossover, the entire Fermi sphere takes part in the pairing. In the BEC-limit, $\phi(k)$ broadens as the pairs become more and more tightly bound. $\phi(r)$ was obtained via numerical integration of $\int_{-\mu}^{\infty} d\xi \frac{\sin(r\sqrt{\xi+\mu})}{\sqrt{\xi^2+\Delta^2}}$ (here, $\hbar = 1 = m$), an expression that follows from Eq. 2.113.

In the **BCS limit**, the fermions taking the most advantage from pairing reside at the Fermi surface $k = k_F$, in a region of width $\delta k \sim \frac{\partial k}{\partial \epsilon}\delta\epsilon \approx \frac{\Delta}{\hbar v_F}$, where v_F is the velocity of fermions at the Fermi surface. We thus expect the spatial wavefunction of Cooper pairs to have a strong modulation at the inverse wave vector $1/k_F$, and an overall extent of the inverse width of the pairing region, $\sim 1/\delta k \sim \frac{\hbar v_F}{\Delta} \gg 1/k_F$. This is indeed the result of Eq. 2.113, which gives (setting $r = |\mathbf{r}_1 - \mathbf{r}_2|$) [23]

$$\phi(r) = \frac{k_F}{\pi^2 r}\frac{\Delta}{\hbar v_F}\sin(k_F r)\, K_0\left(\frac{r}{\pi\xi_{BCS}}\right) \overset{r\to\infty}{\sim} \sin(k_F r)\; e^{-r/(\pi\xi_{BCS})} \tag{2.114}$$

where $K_0(kr)$ is the modified Bessel function that falls off as e^{-kr} at infinity. The envelope function is of the same type as what we have found for a two-body bound state (see table 2.1). The characteristic size of the Cooper pair, or the *two-particle correlation length* ξ_0, can be defined as $\xi_0 = \sqrt{\frac{\langle\phi(\mathbf{r})|r^2|\phi(\mathbf{r})\rangle}{\langle\phi(\mathbf{r})|\phi(\mathbf{r})\rangle}}$, and this gives indeed $\xi_0 \sim 1/\delta k$,

$$\xi_0 \approx \xi_{BCS} \equiv \frac{\hbar v_F}{\pi\Delta} \gg 1/k_F \quad \text{in the BCS-limit} \tag{2.115}$$

In the **BEC limit**, $u_k v_k \propto \frac{1}{1+(ka)^2}$, and so

$$\phi(\mathbf{r}_1 - \mathbf{r}_2) \sim \frac{e^{-|\mathbf{r}_1-\mathbf{r}_2|/a}}{|\mathbf{r}_1 - \mathbf{r}_2|} \tag{2.116}$$

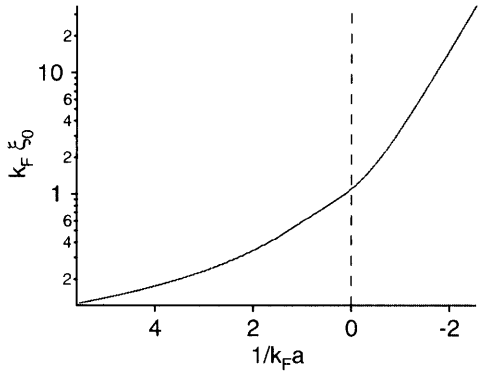

Figure 2-7: From tightly bound molecules to long-range Cooper pairs. Evolution of the pair size $\xi_0 = \sqrt{\frac{\langle\phi(\mathbf{r})|r^2|\phi(\mathbf{r})\rangle}{\langle\phi(\mathbf{r})|\phi(\mathbf{r})\rangle}}$ as a function of the interaction parameter $1/k_F a$. On resonance (dashed line), the pair size is on the order of the inverse wave vector, $\xi_0(0) \sim \frac{1}{k_F}$, about a third of the interparticle spacing.

which is simply the wavefunction of a molecule of size $\sim a$ (see table 2.1). The two-particle correlation length[14] is thus $\xi_0 \sim a$. Fig. 2-6 summarizes the evolution of the pair wavefunction, and Fig. 2-7 shows the pair size given by [23, 197] $\xi_0^2 = \frac{\langle\phi(\mathbf{r})|r^2|\phi(\mathbf{r})\rangle}{\langle\phi(\mathbf{r})|\phi(\mathbf{r})\rangle}$ as a function of the interaction parameter $1/k_F a$.

2.3.3 Single-particle and collective excitations — Landau criterion

The BCS-state $|\Psi\rangle$ describes a collection of pairs $b_k^\dagger |0\rangle = u_k |0\rangle + v_k c_{k\uparrow}^\dagger c_{-k\downarrow}^\dagger |0\rangle$. A *single* fermion that we add in state $\mathbf{k}\uparrow$, say, cannot find a pairing partner and requires a kinetic energy ξ_k. The new state does not profit from pairing in $(\mathbf{k}\uparrow, -\mathbf{k}\downarrow)$, as $-\mathbf{k}\downarrow$ is empty, and we loose the pairing energy $2\xi_k v_k^2 - 2\frac{V_0}{\Omega} u_k v_k \sum_{k'} u_{k'} v_{k'} = \xi_k(1 - \frac{\xi_k}{E_k}) - \frac{\Delta^2}{E_k} = \xi_k - E_k$ (see Eq. 2.98). The total cost for adding one fermion is thus simply $\xi_k - (\xi_k - E_k) = E_k$. In the same way, one calculates the cost for removing a fermion from the BCS-state, which is again E_k.

Fig. 2-8 shows the single-particle excitation energy E_k for different interaction strengths in the BEC-BCS crossover. For $\mu > 0$, the minimum energy required to excite a particle out of the condensate occurs for $\xi_k = \mu$ and is Δ, which gives Δ

[14]This length scale should be distinguished from the *coherence length* ξ_{phase} that is associated with spatial fluctuations of the order parameter. The two length scales coincide in the BCS-limit, but differ in the BEC-limit, where ξ_{phase} is given by the healing length $\propto \frac{1}{\sqrt{na}}$. See [197] for a detailed discussion.

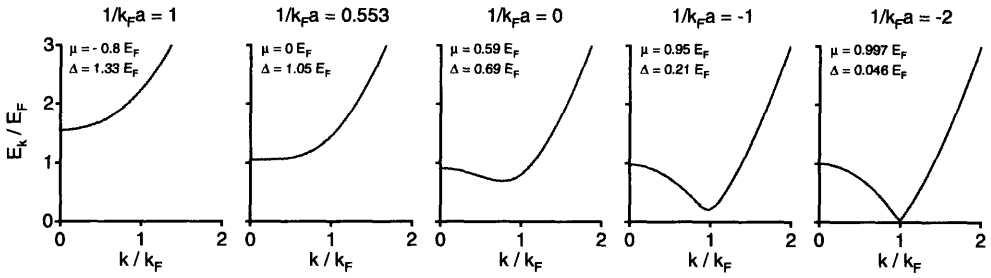

Figure 2-8: Evolution of the single-particle excitation spectrum in the BEC-BCS crossover. On the BEC-side, for $\mu < 0$, the minimum required energy to add a particle is $\sqrt{|\mu|^2 + \Delta^2}$ and occurs at $k = 0$. This qualitatively changes at $1/k_F a = 0.553$ where $\mu = 0$. For $\mu > 0$, the minimum energy is Δ and occurs at $k = \sqrt{2m\mu/\hbar^2}$.

the name of the superfluid gap. Possibly the most visual demonstration of this gap, which prevents single fermions to enter the superfluid, is the phenomenon of phase separation in imbalanced Fermi mixtures (see chapter 7). However, for $\mu < 0$ the minimum energy becomes $\sqrt{|\mu|^2 + \Delta^2}$ and occurs for $k = 0$. Deep in the BEC-regime, this corresponds to $\hbar^2/ma^2$, which is simply the energy needed to break a molecule. If we want to make a distinction between the BEC- and the BCS-limit, that seem to be so smoothly connected, the natural point would be the interaction for which $\mu = 0$, as here the character of single-particle excitations changes from having $k > 0$ to having $k = 0$. In the variational solution, this occurs for $1/k_F a = 0.553$.

We may now ask for the critical velocity of the superfluid in the BEC-BCS crossover. Given the single-particle excitation spectrum above, Landau's criterion for the critical velocity would predict

$$v_{c,\mathrm{BCS}} = \min_k \frac{E_k}{\hbar k} = \sqrt{\left(\sqrt{\mu^2 + \Delta^2} - \mu\right)/m} \quad \overset{\frac{\Delta}{\mu} \to 0_+}{\longrightarrow} \quad \frac{\Delta}{\hbar k_F} \tag{2.117}$$

An object that is dragged through the superfluid at this velocity will break a fermion pair. In contrast, in the BEC-limit of a condensate of tightly bound molecules we would expect density fluctuations, sound waves, to provide the mode of smallest critical velocity, at the speed of sound $c_s = \sqrt{\mu_M/m_M} = \sqrt{\pi\hbar^2 an/m^2}$. This Bogoliubov sound mode of the BEC-limit finds its analog in the BCS-regime, where it is called the Bogoliubov-Anderson mode, propagating at the speed of sound $v_F/\sqrt{3}$, with $v_F = \hbar k_F/m$ the Fermi velocity[15]. The connection is smooth, as expected and

[15]This speed of sound can be calculated using the hydrodynamic equation $c = \sqrt{\frac{\partial P}{\partial \rho}}$, $\rho = mn$

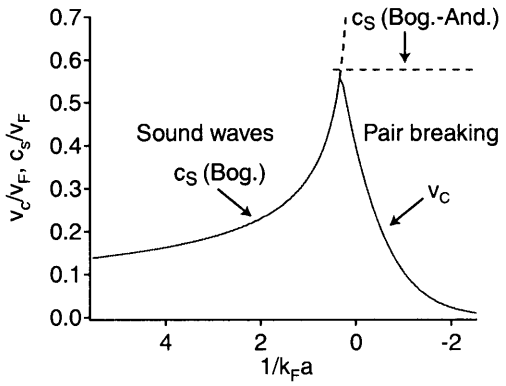

Figure 2-9: Critical velocity v_c in the BEC-BCS crossover. The relevant excitations in the BEC-regime correspond to Bogoliubov (Bog.) sound waves with speed of sound $c_s = \sqrt{\frac{\mu}{m}} = \frac{v_F}{\sqrt{3\pi}}\sqrt{k_F a}$. This sound mode eventually becomes the Bogoliubov-Anderson (Bog.-And.) mode in the BCS-regime, with $c_s = \frac{v_F}{\sqrt{3}}$. The evolution is smooth [74, 176, 27, 64], but only the limiting cases are shown here. In the BCS-regime the excitations with the lowest critical velocity are single-particle excitations that break a Cooper pair. Here, $v_c \approx \frac{\Delta}{\hbar k_F}$. After [64].

found by [74, 176, 27, 64][16].

The critical velocity for the superfluid is given by the smaller of the two velocities, the speed of sound c_s and the critical velocity for pair breaking $v_{c,\mathrm{BCS}}$. For the BEC-side, it is shown in [64] that for small momenta $k \ll 1/a$ which do not resolve the composite nature of the molecules, the expression for the Bogoliubov-dispersion $E_{k,BEC} = \sqrt{(\frac{\hbar^2 k^2}{2m_M} + \mu_M)^2 - \mu_M^2}$ remains valid even well into the crossover region. This allows us to determine the speed of sound in an approximate way in Fig. 2-9. Notable in this figure is the sharp peak in the critical velocity around resonance. It is here that the superfluid is the most stable [219, 64]. Importantly, we observe that the nature of the dominant low-lying excitations changes from rather benign (low k's) sound waves in the BEC-limit to the more violent pair breaking in the BCS-limit (large k). An experimental consequence is that the superfluid is very fragile in the BCS-regime in response to stirring (see chapter 6).

---

and the pressure of a normal Fermi gas $P = \frac{2}{3}\frac{E}{V} = \frac{2}{5}E_F n = \frac{2}{5}\frac{\hbar^2}{2m}(3\pi^2)^{2/3}n^{5/3}$. Thus, the sound mode is already present in the normal Fermi gas, the main effect of pairing being to push low-lying single-particle excitations up in energy, which would otherwise provide damping. While this damping would also vanish in a non-interacting gas at zero temperature, this sound mode cannot propagate, as collisions are absent and the gas can no longer maintain local equilibrium.

[16]Note that in superconductors, density fluctuations can only occur at the plasma frequency, as they are charged superfluids.

2.3.4 Finite temperatures

To study the system at finite temperature, we have to include fluctuations around the BCS variational ground state. This is done most elegantly using the procedure by Bogoliubov [33] and Valatin [249]. The goal is to introduce new quasi-particles that approximately diagonalize the original many-body hamiltonian, just like what was done for the interacting Bose gas in section 2.2.2. For this, new fermionic operators are introduced:

$$\gamma_{k\uparrow} = u_k c_{k\uparrow} - v_k c^\dagger_{-k\downarrow} \tag{2.118}$$

$$\gamma^\dagger_{-k\downarrow} = u_k c^\dagger_{-k\downarrow} + v_k c_{k\uparrow} \tag{2.119}$$

with the requirement that the BCS state presents the new "vacuum" for these quasi-particles: $\gamma_{k\uparrow}|\Psi\rangle = 0 = \gamma_{-k\downarrow}|\Psi\rangle$. If u_k and v_k are chosen as before, the hamiltonian becomes

$$\hat{H} - \mu\hat{N} = \sum_k (\xi_k - E_k) + \sum_k E_k(\gamma^\dagger_{k\uparrow}\gamma_{k\uparrow} + \gamma^\dagger_{k\downarrow}\gamma_{k\downarrow}) \tag{2.120}$$

The first term is the free energy $E - \mu N$ in the BCS state. The second gives the energy of a collection of quasi-particles. $\gamma^\dagger_{k\uparrow}$ simply creates the state we considered above, where a fermion is added in state $k\uparrow$, the paired state $-k\downarrow$ being empty. As we have seen, the energy for this excitation is E_k, as is correctly accounted for in the diagonalized hamiltonian.

Gap equation at finite temperature

The gap equation is modified at finite temperature. With the definitions above one finds

$$\langle c_{k\uparrow}c_{-k\downarrow}\rangle = u_k v_k \left(1 - \left\langle \gamma^\dagger_{k\uparrow}\gamma_{k\uparrow}\right\rangle - \left\langle \gamma^\dagger_{k\downarrow}\gamma_{k\downarrow}\right\rangle\right) \tag{2.121}$$

As the quasi-particles are fermions, they follow the Fermi-Dirac distribution $\left\langle \gamma^\dagger_{k\uparrow}\gamma_{k\uparrow}\right\rangle = \frac{1}{1+e^{\beta E_k}}$. The equation for the gap $\Delta = -\frac{V_0}{\Omega}\sum_k \langle c_{k\uparrow}c_{-k\downarrow}\rangle$ thus becomes (replacing V_0 as above by the scattering length a)

$$-\frac{m}{4\pi\hbar^2 a} = \int \frac{d^3k}{(2\pi)^3}\left(\frac{1}{2E_k}\tanh\left(\frac{\beta E_k}{2}\right) - \frac{1}{2\epsilon_k}\right) \tag{2.122}$$

Temperature of pair creation

We are interested in determining the temperature $T^* = 1/\beta^*$ at which the gap vanishes. In the BCS-limit, this procedure gives the critical temperature for the normal-to-superfluid transition. Setting $\Delta = 0$ in the gap equation, one needs to solve [172, 83, 74]

$$-\frac{m}{4\pi\hbar^2 a} = \int \frac{d^3k}{(2\pi)^3}\left(\frac{1}{2\xi_k}\tanh\left(\frac{\beta^*\xi_k}{2}\right) - \frac{1}{2\epsilon_k}\right) \tag{2.123}$$

This has to be solved simultaneously with the constraint on the total number of atoms. Above the temperature T^*, we have a normal Fermi gas with a Fermi-Dirac distribution, so the number equation becomes

$$n = 2\int \frac{d^3k}{(2\pi)^3}\frac{1}{1+e^{\beta*\xi_k}} \tag{2.124}$$

In the BCS-limit, we can expect $\mu \gg k_B T^*$ and thus find $\mu \approx E_F$. Inserted in the gap equation, this gives the expected critical temperature for BCS superfluidity

$$T^*_{BCS} = T_{C,BCS} = \frac{e^\gamma}{\pi}\frac{8}{e^2}e^{-\pi/2k_F|a|} = \frac{e^\gamma}{\pi}\Delta_0 \tag{2.125}$$

with Euler's constant γ, and $e^\gamma \approx 1.78$. Here, we distinguish Δ_0, the value of the superfluid gap at zero temperature, from the temperature-dependent gap $\Delta(T)$. One can show that

$$\Delta(T) \approx \begin{cases} \Delta_0 - \sqrt{2\pi\Delta_0 k_B T}\, e^{-\Delta_0/k_B T}, & T \ll T_C \\ \sqrt{\frac{8\pi^2}{7\zeta(3)}}\, k_B T_C \sqrt{1-\frac{T}{T_C}}, & T_C - T \ll T_C \end{cases} \tag{2.126}$$

In the BEC-limit, the chemical potential $\mu = -E_b/2 = -\hbar^2/2ma^2$ is again given by half the molecular binding energy as before, and the temperature T^* is found to be

$$T^*_{BEC} \approx \frac{|E_b|}{2\left(\ln\frac{|E_b|}{E_F}\right)^{3/2}} \tag{2.127}$$

This is *not* the critical temperature for the superfluid transition but simply the temperature around which pairs start to form. The logarithmic factor has its origin in the entropy of the molecule-free fermion-mixture, which favors unbound fermions and lowers $k_B T^*$ below the binding energy E_b. There is no phase transition at T^*.

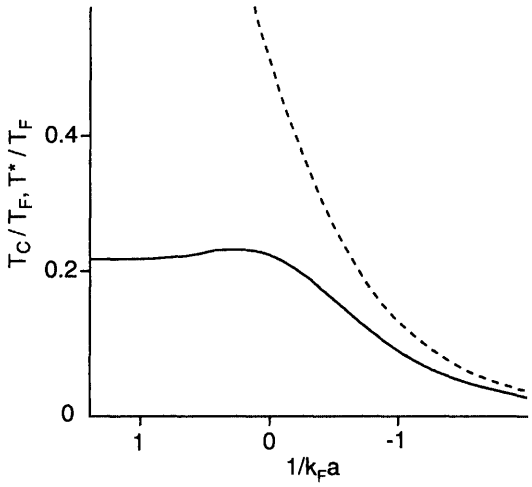

Figure 2-10: Superfluid transition temperature T_C and pair creation temperature T^* (dashed line) in the BEC-BCS crossover. In the BEC regime, T_C corresponds to the BEC transition temperature for a gas of molecules. In the BCS regime, the critical temperature depends exponentially on the interaction strength, drastically reducing T_C. Figure extracted from [74].

Critical temperature

Determining T_C, the temperature at which long-range order is established, is more involved. In the deep BEC-regime, the critical temperature is simply given by the non-interacting value for the BEC transition of a gas of molecules at density $n_M = n/2$ and mass $m_M = 2m$,

$$T_{C,BEC} = \frac{2\pi\hbar^2}{m_M}\left(\frac{n_M}{\zeta(\frac{3}{2})}\right)^{2/3} = \frac{\pi\hbar^2}{m}\left(\frac{n}{2\zeta(\frac{3}{2})}\right)^{2/3} = 0.21E_F \tag{2.128}$$

This result holds for weakly interacting gases, with only a small correction due to interactions. On the BCS-side, the critical temperature should smoothly connect to the BCS result given above. Fig. 2-10 shows the behavior of T_C as a function of the interaction strength. Whether there is a local maximum of T_C somewhere in the crossover region is not fully settled [115].

"Preformed" pairs

In the region between T_C and T^*, we will already find bound pairs in the gas, which are not yet condensed. In the BCS-limit, where $T_* \to T_C$, condensation occurs at the same time as pairing, which we see now is not true for stronger interactions.

On the deep molecular side, it is of course not surprising to find thermal molecules in the gas above T_C. However, the qualitative picture of thermal pairs still holds in the entire crossover region from $-1 < 1/k_F a < 1$. These uncondensed pairs are sometimes called "preformed" (pairing occurs before condensation) and are detected as a "pseudo-gap" in RF spectroscopy experiments [59].

2.3.5 Definition of the condensate wavefunction

As Fritz London proposed in 1938, superfluidity should be a quantum mechanical phenomenon occurring over macroscopic distances. A "wavefunction" $\psi(\mathbf{r})$ should be ascribed to the superfluid, whose "stiffness" against perturbations would result in the peculiar properties of the superfluid.

In the case of weakly interacting Bose-Einstein condensates, we can readily identify $\psi(\mathbf{r})$ with the condensate wavefunction shared by all the bosons in the ground state of the system. Its squared magnitude $|\psi(\mathbf{r})|^2 \equiv n(\mathbf{r})$ is equal to the density of the condensed gas. Thus, taking an absorption image of a weakly interacting Bose-Einstein condensate directly reveals the magnitude of the wavefunction. This has led to the spectacular demonstration of coherence between two Bose condensates [13] and the observation of vortex lattices [160, 2, 120, 87] by straight-forward absorption imaging (to name only a few examples).

For *fermionic* superfluids, it is the center-of-mass wavefunction of the condensed fermion *pairs* which takes on the role of $\psi(\mathbf{r})$. We can define it as the thermal average of the *pair* creation operator $\Psi_\uparrow^\dagger(\mathbf{r})\,\Psi_\downarrow^\dagger(\mathbf{r})$:

$$\psi(\mathbf{r}) = \mathcal{N}\left\langle \Psi_\uparrow^\dagger(\mathbf{r})\,\Psi_\downarrow^\dagger(\mathbf{r})\right\rangle \tag{2.129}$$

where $\mathcal{N}$ is a constant we can conveniently choose.

One realizes an immediate difficulty in measuring this wavefunction: If the pairs are *not* tightly bound, like on resonance or in the BCS-regime, an image of the atomic density will not reveal the *center-of-mass* wavefunction of the pairs. One would rather observe the distribution of, say, the spin-up atoms $n_\uparrow(\mathbf{r}) = \left\langle \Psi_\uparrow^\dagger(\mathbf{r})\Psi_\uparrow(\mathbf{r})\right\rangle$, which turns out to practically not change as one enters the superfluid regime[17]. This presents a more profound difficulty than the mere absence of a bimodal density profile of the gas in the presence of a thermal cloud. It shows that in the BCS-regime, even at zero temperature, we cannot easily detect interference, vortices or other effects related to

[17] We have experimentally observed slight changes in the density profile on resonance, see chapter 5. Note also that for unequal mixtures, there is a dramatic signature, see chapter 7.

the condensate's coherence.

As one can readily check with the tools from previous sections, in a uniform BCS state one has $\psi = \frac{\mathcal{N}}{\Omega} \sum_k \left\langle c^\dagger_{k\uparrow} c^\dagger_{-k\downarrow} \right\rangle = \frac{\mathcal{N}}{\Omega} \sum_k \frac{\Delta}{2E_k} = \frac{\mathcal{N}}{V}\Delta$, where we have used the BCS gap equation. We see that ψ is simply proportional to the superfluid gap Δ, which is zero in the normal and finite in the superfluid state. As such, $\psi(\mathbf{r})$ naturally lends itself as the *order parameter* for the superfluid phase transition, an angle of thought that was pioneered by Landau.

BEC-limit: Gross-Pitaevskii equation

How should we choose the prefactor $\mathcal{N}$? In the **BEC-limit** of tightly bound molecules, $\psi(\mathbf{r})$ should represent the wavefunction of the molecular condensate. As such, its squared magnitude should give the density of condensed molecules n_M, equal to half the total density n at zero temperature: $|\psi|^2 = n/2$. As $\left\langle \Psi^\dagger_\uparrow \Psi^\dagger_\downarrow \right\rangle$ already has units of density, the prefactor $\mathcal{N}$ must be the square root of a volume. We found in section 2.3.1 that in the BEC-limit and at zero temperature, $\Delta = \sqrt{\frac{16}{3\pi}} \frac{E_F}{\sqrt{k_F a}}$. Using $V = 4\pi\hbar^2 a/m$ it can be seen that one should choose $\mathcal{N} = \sqrt{2\pi}\, a^{3/2}$. The resulting condensate wavefunction $\psi(\mathbf{r})$ solves the Gross-Pitaevskii-equation we know from atomic Bose-Einstein condensates:

$$\left(-\frac{\hbar^2 \nabla^2}{2m_M} + V_{\text{ext}}(\mathbf{r}) + g\,|\psi(\mathbf{r})|^2 \right) \psi(\mathbf{r}) = \mu_M \psi(\mathbf{r}) \tag{2.130}$$

with $g = 4\pi\hbar^2 a_M / m_M$, the molecular scattering length a_M, the mass $m_M = 2m$ and the molecular chemical potential μ_M.

In complete analogy with atomic BEC, we directly know that (in the Thomas-Fermi regime, neglecting the kinetic energy) the condensate density will be given by

$$n_M(\mathbf{r}) = |\psi(\mathbf{r})|^2 = \max\left(\frac{\mu_M - V_{\text{ext}}(\mathbf{r})}{g}, 0 \right) \tag{2.131}$$

which results in the famous inverted parabola in the case of harmonic trapping. Note that for experiments in optical traps, the polarizability of molecules is twice that of single atoms, so that V_{ext} for molecules is twice as large as the potential experienced by atoms.

We thus expect a direct signature of condensation in the density profile of the molecular gas. This was therefore our starting point for studying fermionic superfluids, as will be described in chapter 5.

BCS-limit: Ginzburg-Landau equation

In the limit of tightly bound molecules, the fermionic degrees of freedom are not relevant for the description of the condensate. The momenta of the fermions forming the molecules are spread out over the large range of $1/a$, the inverse size of the molecule, which is in this limit much larger than the Fermi momentum k_F. The fermions themselves thus form a non-degenerate gas. In the **BCS-limit**, the fermionic degrees of freedom are dominant, with each spin species forming its respective Fermi sea. We can then no longer expect that there exists a single equation for the center-of-mass wavefunction of pairs $\psi(\mathbf{r})$, which can correctly describe the physics of the fermion pair condensate. The Cooper pairs are spread out in space and overlap strongly, so that a priori, *non-local* equations should replace the *local* Gross-Pitaevskii equation we had found for the condensate of molecules. Indeed, the Gorkov formulation based on Green's functions allows to write BCS theory in the form of two coupled equations for the normal $\left\langle \Psi_\sigma^\dagger(\mathbf{r},t)\,\Psi_{\sigma'}(\mathbf{r}',t')\right\rangle$ and anomalous $\left\langle \Psi_\uparrow^\dagger(\mathbf{r},t)\,\Psi_\downarrow^\dagger(\mathbf{r}',t')\right\rangle$ Green's functions and their complex conjugates (see for example [90]). Still, in the limit where the gap $\Delta(\mathbf{r})$ is small, and close to the critical temperature T_C, one can find a single equation for the center-of-mass wavefunction of the pairs, the Ginzburg-Landau equation. It was introduced in 1950 as a purely phenomenological equation for the condensate wave function $\psi(\mathbf{r})$ with parameters that needed to be fixed by experiments[18]:

$$\left(-\frac{\hbar^2\nabla^2}{2m^*}+b(\mathbf{r})\,|\psi(\mathbf{r})|^2\right)\psi(\mathbf{r})=-a(\mathbf{r})\,\psi(\mathbf{r}) \tag{2.132}$$

Closely resembling the Gross-Pitaevskii equation above, this equation describes the motion of "superfermions" of mass m^*. The condensate wavefunction is normalized to give the density of these "superfermions", $|\psi(\mathbf{r})|^2=n_s^*$. In a uniform system, the two solutions of Eq. 2.132 are $\psi=0$ (the normal state) or $|\psi|^2=-a/b$. The order parameter ψ should vanish at T_C, so a natural choice is to set $a(T)=(T-T_C)a'$. This implies a "superfermion" density that vanishes linearly close to T_C. The simplest choice for b is a constant. For a non-uniform system, we see by inspection that Eq. 2.132 defines a natural length scale over which the order parameter varies, the

[18]We omit the effect of a magnetic field for the case of electron pairs, which could be included by introducing a vector potential $\mathbf{A}$. Rotation of fermion pairs in a neutral fermionic superfluid could be included as well, as it is formally equivalent to the motion of superconducting electron pairs in a magnetic field: One simply replaces $e\mathbf{A}/c$ by $m\mathbf{\Omega}\times\mathbf{r}$, where $\mathbf{\Omega}$ is the rotation frequency.

Ginzburg-Landau coherence length

$$\xi_{\mathrm{GL}}(T) = \sqrt{\frac{\hbar^2}{2m^* \, |a(T)|}} = \sqrt{\frac{\hbar^2}{2m^* \, (T_C - T) \, |a'|}} \tag{2.133}$$

This length scale becomes very large close to the critical temperature, and in particular it can be large compared to the BCS-coherence length $\xi_{\mathrm{BCS}} = \hbar v_F / \pi \Delta_0$, defined above via the zero-temperature gap Δ_0. Spatial variations of the order parameter thus occur at a length scale much larger than the size of a Cooper pair. This is in essence the reason why, even in the BCS-regime of long-range fermion pairs, the condensate can be described by a *local* equation [236]. Remarkably, the Ginzburg-Landau equation, introduced on phenomenological grounds, was later *derived* by Gorkov from BCS theory. The "superfermions" turned out to be fermion pairs, so that a natural normalization of the wavefunction is provided by the density of pairs, $|\psi(r)|^2 = n_s/2$, where n_s is the total superfluid density (at zero temperature, we necessarily have $n_s = n$, the total fermion density). This normalization fixes the phenomenological parameters, $m^* = 2m$ as expected for fermion pairs, $a = -\frac{6\pi^2 (k_B T_C)^2}{7\zeta(3) E_F} \left(1 - \frac{T}{T_C}\right)$ and $|a|/b = n \left(1 - \frac{T}{T_C}\right)$. Comparing with the equation for the superfluid gap close to T_C, Eq. 2.126, and using the result for the critical temperature $T_C = \Delta_0 \, e^{\gamma}/\pi$ in the BCS-limit, we arrive at

$$|\psi|^2 = n \left(1 - \frac{T}{T_C}\right) = \frac{7\zeta(3)}{8e^{2\gamma}} \, n \, \frac{\Delta^2}{\Delta_0^2} \approx 0.33 \, n \, \frac{\Delta^2}{\Delta_0^2} \tag{2.134}$$

The numerical prefactor is not correct at zero temperature, where one should expect $|\psi|^2 = n/2$, as here, the superfluid density must equal the total density. This should not be of concern, however, since $T = 0$ lies outside the applicability of the Ginzburg-Landau equation. The approximate expression for the gap close to T_C in Eq. 2.126 extrapolates to an incorrect value ($\approx 1.7 \Delta_0$) at $T = 0$.

At least close to T_C, Eq. 2.134 finally fixes the normalization parameter $\mathcal{N}$ in Eq. 2.129 for the BCS-regime,

$$\mathcal{N} = \sqrt{\frac{7\zeta(3)}{8e^{2\gamma}}} \, V \, \frac{\sqrt{n}}{\Delta_0} = \sqrt{\frac{56\zeta(3)}{3e^{2\gamma}}} \, \frac{1}{\sqrt{k_F |a|}} \, \frac{E_F}{\Delta_0} \, |a|^{3/2} \tag{2.135}$$

It is satisfying to note that, using the limiting expression for the gap Δ_0 in the BEC-regime, $\Delta_0 = \sqrt{\frac{16}{3\pi}} \frac{E_F}{\sqrt{k_F a}}$, one recovers, up to a numerical constant, the same normalization constant $\mathcal{N} \propto a^{3/2}$ we had found before to arrive at the Gross-Pitaevskii

equation. This suggests that the regime of applicability of the Ginzburg-Landau equation increases from the far BCS-side, where it is $T_C - T \ll T_C$, to the far BEC-side, where it encompasses all temperatures from $T = 0$ up to T_C. In the intermediate regime of strong interactions ($k_F|a| \gg 1$), the Ginzburg-Landau approach is expected to still provide a reasonable, qualitative description of the condensate [74, 236].

Chapter 3

Feshbach resonances

Typical scattering lengths in alkali atoms are on the order of the van der Waals-range $r_0 \approx 50 - 100\,a_0$. Common interparticle spacings in our ultradilute gases are $n^{-1/3} \sim 10\,000\,a_0$. We have seen in the preceding chapter that it is simply hopeless to achieve superfluidity in Fermi gases with such a small interaction strength $k_F\,|a| \sim 0.02$, as the critical temperature depends exponentially on this parameter. Clearly, one needs a way to enhance the interatomic interactions by some sort of scattering resonance.

Early on, ^{6}Li was considered a very promising candidate to achieve fermionic superfluidity [237], as its triplet scattering length was found to be unusually large and negative, about $-2\,000\,a_0$ [3]. As we will see, this is due to an almost bound state in the interatomic potential of ^{6}Li, causing low-energy collisions to be indeed almost resonant. While this seems already too good to be true, ^{6}Li offers in addition a "magic knob" to tune the interaction strength at will, an unusually wide *Feshbach resonance*, predicted in 1997 [124]. These resonances occur as a bound state in the interatomic potential is tuned into resonance with the energy of two colliding atoms. This tuning is possible via an applied magnetic field if the magnetic moment of the bound state differs from that of the two unbound atoms. Feshbach resonances have not only allowed to reach the strongly interacting regime where $k_F\,|a| > 1$ [174, 106, 36], but also to create ultracold molecules from samples of ultracold atoms [205, 69, 239, 128], a new way of doing "quantum chemistry". Of great importance here was the realization that the gas close to resonance is stable [78, 174, 69, 239, 128, 202], a property that is directly linked to the Pauli principle [193].

In the following, I will describe scattering resonances in general and the phenomenon of Feshbach resonances in particular.

3.1 Scattering resonances

Let us consider the archetypical example of a square-well potential of size R and depth V (see Fig. 3-1). We have already seen in the preceding chapter that in order have a 3D bound state for two particles of mass m, the potential well needs to be deeper than a minimum depth V_c. For a square-well potential [145], $V_c = \frac{\pi^2\hbar^2}{4mR^2}$. Let us discuss the relevant situations.

- If no bound state is present, for $V < V_c$, two colliding particles will feel attraction, corresponding to a negative scattering length $a < 0$. That is, the radial wavefunction for their relative motion $u(r) \overset{r>R}{\sim} \sin(k(r-a))$ appears to be "pulled in", to originate from *negative* values of the distance r between the atoms (see upper left panel in Fig. 3-1). The closer V gets to the critical V_c, the more negative the scattering length becomes. It is helpful to think of an "almost" bound state that exists just above the energy of the colliding atoms (the "threshold"). Second-order perturbation theory then shows that this "virtual" state will repel the incoming state, lowering the energy of the colliding particles and thus leading to their attraction. The closer the virtual state lies to threshold, the stronger the attraction.

- If the well is just a bit deeper than the critical V_c, a true bound state is available below zero energy. This state pushes the incoming state up in energy and thus leads to repulsion of the colliding atoms. The closer the bound state lies with respect to the incoming state, the stronger the repulsion. The wavefunction $u(r)$ appears to be "pushed out" from the origin, to originate from $a > 0$. We see that necessarily, whenever a new bound state enters the scattering potential, the wavefunction $u(r)$ acquires a new node.

- Right at $V = V_c$, a true bound state forms at zero energy. Atoms colliding at very low energies are thus in resonance with this state. The scattering length diverges, causing the wavefunction $u(r)$ to look "flat" over distances $r < 1/k$. In fact, over those distances $u(r)$ cannot be distinguished from the equally "flat" wave-function of the very large bound state (see section 2.2.3), the overlap between the two is at its maximum, as we expect for resonant coupling. Like in optics, this situation corresponds to maximum "absorption" of the incoming wave by the potential well, with an absorption cross section given by $\sigma = \frac{4\pi}{k^2}$. This reminds us of the resonant absorption cross section of light by atoms, which

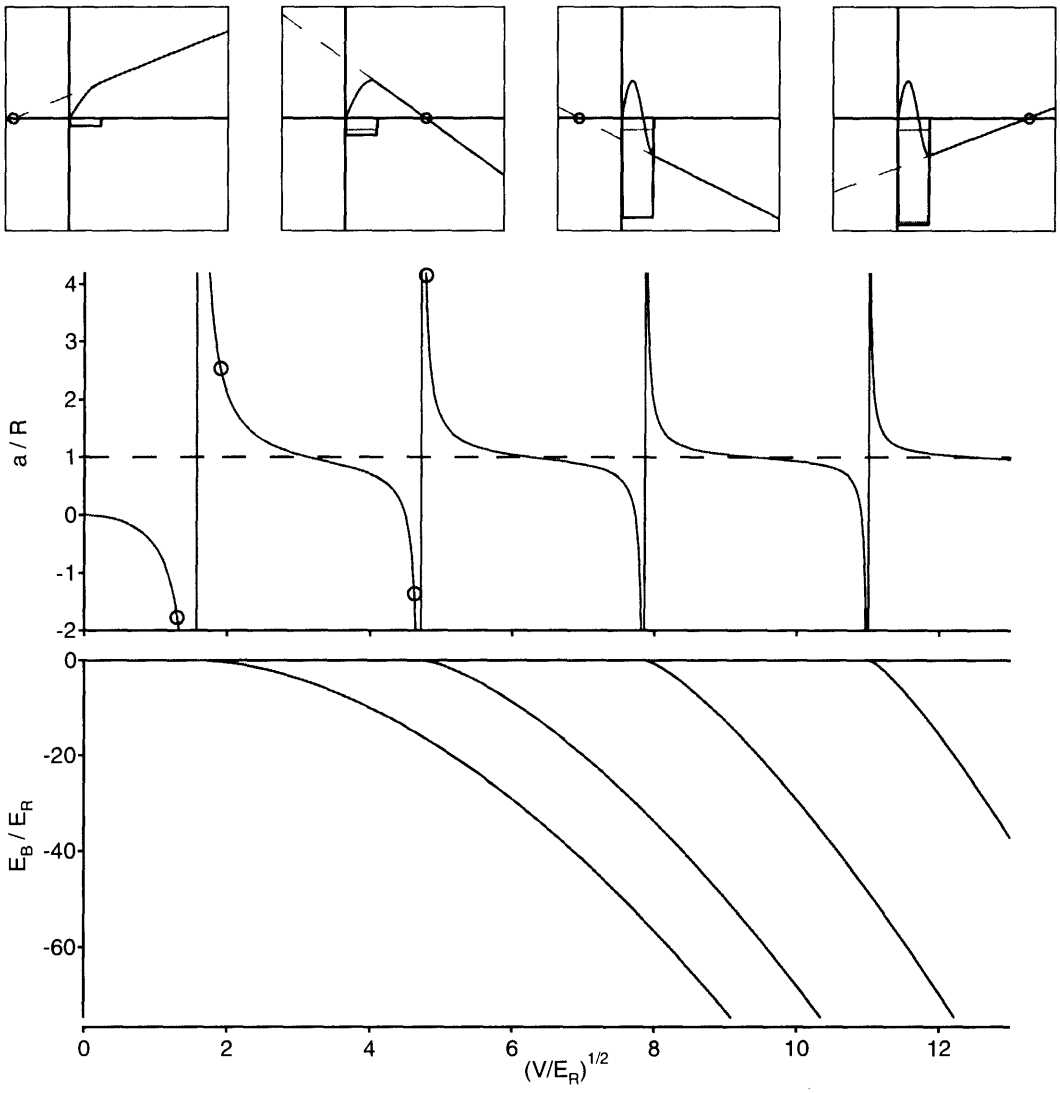

Figure 3-1: Scattering resonances for the square well potential. Shown is the scattering length a and the bound state energies E_B as a function of the square well depth V. Close to a resonance (say at V_c), the energy of the associated bound state depends quadratically on $V - V_c$. The four panels above illustrate the evolution of the wavefunction (red) at selected points (blue circles). The zero-crossing of its tangent (blue dashed line) gives the scattering length. It is negative for a shallow well (left panel), corresponding to attraction. As a bound state enters the well at a critical depth (green), the scattering length diverges and reenters from $+\infty$. The wavefunction now has a new node at a.

is $\sigma = \frac{6\pi}{k^2}$ with k the photon wave vector[1] (see section 2.2.1).

It is not difficult to show that the scattering length a is given by [145]

$$a = R\left(1 - \frac{\tan \kappa R}{\kappa R}\right) \tag{3.1}$$

where $\kappa = \sqrt{\frac{mV}{\hbar^2}}$. Away from any resonances, the scattering length is always close to the "background" scattering length R. However, on top of this background value, scattering resonances occur when $\kappa R = (2n+1)\frac{\pi}{2}$ with integer n. This coincides exactly with the appearance of a new bound state in the potential (see Fig. 3-1). The scattering length is positive if the nearest state is truly bound and negative when it is still "virtual" or almost bound. Close to a resonance (say at $V_c = \hbar^2 k_c^2/m$), the scattering length diverges as

$$a \approx \frac{1}{kR(k-k_c)} \approx \frac{2\hbar^2}{mR(V-V_c)} \tag{3.2}$$

and for $a > 0$ the bound state energy is related to a by

$$E_B = -\frac{1}{4}\frac{(V-V_c)^2}{E_R} = -\frac{\hbar^2}{ma^2} \tag{3.3}$$

We found this general behavior for weakly bound states already in chapter 2.2.3: The binding energy depends quadratically on the "detuning". The beauty of the Feshbach resonance mechanism is that this detuning is indeed an externally controllable parameter.

3.2 Feshbach resonances

We now turn to realistic interaction potentials between alkali atoms. Here, the interaction actually depends on the internal structure of the two colliding atoms, namely on the relative spin orientation of their valence electrons, singlet or triplet. In Fig. 3-2 for example, the atoms enter in a triplet configuration. If there was no coupling between the singlet V_S and the triplet potential V_T, the atoms would simply scatter off each other in $V_T(r)$, acquiring some certain, fixed phase shift. However, the *hyperfine*

[1]The factor "6" is related to the photon being a spin-1 particle, such that atom-photon collisions always involve transfer of angular momentum. The lowest-energy collisions can thus be thought of as being p-wave collisions.

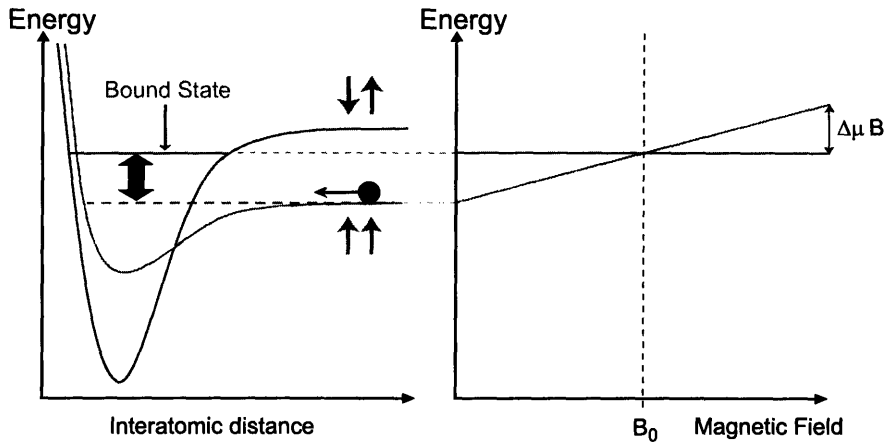

Figure 3-2: Origin of Feshbach resonances. Atoms entering (for example) in the triplet potential are coupled to a singlet bound molecular state. By tuning the external magnetic field, this bound state can be brought into resonance with the incoming state (at B_0 in the right graph).

interaction $V_{\rm hf}$ is not diagonal in the total electronic spin $\mathbf{S} = \mathbf{s}_1 + \mathbf{s}_2$ of the two atoms and thus provides a coupling between singlet and triplet potentials:

$$\begin{aligned} V_{\rm hf} &= a_{\rm hf}\left(\mathbf{s}_1 \cdot \mathbf{i}_1 + \mathbf{s}_2 \cdot \mathbf{i}_2\right) \\ &= \frac{a_{\rm hf}}{2}\mathbf{S}\left(\mathbf{i}_1 + \mathbf{i}_2\right) + \frac{a_{\rm hf}}{2}\left(\mathbf{s}_1 - \mathbf{s}_2\right)\left(\mathbf{i}_1 - \mathbf{i}_2\right) \\ &= V_{\rm hf}^{+} + V_{\rm hf}^{-} \end{aligned} \tag{3.4}$$

with the hyperfine constant $a_{\rm hf}$ and the nuclear spins $\mathbf{i}_{1,2}$ of the two atoms. Given the coupling $V_{\rm hf}^{-}$, the atoms can explore the singlet potential as well. It is in our case a "closed channel", meaning that singlet continuum states are not available as final scattering states by energy conservation. A Feshbach resonance occurs when the state in which the atoms collide (the "incoming" state) is in resonance with a bound state in this potential. The energy difference between the incoming and the Feshbach bound state can be tuned via an applied magnetic field, due to their different magnetic moments (see Fig. 3-2).

3.2.1 A simple model

Let us consider a simple model of a Feshbach resonance, in which there is only one bound state of importance $|m\rangle$ in the closed channel, the others being too far detuned in energy (see Fig. 3-3). The continuum of plane waves of relative momentum $\mathbf{k}$

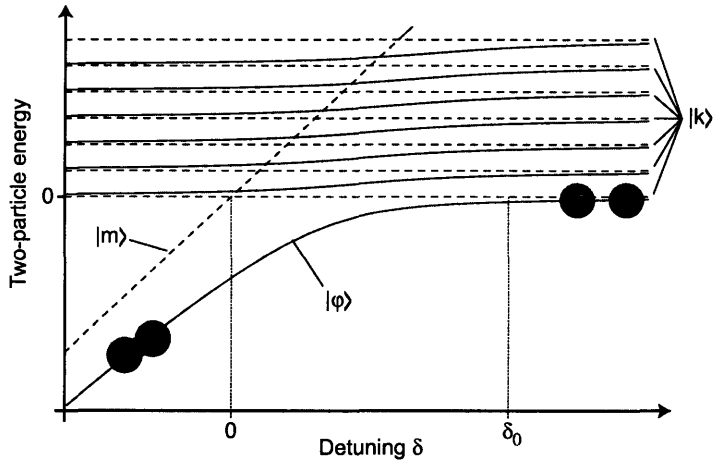

Figure 3-3: Simple model for a Feshbach resonance. The dashed lines show the uncoupled states: The closed channel molecular state $|m\rangle$ and the scattering states $|k\rangle$ of the continuum. The uncoupled resonance position lies at zero detuning, $\delta = 0$. The solid lines show the coupled states: The state $|\varphi\rangle$ connects the molecular state $|m\rangle$ at $\delta \ll 0$ to the lowest state of the continuum above resonance. At positive detuning, the molecular state is "dissolved" in the continuum, merely causing an upshift of all continuum states as φ becomes the new lowest continuum state. In this illustration, the continuum is discretized in equidistant energy levels. In the continuum limit (Fig. 3-4), the dressed molecular energy reaches zero at a finite, shifted resonance position δ_0.

between the two particles in the incoming channel will be denoted as $|k\rangle$. In the absence of coupling, these are eigenstates of the free hamiltonian

$$\begin{aligned} H_0 |k\rangle &= 2\epsilon_k |k\rangle \qquad \text{with } \epsilon_k = \frac{\hbar^2 k^2}{2m} \\ H_0 |m\rangle &= \delta |m\rangle \end{aligned} \tag{3.5}$$

where δ, the bound state energy of the "bare" molecular state, is the parameter we can experimentally control. We will only consider interactions between $|m\rangle$ and the $|k\rangle$'s, neglecting scattering that occurs exclusively in the incoming channel. First, we are interested in seeing how the molecular state is altered due to the coupling to the continuum $|k\rangle$. Thus, we want to solve

$$\begin{aligned} H |\varphi\rangle &= E |\varphi\rangle \\ \text{with } |\varphi\rangle &= \alpha |m\rangle + \sum_k c_k |k\rangle \end{aligned} \tag{3.6}$$

for $E < 0$ where $H = H_0 + V$ and the only non-zero matrix elements of V are $\langle m| V |k\rangle = g_k/\sqrt{\Omega}$ and their complex conjugates (we will take g_k to be real). Ω is the volume of the system and introduced in this definition for later convenience. We quickly find

$$\begin{aligned} (E - 2\epsilon_k)\, c_k &= \frac{g_k}{\sqrt{\Omega}}\, \alpha \\ (E - \delta)\, \alpha &= \frac{1}{\sqrt{\Omega}} \sum_k g_k\, c_k = \frac{1}{\Omega} \sum_k \frac{g_k^2\, \alpha}{E - 2\epsilon_k} \\ \text{and thus} \qquad E - \delta &= \frac{1}{\Omega} \sum_k \frac{g_k^2}{E - 2\epsilon_k} \end{aligned} \tag{3.7}$$

As we only consider low-energy s-wave scattering, one can take the g_k's to be constant g_0 up to some cut-off E_R and zero beyond. The right hand side of Eq. 3.7 side is then identical to Eq. 2.79, and we can read off the solution from table 2.2 (3D case):

$$\begin{aligned} |E| + \delta &= \frac{g_0^2}{\Omega} \int_0^{E_R} d\epsilon \frac{\rho(\epsilon)}{2\epsilon + |E|} = \delta_0 - \sqrt{2E_0 |E|} \\ \text{with} \qquad \delta_0 &\equiv \frac{1}{\Omega} \sum_k \frac{g_k^2}{2\epsilon_k} = \frac{g_0^2}{\Omega} \int_0^{E_R} d\epsilon\, \rho(\epsilon) \frac{1}{2\epsilon} = \frac{4}{\pi} \sqrt{E_0 E_R} \\ \text{and} \qquad E_0 &\equiv \left(\frac{g_0^2}{2\pi} \left(\frac{m}{2\hbar^2} \right)^{3/2} \right)^2 \end{aligned}$$

where we have assumed $E_R \gg |E|$. As illustrated in Fig. 3-3, for positive detuning $\delta > \delta_0$ the original molecular state is "dissolved" in the continuum. For $\delta - \delta_0 < 0$, we find a true bound state at

$$E = -E_0 + \delta - \delta_0 + \sqrt{(E_0 - \delta + \delta_0)^2 - (\delta - \delta_0)^2} \tag{3.8}$$

This "dressed" bound state energy is shown in Fig. 3-4. Far away from the resonance region, for $\delta_0 - \delta \gg E_0$, we have $E \approx -(\sqrt{\delta_0 - \delta} - \sqrt{E_0/2})^2 - \frac{E_0}{2}$, which describes, apart from energy shifts, the original bound state. In the other limit, the bound state crosses the energy of the incoming state at a *shifted* position $\delta = \delta_0$. Close to this point, the energy $E \approx -\frac{1}{2}(\delta - \delta_0)^2/E_0$ depends quadratically on the detuning $\delta - \delta_0$, as expected.

Scattering length

To find the scattering length, it is convenient to project the Schrödinger equation $H|\psi\rangle = E|\psi\rangle$ onto the two relevant subspaces, the space of the scattering states $|k\rangle$ of the incoming channel and the molecular state of the closed channel, $|m\rangle$. The goal is to find out how the coupling to the molecular state affects scattering in k-space. For this, we introduce the projectors $\mathcal{P}_k = \sum_k |k\rangle\langle k|$ and $\mathcal{P}_m = |m\rangle\langle m|$. The weight of all other states being vanishingly small, we have $\mathcal{P}_k + \mathcal{P}_m \approx \mathbb{1}$. The projected wavefunctions are $|\psi_k\rangle = \mathcal{P}_k|\psi\rangle$ and $|\psi_m\rangle = \mathcal{P}_m|\psi\rangle$. The free hamiltonian H_0 acts exclusively within each subspace, so it commutes with the projectors. We define $H_0^k = \mathcal{P}_k H_0 \mathcal{P}_k$ and $H_0^m = \mathcal{P}_m H_0 \mathcal{P}_m$. In contrast, the interaction V couples k-space to the molecular state, and its only non-zero projections are $V_{km} = \mathcal{P}_k V \mathcal{P}_m = \sum_k \frac{g_k}{\sqrt{\Omega}} |k\rangle\langle m|$ and $V_{mk} = \mathcal{P}_m V \mathcal{P}_k = \sum_k \frac{g_k}{\sqrt{\Omega}} |m\rangle\langle k|$. We can now easily calculate the projection of $H|\psi\rangle$ onto k-space: $\mathcal{P}_k H|\psi\rangle = \mathcal{P}_k(H_0 + V)|\psi\rangle = H_0^k|\psi_k\rangle + \mathcal{P}_k V(\mathcal{P}_k + \mathcal{P}_m)|\psi\rangle = H_0^k|\psi_k\rangle + V_{km}|\psi_m\rangle$. In the same way we get $\mathcal{P}_m H|\psi\rangle = H_0^m|\psi_m\rangle + V_{mk}|\psi_k\rangle$. The Schrödinger equation then reads

$$\begin{aligned} (E - H_0^k)|\psi_k\rangle &= V_{km}|\psi_m\rangle \\ (E - H_0^m)|\psi_m\rangle &= V_{mk}|\psi_k\rangle \end{aligned} \tag{3.9}$$

We can formally solve the problem in the closed channel[2], $|\psi_m\rangle = (E - H_0^m + i\eta)^{-1} V_{mk}|\psi_k\rangle$ and insert this into the equation for $|\psi_k\rangle$:

[2]The small positive infinitesimal part $i\eta$ ensures that the scattered wave will correspond to an outgoing wave.

$$(E - H_0^k)\,|\psi_k\rangle = V_{km}(E - H_0^m + i\eta)^{-1}V_{mk}\,|\psi_k\rangle = \frac{V_{km}V_{mk}}{E - \delta + i\eta}\,|\psi_k\rangle \tag{3.10}$$

where we have used $H_0^m\,V_{mk} = H_0^m\,|m\rangle\,\sum_k \frac{g_k}{\sqrt{\Omega}}\,\langle k| = \delta\,V_{mk}$.

The scattering problem is now entirely formulated in the open channel. The molecular state causes an effective interaction that corresponds to two atoms colliding, spending some (infinitesimal) time in the molecular state and exiting again as two unbound atoms. From equations 2.60 and 2.63 we can read off the scattering amplitude for zero-energy collisions and hence the scattering length. We only need to insert the Fourier transform of the effective interaction at $E = 0$, which is $V_0 = \Omega\,\lim_{E,k,k'\to 0}\,\langle k|\,\frac{V_{km}V_{mk}}{E-\delta+i\eta}\,|k'\rangle = -\frac{g_0^2}{\delta}$:

$$\begin{aligned} \frac{m}{4\pi\hbar^2 a} &= -\frac{\delta}{g_0^2} + \frac{1}{\Omega}\sum_k \frac{1}{2\epsilon_k} = -\frac{\delta - \delta_0}{g_0^2} \\ \text{or} \qquad a &= \frac{m}{4\pi\hbar^2}\frac{g_0^2}{\delta_0 - \delta} \end{aligned} \tag{3.11}$$

The scattering length, shown in Fig. 3-4, diverges at the *shifted* resonance position $\delta = \delta_0$. Not surprisingly, we recover $E = -\hbar^2/ma^2$ for the bound state energy close to resonance for positive $a > 0$, as it should be.

In the experiment, the Feshbach resonance occurs for a certain magnetic field B_0. With the magnetic moment difference $\Delta\mu$ between the incoming state and the closed (uncoupled) molecular state, we have $\delta - \delta_0 = \Delta\mu(B - B_0)$ (taking $\Delta\mu$ to be constant). Including the background scattering length a_{bg} for collisions that occur entirely in the open channel, the scattering length can be written in its usual form

$$a = a_{\text{bg}}\left(1 - \frac{\Delta B}{B - B_0}\right) \qquad \text{with } \Delta B = \frac{m}{4\pi\hbar^2}\frac{g_0^2}{\Delta\mu\; a_{\text{bg}}} \tag{3.12}$$

3.2.2 Feshbach resonances in ^{6}Li

We will now discuss the case of ^{6}Li relevant for our experiments. Fig. 3-5 shows the s-wave scattering length for collisions between the two lowest hyperfine states, $|F, m\rangle = |1/2, 1/2\rangle$ and $|1/2, -1/2\rangle$ of ^{6}Li. It shows a broad Feshbach resonance centered around $B_0 = 834.15$ G. The resonance is approximately described by Eq. 3.12 with $a_{\text{bg}} = -1\,405\,a_0$, $\Delta B = 300$ G [24]. These values are highly unusual when comparing scattering lengths and Feshbach resonances in other alkali atoms. Background

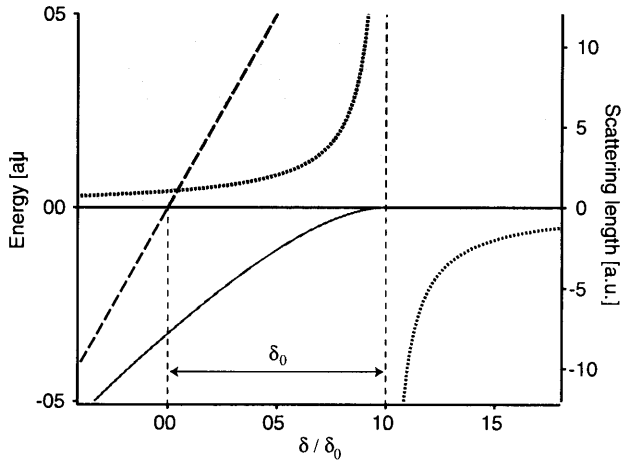

Figure 3-4: Bare, uncoupled molecular state (dashed line), coupled, bound molecular state (solid line) and scattering length (dotted line) close to a Feshbach resonance. The shaded area represents the continuum of scattering states, starting at the collision threshold at $E = 0$. Interaction between the molecular state and the continuum shifts the position of the resonance by δ_0 from the crossing of the uncoupled molecular state with threshold. Note the quadratic behavior of the bound state energy with detuning $(\delta - \delta_0)$ close to resonance.

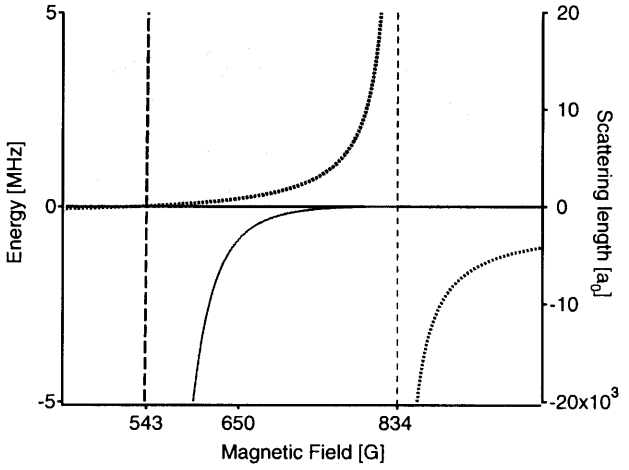

Figure 3-5: Feshbach resonances in ^{6}Li between the two lowest hyperfine states $|F, m\rangle = |1/2, 1/2\rangle$ and $|1/2, -1/2\rangle$. A wide Feshbach resonance occurs at 834.15 G. The resonance position is shifted by an unusually large amount of ~ 300 G from the crossing of the uncoupled molecular state at 543 G. A second, narrow Feshbach resonance occurs right at 543 G, shifted by less than 200 mG.

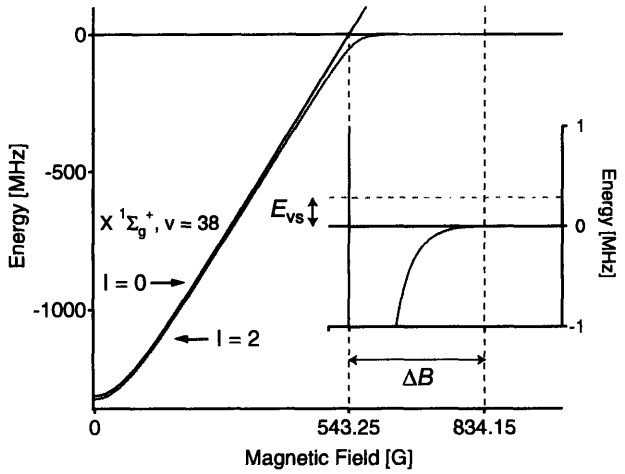

Figure 3-6: Bound state energies for $^6Li_2$ in a magnetic field. The weakest bound state of the singlet potential, $X^1\Sigma_g^+, v = 38$, splits into two hyperfine components with total nuclear spin $I = 0$ and $I = 2$. The state with $I = 0$ is almost not coupled to the triplet scattering continuum, causing the narrow resonance at 543.2 G. In turn, the state $I = 2$ is very strongly coupled and leads to the broad resonance at 834 G, a shift of $\Delta B \approx 300$ G. The strong coupling is caused by a virtual state of the triplet potential (dashed line in the inset), which is only $E_{vs} \approx h \cdot 300$ kHz away from threshold ($E = 0$). It is this virtual state that is responsible for the large background scattering length for triplet collisions.

scattering lengths are typically on the order of $\pm 100\, a_0$ or less, which is roughly the range of the van der Waals-potential. Typical widths of other observed Feshbach resonances are at least two, rather three orders of magnitude smaller than ΔB. Clearly, the broad Feshbach resonance in ^{6}Li is a special case.

The unusually large background scattering length of ^{6}Li that decreases even to $-2\,100\, a_0$ at high fields, hints at a resonance phenomenon even away from the wide Feshbach resonance. Indeed, it turns out that there is an almost bound, virtual state in the triplet potential of ^{6}Li very close to the collision threshold. From the large background scattering length we can estimate that the virtual state must lie approximately $E_{vs} \approx \hbar^2/m a_{bg}^2 \approx h \cdot 300\,\text{kHz}$ above threshold.

It turns out that the wide Feshbach resonance at 834 G is caused by an interplay between the molecular state in the singlet potential and the open channel resonance due to the virtual state. Such a situation has been analyzed in [162] and applied to the case of ^{6}Li in [248]. As a crude approximation, we can argue that the molecular state couples to the scattering continuum exclusively via the virtual bound state. From the equation for the bound state energy, Eq. 3.7, we can estimate a resonance shift of

$\delta \approx g_{\rm vs}^2/E_{\rm vs}$ due to the coupling to the virtual state. Even for a coupling $g_{\rm vs}$ that is not unusually large we expect the resonance position to be shifted considerably (and hence the resonance to be wide) if the virtual state is close to threshold. Indeed, from the resonance width $\Delta B \approx 300$ G we can estimate

$$g_{\rm vs} \approx \sqrt{\delta\, E_{\rm vs}} = \sqrt{\Delta\mu\, \Delta B\, E_{\rm vs}} \approx h \cdot 15\,{\rm MHz} \tag{3.13}$$

where we have used $\Delta\mu \approx 2\mu_B$ on resonance, where the incoming state is essentially a pure triplet, while the molecular state is a singlet. The hyperfine constant for ^{6}Li is $a_{\rm hf} \approx h \cdot 150\,{\rm MHz}$, which sets the scale for the interaction $V_{\rm hf}^-$. A typical coupling g_k is thus $a_{\rm hf}$ times the overlap integral $\int d^3r \varphi_b(\mathbf{r})\psi_k(\mathbf{r})$ of the bound state wavefunction and the scattering states[3]. We see indeed that $g_{\rm vs}$ is not particularly large, and that the cause for the wide Feshbach resonance at 834 G is the virtual bound state[4].

3.2.3 Broad versus narrow Feshbach resonances

We have seen how it is possible to tune the scattering length in atomic gas collisions via Feshbach resonances. To what extent can the many-body description of chapter 2 be carried over to this case?

Let us recall that the derivation of the BEC-BCS crossover made use of a contact potential $V = V_0\delta(\mathbf{r})$, which was adjusted in such a way as to reproduce the correct scattering length a. However, the use of such a contact potential *implies* the relation

$$E_B = -\frac{\hbar^2}{ma^2} \tag{3.14}$$

for the energy of the bound molecular state[5]. This signifies that the character of the molecular state is entirely described by the scattering length, a property of the

[3]To estimate the overlap integral, we assume the weakly bound singlet state to have a characteristic size $a_B \sim 50\,a_0$, the van der Waals-range of the potential. Over this small scale, the virtual state's radial wavefunction $u_{\rm vs} = r\psi_{\rm vs}$ is approximately constant and equal to $\sim 1/\sqrt{a_{\rm bg}}$ (for normalization). The integral $\int dr u_b(r)u_{\rm vs}(r)$ is thus on the order of $\sqrt{a_B/a_{\rm bg}} \approx 0.1 - 0.2$. With this reduction we obtain the correct order of magnitude for g.

[4]The resonance at 543 G has a narrow width, because the molecular state causing it has a vanishing matrix element (Clebsch-Gordan coefficient) with the virtual state.

[5]This can be seen by using a square well potential $V(r) = -V$ for $r < R$ and zero outside. The relation between the scattering length, the Fourier transform of $V(r)$, $\widetilde{V}(\mathbf{q}) \approx \widetilde{V}(\mathbf{0}) = {\rm const}$ (for $q \ll 1/R$) and R is given by Eq. 2.63:

$$\frac{1}{\widetilde{V}} = -\frac{m}{4\pi\hbar^2 a} + \sum_{k<1/R} \frac{1}{2\epsilon_k} \tag{3.15}$$

scattering states in the open channel.

For any real situation, this relation holds only close to resonance. We see from the simple model system of section 3.2.1 that the bound state energy starts to deviate from the above relation once $|E_B| \approx E_0$. E_0 is the energy scale associated with the strength of the Feshbach coupling between the bare molecular state and the scattering continuum. Close to resonance, for $|E_B| \ll E_0$, the "dressed" molecular state

$$|\varphi\rangle = \alpha |m\rangle + \sum_k c_k |k\rangle \tag{3.18}$$

will be almost entirely described by the scattering states of the open channel $|k\rangle$ (one finds $\alpha^2 = \sqrt{\frac{2|E_B|}{E_0}} \ll 1$). However, as $|E_B|$ starts to grow beyond E_0, the dressed molecular state resembles more and more the original "bare" state $|m\rangle$, and $\alpha \approx 1$.

The crucial question for the many-body description is now: How does the Fermi energy E_F compare to the coupling scale E_0? The BEC-BCS crossover occurs for $-1 < 1/k_F a < 1$. If we first reach the weakly interacting regime $k_F a \ll 1$ (equivalently $E_F \ll \hbar^2/ma^2$) *before* $\hbar^2/ma^2 \approx E_0$, we can safely use the single channel description for the crossover. The "dressed" molecular state is almost completely dissolved in the open channel continuum throughout the crossover and the details of the original molecular state $|m\rangle$ do not play a role (case of a "broad" Feshbach resonance). However, if E_0 is comparable to E_F, then the molecular state affects the many-body physics and it needs to be included in the description of the gas (case of a "narrow" Feshbach resonance) [227].

Using Eq. 3.12 and the definition for E_0, Eq. 3.8, we can relate the coupling energy scale E_0 to experimentally observable parameters. One has

$$E_0 = \frac{1}{2} \frac{(\Delta\mu \Delta B)^2}{\hbar^2/m a_{\mathrm{bg}}^2} \tag{3.19}$$

The fraction of the dressed molecular wave function that is in the deeply bound state

---

The equation for the bound state energy $E < 0$ was derived in Eq. 2.79 and is

$$\frac{1}{\widetilde{V}} = \sum_{k<1/R} \frac{1}{2\epsilon_k + |E|} \tag{3.16}$$

We then have

$$\frac{m}{4\pi\hbar^2 a} = \sum_{k<1/R} \left(\frac{1}{2\epsilon_k} - \frac{1}{2\epsilon_k + |E|} \right) = \frac{1}{2\pi^2} \left(\frac{m}{\hbar^2} \right)^{3/2} \sqrt{|E|} \arctan\left(\frac{E_R}{2|E|} \right) \tag{3.17}$$

where we have used the cut-off energy scale $E_R = \hbar^2/mR^2$. For $E_R \gg |E|$ we obtain Eq. 3.14.

$|m\rangle$ is

$$\alpha^2 = \sqrt{\frac{2E_B}{E_0}} = 2\sqrt{\frac{E_F}{E_0}}\frac{1}{k_F a} \tag{3.20}$$

For the resonance used in the experiments by D. Jin on ^{40}K, $E_0/k_B \approx 1\,\mathrm{mK}$, which should be compared to a typical Fermi energy of $E_F/k_B = 1\mu\mathrm{K}$. This resonance is thus broad. Nevertheless, at $k_F a = 1$ the fraction of the wavefunction in the closed channel molecule is $\alpha^2 \approx 6\%$. This might possibly explain the shorter lifetime of the gas of molecules $^{40}K_2$ close to resonance [202] as compared to the case in $^6Li_2$ [35]. For the wide Feshbach resonance in ^{6}Li, one has $E_0/k_B \approx 50\,\mathrm{K}$, which makes it an unusually broad resonance. However, as pointed out above, the simple model of section 3.2.1 does not apply to the case of ^{6}Li, and one has to take into account the influence of the virtual state in the open channel. If this is done, one finds that the energy scale equivalent to E_0 is[6] rather $\approx \Delta\mu\Delta B = k_B \cdot 40\,\mathrm{mK}$, which is still very broad. The simple relation $E_B = -\hbar^2/ma^2$ holds still to better than 3% at a magnetic field of 600 G, 234 G away from resonance, while many-body effects ($k_F a > 1$) start to become important only above 750 G. Indeed, the closed channel contribution to the dressed molecular state has been measured in the group of R. Hulet [188] to be less than 1% at magnetic fields beyond 600 G and less than 10^{-3} throughout the entire strongly interacting regime beyond $k_F a \approx 1$.

The Feshbach resonance in ^{6}Li at 543 G, in turn, has $E_0/k_B \approx 1\,\mu\mathrm{K}$ and is thus narrow. In the case of a narrow resonance, the many-body physics is qualitatively different from the BEC-BCS crossover picture. For a detuning $\delta - \delta_0 < 0$, all fermion pairs are still tightly bound in the closed channel molecular state, where they form a condensate. For $\delta - \delta_0 < 2E_F$, the molecular condensate coexists with a BCS-type fermionic superfluid. Here, the molecular state (unstable in vacuum above threshold) is stabilized by Pauli blocking, as the outgoing momentum states are occupied by fermions in the BCS-state. Only for $\delta - \delta_0 > 2E_F$ is the molecular state truly emptied and we are left with a BCS-type superfluid. However, since the resonance is narrow, the interactions for $\delta - \delta_0 > 2E_F \gg E_0$ will be very small, $k_F\,|a| < \sqrt{\frac{E_0}{E_F}} \ll 1$, rendering the observation of such a state extremely difficult.

[6] At a detuning $\delta - \delta_0 = E_0$, the bound state energy in the simple Feshbach model is about one half times $\hbar^2/ma^2$. We can thus use the detuning where $|E_B| = \frac{1}{2}\hbar^2/ma^2$ as the definition of the coupling energy scale.

Chapter 4

Cooling fermions - The apparatus

Cooling a gas of atoms into the nanokelvin regime appears to be (almost) commonplace: Eight years after the discovery of gaseous Bose-Einstein condensates in 1995, BECs were reliably produced in about 50 laboratories around the world, a number has steadily grown since. At this pace, one would expect the number ultracold fermion experiments to exceed 50: The first degenerate Fermi gas of atoms was created in 1998 [76]. However, by now only thirteen laboratories in the world are studying ultracold fermions. This can hardly be explained by lack of interest in fermions, as they are the building blocks of matter and Fermi statistics governs the structure of nuclei, atoms, and the behavior of metals. The explanation lies in experimental complexity. Of the two corner stones for achieving ultracold temperatures, laser cooling and evaporative cooling, the latter fails to work for a sample of spin-polarized fermions.

In evaporative cooling [118, 73], the most energetic particles are forcibly removed from the trap, while the remaining atoms rethermalize to a lower temperature. In a spin-polarized cloud of fermionic atoms, however, s-wave ("head-on") collisions are forbidden by the Pauli principle, and p-wave collisions will be frozen out at low temperatures[1]. After removal of energetic particles, the sample would not thermalize.

The way out of this dilemma is to use a coolant: This can be either a second spin state of the same fermionic atom [76, 100, 130] or another atomic species [247, 214, 112, 207, 97, 137, 225, 184, 19]. In such a mixture, s-wave collisions between different atoms or spin states are allowed and sympathetic cooling of fermions can

[1]We can estimate the temperature for which p-wave collisions can occur, using the van-der-Waals potential $-C_6/r^6$. The kinetic energy of the colliding particles with angular momentum $\hbar$ must exceed the centrifugal barrier: $E > \hbar^2/\mu r_0^2 - C_6/r_0^6 = 2\hbar^2/3\mu r_0^2$, where $\mu = m/2$ is the reduced mass and $r_0 = \left(3\mu C_6/\hbar^2\right)^{1/4}$ is the position of the barrier. For ^{6}Li, $r_0 = 70\,a_0$ and thus $k_B T \approx 8$ mK. At the temperatures achieved by laser-cooling ($\sim 500\,\mu$K in our magneto-optical trap for ^{6}Li), p-wave collisions are frozen out.

proceed. In our experiment, fermionic ^{6}Li is cooled by a cloud of bosonic ^{23}Na atoms in a magnetic trap, after an initial stage of laser cooling.

The choice of ^{6}Li as the fermion species is simply explained by the relatively high natural abundance of about 7% percent, allowing the use of an atomic beam source, and the ease of laser cooling of alkali atoms. The only other stable fermionic alkali atom, ^{40}K, has a natural abundance of only 0.01%. The common conclusion is that it needs to be enriched in an expensive process, precluding its use in a high-flux atomic beam oven[2]. Our group's expertise in Bose-Einstein condensation of sodium atoms - in 2001 there existed three working sodium BEC-machines - made the choice of the coolant a natural one. With ^{23}Na, the largest alkali condensates (containing up to 100 million atoms) have been produced. The large number of available sodium atoms presents an ideal refrigerator with large heat capacity. However, at the time the project was started, the collision properties between sodium and lithium atoms were completely unknown. It was thus a gamble whether sympathetic cooling would be feasible at all. Nature was kind: The approach led to the production of large clouds of about 50 million degenerate fermions [111] and to condensates containing about 10 million fermion pairs, a number that is a factor of 50-100 larger than that produced in other experiments. This strong atomic signal certainly helped in the discovery of small features such as vortices (chapter 6) or faint kinks (chapters 5 and 7) in the density profile of fermionic superfluids.

4.1 Experimental setup

Table 4.1 summarizes the strategy followed to cool a gas of ^{6}Li fermions from temperatures of 700 K in an oven down to 50 nK deep in the superfluid regime. It involves a series of different techniques which all have to work reliably to produce a consistent sample in every experimental run. From beginning to end, the sequence lasts about 40 s, the longest stage being the $\sim 15 - 20$ s of RF evaporation of sodium in the magnetic trap.

The techniques of laser cooling and evaporative cooling in a magnetic trap, leading to Bose-Einstein condensation, are nicely described in the Nobel lectures of 1997 (laser cooling, S. Chu [60], W. Phillips [194] and C. Cohen-Tannoudji [63]) and 2001 (Bose-Einstein condensation, E. Cornell, C. Wieman [67] and W. Ketterle [136]). Detailed descriptions of a sodium BEC-apparatus can be found in PhD-theses [232, 57] of

[2]An atomic beam source for non-enriched potassium has been demonstrated very recently in the Ketterle group [261].

Stage	Temperature	^{6}Li Atom number	Density	T/T_F
Two-species oven	720 K	$3 \times 10^{11} \frac{\text{atoms}}{s}$	$10^{14}\,\text{cm}^{-3}$	10^8
Laser cooling (*Zeeman slower & MOT*)	1 mK	$\sim 3 \times 10^8$	$10^{10}\,\text{cm}^{-3}$	10^4
Sympathetic cooling (*Magnetic trap*)	1 μK	5×10^7	$5 \times 10^{12}\,\text{cm}^{-3}$	0.3
Evaporative cooling (*Optical trap*)	50 nK	2×10^7	$5 \times 10^{12}\,\text{cm}^{-3}$	0.05

Table 4.1: Different stages during the preparation of a superfluid Fermi gas. Typical numbers for the temperature, atom number, density and degeneracy factor T/T_F are given. Up to the last stage, the gas is spin-polarized. In the optical trap, a spin-mixture of the two lowest hyperfine states of ^{6}Li is evaporatively cooled close to a Feshbach resonance.

former members of the Ketterle group. The addition of fermionic ^{6}Li to an existing sodium BEC apparatus[3] required designing a double-species oven, described in detail in the PhD thesis of Cladiu Stan [233], as well as providing laser light for laser-cooling of ^{6}Li. Details on the latter can be found in my thesis written for the French Magistère de Physique [264], as well as in Zoran Hadzibabic's PhD thesis [110].

The experimental setup is sketched in Fig. 4-1. Hot (~450 degrees C) ^{6}Li and ^{23}Na atoms escape from the oven chamber, traverse a Zeeman slower and are captured in a double-species magneto-optical trap (MOT). We obtain about 10^{10} sodium atoms and $3 \cdot 10^8$ lithium atoms stored at temperatures of about 1 mK and densities of $\sim 10^{10}\,\text{cm}^{-3}$ for ^{6}Li and $\sim 10^{11}\,\text{cm}^{-3}$ for ^{23}Na. The phase space densities of the clouds are about 10^{-7}. The temperature is limited by the natural line width of the optical transition (Doppler limit, see e.g. [194]). Hence, to advance further, the trapping light needs to be switched off and the atoms are transferred into the conservative potential of a Ioffe-Pritchard DC magnetic trap. It is crucial in our scheme to prepare the two species in their respective "stretched hyperfine states", that is, both the nuclear and electronic spins of each atom need to be aligned with the magnetic field. This ensures that interatomic collisions (which to a good approximation preserve the total spin projection on the magnetic field axis) cannot transfer atoms into other spin states (so-called spin-exchange collisions) - a process that could potentially release a large amount of energy and heat the sample.

[3]It is the same apparatus that produced the first sodium Bose-Einstein condensates in 1995.

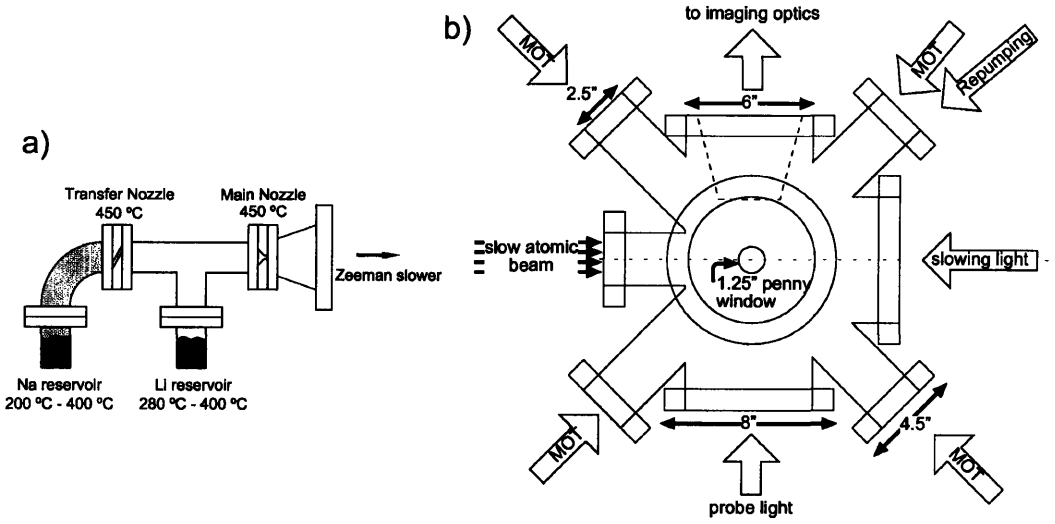

Figure 4-1: Experimental setup. a) The source of atoms, a double species oven for ^{6}Li and ^{23}Na. b) Main chamber, showing the setup for the MOT and slowing beams and one of the two possible imaging directions.

Optical Pumping into the Stretched State Fig. 4-2 provides a closer look at the hyperfine states of ^{23}Na and ^{6}Li. All alkali atoms have a single unpaired valence electron, so $S = 1/2$. As ^{23}Na has a nuclear spin $I = 3/2$, we have $(2S+1)(2I+1) = 8$ hyperfine states available. For ^{6}Li with $I = 1$, there are 6 hyperfine states. Only so-called "low-field seeking" states can be magnetically trapped[4], leaving us in principle with three options for sodium (not counting the weakly trapped $|2,0\rangle$ state) and three for lithium. Inspection of possible (that is, energetically favored) spin-exchange collisions eliminates all combinations but two [110]:

$$\begin{aligned} |2,2\rangle_{\mathrm{Na}} + |3/2,3/2\rangle_{\mathrm{Li}} \quad & \text{(stretched states)} \\ |1,-1\rangle_{\mathrm{Na}} + |1/2,-1/2\rangle_{\mathrm{Li}} & \end{aligned}$$

As we see from Fig. 4-2, the lithium state $|1/2,-1/2\rangle$ is only low-field seeking below 27 G. The lithium cloud would need to be colder than about 300μK in order not to spill out from the trap. Clearly, the robust solution is to prepare both atomic species in their respective stretched state[5].

[4]Maxwell's equations only allow magnetic field minima in free space. Thus, only states that minimize their energy at low field can be trapped.

[5]Historically, the stretched state combination was not the first to be tried [112], since sodium had initially only been condensed in the $|1,-1\rangle$ state, and inelastic losses in the $|2,2\rangle$ state were known

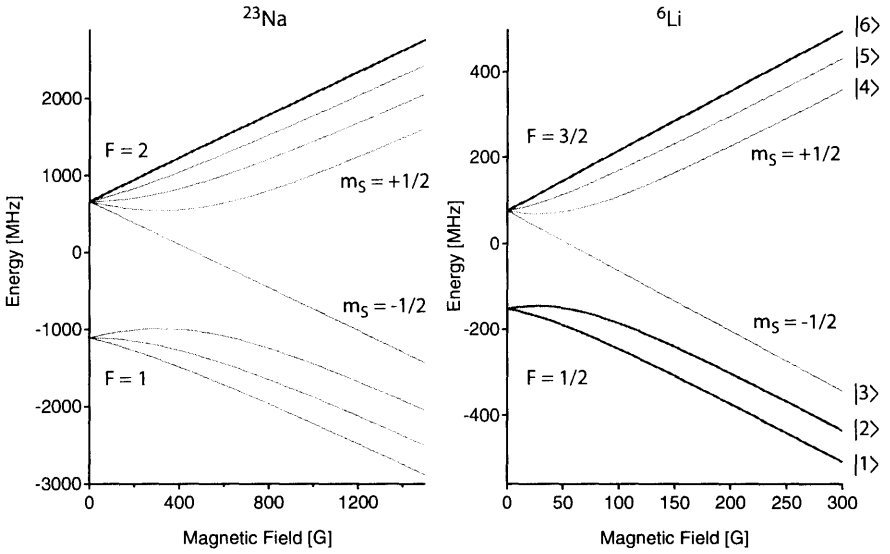

Figure 4-2: Hyperfine states of ^{23}Na and ^{6}Li. Energies are relative to the situation without hyperfine interaction. The sodium hyperfine splitting is $a_{\mathrm{hf}}^{\mathrm{Na}} = 1.77$ GHz, for lithium it is $a_{\mathrm{hf}}^{\mathrm{Li}} = 228$ MHz. Good quantum numbers at low field are the total (nuclear plus electronic) spin F and its z-projection, m_F. At high field, it is the electronic and nuclear spin projections m_S and m_I. The states relevant for the experiment are marked with thick lines. Evaporative cooling of sodium and sympathetic cooling of lithium are performed in the upper, stretched states. In the final stage of the experiment, the strongly interacting Fermi mixture is formed around the Feshbach resonance at 834 G (not shown in the graph) using the two lowest hyperfine states of lithium, labelled $|1\rangle$ and $|2\rangle$.

We achieve spin-polarization of lithium and sodium by optical pumping for ~ 500 μs with σ^+ polarized light right after switching off the MOT trapping light. For ^{6}Li, both F (hyperfine-changing) and m_F (Zeeman-changing) pumping is used, while for ^{23}Na we only employ F-pumping[6]. Next, the Ioffe-Pritchard magnetic trap is switched on. A "purification" stage ensures that only stretched states remain in the trap: With the ^{23}Na F-pumping light (resonantly exciting $F = 1$ atoms) still illuminating the cloud, the bias field of the trap is increased to 80 G. At this field, all hyperfine states are resolved by RF spectroscopy at our initial temperatures of about 1 mK. A 0.6 s

to be more severe. Only later was condensation achieved also in the stretched state [111], greatly facilitating cooling of lithium.

[6]Zeeman or m_F-pumping for ^{23}Na can improve the sodium numbers by ~30%, which is usually not worth the additional effort.

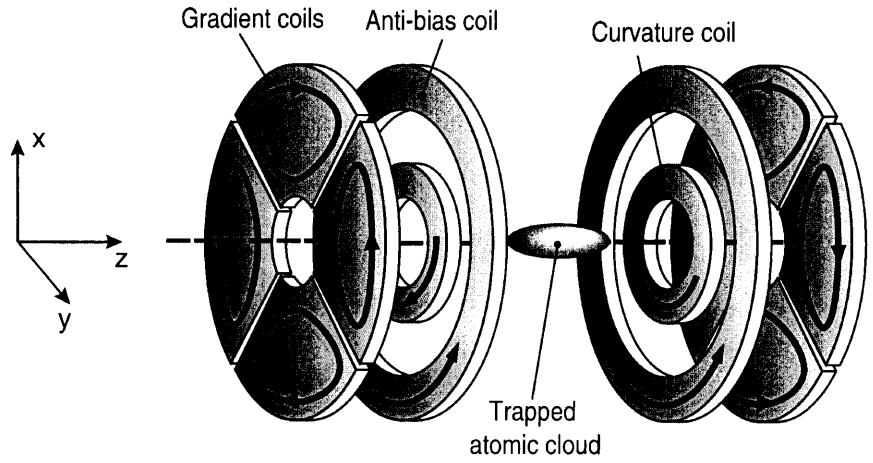

Figure 4-3: Magnetic trap for sympathetic cooling of ^{6}Li with ^{23}Na. The trap consists of a "curvature coil" that produces an axially confining potential. Its offset magnetic field is cancelled to about 0.5 G by the "anti-bias coil". Radial confinement is provided by the gradient coils which are wound in "cloverleaf" configuration. They replace the four Ioffe bars in a standard Ioffe-Pritchard trap. The anti-bias coils are used at a later stage to access the wide Feshbach resonance between states $|1\rangle$ and $|2\rangle$ at 834 G.

microwave sweep near the hyperfine splitting of ^{23}Na at 1.77 GHz transfers possible $|2,1\rangle_{\mathrm{Na}}$ and $|2,0\rangle_{\mathrm{Na}}$ ^{23}Na-atoms into the untrapped $|1,0\rangle_{\mathrm{Na}}$ or $|1,1\rangle_{\mathrm{Na}}$ state. Here, the atoms get "a second chance" to be transferred into the stretched state via absorption of the F-pumping light. If they again end up in the "wrong" m_F-state, they are finally expelled from the trap by another 1.2 s microwave sweep, this time with the pumping light switched off. The final transfer efficiency from the MOT into stretched states in the magnetic trap is about 30-40% for sodium, and about 40-50% for ^{6}Li.

4.2 Sympathetic cooling of ^{6}Li by ^{23}Na

Once the atoms are loaded into the magnetic trap (see Fig. 4-3), ^{23}Na is evaporatively cooled by forcibly removing energetic atoms with a microwave "knife" tuned to the $|2,2\rangle \rightarrow |1,1\rangle$ hyperfine transition above 1.77 GHz. The lithium atoms are insensitive to this frequency and simply cool via thermalization with sodium atoms. After 15 s of evaporative cooling, the trap is adiabatically decompressed over 1 s in order to reduce the effect of inelastic collisions in the increasingly dense sodium cloud. Without the lithium cooling load, another 5 s of evaporative cooling result in a Bose-Einstein

condensate of 10^7 sodium atoms. For experiments with lithium, sodium is completely evaporated over 5 s, leaving a degenerate cloud of about $N = 5 \cdot 10^7$ spin-polarized ^{6}Li fermions at a temperature of $T \approx 0.3T_F$, where $k_B T_F = \hbar\omega(6N)^{1/3}$ is the Fermi energy, and ω is the geometric mean of the trap frequencies.

If less lithium atoms are initially loaded into the magnetic trap, the cooling load for sodium is smaller, resulting in a lower final temperature of the fermionic cloud, with $T \approx 0.05T_F$ [111]. However, it is not preferable to minimize temperature at the cost of atom numbers at this stage, as further manipulations of the cloud necessarily increase entropy. There are two main reasons for this increase in entropy:

1. The next stage of the experiment will require the transfer of the spin-polarized cloud from the magnetic into an optical trap. As the two traps are never perfectly "mode-matched" (e.g. they do not have equal trapping frequencies in the case of harmonic trapping), the non-interacting Fermi gas, initially prepared in equilibrium, is necessarily brought into a non-equilibrium distribution. Once the gas is allowed to thermalize (see below), this will result in an increased entropy.

2. The experiment proceeds by creating a two-state Fermi mixture from the initially spin-polarized cloud. This is achieved in two steps: First, starting with all atoms in the initial state $|1\rangle$, a radiofrequency (RF) Landau-Zener sweep transfers all atoms into a coherent superposition of the initial state and the state that we want to populate, $|2\rangle$. This coherent manipulation obviously preserves entropy. However, as atoms travel along different paths in the trap, they pick up different phases in the inhomogeneous magnetic field and decohere. Even if we had started with a zero-temperature Fermi sea of $|1\rangle$-atoms, we are now left with two Fermi clouds of $|1\rangle$- and $|2\rangle$-atoms in which every second momentum state is unoccupied within the original Fermi sphere. Clearly, the final temperature will not be zero but rather a good fraction of the Fermi temperature.

We see that it does not pay off to reach very low temperatures at the cost of atom number. Further evaporative cooling after loading the optical trap and creating the two-state mixture is needed. This will actually be more efficient than sympathetic cooling by sodium atoms, due to the strong interactions between the two fermionic spin states. The true figure of merit of the sympathetic cooling stage is thus the number of atoms that can be loaded into the finite volume of the optical trap.

4.3 Preparation of an interacting Fermi mixture in an optical trap

At the end of the sympathetic cooling stage, we are left with a degenerate Fermi gas of atoms polarized in the stretched hyperfine state of ^{6}Li, $|F, m\rangle = |3/2, 3/2\rangle$. As p-wave collisions are frozen out and s-wave collisions are forbidden by the Pauli principle, such a non-interacting gas represents indeed one of the most "ideal" gases imaginable. Evidently, in order to study *interacting* Fermions, a second spin state needs to be populated to again allow for s-wave collisions. Unfortunately, all mixtures of two magnetically trappable hyperfine states in ^{6}Li are unstable with respect to spin-changing collisions[7]. However, the lowest two hyperfine states of ^{6}Li, $|1\rangle \equiv |1/2, 1/2\rangle$ and $|2\rangle \equiv |1/2, -1/2\rangle$ are stable. Furthermore, as we have seen in chapter 3, their interactions are tunable over a wide range in the vicinity of a Feshbach resonance. Both states $|1\rangle$ and $|2\rangle$ are high-field seeking at the relevant magnetic fields around the Feshbach resonance. We are thus forced to use an optical trap, which can hold atoms regardless of their spin.

4.3.1 Magnetic plus optical trapping

As atoms are polarizable particles, they are attracted by a static or slowly oscillating electric field (slow on the timescale of electronic transitions). A laser beam detuned to the red of the atomic transition (= slowly oscillating) thus traps the atoms at its intensity maximum. Our optical dipole trap (ODT) consists of a single laser beam [8] at a wavelength of $\lambda = 1064$ nm, a maximum power of 4 W and a waist ($1/e^2$-radius) of about[9] $w = 125\,\mu$m. The maximum trap depth is about $k_B \times 10\,\mu$K, just about enough to catch the degenerate Fermi cloud in the magnetic trap with Fermi energy $k_B \times 3\,\mu$K. We take great care to ensure a radially symmetric trapping potential, needed for the study of rotating quantum gases described in chapter 6. The maximum radial trapping frequency is 300 Hz. The axial trapping provided by the laser beam is very weak, due to the laser beam's large waist and accordingly slow beam divergence (Rayleigh range $z_0 = \pi w^2/\lambda = 4.6\,$cm!). If the optical trap was the only potential acting on the atoms, the aspect ratio of the trapped cloud

[7] $|3/2, 3/2\rangle + |3/2, 1/2\rangle \rightarrow |3/2, 3/2\rangle + |1/2, 1/2\rangle + 11$mK; $|3/2, 3/2\rangle + |1/2, -1/2\rangle \rightarrow |3/2, 1/2\rangle + |1/2, 1/2\rangle$, and $|1/2, 1/2\rangle$ is untrapped; $|3/2, 1/2\rangle + |1/2, -1/2\rangle \rightarrow |3/2, -1/2\rangle + |1/2, 1/2\rangle$, both states are untrapped.

[8] Yb fiber laser, 20 W, IPG Photonics model PYL-20-LP

[9] Waist and maximum power have changed many times over the years. I present here the most recent setup, used to detect vortices in fermionic superfluids (see chapter 6).

would be $\sqrt{2}z_0/w \approx 500$ and the axial trapping frequency only 0.5 Hz. To ensure a more manageable geometry and faster dynamics, we clearly need additional magnetic confinement in the axial direction. This is conveniently provided by the "curvature coils" already used in the magnetic trapping stage. They create a magnetic saddle point potential with typical axial trapping frequency of $\nu_z = 23\,\mathrm{Hz}$. The radial anti-trapping with (imaginary) frequency $\nu_r = i\,23/\sqrt{2}\,\mathrm{Hz}$ is negligible compared to the strong radial confinement provided by the ODT.

4.3.2 Spin transfer

At the end of sympathetic cooling in the magnetic trap, the spin-polarized Fermi gas is loaded into the optical trap by ramping up the laser power over 300 ms. The radial confinement of the magnetic trap can now be removed, which is done by reducing the current in the "gradient coils" (see Fig. 4-3) to zero[10] over 1 s. The atoms, all polarized in the stretched state $|F, m\rangle = |3/2, 3/2\rangle$, experience now the radial confinement of the optical trap plus the axial magnetic curvature. The transfer into state $|1\rangle \equiv |1/2, 1/2\rangle$ can be simply achieved by a RF sweep across the single-photon $|3/2, 3/2\rangle \rightarrow |1/2, 1/2\rangle$ hyperfine transition at 228 MHz. However, state $|1\rangle$ atoms are high-field seekers and thus experience an *anti-trapping* axial curvature after the spin flip. By quickly reversing the sign of the axial magnetic bias field the atoms are trapped again (see Fig. 4-4). To minimize heating of the cloud due to expansion in the transient anti-trap, the field curvature is reduced before the spin transfer, and the magnetic field reversal takes place after less than half a trapping period. A more elegant solution to this spin flip problem would be to use a more tightly focussed ODT (which we avoid for other reasons, see chapter 6) or a second optical dipole trap that provides axial confinement regardless of the atomic spin. However, subsequent evaporative cooling of the interacting $|1\rangle$-$|2\rangle$ mixture (see below) will efficiently remove the produced heat.

At this stage, the magnetic field is now increased to values around the Feshbach resonance between state $|1\rangle$ and $|2\rangle$ (see chapter 3), located at $B = 834\,\mathrm{G}$. Here, the ^{6}Li hyperfine states are in the Paschen-Back regime, that is, the electron and nuclear

[10]This is a slightly delicate process, as one needs to ensure that the center of the magnetic trap remains aligned with the optical trap at all times during the current ramp. In the radial direction, this trap center is defined by the zero-point of the radial magnetic fields. To this one must add the influence of gravity, leading to sag. The position of the optical trap can be different, due to requirements at later stages of the experiment (as in chapter 6). Additional bias fields in the radial direction allow to overlap the magnetic trap with the optical trap, but the required field values depend on the current in the cloverleaf coils. Hence, the bias fields need to be dynamically adjusted as the gradient current is reduced.

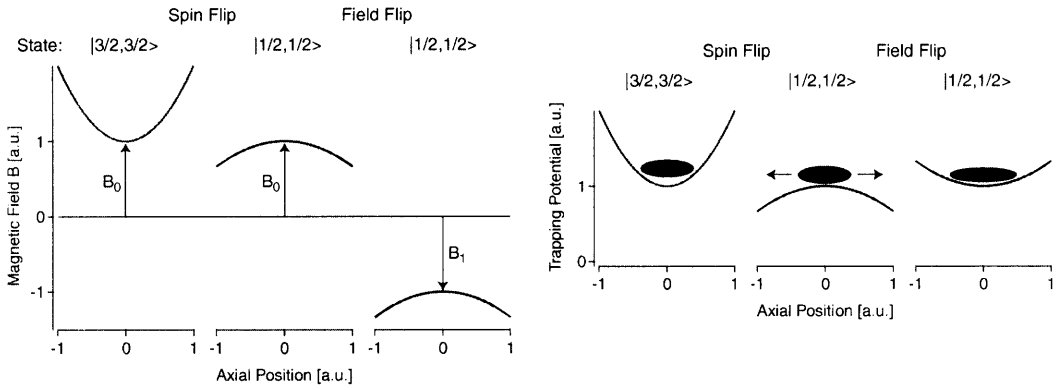

Figure 4-4: Hyperfine transfer of the cloud in a magnetic field curvature. The atoms are initially trapped in state $|3/2, 3/2\rangle$. After the spin transfer into state $|1/2, 1/2\rangle$, the atoms are no longer trapped. Quickly reversing the sign of the magnetic field retraps the atoms.

spins are decoupled. Both state $|1\rangle$ and $|2\rangle$ have their electronic spin aligned with the applied magnetic field and thus have practically identical magnetic moments of 1 Bohr magneton. They only differ by the projection of the nuclear spin, $m_I = +1$ for state $|2\rangle$, and $m_I = 0$ for state $|1\rangle$. An RF Landau-Zener sweep at about 80 MHz can easily transfer atoms in state $|1\rangle$ into state $|2\rangle$. The final population in the two spin states can be controlled by the sweep rate: The Landau-Zener probability for the transfer $|1\rangle \rightarrow |2\rangle$ is

$$P_{|1\rangle \rightarrow |2\rangle} = 1 - \exp(-2\pi \frac{\Omega_R^2}{\dot{\omega}}),$$

where Ω_R^2 is the square of the Rabi frequency, proportional to the power of the RF wave, and $\dot{\omega}$ is the frequency sweep rate. For a fully adiabatic transfer, $\Omega_R^2 \gg \dot{\omega}$ and all atoms are transferred into state $|2\rangle$. A non-adiabatic transfer can produce any final spin mixture.

One should note that the RF sweep is a coherent process that does not directly convert atoms into another spin state (see [266], reprinted in appendix A). Rather, each atom is brought into a coherent superposition state $\sim a\,|1\rangle + b\,|2\rangle$. A non-interacting, degenerate Fermi gas of atoms in state $|1\rangle$will still be a spin-polarized Fermi gas after the sweep, but now all atoms are polarized in the superposition state. Clearly, we require a decoherence mechanism to truly *populate* the two distinct spin states. This mechanism is found in the inhomogeneous magnetic field experienced by the atoms, which scrambles their relative phase as they follow different paths in the

trap. By recording the onset of interactions in our cloud, we have measured [106] the typical timescale for this decoherence to be tens of milliseconds for our magnetic field curvatures. This is on the order of the axial trapping period, which is a sensible result.

Once the fully decohered spin-mixture is created, efficient evaporative cooling of the gas can begin. We typically lower the trap depth U over several seconds down to about $1\,\mu$K to enforce evaporative cooling. At this point, U becomes comparable to the Fermi energy of the cloud, and further reduction in trap depth leads to strong losses as atoms spill out from the trap. We reach temperatures of $T/T_F \approx 0.05$ in a Fermi mixture containing a total of about 10^7 fermion pairs.

Chapter 5

Bose-Einstein condensation of fermion pairs

The hallmark of Bose-Einstein condensation in atomic gases was the sudden appearance of a dense central core in the midst of a large thermal cloud [12, 72]. This direct signature in the density distribution derives from a clear separation of energy scales in weakly interacting gases. The condensate's repulsive mean-field $\mu \propto na$ is much smaller than the critical temperature (times k_B) at which condensation occurs, $T_C \propto n^{2/3}$: The gas parameter na^3 is much less than 1 (about 4×10^{-6} for our sodium condensates). In a harmonic trap, the different energy scales directly translate into the different sizes of a thermal cloud, $R_{\rm th} \propto \sqrt{T}$, and of a condensate $R_C \propto \sqrt{\mu}$. However, in the case where μ becomes comparable to $k_B T_C$, the condensate is no longer clearly separated from the thermal cloud, hindering the direct observation of condensation.

This is the situation we encounter in our Fermi mixture close to the Feshbach resonance. In not too strongly interacting gases of *molecules*, it was indeed possible to observe the characteristic bimodal density distribution known from atomic BEC [102, 271, 26, 36, 188] (section 5.1). The fact that molecules could be created [205] and were found to be stable and long-lived close to a Feshbach resonance [69, 128, 239, 202] was crucial for this observation. It finds its explanation in the fermionic nature of the molecules' constituents [193].

As the interactions between molecules are increased by moving closer to the Feshbach resonance, the size of the molecular condensate grows and the bimodal feature close to T_C becomes invisible[1]. Now interactions dominate the appearance of both the normal and the condensed cloud. At the same time - this is the essence of the

[1]This is *almost* true. See section 5.3 below and section 7.4.

BEC-BCS crossover - the composite nature of the molecules starts to play a role. The constituent fermions, no longer spread out in k-space due to the molecular binding, start experiencing Pauli pressure from the presence of others. The cloud size increases even further until finally, on the BCS-side of the resonance, the size is completely dominated by the single-particle energy, the Fermi energy E_F. This is evidently the same size the system would have in the normal state.

For this reason it seems no longer possible, in the strongly interacting regime, to detect the superfluid phase transition in the density profile of the gas. To the rescue comes the fact that in atomic Fermi gases, the interaction strength can be tuned at will, on timescales short compared to the growth time of the condensates. This allows to effectively "map" the condensate wavefunction in the strongly interacting regime onto a molecular condensate wavefunction far away from resonance. If this is done in the moment of releasing the gas from the trap, the final image of a molecular cloud will again reveal a bimodal density distribution: The condensate surrounded by a thermal cloud.

This method was employed by the JILA group [203] in a Fermi mixture of ^{40}K, and subsequently in our group for ^{6}Li [272] to infer condensation of fermion pairs on the BCS-side of the Feshbach resonance.

In the following I will first introduce the methods that have allowed the formation of molecules, and present the observation of one of the first molecular Bose-Einstein condensates. Next, I will describe the technique that has allowed to infer condensation of fermion pairs on the BCS-side of the Feshbach resonance, where pairing is purely a many-body effect. Finally, I will present unpublished data showing a direct signature of the condensate in the density profile of the gas on resonance.

5.1 Bose-Einstein condensation of molecules

5.1.1 Feshbach resonances

Even before one could enter the realm of many-body physics, Feshbach resonances have opened a new avenue in the physics of atoms and molecules: They have allowed the production of ultracold molecules starting with ultracold atoms. The first observation of a Feshbach resonance in ultracold atoms [126, 235] showed strong losses in the atomic signal that were attributed [250, 168, 259] to the formation of ultracold, highly vibrationally excited molecules. It was predicted that these molecules, formed out of two bosonic atoms, would undergo fast vibrational relaxation into more tightly

bound molecules. Still, in experiments on ^{85}Rb, the presence of the molecules, as short-lived as they were (lifetime $\sim 100\,\mu s$) could be detected via coherent beats between the free atomic and the bound molecular state [81]. Studies of the decay of *fermionic* gases close to a Feshbach resonance [78, 36, 202] held a peculiar surprise: The maximum atom loss was not centered on resonance, but was shifted towards regions where the Feshbach molecular state was already quite deeply bound. The gas close to resonance was *stable* [78, 174, 36, 204], in stark contrast to the bosonic case. This molecular state could be *reversibly* populated via a magnetic field sweep across resonance [205], at a conversion efficiency exceeding 90% [69, 121]. Most importantly, it was found to be long-lived [69, 128, 239], with lifetimes between about 100 ms (for ^{40}K) and several 10 s (for ^{6}Li). This is to be compared to the conversion efficiencies of only 5%-10% and lifetimes on the order of 5 ms observed in bosonic gases [117, 255, 84].

It is this long lifetime which in the case of ^{6}Li has allowed to simply evaporatively cool the gas close to the Feshbach resonance to create molecules [128], populating the molecular state via collisions, and not via a magnetic field sweep.

5.1.2 Methods for making molecules

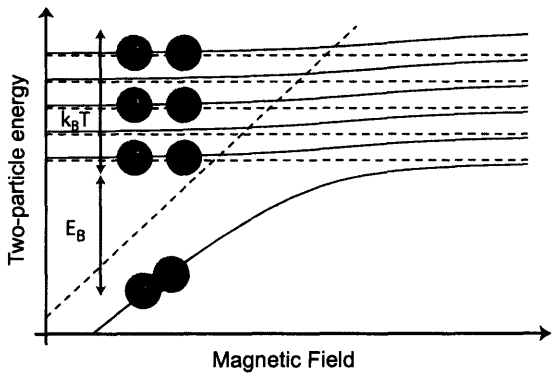

Figure 5-1: Creating molecules via three-body collisions. A molecular state is coupled to the continuum (see Fig. 3-3). As the gas is cooled on the molecular side, the molecular state is populated vie three-body collisions. If the binding energy is not much larger than k_B times the temperature, the energy carried away by the third body does not substantially heat the sample. For fermionic particles, further vibrational decay into small molecules is strongly suppressed due to Pauli blocking.

There are essentially two ways to create molecules out of unbound atoms close to a Feshbach resonance. Three-body collisions and coherent two-body adiabatic transfer.

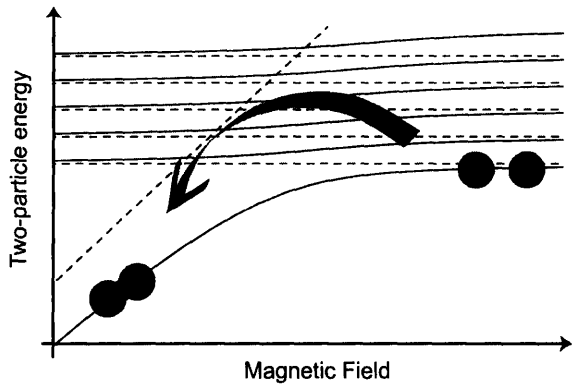

Figure 5-2: Creating molecules via magnetic field ramps. A magnetic field sweep can transfer unbound atoms adiabatically into the molecular state, much like a two-level Landau-Zener transition.

In the three-body process, two of the colliding particles form a molecule, the third carrying away the leftover energy and momentum. In a typical situation, molecular states are deeply bound compared to the temperature of the gas (times k_B). The released energy in such a collision thus usually heats up the cloud, leading to trap loss (hence the name "bad collisions"). However, in the case of a very weakly bound molecular state close to a Feshbach resonance, the binding energy can be on the order of the temperature, and molecules can efficiently form without severe heating and trap loss (Fig. 5-1). Subsequently, leftover atoms can be efficiently evaporated from the optical trap. Weakly bound molecules have twice the atomic polarizability, hence the optical trap is twice as deep for molecules than for single atoms.

The molecules are only stable if the decay into more deeply bound molecular states is suppressed in some ways. It turns out that for fermions there is such a suppression mechanism: The Pauli principle. Decay into a deeply bound state requires three fermions to be very close to each other in the final state of this process. With only two spin states available, this is strongly forbidden [193]. For bosons, the decay process is actually enhanced close to a Feshbach resonance, which results in molecular lifetimes of only a few ms [117, 255, 84].

The second process is reversible, it does not generate heat and makes use of the tunability of the molecular state: Starting with unbound atoms in the continuum, one can adiabatically sweep the magnetic field across resonance and form a bound molecule (Fig. 5-2). It is very helpful to think of this sweep in terms of a two-level Landau-Zener sweep through an avoided crossing. For a coupling matrix element V

between two "bare" states, $|a\rangle$ and $|b\rangle$, and an energy sweep rate $\dot{E}$, one finds [168]

$$P_{|a\rangle\to|b\rangle} = 1 - e^{-c\frac{|V|^2}{\hbar\dot{E}}} \tag{5.1}$$

for the probability $P_{|a\rangle\to|b\rangle}$ to make a transition from $|a\rangle$ to $|b\rangle$ as the bare state energies are swept through resonance. Here c is a numerical constant on the order of 1.

In the case of Feshbach resonances, the two "levels" are the molecular state and the energy of two unbound atoms. V is the coupling matrix element $V = \sqrt{N/\Omega}\, g_0 = \sqrt{N}\, \langle\varphi_b| V_{\rm hf}^- |\Psi_k\rangle$ that we have encountered in chapter 3. The number N of atom pairs that appears in $|V|^2$ accounts for the fact that each spin up atom has N chances to form a molecule with a spin down atom per volume Ω. If we take our simple Feshbach model of chapter 3, we can replace $g_0^2 = \frac{4\pi\hbar^2}{m} a_{\rm bg}\, \Delta\mu\Delta B$. The bare state energies are tuned via the magnetic field, so $\dot{E} = \mu_B \dot{B}$. We have then

$$P_{\rm atoms\to molecules} \simeq 1 - e^{-A\frac{n}{\dot{B}}} \tag{5.2}$$

with $A = c\frac{4\pi\hbar a_{\rm bg}\Delta B}{m}$. That is, the higher the density and the slower the magnetic field ramp across resonance, the more efficient the production of molecules [141].

The simple two-state picture is obviously flawed, as the state of two unbound atoms belongs to a continuum. Also, we neglect here the fact that two atoms need to encounter each other in real space before the transition to the molecular state can take place. In a "hot" atomic cloud, the production efficiency for adiabatic sweeps will thus be less than 100%. In a semi-classical picture, we can expect that the efficiency will be maximum if the two atoms belong to the same phase space cell. In a zero temperature cloud, one would expect 100% efficiency of the sweep, as was discussed in [121].

It should be noted that this coherent way of producing molecules generally does not lead to a thermal equilibrium state if the sweep is too fast. The molecular cloud needs to thermalize via collisions before it can settle into equilibrium (where, for example, parts of it might be Bose condensed).

Distinguishing atoms from molecules

An amazing property of the molecular state close to resonance is its long range. A most important consequence is that we can directly *image* the molecules using the same laser light that is absorbed by unbound atoms. This is possible as long as the

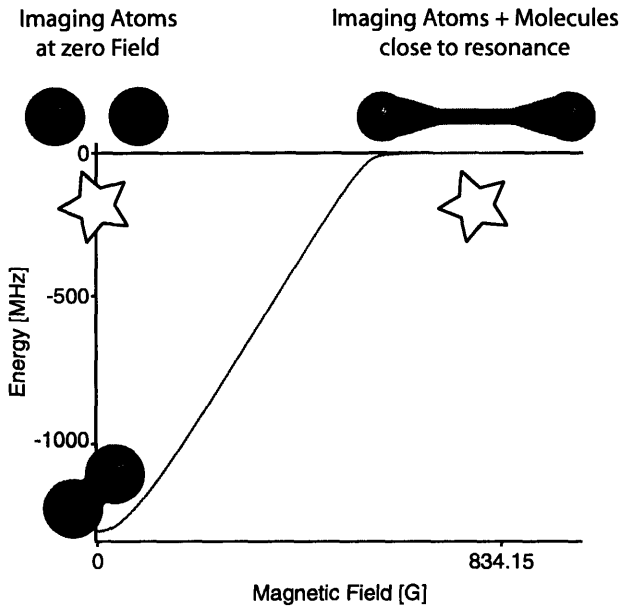

Figure 5-3: Imaging atoms and molecules. At zero field, only unbound atoms are imaged. Tightly bound molecules do not absorb the imaging light resonant with unbound atoms. Close to resonance, the molecules are so weakly bound that their constituent atoms absorb light just like unbound atoms.

molecular size is much larger than the wavelength (divided by 2π).

The easiest way to *distinguish* atoms from molecules is to take an image at low field, where the tightly bound molecules are detuned far from resonance (and their line strength is diluted over the many excited molecular states), see Fig. 5-3. Alternatively, one can dissociate the molecules into an unoccupied state using an RF pulse [205] and subsequently image that state with a resonant laser beam. Yet another diagnostic tool is the use of a Stern-Gerlach field gradient [128] to separate molecules from atoms in a regime where their magnetic moments already differ substantially.

5.1.3 Formation of molecules

In a first experiment to locate the resonance, one can prepare a Fermi mixture on the "BCS"-side of the Feshbach resonance, where no two-body molecular bound state is available to atom pairs. As the magnetic field is swept across resonance, molecules will form and, accordingly, the signal from unbound atoms taken with low-field imaging will diminish (Fig. 5-4). This is a standard technique to locate Feshbach resonances [205, 117, 234]. From Fig. 5-4 we determine a value of $B_0 = 838 \pm 27$ G

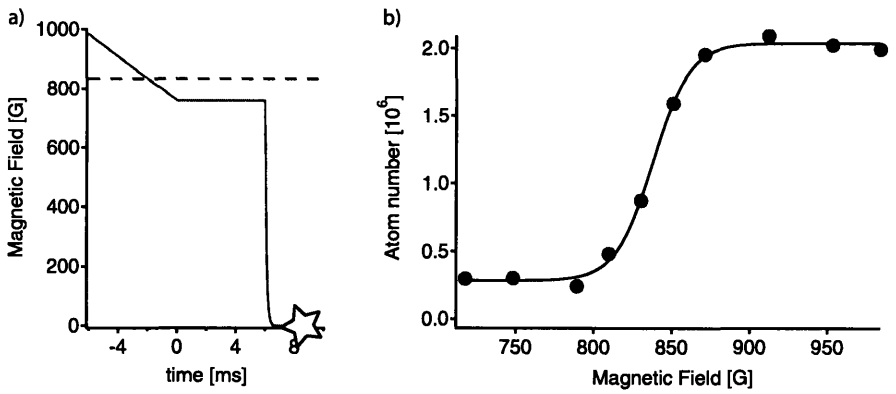

Figure 5-4: Molecule formation by magnetic field sweep across the Feshbach resonance. a) Experimental procedure. A Fermi mixture prepared on the BCS-side of the Feshbach resonance is swept across resonance (shown as the dashed line) to form molecules. The gas is released from the trap at the end-point of the ramp at time $t = 0$ ms. Zero-field imaging is used to be sensitive to only the leftover atoms. b) Atomic signal vs end-point of the magnetic field sweep. The line is a fit to an error-function, whose center is determined to be 838 ± 27 G, with an uncertainty given by the 10%-90% width (54 G).

for the position of the resonance.

Seeing the atomic signal disappear can easily mislead one to believe that the atoms are simply lost from the trap. However, the process is reversible: Ramping back across resonance will dissociate the molecules (if done non-adiabatically, this process can heat the cloud in the trap [171]).

In fact, the dissociation method gives a more accurate determination of the location of the Feshbach resonance [203, 272]. To avoid effects due to the high density in the trap (i.e. many-body physics), the molecular cloud is expanded to a 1000 times lower density, about $10^{10}\,\mathrm{cm}^{-3}$. Then the magnetic field is ramped to a value B_{test}. If B_{test} lies above the Feshbach resonance, the molecules will dissociate into unbound atoms, which can subsequently be detected at low field.

The very sharp onset of the atomic signal at $B_{\mathrm{test}} = 821 \pm 1$ G is striking (see Fig. 5-5) and suggests this magnetic field value as the position of the Feshbach resonance. However, using molecular RF spectroscopy on a bound-bound transition between two different Feshbach molecular states, the group of R. Grimm in collaboration with the NIST theory group was able to infer the location of the Feshbach resonance [2] at

[2] A reason for our lower value could be few-body collisions, even at 1000 times lower density: At 821 G, $a = 30\,000\,a_0$ and $k_F a$ is still on the order of 1. Another systematic shift could be the finite ramp speed employed, that might dissociate the extremely weakly bound molecules at 821 G

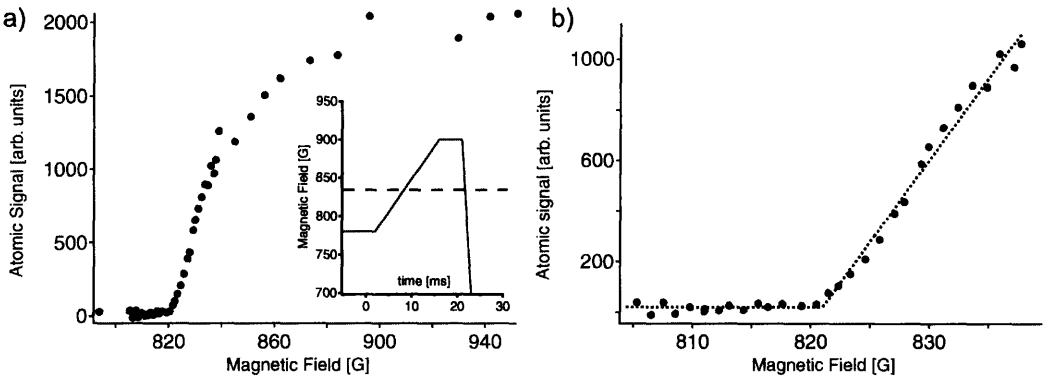

Figure 5-5: Locating the Feshbach resonance by molecule dissociation. The experimental procedure is shown in the inset. A molecular cloud is prepared on the BEC-side of the Feshbach resonance, at 780 G, and released from the trap at $t = 0$ ms. After some expansion, the field is ramped to a test value around resonance (shown as the dashed line), held constant and is finally brought to zero field, where only unbound atoms are imaged. a) The atomic signal as a function of the test field shows a sharp threshold behavior at 821 ± 1 G, where the uncertainty is the statistical error of a threshold fit, shown in b).

834.1 ± 1.5 G [24].

From Fig. 5-5 we can directly see that before dissociation, more than 99% of the gas exists in form of molecules. The reason is that this molecular cloud was formed via the three-body process, by simply cooling the gas at the fixed field of 780 G (the BEC-side of the resonance). The lifetime of the weakly bound molecules is so long, and the binding energy is so small that losses and heating are negligible, and, after evaporation of leftover unbound atoms, essentially all particles are bound into molecules.

Coupling strength

Fig. 5-6 demonstrates the extremely strong coupling strength of the ^{6}Li Feshbach resonance. In this experiment, a Fermi mixture is released from the trap at $B = 840$ G, slightly above the Feshbach resonance. After a varying expansion time, the magnetic field is switched off to zero field (at an initial slew rate of $\dot{B} = 30\,\mu$s/G), where the remaining atomic signal is detected. At the high density of the trap, almost

(binding energy 30 nK!). We searched for a dependence of the resonance location on these effects and estimated that they could contribute an up-shift of the position by 3 ± 3 G each. This is barely within the error margin of the RF spectroscopy result.

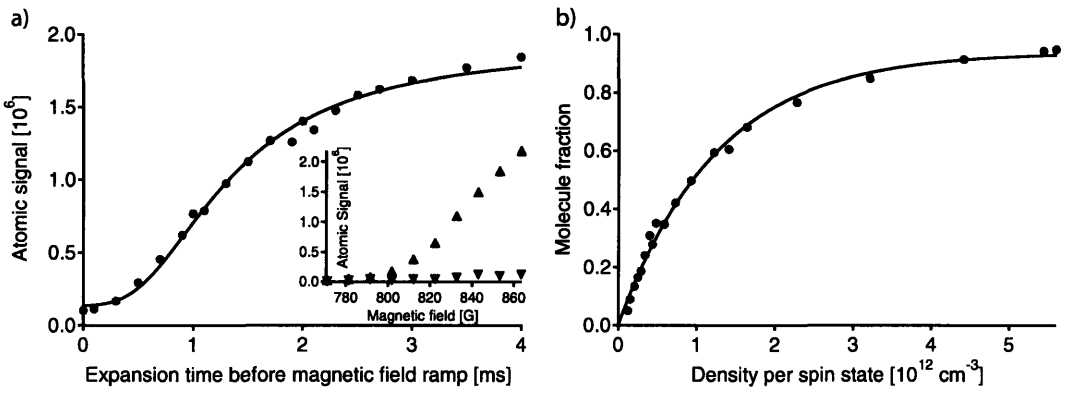

Figure 5-6: Revival of the atomic signal during expansion and strength of Feshbach coupling. a) The magnetic field is switched off after varying expansion times for a cloud released at 840 G. The field ramp creates molecules more efficiently at the high densities of the trap than at low densities after long expansion. The inset shows the atomic signal for immediate switch off (triangles pointing down) and for a switch off after 4 ms expansion (triangles pointing up). In b), all of the atomic signal loss is interpreted as molecular conversion and plotted as a function of density. The density was calibrated by imaging the cloud at high field for varying expansion times. All fits are for the simple Landau-Zener-model described in the text.

the entire atomic signal has vanished, the loss being almost 95%. However, as the density decreases during expansion, the atomic signal revives, indicating that the atoms were not truly "lost" but only "hidden" in the molecular state. In Fig. 5-6 b) we tentatively interpret all the atomic signal loss as conversion into the weakly-bound molecular state[3]. This conversion efficiency is plotted versus the density per spin state at the given expansion time. Using the simple fit function given by the Landau-Zener formula Eq. 5.2, we find $A \approx 24 \frac{\mathrm{G}}{10^{12}\,\mathrm{cm}^{-3}\,\mu\mathrm{s}}$ with a relative error of 50% due to the uncertainty in the atom number.

The prediction is Eq. 5.2 with $c = 2\pi$, and using the lithium parameters we find

$$A = \frac{8\pi^2 \hbar a_{\mathrm{bg}} \Delta B}{m} = 19 \frac{\mathrm{G}}{10^{12}\,\mathrm{cm}^{-3}\,\mu\mathrm{s}} \tag{5.3}$$

The agreement is quite good but might be fortuitous, as the simple formula does not take temperature and other effects into account (see [121] for a discussion of more complete models and comparison with experiments). Also, here we have not directly observed the molecular state, but only the loss in atomic signal, which could

[3]Other loss-channels like unobserved molecular states cannot be excluded here.

be enhanced due to collisions after the ramp, leading to the formation of more deeply bound molecules. Nevertheless, while the maximum conversion efficiency might be subject to these systematics, the shape of the density dependence is likely less affected, especially at low densities where collisions after the ramp should be negligible.

The strong coupling to the molecular state does not allow us to be fast compared to the two-body time scale at the density of the trapped gas. For a typical $n = 5 \times 10^{12}\,\mathrm{cm}^{-3}$, in order to convert less than 10% of the atoms into molecules, we would have to ramp at a rate of 1200 G / μs, about 40 times faster than the limit set by our coil inductance.

On the other hand, this efficient molecule conversion will be very useful in section 5.2, where the state of the fermion pair condensate above resonance is "frozen in" by the rapid ramp into a condensate of molecules. That is, the ramp can be faster or comparable to the many-body time scale but still slow enough for efficient molecule formation.

For comparison, for the Feshbach resonance at $B = 202$ G used in experiments with ^{40}K we have $A = 0.9 \frac{\mathrm{G}}{10^{14}\,\mathrm{cm}^{-3}\,\mu\mathrm{s}}$ (close to the measured value $0.7 \frac{\mathrm{G}}{10^{14}\,\mathrm{cm}^{-3}\,\mu\mathrm{s}}$ [205]), resulting in efficient conversion into molecules at about 2000 times slower ramp rates.

5.1.4 Observation of molecular Bose-Einstein condensates

After the successful creation of ultracold molecules out of ultracold atoms via Feshbach resonances in gases of fermions [205, 69, 128, 239] and bosons [81, 117, 255, 84] the intriguing question was whether thermal equilibrium could be reached and cold enough temperatures realized to observe the onset of Bose-Einstein condensation in gases of molecules.

In the case of ^{6}Li the long lifetime of molecules [36] (see Fig. 5-7) enables us to evaporate the Fermi mixture at a fixed magnetic field, just as if one were to cool a cloud of bosonic atoms towards BEC. As the mixture is cooled by ramping down the trapping laser power, molecules form as the temperature becomes comparable to the binding energy. Accordingly, the atomic signal observed in zero-field imaging vanishes: We can see this in Fig. 5-5 for fields below resonance, where essentially no atomic signal is measured. What renders evaporation very efficient is the fact that molecules, having twice the polarizability of an atom, experience twice the trap depth for unpaired atoms. The potentially energetic atoms produced during a molecule-forming three-body collision are efficiently removed from the trap.

To observe the molecules directly, one can either use high-field imaging (see Fig. 5-

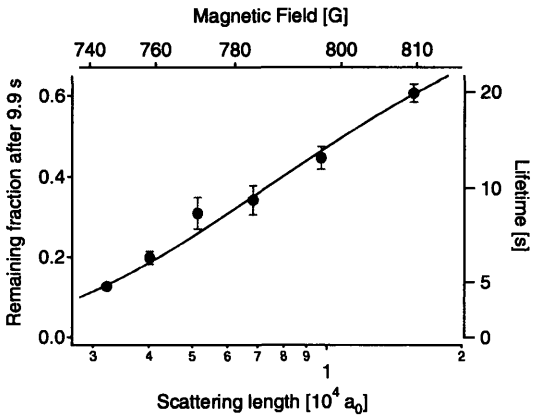

Figure 5-7: Lifetime of molecules in partially condensed clouds. The cloud with initially about 1×10^6 molecules was held for 9.9 s (initial density about $5 \times 10^{12}\,\mathrm{cm}^{-3}$, slightly varying with the interaction strength). Shown is the remaining fraction as a function of scattering length. The lifetime $1/\Gamma$ is calculated under the simplifying assumption of a pure exponential decay $e^{-\Gamma t}$. The line is a fit with a power law for $\Gamma = ca^{-p}$, giving $p = -0.9$. The clouds were partially condensed (up to 80% condensate fraction at the largest scattering length), and all measurements were done in the strongly interacting regime where $a > 1/k_F$, so the expression for the relaxation rate differs from the prediction for weakly interacting, thermal molecules ($\Gamma = ca^{-2.55}$) [193].

3) or one can dissociate them as in Fig. 5-5 by crossing the resonance shortly before taking an absorption image at zero field. Below a certain temperature, one observes the striking onset of a bimodal density distribution, the hallmark of Bose-Einstein condensation (see Figs. 5-8 and 5-9). In contrast to weakly interacting Bose gases, the condensate peak is not much smaller than the thermal cloud, indicating a large mean-field energy of the BEC, comparable to k_B times the condensation temperature. As we move closer to the Feshbach resonance, the size of the condensate grows to be almost that of a degenerate Fermi gas. Figure 5-10 illustrates this fact for an essentially pure condensate at 780 G.

We thus start entering the situation outlined in the introduction: All energy scales approach each other. The molecules are no longer tightly bound and far from each other, but rather their average distance $n_M^{1/3}$ from each other becomes comparable to the molecular size in free space, given approximately by the scattering length. One has already entered the strongly interacting regime of the BEC-BCS crossover.

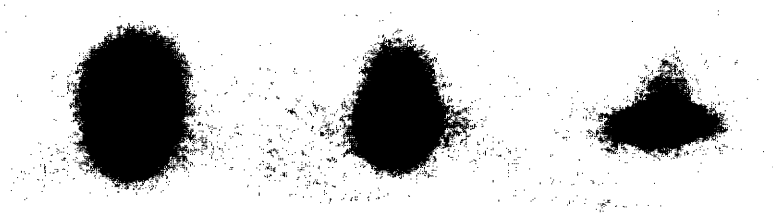

Figure 5-8: Observation of Bose-Einstein condensation of molecules. As the trap depth is lowered (from left to the right image), the characteristic bimodal density distribution appears in the molecular cloud.

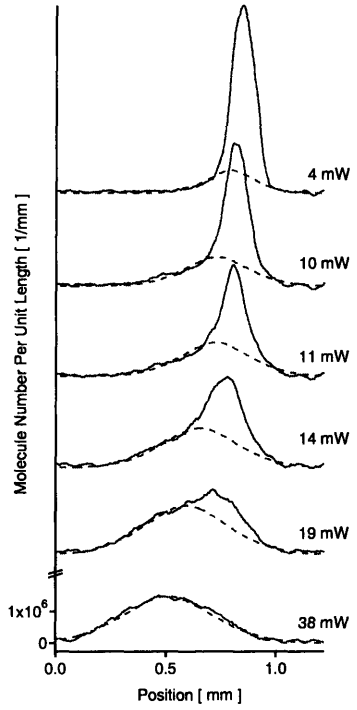

Figure 5-9: Bimodal density distribution emerging in a cloud of molecules. Shown are radially integrated profiles of absorption images such as those in Fig. 5-8, as a function of final laser power. The dashed lines are fits to the thermal clouds.

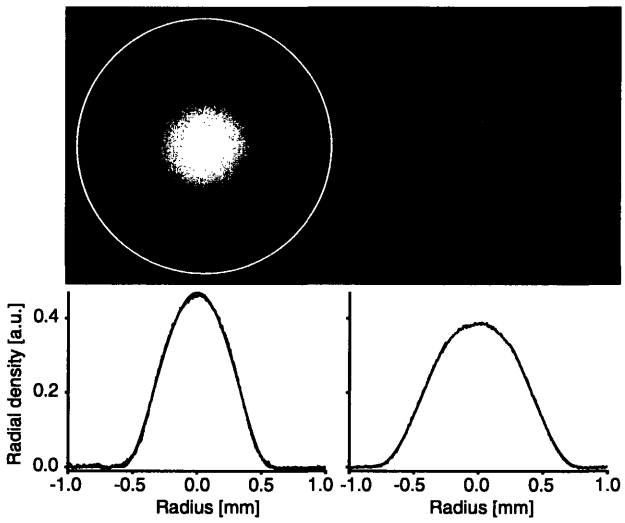

Figure 5-10: Comparison between a molecular BEC (a) and a degenerate Fermi sea (b). The condensate containing $N_m = 6 \times 10^6$ molecules is in the strongly interacting regime at a magnetic field of 780 G ($1/k_F a = 0.6$). Its size is almost as large (factor ~ 0.7) as a non-interacting Fermi sea containing N_m atoms, indicated by the white circle. Image and profile b) show an essentially spin-polarized Fermi sea (minority component of $< 2\%$ not shown) containing $N = 8 \times 10^6$ atoms at the same field. The images were taken after 12 ms expansion with the probe light aligned with the long axis of the cigar-shaped clouds.

5.2 Condensation of fermion pairs close to a Feshbach resonance

In contrast to the case of molecular condensates, the superfluid in the strongly interacting regime does not appear to spatially separate from the normal state. This is the main "dilemma" with strongly interacting Fermi gases, dramatically shown in recent high-resolution images (see Fig. 5-11). A second difficulty with Fermion pair condensates on the BCS-side is the fragility of the pairs: During expansion, the gas becomes more dilute, and the pair binding energy can decrease below (k_B times) the local temperature. Thus, the pairs can break in time of flight (see chapter 6 for a study of this effect using vortices). Clearly, a new detection method is needed to infer condensation on the BCS-side of the resonance.

5.2.1 The rapid ramp technique

Such a method was introduced by the JILA group [203], and later adapted to ^{6}Li by our group [272]. The idea behind the rapid ramp technique is to "rescue" the fragile fermion pairs by sweeping the magnetic field towards the BEC-side of the resonance, thereby transforming them into stable molecules (see Fig. 5-12). This is done in the moment the trap is switched off for expansion. If each fermion pair is transferred into a tightly bound molecule, the momentum information of the original pair is preserved. Time-of-flight analysis of the resulting molecules should thus allow to infer the momentum distribution of pairs in the gas above resonance.

This technique has enabled us to demonstrate fermion pair condensation in the entire BEC-BCS crossover. Sample images and profiles of the resulting molecular clouds are shown in Fig. 5-13. The drastically reduced interaction results in a clear separation of the condensate from the "thermal" or uncondensed part of the cloud[4]. The fact that this can be seen even with low-resolution imaging (compare the profiles in Fig. 5-13 from February 2004 with those in Fig. 5-11 obtained two years later) demonstrates the power of the method. Note that the rapid ramp converts atoms into molecules with higher than 90% efficiency for all fields in the BEC-BCS crossover,

[4]At zero field, the scattering length between molecules should be on the order of the singlet scattering length of lithium atoms, which is about 40 a_0. The exact value is not known. In fact, the residual mean-field interaction at zero field is so low that the condensate practically does not expand if the rapid ramp is performed immediately after switching off the trap. For this reason, it is sometimes beneficial to let the cloud expand by some amount *before* the rapid ramp is performed. This converts some of the interaction energy in the cloud into kinetic energy, which lets one "choose" the final expanded size of the molecular condensate.

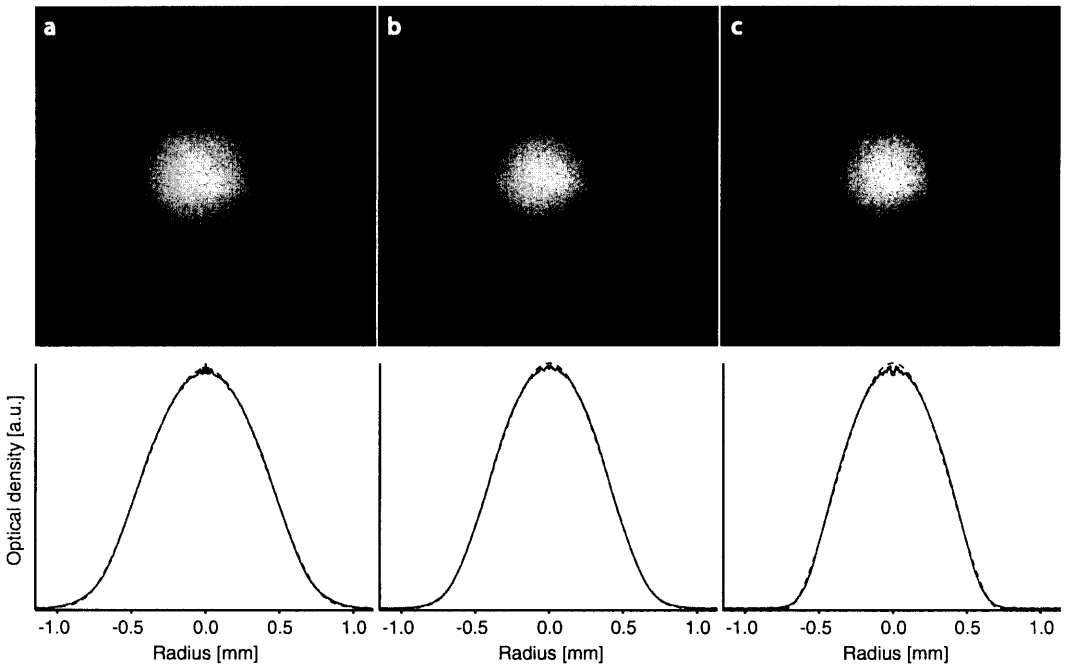

Figure 5-11: The dilemma with strongly interacting Fermi gases: The superfluid appears not to leave a trace in the density profile of the gas. Shown are high-resolution images (from February 2006) of spin up atoms in a resonantly interacting, equal mixture of spin up and spin down for different temperatures. The lower graphs show aximuthally averaged radial profiles (noise level well below 1% of the maximum optical density). All three clouds are very well fit using a finite-temperature Thomas-Fermi distribution (with fugacity $e^{\mu/k_B\widetilde{T}}$, central density n_0 and mean square radius $\langle r^2 \rangle$ as free parameters, see Eq. 2.28). However, the empirical temperatures of $\widetilde{T}/T_F = 0.22$ (a), 0.13 (b) and 0.075 (c) determined from the profiles' wings indicate that at least clouds b and c should be in the superfluid regime (which is indeed the case, see chapter 6). Trap parameters $\nu_r = 162$ Hz, $\nu_z = 22.8$ Hz, 10 ms time of flight, expansion factor 13.9, atom numbers N per spin state were 10.2 (a), 9.5 (b) and 7.5 $\times 10^6$.

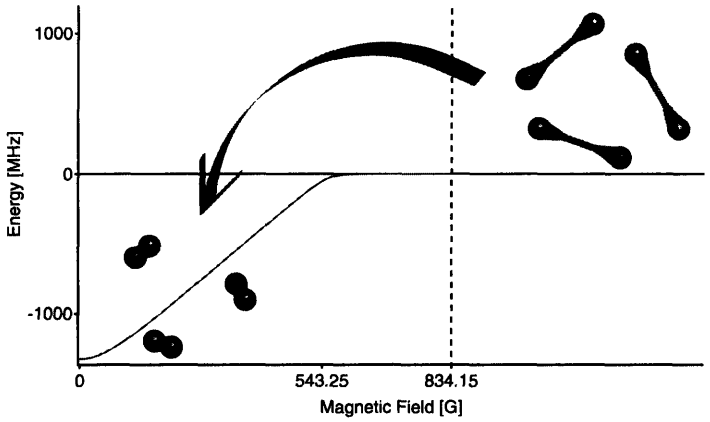

Figure 5-12: Rapid ramp to the molecular side to observe pair condensation. Immediately after switching off the trapping beam, the magnetic field is ramped to zero field. This converts long-range pairs into stable, tightly bound molecules. Momentum information of the original pairs is thus preserved.

see the discussion in section 5.1.3 above and Fig. 5-6.

5.2.2 Condensate fraction in the BEC-BCS crossover

The condensate fraction was determined by fitting a bimodal distribution to the profiles like those in Fig. 5-13, a parabola for the central dense part and a gaussian for the thermal background. To our surprise, we found very large condensate fractions throughout the entire BEC-BCS crossover, with a peak of 80% at $B \approx 820\,\mathrm{G}$, close to, but still on the BEC-side of the resonance (determined via RF spectroscopy and theory [24] to be $B_0 = 834$ G)[5] (see Fig. 5-14). It is intriguing to note that around the same field, a minimum in the damping of collective excitations was found [25].

The high condensate fraction might be a hint that the pairs in the strongly interacting regime on the BCS-side of the resonance are still smaller than the interparticle spacing, and not larger as one would expect from long-range Cooper pairs. In this case, it is intuitive that each atom of a given pair can still form a molecule with its original partner during the rapid ramp. If the pairs were much larger than the interparticle spacing, molecules might rather form out of uncorrelated atoms, resulting in a thermal cloud after the ramp. In accord with this argument, BEC-BCS crossover theory predicts that the pairsize ξ will be smaller than the interparticle spacing $n^{-1/3}$

[5]Interestingly it is at this magnetic field where the sharp onset of the dissociation threshold was found (see discussion of Fig. 5-5 above).

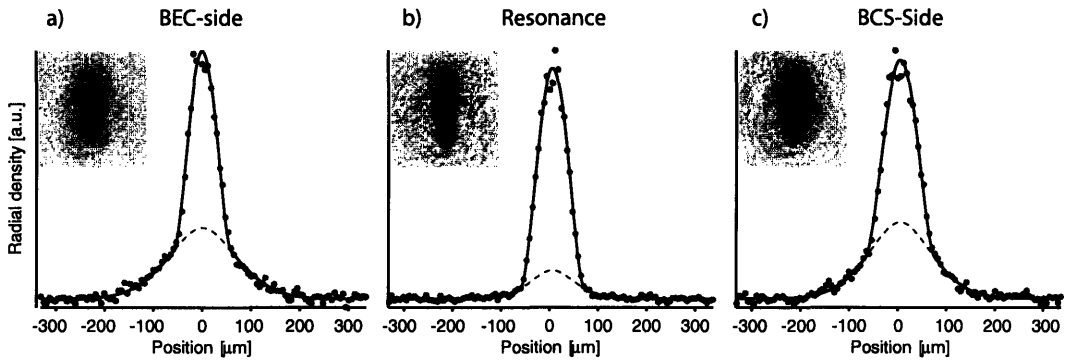

Figure 5-13: Fermion pair condensates. Axial density of the atomic cloud after the rapid ramp to zero field (in $< 100\,\mu s$), further expansion (for 10 ms), and dissociation of the resulting molecules by ramping back across resonance. The initial field B_0, the number of fermion pairs N, the condensate fraction and the interaction parameter $1/k_F a$ where a) 745 G, 700 000, 47%, 1.2; b) 835 G, 1.4×10^6, 81%, 0.0 (resonance); c) 912 G, 1×10^6, 49%, -0.5.

up to $k_F a = -1$ (see chapter 2), which is indeed on the BCS-side of the resonance. So far no experiment on Fermi gases has shown condensation or superfluidity in a regime where $k_F|a|$ ($a < 0$) is significantly less than 1 and hence where pairing is truly long-range.

Let us also note that the high condensate fraction is in stark contrast to the maximum fraction of about 14% found in experiments with ^{40}K [203]. The cause for this discrepancy might be connected with the shorter lifetime of the Fermi mixture in ^{40}K close to resonance, on the order of 100 ms [202]. This lifetime might not have been sufficient to reach full thermal equilibrium of the gas in all three dimensions[6].

In our experiments, the condensates were found to be very long-lived. For a hold time of 10 s, the condensate fraction on resonance was observed to still be close to its initial value[7]. In fact, these lifetimes can very favorably compare to those found for atomic Bose-Einstein condensates.

[6]The axial trapping period in [203] was about 200 ms, comparable to the lifetime of atoms in the regime where condensation has been reported [202].

[7]On the BEC-side, it decayed more rapidly due to the increasing rate of vibrational relaxation of the molecules away from resonance. The decay in the condensate fraction on the BCS-side is likely caused by atom loss without change in temperature.

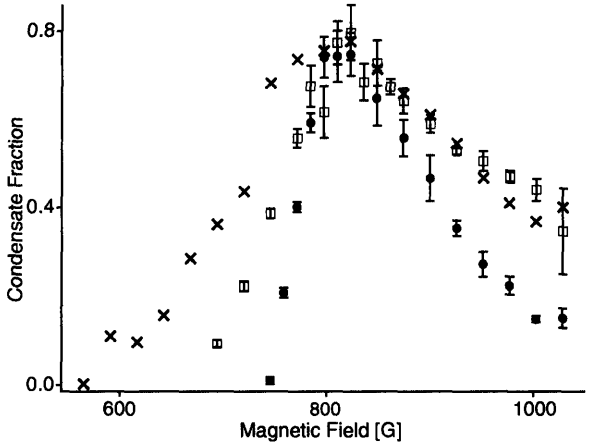

Figure 5-14: Condensate fraction in the BEC-BCS crossover as a function of the magnetic field before the rapid ramp. The symbols correspond to different hold times, 2 ms (crosses), 100 ms (squares) and 10 s (circles).

5.2.3 Discussion of the condensate fraction

Fig. 5-15 shows a "phase diagram" for the condensate fraction as a function of temperature. Several theoretical works [79, 20, 51] have confirmed the general behavior of the "critical temperature" of the observed condensation phenomenon in ^{40}K and in ^{6}Li. Also, the fact that high condensate fractions were found in our experiment could be explained within the BEC-BCS crossover model [191, 209, 181] and by Quantum Monte-Carlo simulations [18].

How does the condensate fraction change in the BEC-BCS crossover? On the molecular side of the resonance, even in the absence of losses due to vibrational relaxation, one would expect quantum depletion to reduce the condensate fraction. The Bogoliubov theory of chapter 2 predicts $\frac{8}{3}\sqrt{\frac{n_M a_M^3}{\pi}}$ for the condensate depletion in a molecular gas of density n_M and scattering length a_M. At $k_F a = 1$ (at about 750 G in our experiment) this would give 9% (we assume $a_M = 0.6a$ [193]). Evidently, close to resonance this first-order expression diverges. The quantum depletion on resonance will be a universal number.

On the BCS-side of the resonance, it is a priori not evident how a "condensate fraction" should be defined. If we ask for the superfluid density, this must of course equal the total density of the gas at zero temperature. This was in fact the way we normalized the order parameter $\psi(\mathbf{r})$ on the BCS-side in section 2.3.5. If the question concerns the fraction of paired fermions, this, too, would be given by 100% at $T = 0$.

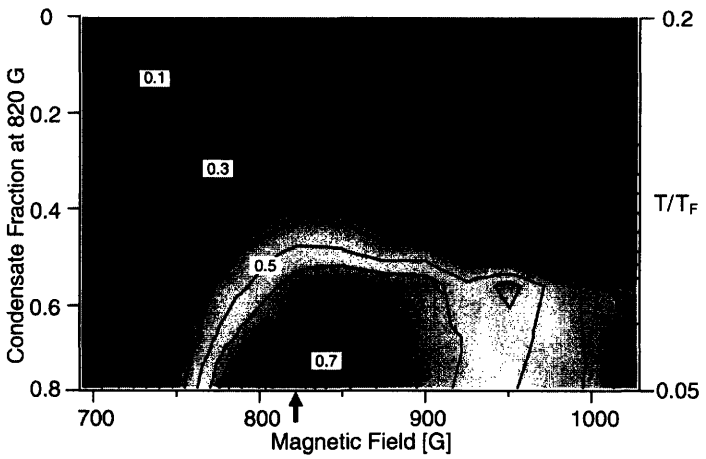

Figure 5-15: "Phase diagram" for the condensate fraction as a function of magnetic field and temperature. Condensates are obtained in the entire BEC-BCS crossover. The highest condensate fraction and highest onset temperature are obtained on the BEC-side close to resonance. As a model-independent measure of temperature, the condensate fraction at 822 G (see arrow) is used as the vertical axis. The Feshbach resonance lies close to this point, at 834 G.

However, we have seen in section 2.3 that we should not regard the BCS-state as a condensate of *bosonic* pairs: Anti-symmetrization of the many-body wavefunction spoils this picture. The definition of "condensate fraction" that is usually employed is a measure of coherence in the gas, the long-range order due to condensation. The quantity that expresses this coherence is the "Cooper pair wavefunction" $\phi(\mathbf{r}_1 - \mathbf{r}_2) = \left\langle \Psi_\uparrow^\dagger(\mathbf{r}_1)\Psi_\downarrow^\dagger(\mathbf{r}_2) \right\rangle$. The number of "condensed pairs" N_0 is the norm of $\phi(\mathbf{r}_1 - \mathbf{r}_2)$. With the tools of chapter 2 and following [209], we can calculate the condensate fraction within the variational BCS Ansatz:

$$N_0 = \int d^3r_1\, d^3r_2\, |\phi(\mathbf{r}_1 - \mathbf{r}_2)|^2 \tag{5.4}$$

Calculating this quantity for the BCS state one observes that the density of condensed pairs is

$$n_0 = \frac{N_0}{\Omega} = \frac{1}{\Omega}\sum_k u_k^2 v_k^2 = \frac{1}{4}\int \frac{d^3k}{(2\pi)^3}\frac{\Delta^2}{\xi_k^2 + \Delta^2} \tag{5.5}$$

Quite satisfactorily, the integral can be obtained analytically and we find with [209]

$$n_0 = \frac{m^{3/2}}{8\pi\hbar^3}\Delta^{3/2}\sqrt{\frac{\mu}{\Delta} + \sqrt{1 + \frac{\mu^2}{\Delta^2}}} \tag{5.6}$$

μ and Δ were calculated in chapter 2. In the BEC-limit, with the help of Eq. 2.111, this becomes the density of molecules or half the total atomic density n, as expected,

$$n_0 = n/2 \tag{5.7}$$

that is, all molecules occupy the same single-particle ground state. In the BCS-regime, where the gap is exponentially small, one finds [209]

$$n_0 = \frac{mk_F}{8\pi\hbar^2}\Delta = \frac{3\pi}{16}\, n\, \frac{\Delta}{E_F} \tag{5.8}$$

Also this result is natural: Loosely speaking, the pairs that truly contribute to coherence in the system reside mainly close to the Fermi surface, in an energy width of size Δ, so their density is simply $\sim n\Delta/E_F$.

On resonance, μ/Δ and Δ/E_F are universal numbers, for which the variational BCS approach provides the approximations 0.85 and 0.69, respectively. One finds a condensate fraction of

$$\frac{2N_0}{N} = 0.70 \tag{5.9}$$

Hence, the variational BCS-Ansatz provides a hint that the condensate fraction on resonance can indeed be large. Other studies have come to the same conclusion. For example, a Monte-Carlo study gives $2N_0/N \approx 0.60$ [18].

It is not evident that the rapid ramp method of the experiment directly measures this condensate fraction. Our experiments on the growth time of fermion pair condensates [270] and on the in-situ detection of condensation (see section 5.3 and chapter 7) and theoretical modelling of the ramp [79, 191, 10, 260] have shown that the observed bimodal density distributions provide a qualitative signature of a condensate on the BCS-side. It is an open question whether the obtained condensate fractions can provide a good quantitative measure of the coherent part on the BCS-side. Fig. 5-16 compares the variational BCS prediction to the data obtained via the rapid ramp. The very close agreement is fortuitous, but it is encouraging to see the correct trend on the BCS-side.

5.2.4 Discussion of the time scales involved

One objection to the rapid ramp method might be that the condensates could be formed *during* the ramp, on the molecular side of the Feshbach resonance. To rule out this possibility, we need to address the question on what time scales condensate

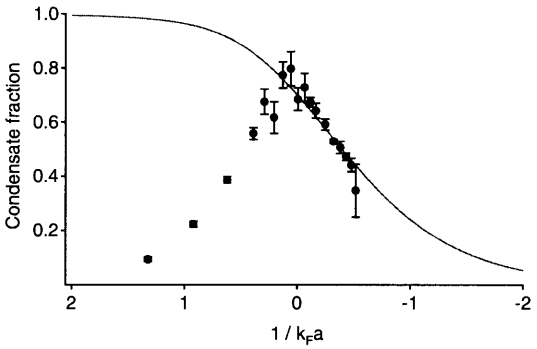

Figure 5-16: Condensate fraction as a function of the interaction strength in the BEC-BCS crossover. The circles show the 100 ms data of Fig. 5-14. The interaction strength is calculated using the known scattering length as a function of magnetic field and the experimental value $1/k_F = 2\,000\,a_0$. The curve shows the variational BCS prediction for the condensate fraction. The good agreement on the BCS-side should not be taken as proof that the rapid ramp truly measures the condensate fraction. On the BEC-side, heating due to vibrational relaxation leads to fast decay on the condensate. Figure adapted from [209] using Eq. 5.6.

formation takes place. Table 5.1 lists the different time scales of importance in our experiment.

Time scale	Formula	Value
Two-body physics	$\hbar/g_0\sqrt{2\pi n}$	20 ns
Magnetic field ramp (*timescale on which the molecular state changes with respect to threshold*)	$g_0\sqrt{2\pi n}/\Delta\mu\dot{B}$	80 ns
Fermi energy	$\hbar/E_F$	3 μs
Time required to leave resonance	$\Delta B/\dot{B}$	10 μs
Evolution of the gap at $k_F\lvert a\rvert = 2$	$\Delta/\dot{\Delta}$	10 μs
Gap at $k_F\lvert a\rvert = 2$	$\hbar/\Delta$	15 μs
Inverse collision rate at unitarity and $T/T_F = 0.1$	$\approx 0.23\,\hbar E_F/(k_B T)^2$ [95]	70 μs
Growth time of a pair condensate at $k_F\lvert a\rvert = 2$	$\approx \hbar E_F/\Delta^2$ [21]	75 μs
Radial trapping period	$2\pi/\omega_r$	2 ms

Table 5.1: Time scales involved in the rapid ramp technique

The fastest timescale is that relevant to two-body physics, the Feshbach coupling strength. At the high densities of our trapped samples, we cannot beat this even with our fastest magnetic field ramps (that is, switching off the power supply). As discussed in section 5.1.3, for our ramp speeds the conversion into molecules is always better than 90% for in-trap densities. The next fastest time scale is that set by the Fermi energy, which in the unitarity regime on resonance would set the timescale

for collisions in the normal Fermi gas, were it not for Pauli blocking (and factors of 2π etc.). The time it takes to leave the resonance region in our gas is a bit longer than the Fermi time scale, but might be smaller than the inverse collision rate. This would mean that the original momentum distribution of fermion pairs is truly "frozen in" during the ramp. The momentum distribution of the final molecules would then reflect that on the BCS-side.

The ramp is non-adiabatic on the time scale of the gap, which is forced to evolve faster than it can respond to the change in interaction strength, $\dot{\Delta}/\Delta \gtrsim \Delta/\hbar$. Finally, there is the relaxation time scale of the gas in response to a change in the particle distribution. In a normal Fermi gas of N particles at temperatures $T \ll T_F$, relaxation occurs via collisions of particles close to the Fermi surface, of number NT/T_F. Pauli blocking reduces the available final states for collisions by another factor of T/T_F, giving a relaxation time $\tau_R \approx \hbar E_F/(k_B T)^2$. In general, if the Fermi surface is smeared over an energy width ΔE, the relaxation time is $\tau \approx \hbar E_F/\Delta E^2$. In the case of a (BCS-type) superfluid, $\Delta E = \Delta$, and the relaxation time thus scales as $\tau_R = \hbar E_F/\Delta^2$.

We were able to show that fermion pair condensates grow indeed on a time scale long compared to the ramp time, comparable to the expected relaxation time scale [270]. This lends validity to the rapid ramp method.

This technique actually poses a difficult problem for many-body theory. For a Bose-Einstein condensate, problems that involve time variations can be treated with the time-dependent Gross-Pitaevskii equation (Eq. 2.65), which is applicable also at zero temperature. The single characteristic timescale involved is the mean-field timescale $\tau_\mu = \hbar/\mu$. For the BCS-case, the pendant to the Gross-Pitaevskii equation is the time-dependent Ginzburg-Landau equation for the order parameter $\Delta(\mathbf{r}, t)$ (see section 2.3.5), which is unfortunately only valid in a region of size $(T_C/E_F)^4$ close to the critical temperature, and other approaches are needed. It turns out that the gap introduces the time scale of coherent evolution of the wavefunction, while the relaxation time $\hbar E_F/\Delta^2$ gives the time scale for incoherent redistributions of the many-body state.

If the ramp is faster than all many-body time scales, the BCS-state needs to "project" itself onto the eigenstates on the BEC-side [79, 191, 10, 260], a process similar to an orthogonality catastrophe [260]. As the BCS-state can either decay into condensed or excited molecules, it is natural to expect the typical image of a condensate embedded in a thermal cloud after expansion.

In summary, our experiments show that one can indeed infer the existence of a fermion pair condensate on the BCS-side using the rapid ramp technique. It provides

us with a *qualitative* signature of condensation. The *quantitative* comparison between the observed condensate fractions and what is usually *defined* as a condensate fraction in BCS theory is, however, far from trivial [79, 191, 10, 51].

5.3 Direct observation of the phase transition in a resonantly interacting, equal mixture of fermions

5.3.1 The normal and the superfluid gas on resonance

Let us now return to the dilemma with strongly interacting Fermi gases we have seen in Fig. 5-11: The superfluid does not appear to leave a detectable trace in the density profiles of the gas on resonance. We can understand this qualitatively from the principle of universality: As the scattering length diverges, the only length scale of relevance is the interparticle spacing, $n^{-1/3}$. Accordingly, the only energy scale available is the Fermi energy, $\epsilon_F = \frac{\hbar^2}{2m}(3\pi^2 n)^{2/3}$. The chemical potential μ of the gas can thus only be ϵ_F times a universal constant:

$$\mu = \xi_s \, \epsilon_F \tag{5.10}$$

In a trap, the local chemical potential varies like $\mu(\mathbf{r}) = \mu - V(\mathbf{r})$, so we immediately deduce that for harmonic trapping the shape of the cloud, at least at zero temperature, must be given by

$$n(\mathbf{r}) = n_0 \left(1 - \frac{r^2}{R_{\mathrm{TF}}^2}\right)^{3/2} \tag{5.11}$$

with $n_0 = \frac{1}{3\pi^2}\left(\frac{2m\mu}{\xi_s \hbar^2}\right)^{3/2}$ and the Thomas-Fermi radius $R_{\mathrm{TF}} = \sqrt{\frac{2\mu}{m\omega^2}}$ (we consider a spherical trap without loss of generality). This shape is *identical* to the one we expect for a *normal* Fermi gas (see chapter 2). The only difference is the universal constant ξ_s appearing in μ and n_0. This parameter can indeed be measured for example by determining the cloud size [174, 26, 139, 187], or the release energy of the gas [37]. It is not difficult to check that

$$\mu = \sqrt{\xi_s}\, E_F \tag{5.12}$$

$$R_{\mathrm{TF}} = \xi_s^{1/4}\, R_F \tag{5.13}$$

with the usual expression for the Fermi energy of an equal mixture in a harmonic trap, $E_F = \hbar\omega(3N)^{1/3} \equiv \frac{1}{2}\, m\omega^2\, R_F^2$ and the total number of atoms, N.

The above consideration holds strictly only at zero temperature, where the gas we describe is the superfluid (hence the subscript s). The crucial point is now that *above* the critical temperature T_C, the normal state can have a *different* universal parameter ξ_n describing its zero temperature energy and size (which are, of course, never attained due to the transition to the superfluid state). It should then, in principle, be possible to directly observe the superfluid phase transition by a faint change in the density profiles, as an inner superfluid core emerges with a different equation of state (that is, if not accidentally $\xi_n = \xi_s$). It turns out that the superfluid constant ξ_s has been measured [174, 26, 139, 187] and calculated [43, 17, 44, 39] to be about

$$\xi_s \approx 0.45 \tag{5.14}$$

while the universal constant for the normal state has been obtained in [38, 39] to be about

$$\xi_n \approx 0.59 \tag{5.15}$$

Hence the characteristic size of a normal and a superfluid gas in a trap are expected to differ.

5.3.2 Anomalous features in the density profiles of expanded clouds at unitarity

To test this hypothesis, we have studied the density profiles of the unitary gas on resonance after expansion. To a very good approximation, the trapping potential was cylindrically symmetric (see chapter 6). This allowed us to obtain high-resolution profiles via azimuthal averaging. Temperature was varied by changing the final trap depth used during evaporation. After evaporative cooling, the trap was recompressed to a fixed trap depth ($U = 2.6\,\mu$K) before expansion. As an independent check for the superfluid phase transition, the condensate fraction was determined using the rapid ramp method, described in the previous section.

Sample profiles are shown in Fig. 5-17. The goal is to detect a *deviation* from the shape of a single-component fermionic cloud. We thus fit an unconstrained finite-temperature Thomas-Fermi function to the profiles. The relevant information is now contained in the residuals of such a fitting procedure. The quality of the fit, given by the parameter χ^2, is shown in Fig. 5-18 as a function of the trap depth. At tem-

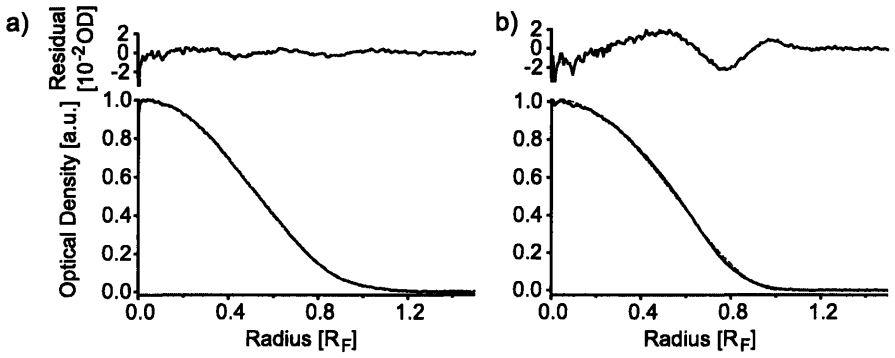

Figure 5-17: Density profiles of an equal Fermi mixture on resonance. The temperature in a) was $T/T_F \approx 0.15$, whereas in b) it was $T/T_F \approx 0.09$. Temperatures were determined from the thermal molecular cloud after the rapid ramp, and might not be quantitatively accurate. Both gas clouds contained a condensate after the rapid ramp to the BEC-side. The condensate fraction was: a) 7%. b) 60%.

peratures above 200 nK, the cloud is well fit by the Thomas-Fermi profile. However, as we lower the trap depth during evaporation below a certain value, the fits become suddenly worse than at high temperatures. Small "kinks" or changes in slope appear in the profiles. This could indicate that now (at least) two "species" in the gas compete for space. At our lowest temperatures, we see the quality of the fits to improve again, indicating that now a large fraction of the gas is in the superfluid state. The size of the cloud is then $R_{\mathrm{TF}} = 0.83R_F$, which gives $\xi_s \approx 0.47$, which is in accord with other experiments and theory [174, 26, 139, 187, 43, 17, 44, 39].

One should note that we never observe the fit residuals to deviate by more than 2% from the Thomas-Fermi shape. This explains why this effect has so far been too small to be observable. Note that the conventional way of measuring an effective temperature is to fit a Thomas-Fermi profile to the *entire* cloud. The small features we observe will bias the fits and thus systematically affect such temperature measurements. For example, the Thomas-Fermi fit to Fig. 5-17b would yield an unrealistically low temperature of $T/T_F < 0.01$. A better way to determine temperature would probably be to only fit the profile's wings, where the gas should be normal. The region to be included in the fit could be defined by requiring the quality indicator χ^2 to be as low as that found for normal, "hot" clouds above the phase transition. In Fig. 5-17b), such a procedure yields $\tilde{T}/T_F \approx 0.11$. This compares quite well to the value $T/T_F \approx 0.09$ obtained from the thermal distribution of molecular clouds observed after a rapid ramp to the BEC-side. However, the fact that the normal state

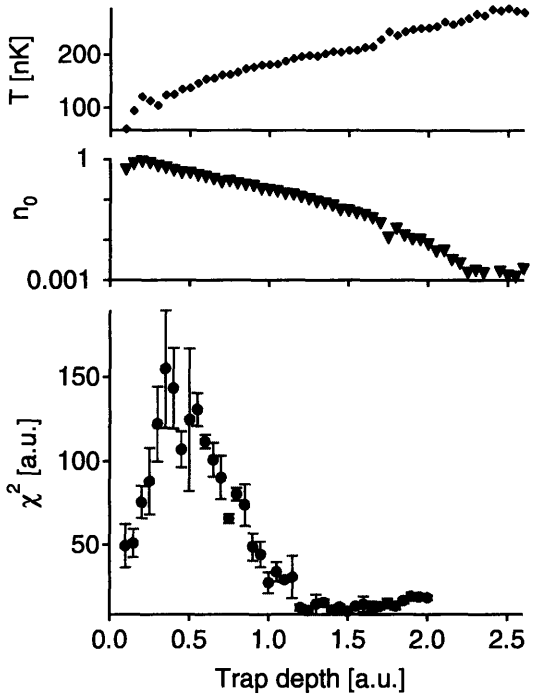

Figure 5-18: χ^2 of the Thomas-Fermi fit as a function of the final evaporation trap depth. χ^2 shows a strong dependence on temperature, as expected from theory [122, 190, 119, 230]. The condensate starts to form already around a trap depth of $U \sim 2.2$, and the fit-residuals in Fig. 5-19 indicate the same transition. The quality of the global fit does not appear to be sensitive to small condensates. The temperature was determined from the thermal wings of expanding molecular clouds after the rapid ramp. The Fermi temperature decreased slowly from 1.5 μK for $U = 2.6$ to 1.4 μK at $U = 0.4$, and dropped quickly due to atom spilling below $U = 0.2$. All measurements were done after recompression into a deeper trap with $U = 2.0$.

on resonance is still strongly interacting limits its use as a reliable thermometer.

A convenient way to graph fit residuals as a function of temperature is by means of a "density" plot of gray shades, with white and black corresponding to positive or negative deviations of the measured profile from the fit. This is shown in Fig. 5-19. Also included in this figure is the information on the density profiles and their curvature. While the profiles themselves do not appear to change with temperature (trap depth) on the scale of the plot, we observe an intriguing structure appearing in the residuals at an evaporation depth of about $U = 2\,\mu$K. The curvature of the density profiles shows a similar qualitative behavior.

As a strong indication that the observed feature indeed stems from the superfluid,

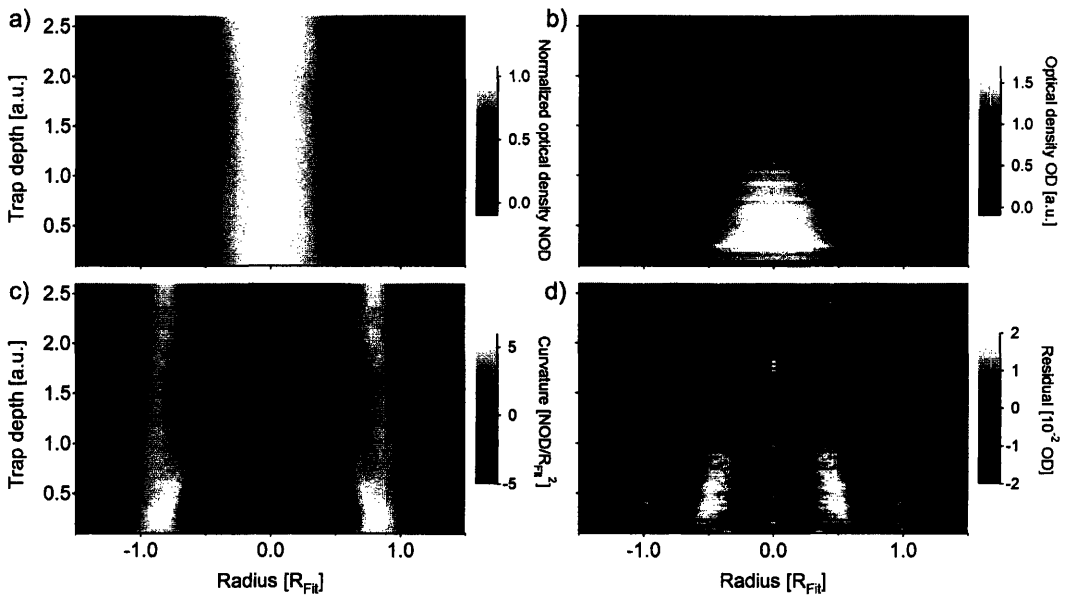

Figure 5-19: Density profiles, their curvature and their fit-residuals on resonance. a) Density profiles on resonance as a function of trap depth. There is no sign of a phase transition at this resolution. b) After the rapid ramp to the BEC-side and expansion, a condensate is clearly visible below a certain trap depth. c) The curvature of the density profiles on resonance in a) carries a signature of the condensate. No field ramp is required. d) The fit residuals for a finite temperature Thomas-Fermi fit. Also here, the condensate's imprint in the density profile is clearly visible. To obtain the curvature, the noisy central region of $\pm 0.1 R_F$ in each profile was replaced by a fit.

we also include a density plot of the profiles obtained with the rapid ramp method. As explained in the previous section, this allows to clearly separate the condensate and thermal cloud in expansion. The condensate fraction is included in Fig. 5-18, and shows, as one would guess from inspection of Fig. 5-19, that the condensate appears around $U = 2.2$ (in a.u.), a trap depth of 4.2 μK in real units. We conclude that a small condensate does not leave a strong signature in the gas cloud, unlike the case of weakly interacting Bose gases. Only when the condensate has grown to an appreciable size (about 20% in our data) does it significantly deform the density profiles.

To conclude, we have shown that the dilemma stated in the beginning of this chapter does not truly exist on resonance. The gas *does* show features in the density profiles upon condensation. Such features have been predicted by several authors [122, 190, 119, 230], but up to now they were too small to be seen after column integration.

Chapter 6

High-temperature superfluidity: Observation of vortices in a strongly interacting Fermi gas

Δῖνος βασιλεύει τὸν Δί' ἐξεληλακώς.
Vortex is king, having kicked out Zeus.
Aristophanes, *Clouds* 828 (423 B.C.)

Πάντα τε κατ' ἀνάγκην γίνεσθαι, τῆς δίνης αἰτίας
οὔσης τῆς γενέσεως πάντων, ἣν ἀνάγκην λέγει.
All things happen by virtue of necessity, the vortex being the cause of the creation of all things, and this he calls necessity.
Diogenes Laertius, *Lives of eminent Philosophers*, IX 45
(DEMOCRITUS, 460-357 B.C.)

Superfluidity is the hallmark property of interacting quantum fluids, whether it occurs in superconductors, in liquid helium or inside a neutron star. It is intimately, although not directly related to the presence of a condensate. It might be evident from analogy with atomic BEC that the molecular condensates of the preceding chapter are indeed superfluid. But how can one demonstrate superfluidity for the strongly interacting Fermi gas on resonance?

Quantized vortices in superfluids and superconductors

One of the most striking properties of superfluids is their response to rotation. In contrast to a normal fluid, which rotates just like a rigid body, a superfluid can carry

angular momentum only in the form of quantized vortices. Their mutual repulsion results in a regular distribution of the vortex lines, the Abrikosov lattice [4]. In superconductors it is an applied magnetic field that attempts to set the charged superfluid of electron pairs in rotation. The superconductor responds by either completely expelling the magnetic field (the Meissner effect) or by allowing quantized magnetic flux lines, vortices, to penetrate it. Quantized magnetic flux was measured by Deaver and Fairbanks [75] and Doll and Näbauer in 1961 [80] by moving a thin superconducting cylinder of tin toward and away from a conducting coil and measuring the electromotive force induced in the coil as a function of applied field. Entire Abrikosov lattices of magnetic flux lines were observed by using ferromagnetic particles that were trapped at the lines' end-points (Träuble and Essmann [246], Sarma [212], independently in 1967). Preceding these experiments in superconductors, quantized circulation in superfluid helium-4 [252] was observed by Vinen in 1958 by measuring the frequency of circular motion of a thin wire placed at the center of the rotating superfluid. The direct observation of vortex lattices in superfluid ^{4}He was achieved in 1979 by Yarmchuk, Gordon and Packard [257] by imaging ions trapped in the core of the vortex lines. Using the method of the vibrating wire, the presence of quantized circulation was confirmed for the fermionic superfluid ^{3}He in 1990 by Davis, Close, Zieve and Packard [71]. Our work presents the first direct imaging of vortices in neutral fermionic superfluids. It is interesting to add to this list that glitches in the frequency of pulsars, fast rotating neutron stars, have been attributed to the spontaneous decay of vortex lines leaving the neutron pair superfluid [9, 82].

Superfluidity in dilute gases

The observation of superfluidity in gaseous Bose-Einstein condensates had been the subject of many experimental efforts. One class of experiments performed at MIT consisted in observing the energy dissipated in the cloud by a moving obstacle [200, 58, 179]. Another class of experiments addressed the change of the moment of inertia as the gas turns superfluid. This could be evidenced by the observation of the scissors mode for a Bose-Einstein condensate [161], the oscillation of a dilute gas generated by the sudden rotation of the confining trap [108]. Finally, the observation of vortices in weakly interacting BECs provided the most spectacular demonstration of superfluidity. In a two-component condensate, the JILA group created a single vortex using a phase-imprinting technique, in which one component was stationary while the other was rotating around it [164, 11]. In an adaption of the "rotating bucket" idea, vortex lattices in single-component BECs were created [160, 2, 120, 87] by driving surface

excitations [178].

In Fermi gases, the direct observation of superfluidity was hindered by the fact that the normal cloud above T_C is still strongly interacting and obeys (collisional) hydrodynamic equations of motion, of the same form as that expected for superfluid hydrodynamics. The observation of an inversion of the aspect ratio of the cloud during expansion [174], a hallmark for Bose-Einstein condensation in weakly interacting Bose gases, indicated strong interactions in the gas but could not provide proof for superfluidity [105, 36, 204]. Condensation on both sides of the Feshbach resonance [102, 129, 271, 203, 272] showed the presence of very low-energetic fermion pairs, but did not directly address questions of superfluidity or phase coherence. Evidence for superfluidity was provided via measurements of collective excitations of the gas [138, 25], and via the observation of pairing in the strongly interacting regime [59]. A signature of a phase transition was not observed in these experiments, in the form of an abrupt change of the physical behavior of the gas as a function of temperature. It is a remarkable fact that the BEC-BCS crossover supports bound fermion pairs even above T_C, in an uncondensed state. Superfluid pairs could not be distinguished from uncondensed pairs, and theoretical modelling was needed to infer the presence of a superfluid.

In the experiments I will describe in the following, superfluidity was directly demonstrated in ultracold Fermi gases through the observation of vortices. At the same time, these results established phase coherence in gases of molecules and of fermionic atom pairs. Vortices have now become a tool to study the limits of superfluidity close to the phase transition (section 6.3.3) or in imbalanced Fermi mixtures (chapter 7).

In the following, I will present the experimental techniques used to set strongly interacting gases into rotation (section 6.2), the observation of vortex lattices in section 6.3 along with measurements on the damping time, and the phenomenon of pair breaking in expanding superfluids (section 6.3.3).

6.1 Origin of the vortex phenomenon

Superfluids are described by a macroscopic wavefunction $\psi(\mathbf{r})$ (see chapters 2 and 5). It is this quantity which is zero in the normal state and non-zero in the superfluid state, so it qualifies as the order parameter of the superfluid phase transition. As a

wavefunction, it is a complex quantity, with a magnitude and phase ϕ

$$\psi(\mathbf{r}) = |\psi(\mathbf{r})| \, e^{i\phi(\mathbf{r})} \tag{6.1}$$

The velocity of the superfluid is simply the gradient of its phase,

$$\mathbf{v} = \frac{\hbar}{m^*} \nabla\phi \tag{6.2}$$

where m^* is the mass of the bosonic entities forming the superfluid. In the case of fermionic superfluids, we have $m^* = 2m$, where m is the fermion mass. If we integrate Eq. 6.2 around a closed loop inside the superfluid, we immediately arrive at the Onsager-Feynman quantization condition [180, 91, 92],

$$\oint \mathbf{v} \cdot d\mathbf{l} = n \frac{h}{m^*} \tag{6.3}$$

with integer n. If the superfluid wavefunction has no nodal lines and the loop fully lies in a simply connected region of space, we must have $n = 0$. However, Eq. 6.3 can be fulfilled with $n \neq 0$ if the wavefunction contains a *vortex*, that is, a flow field that depends on the vortex core distance r like $v \sim 1/r$. At the location of the vortex, the wavefunction identically vanishes, it has a nodal line. This is the way a superfluid can carry angular momentum. In case of cylindrical symmetry, the angular momentum per boson or fermion pair is quantized in units of $\hbar$. Note that the vortices are an equilibrium property of the superfluid at given angular momentum. This is in marked contrast to *classical* vortices, which can only be found in non-equilibrium situations (dynamical equilibrium). Here, vorticity must decay whenever the viscosity is non-zero. Also, classical vortices do not obey any quantization rule and can occur with any circulation.

It turns out that for quantized vortices, only the case of $n = \pm 1$ is of relevance, since more highly "charged" vortices are energetically not favorable and quickly decay into singly charged vortices [222].

How can quantized vortices nucleate? Imagine that we move a stick or spoon through the condensate. We know that the condensate will not respond to the spoon if its motion is slower than a certain critical velocity. Another fact is that vortices cannot suddenly appear within the condensate, as the angular momentum contained within a closed loop inside the condensate cannot abruptly jump. Rather, the nodal lines have to enter the condensate from its *surface*, where the condensate's wavefunction is zero. This surface can also be the surface of the stirrer, if it fully expels the condensate.

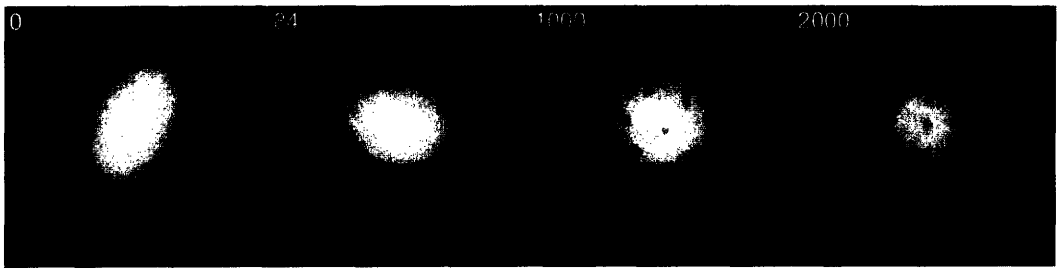

Figure 6-1: Fate of a quadrupole oscillation in a rotating atomic Bose-Einstein condensate. The images show a sodium condensate in the magnetic trap after stirring slightly above the quadrupole resonance (at 52 Hz, trapping frequencies $\nu_\perp = 73$ Hz and $\nu_z = 18$ Hz) and equilibrating for a certain time t (time given in ms). First, the condensate rotates in the form of a perfect quadrupolar collective excitation. After about 100 ms, density depletions looking like vortex cores start to appear at the edges of the condensate. Between 500 ms and 1 s, some of these penetrate inside the condensate as vortex lines, which arrange themselves into an ordered lattice after about 1-2 s.

We conclude that the spoon has to excite *surface* excitations, moving faster than the local critical velocity v_c for such excitations [14]. What surface excitations are efficiently created depends on the shape of the stirrer [70], or, in the case of a rotating container, the roughness of the container walls. Accordingly, the necessary critical angular velocity Ω_c to nucleate vortices will likewise depend on the stirrer's shape. Note that Ω_c is typically much higher than the *thermodynamic* critical angular velocity Ω_{th}. The latter is the angular velocity at which, in the rotating frame, the ground state of the condensate contains a single vortex. But simply rotating the condensate at Ω_{th} will not lead to this ground state. If the condensate contains N bosons, N units of angular momentum have to be provided to form the vortex. This presents an energy barrier between the metastable state without vortex and the ground state with vortex. Driving a surface excitation provides the necessary coupling mechanism to "pump" angular momentum into the condensate, which can subsequently relax into a state containing vortices.

6.2 Experimental techniques

In the case of weakly interacting Bose gases in magnetic traps, the techniques for setting the cloud in rotation are well established [178, 160, 2, 113, 120]. In [113, 120], the initially axially symmetric magnetic potential is deformed into an ellipse in the

radial plane, which is then set in rotation. In [160], an asymmetric optical dipole potential is superimposed onto a cylindrically symmetric magnetic trap, again resulting in an elliptically deformed potential. In these cases, the role of the "rough container walls" needed to nucleate vortices is played by the smooth elliptical deformation. In contrast to the case of a sharp object or "spoon" stirring in the superfluid, this smooth potential can only excite a specific surface excitation of the condensate, a rotating quadrupole mode. This collective excitation carries angular momentum $m = \pm 2$ (the third component of angular momentum) and can only be excited at a certain angular frequency[1] $\Omega_Q = \omega_\perp/\sqrt{2}$, where $\omega_\perp$ is the radial trapping frequency[2]. Below this threshold angular frequency, the rotating elliptical potential cannot excite the condensate. Above this threshold frequency, the condensate's quadrupolar mode is excited, and will eventually decay (via a dynamical instability) into vortices [159] (see Fig. 6-1).

In the MIT experiments [178, 2, 1], two small, focussed laser beams were symmetrically rotated around the cloud. Vortices could be created efficiently over a large range of stirring frequencies [2, 199]. The small beams presented a sharp obstacle to the superfluid, most likely creating vortices *locally* at their surface [199], corresponding to high angular momentum excitations at low critical angular velocities. This is the strategy followed in our experiment on rotating Fermi gases.

6.2.1 Roadblocks

However, in contrast to the case of weakly interacting Bose gases in magnetic traps, the rotation of Fermi gases and the observation of vortices is hindered by several issues, some of them technical and some of them due to the physics of Fermi gases.

Technical difficulties:

1. Strongly interacting fermions in ^{6}Li require an optical trap formed by a laser beam. In contrast to magnetic traps, which can be designed to be very round in the transverse plane, laser beams typically suffer from aberrations, such as a non-uniform beam profile with potentially high spatial frequency noise, and - without special care - are generally not round.

[1] While a collective excitation carrying angular momentum m has an energy $\hbar\omega_\perp\sqrt{m}$, it m-fold symmetric and is thus excited at a frequency $\Omega = \omega_\perp/\sqrt{m}$, see [240].

[2] In the presence of an elliptic deformation, one needs to replace $\omega_\perp$ by $\sqrt{(\omega_x^2 + \omega_y^2)/2}$, where $\omega_{x,y}$ are the trapping frequencies in the direction of the long and short axis of the ellipse.

2. The experiments have to be carried out at high magnetic fields[3]. Stray gradients can distort the optical trapping potential. Also, the expansion from the optical trap, crucial for the magnification of the vortex cores, can be strongly affected by the curvature of the magnetic potential.

3. Gravity is usually not considered a problem in magnetic traps, since it merely shifts the center of the (to a very good approximation) harmonic trapping potential. However, optical traps provide a gaussian potential for the atoms. Gravitational sag can thus distort the trapping potential.

The technical difficulties can be overcome one by one using an atomic BEC of sodium atoms as the "testbed". However, the following problems are specific to Fermi gases:

Difficulties arising from the physics of Fermi gases:

1. Far on the molecular side of the Feshbach resonance, in the regime where $k_F a$ is small, the situation should be fully analogous to the case of atomic condensates. This is thus the natural starting point for observing vortices. However, too far away from resonance, the molecules (which are in the highest vibrational state of the interatomic potential!) can undergo rapid vibrational relaxation via three-body collisions, leading to heating and trap loss. The lifetime of the gas needs to be longer than the vortex nucleation and equilibration time (typically 1 s). This limits the smallest values of $k_F a$ one can study ($k_F a \gtrsim 3$ in our experiment).

2. On the other hand, closer to resonance, quantum depletion becomes important: The density of atoms in one spin state is no longer given by the square of the superfluid wavefunction $|\psi(\mathbf{r})|^2$ as was the case in the deep molecular regime. The contribution of the coherent part of the gas to the atomic density actually becomes exponentially small in the BCS regime (for definitions of the condensate wavefunction see sections 2.3.5 and 5.2.3). Loosely speaking, only the Cooper pairs, of weight $N\Delta/E_F$, contribute to the condensate wavefunction $\psi(\mathbf{r})$. Even though $\psi(\mathbf{r})$ still has to identically vanish inside the vortex core, the density $n(\mathbf{r})$ does not anymore, and the vortex contrast is greatly reduced. This will

[3]"High" refers to the scale of atomic physics experiments, that is, the scale set by the hyperfine interaction, ranging from about 100 G to several 1000 G. In condensed matter, magnetic fields around tens of Tesla are considered "high", as here $\mu_B B$ becomes comparable to the gap energy and k_B times the critical temperature.

set a technical limit on how deep into the strongly interacting regime one can observe vortices as density depletions.

3. The vortex core size in the molecular Bose-Einstein condensate is given by the healing length $\xi \propto \frac{1}{k_F}\frac{1}{\sqrt{k_F a}}$. As $k_F a$ is increased moving into the strongly interacting regime, the vortex core shrinks. The core size will of course never decrease below the value at unitarity, where it has to be on the order of $1/k_F$, the only length scale available when $a \to \pm\infty$. Still, one might be concerned whether this length scale can be resolved.

4. It is well-known from studies on atomic BECs [1] that vortices are strongly damped by friction with the normal gas as the temperature approaches T_C. As we move to the BCS-side of the resonance, T_C is strongly reduced (see chapter 2) and we might expect vortices and rotation to be heavily damped.

5. On the BCS-side, the lowest lying excitations in the superfluid are those which break a pair. However, as experience with sodium condensates in magnetic traps suggests (see Fig. 6-2), one needs to strongly perturb the cloud in order to nucleate many vortices. In the case of a gas in the BCS-regime, such a strong perturbation is likely to simply destroy the superfluid via pair-breaking.

We will first describe the solutions to the technical problems, using an atomic sodium BEC as the stepping stone.

6.2.2 "Sanding off the bumps"

Optical Trap

The experimental setup used for rotating Fermi gases is shown in 6-3. The atom trap is formed by the combination of an optical dipole trap (waist w), confining the atoms radially, and a magnetic saddle point potential that provides axial confinement (and weak radial anti-confinement). We favored this geometry out of several reasons:

- The large waist for the optical trap allows for a smooth beam profile, suppressing high spatial frequency noise that is usually introduced when focussing light down to sizes not much larger than the wavelength.

- We aim for a small aspect ratio of the cigar-shaped trap (about $\nu_z/\nu_r = 5$), so that the stirring beam can rotate the entire cloud at once. For very elongated clouds, a tightly focussed stirrer will excite the sample only locally, leading to inefficient transfer of angular momentum into the cloud.

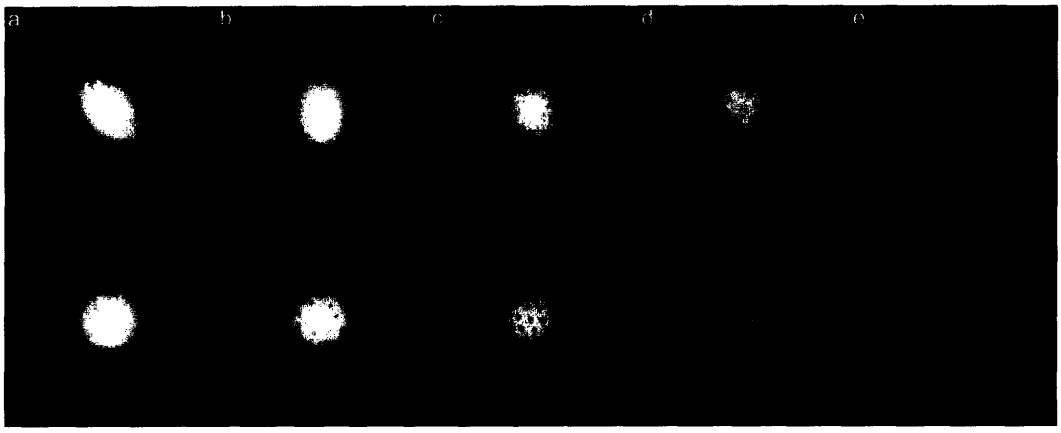

Figure 6-2: Vortex nucleation for violent stirring in an atomic BEC. The upper row shows expansion images of sodium condensates after 500 ms of stirring at the quadrupole frequency, for different laser powers of the stirring beam. The lower row shows the resulting BEC after 300 ms of equilibration time. This suggests that the condensate has to be severely excited to generate many vortices. From left to right, the laser power was increased for each subsequent image by a factor of two.

The aspect ratio of purely optical traps at wavelength λ (= 1064 nm in our experiment) is given by $\sqrt{2}\pi w/\lambda$. We see that it is not possible to fulfill both requirements with purely optical (near-infrared) traps. In the combined optical and magnetic trap, the trap frequencies are essentially decoupled, ν_r being given by the optical trap and ν_z fixed by the magnetic field curvature.

Another important requirement is that the cloud is allowed to cool after stirring. Without dissipation, the excited cloud would never form an ordered vortex lattice. In experiments using magnetic traps, this could be achieved by leaving an "RF-knife" on during equilibration, which removed energetic atoms from the trap. Optical traps have a finite trap depth "built in". Cooling of the cloud will be efficient if the trap depth U is not much higher than the Fermi energy E_F. This constraint fixes the waist, once the aspect ratio $a = \nu_r/\nu_z$ and the axial trapping frequency ν_z is given:

The relation between U and the waist w is

$$U = \frac{1}{4}m\omega_r^2 w^2 = \frac{1}{4}m\omega_z^2 a^2 w^2 \tag{6.4}$$

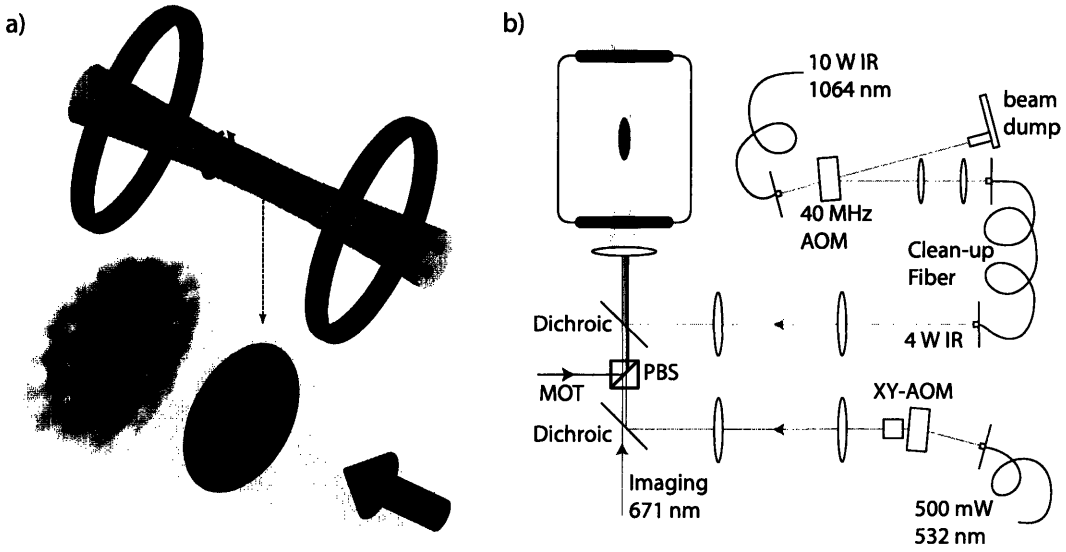

Figure 6-3: Experimental setup for the observation of vortices in a Fermi gas. a) Sketch of the geometry. The atomic cloud (in red) is trapped in a weakly focussed optical dipole trap (pink). The coils (blue) provide the high magnetic offset field to access the Feshbach resonance as well as the axial confinement (additional curvature coils not shown). Two blue-detuned laser beams (green) rotate symmetrically around the cloud. An absorption image of the expanded cloud shows the vortices. b) Optical setup for the vortex experiment. The laser beam forming the dipole trap is spatially filtered using an optical fiber tolerating high laser power. The stirring beam (green) passes through two crossed AOMs that deflect it in the transverse (XY) plane. These beams are overlapped with the imaging light by dichroic mirrors. The light for the magneto-optical trap (MOT) is overlapped on a polarizing beam splitter cube (PBS).

The Fermi energy per spin state for a total number of atoms N is given by (using the harmonic approximation for the radially gaussian potential):

$$E_F = \hbar(\omega_r^2\omega_z)^{1/3}(3N)^{1/3} = \hbar\omega_z a^{2/3}(3N)^{1/3} \tag{6.5}$$

Requiring $U \gtrsim E_F$ results in

$$w \gtrsim 2\sqrt{\frac{\hbar}{m\omega_z}}a^{-2/3}(3N)^{1/6} \tag{6.6}$$

If we want to trap $N = 1\times10^7$ atoms with an aspect ratio $a = 5$ and an axial trapping frequency $\nu_z = 20\,\mathrm{Hz}$ (a typical value), we need the waist to be larger than 100 μm. Note that this requirement is quite stringent: Changing ω_z is limited: Increasing the

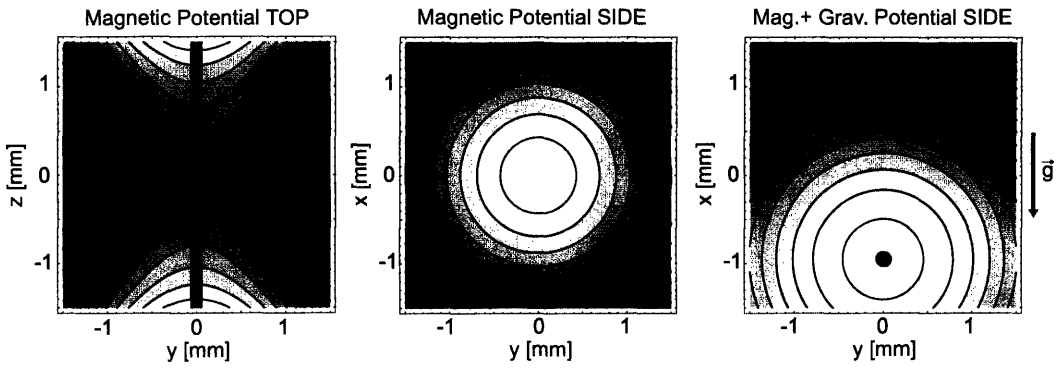

Figure 6-4: Trapping potential for the study of rotating Fermi gases. The magnetic field produces a saddle potential (left), confining in the axial and anti-confining in the radial direction. The optical trap needs to be aligned with the confining axis in order to avoid stray gradients. In the vertical direction, gravity shifts the center of the potential seen by the atoms (middle + right). The optical trap thus needs to be *below* the symmetry axis of the magnetic fields.

current in the curvature coils by a factor of two (which increases power dissipation by four) only reduces the required waist by 20%. Allowing for an aspect ratio of 10 would only give another reduction by 35%, at the expense of making uniform stirring across the longer cigar more difficult.

We choose $w = 120\,\mu$m. The large waist ensures that there is negligible variation of the optical trap along the axial direction of the cloud: The Rayleigh range of the beam is $z_0 = \pi w^2/\lambda > 4\,$cm while a typical axial cloud size is 1 mm. The optical trap is thus quite perfectly a cylindrically symmetric potential. The symmetry in the radial plane is ensured using a high-power optical fiber to spatially filter and shape the beam profile. Care is taken not to deteriorate the quality of the gaussian beam's roundness when passing through several lenses after the fiber exit.

The maximum power in the laser beam is 4 W, which limits the trap depth to about 10 μK. This is still deep enough to load about 3×10^7 degenerate fermions from the magnetic trap after the sympathetic cooling stage with sodium (The Fermi temperature in the combined magnetic and optical trap during this loading is 5 μK, and the degenerate cloud at $T/T_F \approx 0.3$ is not much larger than a zero-temperature Fermi sea).

Magnetic Field profile

The offset magnetic field tunes the interatomic interactions close to the Feshbach resonance. We would like this to be an independent parameter, so one requires two coils in Helmholtz configuration that create a very flat magnetic field along the axial dimension. Our "Feshbach" coils provide a residual magnetic field curvature that corresponds to an axial trapping frequency of 11.0 Hz at 834 G (resonance). While this frequency depends only as $\sqrt{B_{\mathrm{FB}}}$ on the offset field B_{FB} due to these coils, we can render the dependence negligible by adding an additional magnetic field curvature via independent sets of "curvature" coils. These coils also produce an offset field that is directed opposite to the field from the Feshbach coils, yielding a total offset field $B_0 < B_{\mathrm{FB}}$. The final curvature corresponds to $\nu_z = 22.8$ Hz axial confinement, and varies only by 1 Hz from $B_0 = 700$ G to $B_0 = 1000$ G. The optical trap providing radial confinement with ν_r in the range of 50 to 300 Hz, the aspect ratio of the cloud can be varied between about 2 and 12.

The combined potential of Feshbach and curvature coils creates a magnetic saddle potential $V(x, y, z) = \frac{1}{2}m\omega_z^2(z^2 - \frac{1}{2}x^2 - \frac{1}{2}y^2)$. It is then necessary to align the optical trapping beam judiciously on top of the saddle, aligned with its confining (z-)axis (see Fig. 6-4). Otherwise the cloud would experience stray gradients, distorting the round trapping potential provided by the laser beam.

Gravity

Along the vertical (x-)axis, the combined potential of gravity+magnetic fields is $-\frac{1}{4}m\omega_z^2x^2 - mgx$. Thus, gravity shifts the saddle potential by an amount $2g/\omega_z^2 \approx 1\,\mathrm{mm}$. The "sweet spot" in the radial plane to which the ODT needs to be aligned is thus not the center of the magnetic field coils, but about 1 mm below it (see Fig. 6-4). In this position no gradients act on the atoms. If the optical trap is round in the radial plane, the combined potential experienced by the atoms is round as well.

The alignment procedure of the ODT is shown in Fig. 6-5. At the end of evaporation of the lithium condensate, the trap depth is reduced in about 30 ms to a very shallow depth which is not sufficient to hold the atoms if they are not in the "sweet spot". After 10 ms of expansion from the optical trap one clearly observes in which direction the atoms spill out, and one can counteract by moving the optical trap.

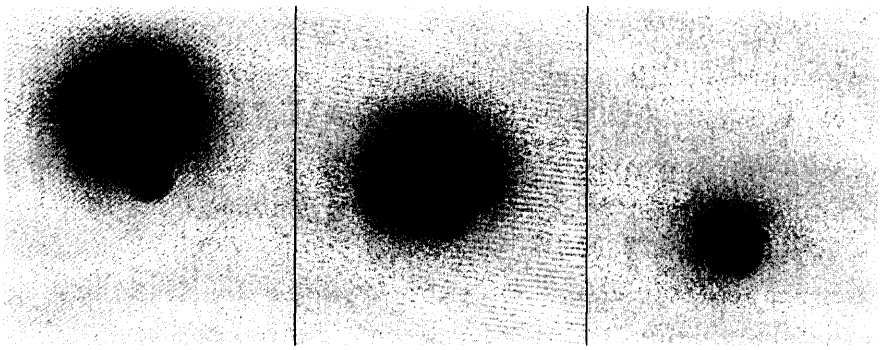

Figure 6-5: Alignment of the optical trap to achieve a radially symmetric potential. In the left image, the trap is still far from the "sweet spot". In the right image, stray gradients are almost completely cancelled. The absorption images are of a lithium pair condensate. The field of view for each image is 1.1 × 1.3 mm.

Expansion

While the trap is now round and the cloud can be set in rotation, one still needs to observe the vortex cores. In the trap, the vortex size is on the order of the healing length (for an atomic or a molecular BEC) or the inverse wavevector (for a strongly interacting Fermi gas), about 200 nm. It is essentially impossible to detect them in-situ using absorption imaging with larger optical wavelength (589 nm for ^{23}Na, 671 nm for ^{6}Li). Fortunately, vortices survive the expansion of the condensate, which we can thus use as a "magnifying glass". However, only in simple geometries is the expansion a faithful magnification. Complications arise due to the expansion into a saddle potential.

Let us discuss the case of an atomic or molecular condensate containing a single vortex, initially confined in our cigar-shaped trap and with axial and radial Thomas-Fermi radii R_a and R_r. It is well-known that the condensate preserves its parabolic density profile during expansion, and its radii scale according to a simple scaling law [48, 131, 167, 47]. For very long cigars, $R_a \gg R_r$, the condensate's mean-field mostly escapes in the tight radial dimension and the expansion is effectively 2D. For free space expansion, $R_r(t) = R_r(0)\sqrt{1+\omega_r^2 t^2}$, while for expansion into our radial anti-confining potential,

$$R_r(t) = R_r(0)\sqrt{\cosh^2\left(\frac{\omega_z}{\sqrt{2}}t\right) + \left(\frac{\sqrt{2}\omega_r}{\omega_z}\right)^2 \sinh^2\left(\frac{\omega_z}{\sqrt{2}}t\right)} \tag{6.7}$$

Figure 6-6: Decrease of vortex visibility for a sodium condensate expanding from the optical trap into a magnetic saddle potential. Top and bottom row show axially and radially integrated optical densities, respectively. The saddle potential is confining in the axial and anti-confining in the radial direction. As the condensate expands radially, it collapses in the axial dimension, a direct consequence of hydrodynamic flow. The vortex cores shrink and collapse onto themselves, thereby filling in completely and forming ring-like structures (see text for details). For the images, the magnetic field curvature ($\nu_z = 26\,\mathrm{Hz}$) was switched off after, from left to right, 0, 2, 3, 4, 5, 7 and 10 ms. The total time of flight was constant at 35 ms.

where $\omega_z/\sqrt{2}$ is the rate of radial anti-trapping[4].

How does the vortex core size change during expansion? There are two regimes one can simply understand, the initial hydrodynamic expansion and the ballistic expansion at long times of flight. In the first part of the expansion, the mean-field $\mu \propto na$ changes so slowly that the condensate wavefunction can still react to the change in density: Adjustments on the healing length scale ξ - about the size of a vortex in equilibrium - can occur at a rate $\hbar/m\xi^2 = \mu/\hbar$. As long as the rate of change of μ - essentially the rate of change of R_r - is smaller than $\mu/\hbar$, the vortex core can still adjust in size to the local mean-field. It thus grows as $\xi \propto 1/\sqrt{n(t)a} \propto R_r(t)\sqrt{\frac{R_a(t)}{a}}$. If R_a does not vary appreciably, $\xi/R_r(t)$ will remain *constant* during the expansion, the vortex core grows just as the size of the condensate, and the magnification is faithful.

Once the rate of change of $\mu(t)$ becomes comparable to $\mu(t)/\hbar$, the condensate can

[4]In the case of hydrodynamic expansion of a gas with arbitrary equation of state $\epsilon \propto n^\gamma$, the scaling factors $b_{r,z}(t)$ for the radial (r) and axial (z) direction do not have an analytic expression, but can be easily calculated as the solution to the differential equations [167]

$$\ddot{b}_z = \frac{\omega_z^2}{b_z^{\gamma+1} b_r^{2\gamma}} - \omega_z^2 b_z \tag{6.8}$$

$$\ddot{b}_r = \frac{\omega_r^2}{b_r^{2\gamma+1} b_z^{\gamma}} + \frac{1}{2}\omega_z^2 b_r \tag{6.9}$$

Here we assume that the axial confinement is still on during expansion, only the radial confinement from the optical trap being switched off.

no longer adiabatically adapt to the lowering density. The characteristic expansion rate being ω_r, this occurs when $\mu(t) \approx \hbar\omega_r$. For much longer expansion times, we are in the limit of ballistic expansion. Here, each particle escapes outward with the given velocity (in free space) or, in the case of the saddle potential, with a radial acceleration proportional to its distance from the origin. This simply rescales the radial dimension, and thus stretches the vortex core and the cloud size by the same factor. Again the magnification is faithful.

However, in our experiment we are not in the quasi-2D regime where $R_a \gg R_r$. The saddle potential "squishes" the cloud in the axial dimension, as the decreasing mean-field no longer stabilizes the condensate's axial size. According to the above estimate, the vortex cores will *shrink* in comparison to the cloud size by a factor $\propto \sqrt{R_a(t)}$. We can see the effect on a sodium condensate in our optical trap in Fig. 6-6, where the axial curvature was left on for longer and longer times.

To work around this problem, we quickly reduce the magnetic field curvature during expansion by ramping down the curvature coils (in about 1 ms). As this increases the overall offset field (see above), the current in the Feshbach coils is decreased accordingly, so as to leave the offset field B_0 - and the interaction parameter of the Fermi mixture - constant. We can speed up the radial expansion even further in comparison to the axial evolution by actively "squishing" the cloud about 3 ms before release. This is done by simply ramping up the power in the optical trapping beam by a factor of 4. Not only does this increase the radial trapping frequency, but it also excites a "breathing" mode in the condensate. The result is that the condensate expands almost twice as fast as without these steps.

Overcoming all technical difficulties, the resulting trapping potential can now favorably compare with our magnetic traps. The residual ellipticity of the transverse potential is estimated to be less than[5] 2%. Large vortex lattices containing about 120 vortices can be created in sodium Bose-Einstein condensates (see Fig. 6-7). The vortex lifetime is about 4 s, which is at least half the lifetime of vortices in our magnetic trap.

[5]Of course, this cannot compare with the almost perfect roundness of a (magnetic) TOP trap, with residual ellipticity of less than 0.1% [113].

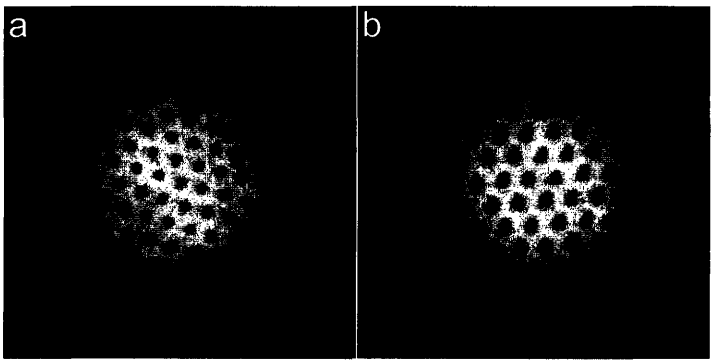

Figure 6-7: Vortex lattice in a Bose-Einstein condensate of sodium atoms in the magnetic trap (left) and the optical trap (right image). The optical trap (highest number obtained $\sim$ 120 vortices) can favorably compare with the magnetic trap (highest number in our experiment $\sim$ 150 vortices).

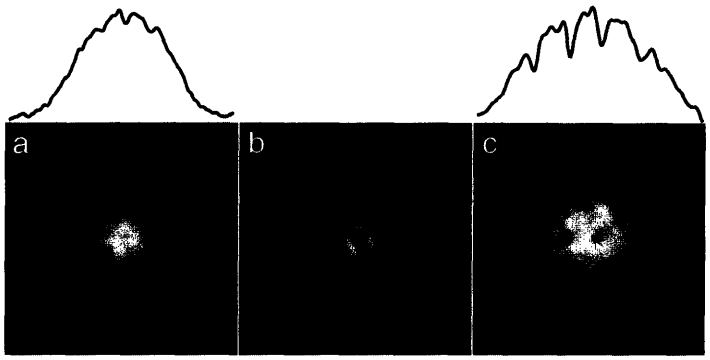

Figure 6-8: Vortex lattice in a $^6Li_2$ molecular condensate. In a), stirring, equilibration and imaging of the vortex lattice all took place at a fixed field, 766 G ($1/k_Fa$). Image a) shows the very first clear signature we observed. The vortex core depletion is barely 10%. b) A Fourier filter applied to a) clearly shows the Abrikosov vortex lattice. c) The improved scheme of "squishing and release" (see text), as well as a sudden reduction of the interaction strength led to an improved vortex contrast.

6.3 Observation of vortices in a Fermi gas

The search for vortices in Fermi gases started on the molecular side of the resonance, to stay close to the analogous case of an atomic BEC. It was not clear whether there would be a window in which 1. the molecular condensate lives long enough to nucleate vortices and 2. the interactions are weak enough such that vortices show up as clear density depletions.

It turned out that at a field of 766 G ($1/k_Fa = 1.3$), we were successful: After stirring the cloud for 800 ms and letting the cloud equilibrate in 400 ms, we observed a vortex lattice in the density profile (Fig. 6-8). This established superfluidity for molecular condensates.

With this as the starting point, different methods could be tried to improve the vortex contrast. What turned out to be crucial for good contrast was - as expected - the reduction of the interaction strength. In the moment the vortex lattice is released from the trap, the magnetic field is lowered to fields around 700-740 G ($1/k_Fa \approx 2-4$ initially, further growing during expansion). If the condensate still has time to react to this change in scattering length, the vortex size $\xi \propto R_r(t)/\sqrt{a}$ will increase relative to the condensate's radius (the expression for ξ is valid in the BEC-limit, and assumes radial expansion, see previous section). Also, at the new interaction strength, quantum depletion of the condensate wavefunction is reduced.

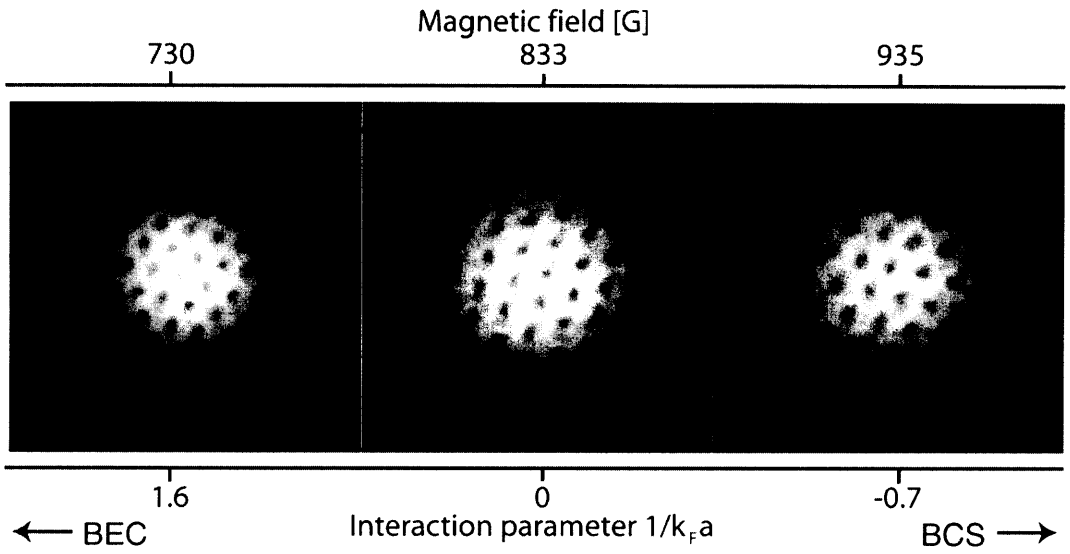

Figure 6-9: Observation of vortices in a strongly interacting Fermi gas. This establishes superfluidity and phase coherence in gases of fermions.

The vortices are effectively "emptied" by weakening the interactions[6].

This technique proved to work on both sides of the Feshbach resonance. Stirring, equilibration and initial expansion could be performed at magnetic fields between 740 G ($1/k_F a = 2$) and 860 G ($1/k_F a = -0.35$), before switching to the BEC-side during expansion for imaging. The observation of ordered vortex lattices above the Feshbach resonance at 834 G, on the BCS-side of the resonance, establishes superfluidity and phase coherence of fermionic gases at interaction strengths where there is no two-body bound state available for pairing.

One might argue that the gas could have been in the normal state above resonance, while the vortex lattice might have formed during the 10 ms of expansion at the imaging field, on the BEC-side of the resonance. This is not possible. We showed that the vortex lattice needs many hundreds of milliseconds to form in the stirred cloud. This is the same time scale found for the lattice formation time in atomic BECs [159, 1]. It is also in agreement with a theoretical study of vortex formation

[6]The ramp should not move too far into the weakly interacting regime: The condensate would simply not expand anymore as practically all the repulsive mean-field has been taken out of the cloud. On the other hand, letting the condensate expand for too long *before* the ramp should be avoided as well. At reduced density the ramp would not allow the condensate to adjust to the new interaction strength and modify the vortex size. The condition is again (see previous section) that the "reaction time" of the condensate wavefunction, $\mu/\hbar$, evaluated at the final field, should be faster than the rate of change of μ, that is, the rate of change of $R_r(t)$.

in strongly interacting Fermi gases [245]. When a thermal cloud is slowly cooled through the transition temperature [113], the condensate first forms without a vortex. As the condensate grows, vortices are nucleated at the surface and then enter the condensate [14]. When a thermal cloud is suddenly cooled, a condensate with phase fluctuations will form [16, 224] which can arrange themselves into a vortex tangle. In either case, one would expect a crystallization time of at least several hundred milliseconds before a regular vortex lattice would emerge. It simply needs several axial trapping periods for the vortex tangle to stretch out. It should be noted that this time scale was found to be independent of temperature [1] and seems to represent an intrinsic time scale of superfluid hydrodynamics.

Even if these timescales were not known, it is not possible to establish a regular vortex lattice with long-range order in a gas that expands at the speed of sound of the trapped gas. Opposing edges of the expanding cloud simply cannot "communicate" fast enough with each other.

The regularity of the lattice proves that all vortices have the same vorticity. From their number, the size of the cloud and the quantum of circulation $h/2m$ for each vortex, we can estimate the rotational frequency of the lattice. For an optimized stirring procedure, we find that it is close to the stirring frequency. This excludes a quantum of circulation of h/m or doubly charged vortices.

6.3.1 Vortex number and lifetime

The number of vortices that could directly be created on the BCS-side was rather low in the first experiments, as the stirring seems to have had an adverse effect on the stability of the pairs. This corresponds to the expectation that the gas is more robust on the BEC-side, where the lowest excitations are sound waves, while on the BCS-side it is pair breaking. To optimize the vortex number on the BCS-side, first a large vortex lattice was produced close to resonance, at 812 G, before ramping the magnetic field beyond the Feshbach resonance. In this way, large numbers of vortices could be obtained in the entire BEC-BCS crossover (see Fig. 6-9).

The vortex lifetime is on the same order of what was found for atomic BECs. This displays the high degree of metastability of vortices in superfluids. The longest lifetime is found close to, but not right on resonance. In fact, there is a peculiar dip in the lifetime on resonance, which we speculate to be caused by pair breaking. The idea is the following: Pairs far outside, in the low-density regions of the cloud, and close to resonance, have very small binding energies. For example, the (two-body)

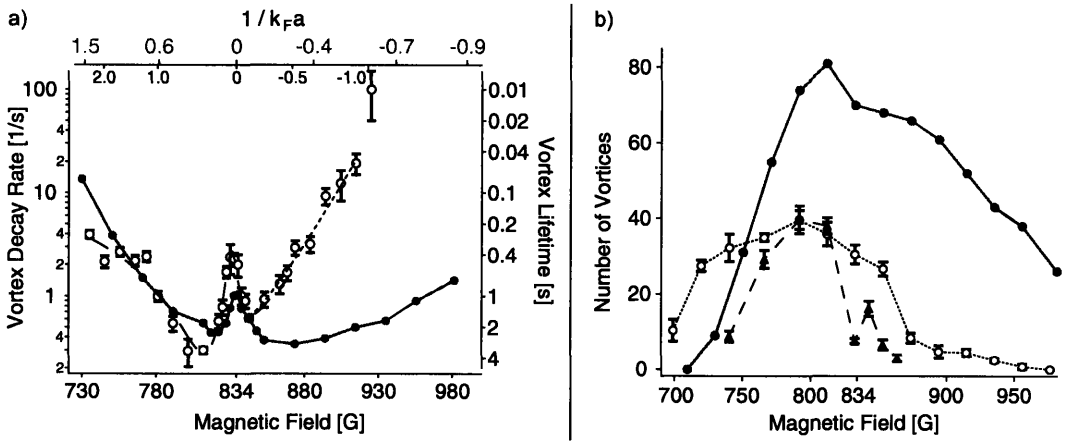

Figure 6-10: 1/e-Lifetime (a) and number (b) of vortices in the BEC-BCS crossover. Vortices are long-lived across the entire BEC-BCS crossover. A narrow dip in the lifetime on resonance is presumably due to breaking of pairs whose binding energies are comparable to $h\times$ the rotation frequency (several tens of Hz, corresponding to the binding energy of free molecules a few G away from resonance). Open symbols are data from April 2005. Optimization of the system using a deeper trap resulted in improved characteristics on the BCS-side, shown by the full symbols (data from June 2005). In b), the triangles give the number obtained by stirring and equilibrating both at the given field. Stirring at 812 G and subsequently ramping to the final field for equilibration resulted in the data shown as circles.

molecular binding energy at 830 G, 4 G away from resonance, is only $k_B \times 3\,\mathrm{nK}$ or $h \times 60\,\mathrm{Hz}$. This is on the order of $\hbar\times$ the rotation frequency Ω of the lattice. If there are small "bumps" in the trapping potential, the molecules rotating around the trap are excited at their binding energy and thus tend to break. The effect could thus be an interesting coupling of the external degrees of freedom with the internal ones. Why do clouds in the BCS-regime not suffer from this pair breaking as well? Here, the binding energy in the low-density regions is even smaller if not identically zero. We speculate that this is because *only* the pairs that have a binding energy $\sim \hbar\Omega$ are in danger. Such pairs reside in a certain shell within the condensate. If this is not the outermost paired shell, the surrounding superfluid "protects" the endangered pairs from breaking.

This scenario might also explain why stirring the cloud on the BCS-side creates heating and creates vortices only inefficiently. As the cloud is spun up, all frequencies from $\Omega = 0\,\mathrm{Hz}$ up to the final value will occur, thus destroying one shell of pairs after the other.

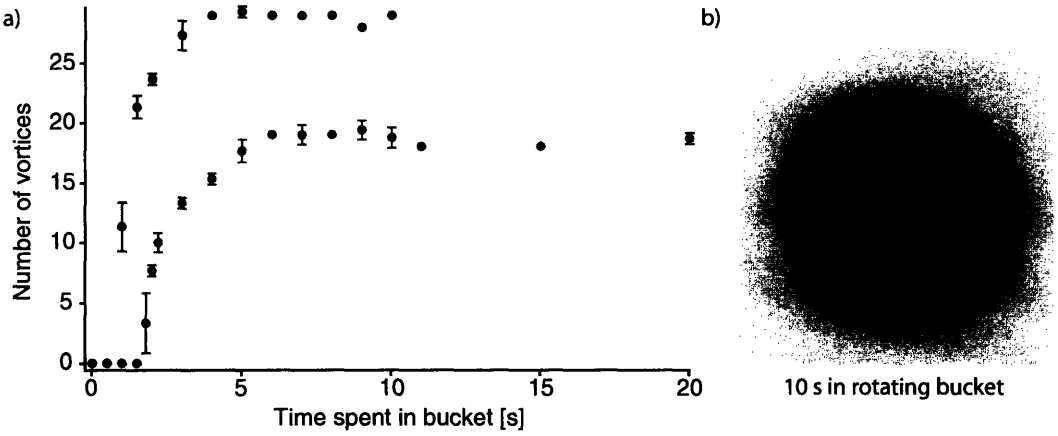

Figure 6-11: Rotating bucket for superfluid Fermi gases. a) Vortex number vs time spent in the rotating trap. After a certain nucleation time the number of vortices saturates and stays constant. The final vortex number depends on the power of the green beam, indicating slippage due to residual friction with the "container walls". The lower and upper curve correspond to lower and higher green beam power. b) Absorption image of an optimized vortex lattice, containing about 75 vortices, after 10 s hold time in the rotating bucket. The magnetic field for all data was 812 G, corresponding to $1/k_F a \approx 0.2$.

The dip in the vortex lifetime on resonance might thus be a spurious effect due to residual trap anisotropy. Its presence is a curiosity, since the critical velocity of the superfluid should be highest, and thus the superfluid the most stable close to resonance [219, 64].

6.3.2 A rotating bucket

All the experiments described before first set the cloud in rotation using the stirring beam and then let the gas equilibrate in the stationary trap to settle into a vortex lattice. In the stationary trap, the configuration is of course only metastable. Granted, if the trap was perfectly round, there would be no way for angular momentum to escape and the vortex lattice would persist indefinitely. In this case, the vortex configuration is the ground state of the equivalent system with a given angular momentum imposed (mathematically speaking, it is the ground state for the hamiltonian in the rotating frame $H - \Omega L_z$, where H is the hamiltonian in the absence of rotation and L_z plays the role of a lagrangian multiplier: the angular momentum imposed on the system that fixes the rotation frequency Ω). At zero temperature, it would not even matter if the trap was not round, as the superfluid does not experience friction with the

container walls. The only way the superfluid can spin down is via friction with the thermal cloud [263, 88]. The thermal cloud's rotation, in turn, is slowed down quickly by the container walls [107].

However, in the original "rotating bucket" experiments on helium-4 [257], it was actually possible to continue rotating the trap practically indefinitely (for as long as the refrigerator helium supply lasted). In the case of atomic condensates, the rotating anisotropy or the "spoon" used to stir up the cloud usually needs to be switched off before an ordered vortex lattice can form[7]. This is possibly because the spoon is not moving smoothly enough to allow equilibration into a vortex lattice. Before their observation of ordered vortex arrays, the experiments on helium-4 initially suffered from similar perturbations [257].

In contrast to previous experiments, we have found that it is possible to keep the stirring beams on during formation of the vortex lattice. The experiment was performed at 812 G in a trap with radial trapping frequency $\nu_R = 90$ Hz. The two stirring laser beams (power in each beam ≈ 100 μW, waist $w = 16\,\mu$m) created only a weak potential of about 20 nK each on the cloud (mean-field $\mu \approx 400$ nK). They were rotated around the cloud at a frequency of 70 Hz. For imaging, the atoms were released from the combined trap, the confining optical potential plus the repulsive stirring beam. We found that it was possible to stabilize a vortex lattice containing 19 vortices for 20 s (see Fig. 6-11). The maximum time studied was only limited by the memory of the computer controlling the experiment.

The final vortex number depended on the laser power or the "stiffness" of the stirrer. Increasing the power in the stirring laser by 60 % allowed a larger equilibrium vortex number, 29. This suggests that the stirrer is fighting a residual trap anisotropy. The "slippage" is worse for a weaker drive, and causes the condensate to rotate at a lower speed.

It is interesting to note that vortices become visible in the condensate only after a considerable delay of $1 - 2$ s. In contrast to the more severe perturbations used in the previous studies (stirring potential ~ 100 nK), where the total stirring time was about 500 ms to 1 s, the more gentle but continuous stirring is less efficient in nucleating vortices. The system is stuck longer in the metastable state without vorticity. Again, with the stronger stirrer, the time needed to nucleate the first vortices was considerably reduced. That indicates that the barrier to the energetically more favorable state containing vortices could now be overcome more easily.

[7] In Paris, 11 vortices ordered in a lattice were observed in expansion after ramping down the stirring beam in only 8 ms [160, 54].

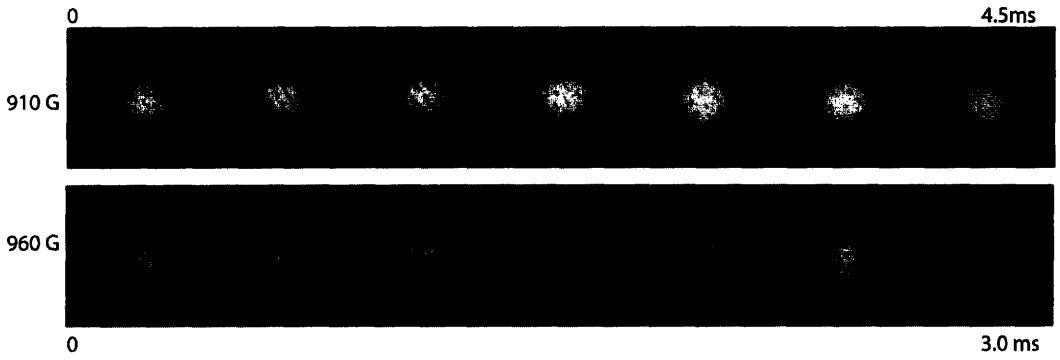

Figure 6-12: Observation of pair breaking in a superfluid Fermi gas. Shown are absorption images for different expansion times on the BCS-side of the Feshbach resonance at 910 G (0,1,2,3,3.5,4, and 4.5 ms) and at 960 G (0, 0.5, 1, 1.5, 2, 2.5, and 3 ms), before ramping to the BEC-side for further expansion and imaging. The total time-of-flight was constant. The vortices served as markers for the superfluid parts of the cloud. Superfluidity survived during expansion for several ms, and was gradually lost from the low-density edges of the cloud towards its center. The field of view of each image is 1.2 mm $\times$ 1.2 mm.

At later stages of the experiment, we were able to stabilize 75 vortices for 10 s in a deeper trap with $\nu_r = 120$ Hz.

6.3.3 Pair breaking

A true qualitative distinction between the BEC- and the BCS-limit in fermionic superfluids is the fragility of the pairs on the BCS-side. Here, pairing is purely a many-body effect. In contrast to the case of Bose-Einstein condensates, the simple expansion from the trap can destroy the superfluid (at finite temperatures): The now isolated pairs will break. All information about the center-of-mass wavefunction of the pairs $\psi(\mathbf{r})$ and hence the vortices, will be gradually lost. In our experiments, the rapid ramp to the BEC-side ensures that the pairs survive as stable molecules.

It is now natural to *delay* the "rescuing" ramp to the BEC-side and observe when exactly this breakdown of superfluidity occurs, using the presence or absence of vortices as markers for superfluidity [216]. We thus let the gas expand on the BCS-side for a certain time t_{BCS}, then ramp down to the BEC-side for further expansion and imaging. The total expansion time is kept constant.

It is found that superfluid flow initially persists during the expansion. Then, vortices start to disappear first at the edges of the cloud, then, for longer BCS-

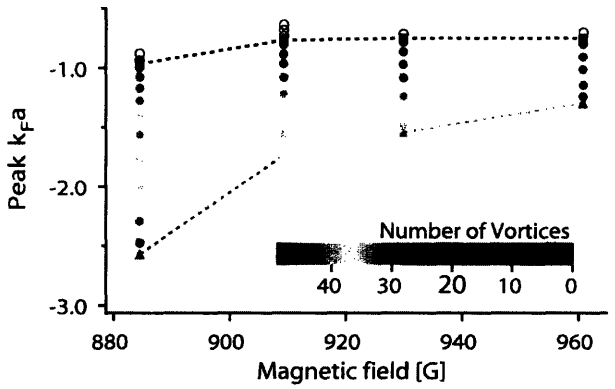

Figure 6-13: (Color online) Peak interaction strength $k_F a$ during superfluid expansion. Starting at a peak $k_F a$ in the optical trap, vortices survive up to an interaction strength $k_F a \approx -0.8$, almost independent of the magnetic field (scattering length a). Filled circles correspond to partially superfluid, open circles to normal clouds. The observed number of vortices is color coded.

expansion t_{BCS}, further inwards until the last vortex disappears at the cloud's center (see Fig. 6-12). The time t_{BCS} for which the last vortex disappears, increases the closer we are to resonance, that is, the larger the interaction strength and the stronger the fermion pairs are bound.

In fact, by varying the magnetic field and thus the scattering length, we find that the last vortex always disappears at about the same value of the interaction parameter $k_F a \approx -0.8$ (see Fig. 6-13). Here one enters the regime of weak interactions, where the pair size is large, the critical temperature for superfluidity is small and hence the superfluid state is fragile.

The simplest explanation for our observation is naturally that we cross the phase transition line during expansion. While T/T_F is an adiabatic constant for the expansion, T/T_C is not, as T_C/T_F depends exponentially on the density. As the density decreases, the critical temperature in the outer regions of the cloud eventually drops below T, superfluidity is lost starting from the edges inwards.

We can estimate the critical interaction strength for this breakdown to occur. At our coldest temperatures, $T/T_F = 0.05$ (see chapter 7). The formula for T_C due to Gorkov and Melik-Barkhudarov [98] gives $T_C = \frac{e^\gamma}{\pi}\left(\frac{2}{e}\right)^{7/3} T_F\, e^{-\pi/2k_F|a|} = 0.28\, T_F\, e^{-\pi/2k_F|a|}$. This formula should be valid in the BCS-regime where $k_F|a| \lesssim 1$. We can now equate

$$1 = \frac{T}{T_C} = \frac{T}{T_F}\frac{T_F}{T_C} \approx 0.05\,\frac{T_F}{T_C} = 0.18\, e^{\pi/2k_F|a|} \tag{6.10}$$

Figure 6-14: Loss of vortex contrast on resonance, at $B = 834$ G. Shown are absorption images at fixed total time-of-flight, but for different expansion times on resonance (2, 2.5, 3, 3.5, 4,5, and 6 ms) before the magnetic field ramp to the BEC-side for further expansion. The vortex contrast decreases uniformly across the cloud from 15% (for 2 ms resonant expansion) to about 3% (for 5 ms). The field of view of each image is 1.2 mm $\times$ 1.2 mm.

The result gives the critical interaction strength $k_F\,|a| = 0.9$. This is close to the observed value.

However, we can think about other scenarios that might explain the observed disappearance of vortices: In the BCS-regime around $k_F|a| = 1$, the pairs are large and fragile. The expansion itself might be too much of a perturbation so that they break apart. This dynamic pair breaking will occur if the rate of change in the binding energy Δ is larger than the rate at which the pairs can respond to the reduced density, $\Delta/\hbar$. For our experimental parameters, we find $\frac{\hbar\dot{\Delta}}{\Delta^2} \leq 0.4$, so the pair binding energy still changes more slowly than the characteristic response time. However, the rates are not too different, and this dynamic pair breaking mechanism might not be negligible.

Note that in the images, even for short "BCS-expansion" times, we see a clear boundary between the coherent part containing vortices and a part of the fluid which does not contain vortices and appears normal. For these short expansion times, the dynamic pair breaking mechanism is ruled out and the most plausible scenario is that we are simply seeing the normal-to-superfluid transition in the gas cloud: $T_C = T$ defines a certain density in the cloud beyond which the gas is necessarily normal.

On resonance, $T_C \propto T_F$, and one would not expect to loose superfluidity during expansion. Indeed, here we observe that vortices survive expansion even in the low-density edges of the cloud (see Fig. 6-14). However, the longer the ramp to the BEC-side is delayed, the lower the vortex contrast in the final cloud, and the smaller the apparent size of the vortex cores. We believe that this is due to the low density of the cloud after long expansion on resonance. Then the gas is so dilute that, after the ramp, the vortex cores cannot adjust anymore to the larger equilibrium size and the increased contrast they should have on the BEC-side. It is expected that expansion on resonance simply scales the dimensions of the cloud (at least for purely radial

expansion) [47]. Hence we can speculate that, the longer we delay the ramp to the BEC-side, the closer the final vortex contrast and vortex size will correspond to the situation on resonance. Here, vortices are expected to be small, of size $\xi \sim 1/k_F$, and to show a reduced contrast [41].

To conclude, we observe superfluid flow in an expanded Fermi gas down to densities of about $10^{11}\,\mathrm{cm}^{-3}$. At these densities, the average distance between two atoms is 2 μm! The average distance between neutrons in a neutron star is a few fm, corresponding to densities of $10^{38}\,\mathrm{cm}^{-3}$. This nicely illustrates how general the phenomenon of fermionic superfluidity is.

Chapter 7

Fermionic superfluidity with imbalanced spin populations

In previous chapters, we have exclusively studied an *equal* spin-mixture of fermionic atoms. Here, pairing can be complete and the entire gas can become superfluid at zero temperature. What, however, happens if we deliberately imbalance the populations in the two spin states? In this case, not every spin up (majority) fermion can find a spin down (minority) partner. Immediately, several questions arise: Can the gas still be superfluid? If so, are the excess fermions tolerated inside the gas of pairs or are they expelled from the superfluid? If superfluidity breaks down, what is the nature of such a strongly interacting, imbalanced normal mixture?

We studied these questions in a strongly interacting Fermi mixture by varying the spin imbalance, temperature and interaction strength. Superfluidity was found to be robust against population imbalance in the strongly interacting regime. We could show that, below a certain temperature, the superfluid state requires equal spin densities, and phase separates from the partially polarized normal state. At a critical population imbalance, we observed the final breakdown of the superfluid state, the Clogston or Pauli limit of superfluidity. Studying imbalanced Fermi mixtures enabled us to directly observe the superfluid transition in situ, without any magnetic field ramps into the molecular regime. The non-interacting, fully polarized part of the cloud served as a reliable thermometer, solving, for the imbalanced case, the problem of measuring temperature in a strongly interacting gas.

In contrast to the smooth BEC-BCS crossover physics in an equal Fermi mixture with varying interaction strength, the imbalanced mixtures provide us with a rich phase diagram, including zero temperature phase transitions, which challenges present many-body theories.

7.1 Historic overview

The question of imbalanced superfluidity has a 50 year old history. Bardeen, Cooper and Schrieffer described the superconducting state as a condensate of pairs of electrons carrying opposite spin. However, an applied magnetic field tends to align the electron spins, thereby putting a "stress" on the fully paired superfluid state. Following this thought, Clogston [61] derived in 1962 an upper limit for the critical magnetic field of a superconductor: Once the energy gain for aligning the electron spins is larger than the energy gain from pairing opposite spins, Cooper pairs must break and the system should turn normal. This is the Pauli or Clogston limit of superconductivity. In 1964, Fulde and Ferrell [94] and independently Larkin and Ovchinnikov [146] found that not all the pairs necessarily break at once, but that there exists a novel superfluid state which tolerates a certain amount of broken pairs by allowing the remaining Cooper pairs to have a common non-zero momentum $\mathbf{Q}$ (FFLO or LOFF state). Thus, the order parameter (the gap) is not a constant, but it oscillates at a wavelength $\sim 1/Q$, where the typical value of Q is given by the Fermi momentum difference between the two spin states. This state of the imbalanced superconductor will thus break translational and rotational symmetry by picking out a certain direction $\mathbf{Q}$. Forty years later, the debate about the ground state of imbalanced superfluidity is still ongoing. The topic had been revived from several directions: From condensed matter, through studies of exotic superconductors [46, 198, 30] that are essentially Pauli limited, and from nuclear physics and the study of the quark-gluon plasma, where similar questions arose in the study of superfluid pairing of quarks at unequal Fermi energies [7], and from atomic physics, were the advent of ultracold atomic Fermi gases presented a new opportunity to study imbalanced superfluidity.

Preceding the experimental studies, Liu and Wilczek [151] proposed the breached pair or Sarma state [211] as an alternative to the FFLO state. Another suggestion, that did not require breaking of translational, only rotational symmetry, was a state with a deformed fermi surface [218]. Combescot and Mora [65] studied the FFLO-state in Fermi gases in the BCS regime. Its direct detection by imaging the gas was proposed by Mizushima et al. [169] (see also [49]). Bedaque et al. [28] noted that it is favorable for a weakly interacting imbalanced Fermi mixture to phase separate into a superfluid part at equal densities and a normal part at unequal densities. In the regime of strong interactions, a Monte-Carlo study of the problem of imbalanced superfluidity was performed by Carlson and Reddy [44]. They found that the imbalanced Fermi gas on resonance was intriguingly close, within their error margins, to be a polarized

superfluid, where unpaired excess fermions were tolerated by the Cooper pairs. The implications of universality on resonance were discussed by Cohen [62]. Pao et al. [185] performed a stability analysis of the superfluid state across a Feshbach resonance at fixed densities, and found that homogeneous superfluidity was unstable on the BCS-side and in the strongly interacting regime.

The subject has received much attention since our first observation of superfluidity with imbalanced spin populations, reported in June 2005 [135]. We determined the phase diagram of imbalanced Fermi gases, and found the Clogston limit of superfluidity [268]. Hints of phase separation were seen in our work and at Rice University [187]. Imbalanced Fermi mixtures allowed us to observe the superfluid phase transition directly, without the necessity of field ramps [269]. Finally, using a novel imaging technique, we were able to demonstrate phase separation in strongly interacting Fermi mixtures [223].

Motivated by these findings, phase diagrams for imbalanced mixtures close to a Feshbach resonance were obtained[1] [185, 221, 229, 256, 152, 157, 103, 50, 127, 186], and the shape of imbalanced Fermi gases in atom traps was studied [196, 140, 226, 258, 53, 114, 55, 220]. Insight into the equation of state on resonance was gained by exploiting the principle of universality [52, 40] and via Monte-Carlo calculations [153]. The properties of the vortex state in imbalanced fermionic superfluid was discussed in [242], showing that particles of the majority spin species will be trapped inside the vortex cores.

Naturally, there are still many open questions: The role of temperature, finite size effects or the nature of the strongly interacting normal state. The search is still ongoing for a signature of the FFLO-state or other proposed new forms of superfluidity. We can expect that the next months and years will bring us exciting new experimental results and theoretical insight.

7.2 The Clogston limit of superfluidity

7.2.1 The Clogston limit of superconductors

Naturally, it is not a simple task to magnetize a superconductor because of the Meissner effect [166]: Magnetic fields are actively expelled from charged superfluids. They can only enter as magnetic flux lines or vortices (and only in so-called Type II super-

[1] This list is far from complete. Over 80 articles have been written on the topic over the past nine months. I refer the reader to the cited publications and references therein.

conductors). Once the energy cost per volume for expelling the field, $B^2/2\mu_0$, exceeds the difference in the free energy density F between the normal and the superconducting state, the superconductor turns into a normal metal. If the critical field is B_c, we have

$$\mathcal{F}_N = \mathcal{F}_S + \frac{B_c^2}{2\mu_0} \tag{7.1}$$

where the subscripts N and S stand for the normal and the superconducting state, respectively. The free energy density difference $\mathcal{F}_N - \mathcal{F}_S$ is given by the pairing energy Δ of $\rho(E_F)\Delta$ electron pairs at the Fermi surface per unit volume ($\rho(E_F)$ is the density of states per spin state at the Fermi energy),

$$\mathcal{F}_N - \mathcal{F}_S = \frac{1}{2}\rho(E_F)\Delta^2 \tag{7.2}$$

which relates the critical magnetic field B_c to the superconducting gap,

$$B_c = \sqrt{\mu_0 \rho(E_F)}\Delta \tag{7.3}$$

To get a sense of scale, for free electrons, $\rho(E_F) = \frac{3}{4}\frac{n}{E_F}$, with $n \approx 1 - 10 \cdot 10^{22}\,\mathrm{cm}^{-3}$ the density of electrons and $E_F \approx k_B \times 50\,000 - 100\,000\,\mathrm{K}$, and assuming $\Delta = 1.76\, k_B T_C$ from BCS theory (see Eq. 2.125 in chapter 2), we get

$$B_c \approx 50\,\mathrm{G}\,\frac{T_C}{\mathrm{K}} \tag{7.4}$$

This is a very small field compared to the natural scale set by the critical temperature and the electron's magnetic moment, $B_{T_C} \sim k_B T_C/\mu_B = 15\,000\,\mathrm{G}\,\frac{T_C}{\mathrm{K}}$. However, at the surface of a superconductor, the magnetic field does not suddenly drop to zero, but only over a certain penetration depth. For very thin superconductors or certain special materials, the magnetic field *can* enter the superconductor, increasing the critical magnetic field substantially. It was Clogston's insight that under the extreme condition that there is *no* Meissner effect, there will still be a critical magnetic field that destroys superconductivity à la BCS.

The reason is the following: The superconducting state is fully paired, that is, there must be an equal number of spin up and spin down electrons present. In fact, by changing a spin down into a spin up electron one gains an energy $2\mu_B B$, but this would necessitate breaking the initial pair (cost Δ), and in addition there is no pairing partner for the new spin up electron (cost another Δ) (for adding and removing single particles to the BCS state see section 2.3.3). Thus, for $\mu_B B < \Delta$ this

cannot occur. However, the normal state is free to adjust the number of spin up vs spin down electrons, thereby reducing its energy.

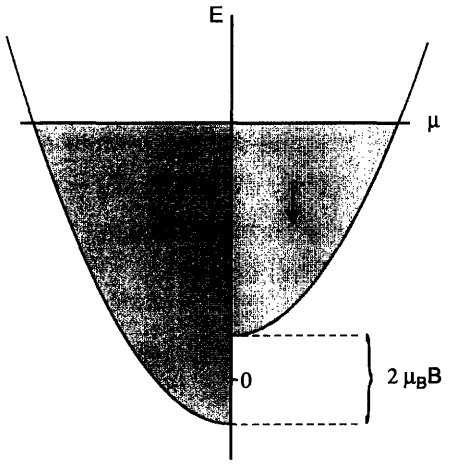

Figure 7-1: Imbalanced chemical potentials for electrons in the normal state under the influence of a magnetic field.

Let us calculate this reduction of free energy density in the normal state in the presence of a magnetic field. The field changes the energies of spin-up electrons according to $\epsilon_{k\uparrow} = \epsilon_k - \mu_B B$, which we can incorporate into the chemical potential $\mu_\uparrow = E_F + \mu_B B$ of the up-electrons[2] (see Fig. 7-1). The energy density of a Fermi gas at chemical potential $\mu_\uparrow$ is $\epsilon = \frac{3}{5}\mu_\uparrow n_\uparrow$, with the density $n_\uparrow = \frac{1}{6\pi^2}k_{F\uparrow}^3$ and the Fermi wave vector $k_{F\uparrow}$ related to $\mu_\uparrow$ via $\mu_\uparrow = \frac{\hbar^2 k_{F\uparrow}^2}{2m}$. Hence, the free energy density of the "two-species mixture" of spin-up and spin-down electrons is given by

$$\mathcal{F}_N(B) = \frac{3}{5}\mu_\uparrow n_\uparrow + \frac{3}{5}\mu_\downarrow n_\downarrow - \mu_\uparrow n_\uparrow - \mu_\downarrow n_\downarrow \tag{7.5}$$

$$= -\frac{4}{15}\rho(1)\left(\mu_\uparrow^{5/2} + \mu_\downarrow^{5/2}\right) \tag{7.6}$$

with $\rho(1) = \frac{m^{3/2}}{\sqrt{2}\pi^2\hbar^3}$. Inserting the chemical potentials given as a function of E_F and B, we finally have

$$\mathcal{F}_N(B) = -\frac{4}{15}\rho(E_F)\,E_F^2\left\{\left(1+\frac{\mu_B B}{E_F}\right)^{5/2} + \left(1-\frac{\mu_B B}{E_F}\right)^{5/2}\right\} \tag{7.7}$$

$$\approx \mathcal{F}_N(0) - \rho(E_F)\,\mu_B^2\,B^2 \qquad \text{valid for } \mu_B B \ll E_F \tag{7.8}$$

[2]The sign-convention makes sure the spin-up electrons will be the majority species. This means, the electron spin of spin-up electrons points into the direction *opposite* the magnetic field.

The *magnetization* of the normal state is $\mathcal{M} = -\frac{\partial \mathcal{F}_N}{\partial B} = \rho(E_F)\mu_B^2 B$, proportional to the applied field.

If the reduction in $\mathcal{F}_N$ is larger than the energy gain from forming a fully paired superconducting state, Eq. 7.2, the metal favors the normal state. The critical magnetic field found by Clogston is thus

$$B_{\text{Clogston}} = \frac{1}{\sqrt{2}}\frac{\Delta}{\mu_B} \tag{7.9}$$

$$= 18\,500\,\text{G}\frac{T_C}{\text{K}} \tag{7.10}$$

The expression holds for weak interactions, where $\Delta \ll E_F$. This is evidently very well satisfied by conventional superconductors, but it will be interesting to see whether such a critical field might still exist in the strongly interacting regime.

7.2.2 Translation to dilute Fermi gases in atom traps

In dilute Fermi gases, the chemical potential difference $\delta\mu \equiv 2h = \mu_\uparrow - \mu_\downarrow$ is not directly controlled, as it was the case for superconductors in a magnetic field where $h = \mu_B B$. What can be freely chosen in our case are the *numbers* of spin-up and spin-down fermions, i.e. the populations of the two hyperfine states $|1\rangle$ and $|2\rangle$.

Furthermore, the experiments take place in the presence of a trapping potential $V(\mathbf{r})$. The chemical potentials of the two species are determined by the *global* requirement that they must correspond to the state that has the given particle numbers $N_\uparrow$ and $N_\downarrow$ in the two spin states. Let us say the system finds that $\mu_\uparrow^0$ and $\mu_\downarrow^0$ are the correct (global) chemical potentials. *Locally*, the chemical potentials at point $\mathbf{r}$ in the trap will thus be[3]

$$\begin{aligned} \mu_\uparrow(\mathbf{r}) &= \mu_\uparrow^0 - V(\mathbf{r}) \\ \mu_\downarrow(\mathbf{r}) &= \mu_\downarrow^0 - V(\mathbf{r}) \end{aligned} \tag{7.11}$$

While the average chemical potential $\mu(\mathbf{r}) = \frac{\mu_\uparrow(\mathbf{r})+\mu_\downarrow(\mathbf{r})}{2}$ varies across the trap, the *difference* chemical potential is constant throughout,

$$\delta\mu(\mathbf{r}) = 2h = \mu_\uparrow^0 - \mu_\downarrow^0 \tag{7.12}$$

Thus, effectively, the trapping potential *tunes* the ratio h/μ over a certain range. An

[3]We assume here that the system *can* be described by local quantities, that is, we assume that the local density approximation holds (see section 7.5).

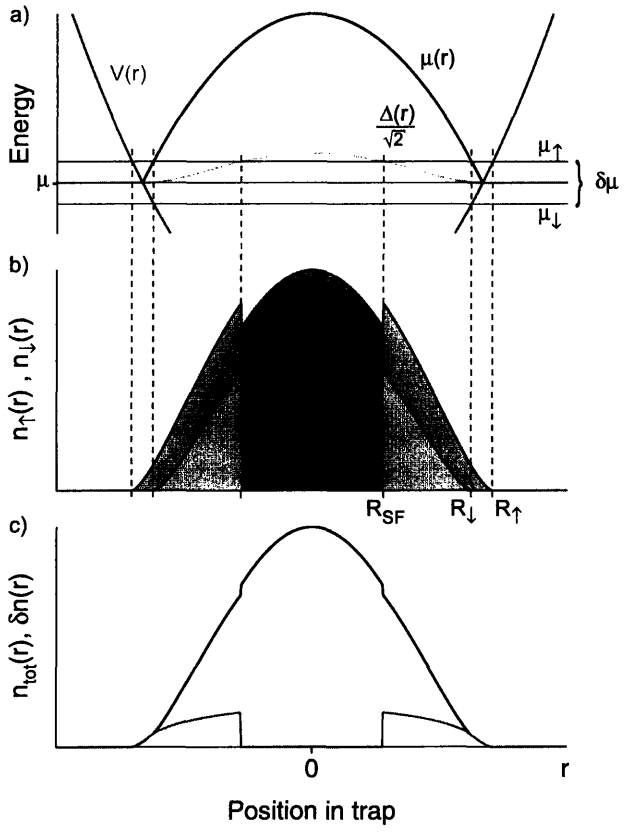

Figure 7-2: A weakly interacting, imbalanced Fermi mixture with superfluid component in a harmonic trap. a) Trapping potential $V(r)$, local, average chemical potential $\mu(r)$ and Clogston limit $\Delta(r)/\sqrt{2}$. Where $\Delta(r)/\sqrt{2} > \delta\mu/2$, the gas is in the superfluid phase. b) shows the densities of spin up and spin down atoms, c) the total and the difference density distribution. For this illustration, the peak gap was chosen to be $\Delta(0) = 0.25\mu(0)$.

imbalanced Fermi mixture in a trap can thus explore several local phases. Let us for example consider the Clogston limit above. It occurs when the "field" h satisfies

$$h = \frac{1}{\sqrt{2}}\Delta(\mathbf{r}) \qquad \text{for } \Delta \ll \mu \tag{7.13}$$

where the superfluid gap $\Delta(\mathbf{r})$ is to be calculated as usual using the average chemical potential $\mu(\mathbf{r})$, that is in the weakly interacting regime[4] $\Delta(\mathbf{r}) = \left(\frac{2}{e}\right)^{7/3}\mu(\mathbf{r})\, e^{-\pi/2k_F(\mathbf{r})|a|}$, with the Fermi wave vector $k_F(\mathbf{r})$ given by $\mu(\mathbf{r}) = \hbar^2 k_F(\mathbf{r})^2/2m$. The situation is sketched in Fig. 7-2: The Clogston criterion defines a critical radius $R_{\rm SF}$ where $\Delta(R_{\rm SF}) = \sqrt{2}h = \frac{1}{\sqrt{2}}\delta\mu$. For radii $r < R_{\rm SF}$, the gas is in the BCS-type superfluid state and thus fully paired. For radii exceeding $R_{\rm SF}$, the gas is in the normal state. Here we can further distinguish the region where both spin up and spin down particles are present, $R_{\rm SF} < r < R_\downarrow$ and the region where *only* spin up atoms are present, $R_\downarrow < r < R_\uparrow$, the case of a fully polarized sample. These radii are - in this weakly interacting case - simply given by the usual relations $V(R_{\uparrow,\downarrow}) = \mu_{\uparrow,\downarrow}$, that is $R_{\uparrow,\downarrow} = \sqrt{\frac{2\mu_{\uparrow,\downarrow}}{m\omega^2}}$, for harmonic trapping. The densities are given by $n_{\uparrow,\downarrow}(r) = \frac{1}{6\pi^2}(\frac{2m\mu_{\uparrow,\downarrow}}{\hbar^2})^{3/2}(1-\frac{r^2}{R^2_{\uparrow,\downarrow}})^{3/2}$ (for $R_{\rm SF} < r < R_{\uparrow,\downarrow}$), whereas for the superfluid state at $r < R_{\rm SF}$ one has $n_{\rm SF}(r) = \frac{1}{6\pi^2}(\frac{2m\mu}{\hbar^2})^{3/2}(1-\frac{r^2}{R^2})^{3/2}\cdot(1+\mathcal{O}(\frac{\Delta^2}{\mu^2}))$ with $R = \sqrt{\frac{2\mu}{m\omega^2}}$ given by the average chemical potential and a small enhancement of the density ($\mathcal{O}(\frac{\Delta^2}{\mu^2})$ due to pairing [220].

We will see in the experiments that the important qualitative features, a central superfluid region of equal densities, a mixed normal region and a fully polarized region further outside, remain valid also in the strongly interacting regime where $k_F|a| \gg 1$.

7.2.3 Phase separation in the BCS-regime

Fig. 7-2 shows that the densities of the two spin components are expected to jump from their respective values in the normal state to a common value in the superfluid state. This discontinuity nicely illustrates that the Clogston limit is a first-order transition: As h/μ is tuned starting from zero (either directly via a magnetic field for a superconductor, or implicitly via the varying trapping potential), the density difference is first zero, as one is still in the BCS superconducting phase. At the Clogston limit $h/\mu = \frac{1}{\sqrt{2}}\frac{\Delta}{\mu}$ the system suddenly turns normal and the density difference jumps to a finite value. In the language of thermodynamics, the free energy density, con-

[4]This is the BCS-gap when density fluctuations are taken into account [98]. Note that in the weakly interacting regime, μ does not depend on the interaction strength and is equal to the average Fermi energy of a non-interacting Fermi mixture.

sidered a function of the superfluid gap Δ, has developed a new global minimum at $\Delta = 0$, the normal state.

We thus see that in the presence of a trapping potential, which tunes h/μ, we expect to observe phase separation between an inner superfluid core of equal densities and a normal state outside. However, phase separation would also occur in the case of an imbalanced Fermi mixture confined in a large box potential. In this case, the global densities $n_\uparrow$ and $n_\downarrow$ are fixed. We can consider three possibilities: 1. A uniform superfluid state with imbalanced densities. 2. A uniform normal state with imbalanced densities. 3. A phase separated state containing bubbles of a superfluid equal mixture, surrounded by a mixed normal state.

A uniform BCS state with imbalanced densities is not possible, as we have already seen in the case of superconductors. Polarization of the BCS state could only happen if the "Zeeman field"

$$h = \frac{\delta\mu}{2} > \Delta \tag{7.14}$$

Before h could ever equal the gap, however, the system already turns normal at $h = \Delta/\sqrt{2}$, the Clogston limit. The BCS state thus does not tolerate imbalanced densities.

One might consider other possible states than the fully paired BCS-state, for which, for increasing mismatch between the two Fermi surfaces of the homogeneous superfluid, pairing still occurs, but becomes less efficient with decreasing Fermi surface overlap, and the gap decreases until superfluidity finally disappears. One candidate is the Sarma (or breached pair) state [211, 151]. For fixed "magnetic field" h, this state is a maximum of the thermodynamic potential, hence unstable, but it was argued that it might be stable in the case of fixed *densities*. For the BCS-case it turns out that the phase separated state containing superfluid bubbles of equal densities is energetically favored compared to a uniform normal state of unequal densities and the Sarma phase, as was first pointed out by Bedaque, Caldas and Rupak [28]. In a certain parameter regime, calculations indicate that the FFLO-state, where Cooper pairs have finite momentum, should be the ground state of the system [94, 146, 169, 221, 157].

7.2.4 Critical number imbalance

In the case of weak interactions ($\Delta \ll \mu$) and harmonic trapping, it is easy to derive a critical population imbalance for which there will be *no* superfluid region. The

condition is simply $R_{\rm SF} = 0$ or

$$h = \frac{1}{\sqrt{2}}\Delta(0) \tag{7.15}$$

$$\Rightarrow \frac{h}{\mu} = \frac{1}{\sqrt{2}}\left(\frac{2}{e}\right)^{7/3} e^{-\pi/2k_F|a|} \tag{7.16}$$

where, as before, μ is the average Fermi energy of a non-interacting, equal Fermi mixture, $\mu = E_F$. The numbers of particles in the normal state are given by the usual relation for a harmonic trap (see Eq. 2.40 in chapter 2), $N_{\uparrow,\downarrow} = \frac{1}{6}\left(\frac{\mu_{\uparrow,\downarrow}}{\hbar\omega}\right)^3$. We thus find the critical population imbalance for weak interactions

$$\delta_c \equiv \frac{N_\uparrow - N_\downarrow}{N_\uparrow + N_\downarrow} = \frac{(1+\frac{h}{\mu})^3 - (1-\frac{h}{\mu})^3}{(1+\frac{h}{\mu})^3 + (1-\frac{h}{\mu})^3} \approx 3\frac{h}{\mu} = \frac{3}{\sqrt{2}}\frac{\Delta(0)}{\mu} \tag{7.17}$$

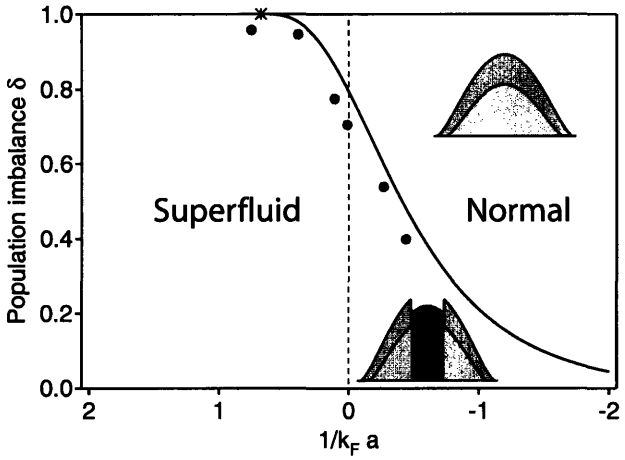

Figure 7-3: Critical population imbalance $\delta = \frac{N_\uparrow - N_\downarrow}{N_\uparrow + N_\downarrow}$ for BCS-type superfluidity in a harmonic trap. The data-points give the experimental result [268]. The cross marks the point on the BEC-side of the resonance where superfluidity occurs at any imbalance smaller than 1. Using the Gorkov expression for the gap, this point lies at $1/k_F a = 0.7$, outside the applicability of our derivation. However, the point should lie at $1/k_F a > 0$, probably around $1/k_F a \approx 1$, where the chemical potential μ changes from positive to negative values and BCS-type physics is replaced by condensation of small molecules.

Fig. 7-3 shows the resulting phase diagram, along with the experimental results described in the next section. The calculation assumes the expression for h/μ, Eq. 7.16, to still hold in the strongly interacting regime, which is discussed below. In the

weakly interacting regime, where $h \ll \mu$, we see that δ_c is proportional to the gap and thus depends exponentially on the interaction strength $1/k_F|a|$. This presents - apart from the exponentially low critical temperature T_C - another reason why in the beginnings it was not clear whether experiments with fermionic atoms were able to observe superfluidity. It appeared that the two spin populations had to be essentially perfectly matched: For a Fermi energy of $E_F = 1\,\mu$K ($1/k_F \approx 3800\,a_0$) and a scattering length of $a = -500\,a_0$, still ten times larger than "typical" scattering lengths in alkali atoms, the critical population imbalance δ_c is already smaller than one out of 10^5 atoms! If experiments do not control the number difference to better than 1%, they cannot explore superfluidity at interaction strengths smaller than $k_F|a| \approx 0.35$. Obviously, the use of Feshbach resonances solved this problem.

Using several independent techniques described in the following sections, we measured the critical number imbalance as a function of interaction strength. The data for one type of measurement (via the condensate fraction) is shown in Fig. 7-3. It is satisfying to see that the experimental data closely follows the expected trend for the critical number imbalance.

Resonance

Note that in the above calculation of the critical number imbalance we have assumed that the normal state is *non-interacting*. Also, the BCS-approach neglects Cooper pairs at finite momenta as well as interactions between different Cooper pairs. In addition, the simple formula Eq. 7.2 for the free energy density difference between the normal and the superfluid state will be altered for large $k_F|a|$. For these reasons, the results cannot be trusted in the strongly interacting regime. Nevertheless, it is reasonable that the *qualitative* behavior remains unchanged all the way to ($1/k_F a = 0$), in the same way the qualitative behavior of the BEC-BCS crossover model appears to capture the essential physics of an equal mixture. Moreover, the expression for the gap used in Eq. 7.16 above, due to Gorkov and Melik-Barkhudarov [98], gives for the resonance case $\Delta = (2/e)^{7/3} E_F = 0.49 E_F$, which agrees surprisingly well with the result of Monte-Carlo calculations, $\Delta = 0.50 E_F$ [44]. With all caveats in mind, we give the critical population imbalance on resonance, using the expression for the gap due to Gorkov and Melik-Barkhudarov

$$\delta_c = 80\% \qquad \text{at } 1/k_F\, a = 0 \tag{7.18}$$

We have measured this critical imbalance on resonance (see below) and find $\delta_c^{\text{exp}} =$

74(5)%. A recent Monte-Carlo study predicts $\delta_c = 77\%$ [153]. Using the variational BCS-approach, for which $\Delta = 0.69E_F$ on resonance, yields $\delta_c = 92\%$. However, one should not expect the variational Ansatz to predict any parameter on resonance in a quantitative way. Fluctuations, such as those included by Gorkov and Melik-Barkhudarov in the BCS-regime, seem to play an important role. This example gives hope that the study of imbalanced Fermi mixtures will substantially improve our understanding of strongly interacting fermions.

Both experiment and recent theory obtain $\delta_c < 1$ on resonance. By continuity, this implies that there is a region *on the BEC-side* of the BEC-BCS crossover where *condensation cannot occur*, even at zero temperature, in the presence of large spin imbalance. This is surprising, since for $a > 0$, there is a molecular state available for two atoms in vacuum, and one would expect these bosonic molecules to condense at zero temperature (essentially, bosons have no other choice at zero T). A simple way out of this dilemma is of course that the very presence of the large Fermi sea of spin up atoms prohibits the formation of the molecular state. Essentially, the (two-body) molecular state requires a width $k \sim 1/a$ in k-space. Once $a \approx 1/k_F$ in the strongly interacting regime close to resonance, the required momenta are Pauli-blocked by the presence of spin-up atoms occupying k-space from $k = 0$ to $k = k_{F\uparrow} > 1/a$. Hence, the molecular state is not available anymore.

7.3 Fermionic superfluidity with spin imbalance

In this experimental section, we will demonstrate superfluidity for imbalanced mixtures. The first experiment is a study of rotating fermionic mixtures. Vortices directly demonstrate that superfluidity persists in trapped, imbalanced Fermi mixtures. The second experiment determines the condensate fraction using the rapid ramp method of chapter 5. Hereby we could show the robustness of the superfluid in the strongly interacting regime and directly demonstrate the Clogston limit of superfluidity. In the first paragraph I describe how the population imbalance can be varied in our experiment.

7.3.1 Creation of imbalanced Fermi mixtures

The experiments start at maximum optical trap depth with a fully polarized sample in the lowest hyperfine state of lithium, $|1\rangle$, and at a magnetic field above resonance (typically at 875 G). The energies of states $|1\rangle$ and $|2\rangle$ are split by about $h \times 76\,\mathrm{MHz}$.

A radiofrequency sweep then transfers a certain fraction from state $|1\rangle$ into state $|2\rangle$ according to the Landau-Zener law $P = 1 - e^{-2\pi\Omega_R^2/\dot{\omega}}$, where $\hbar\Omega_R$ is the Rabi-frequency of the transition, tunable via the power of the radiofrequency drive, and $\dot{\omega}$ is the sweep rate at which the transition is crossed. We typically keep $\hbar\Omega_R$ fixed and vary $\dot{\omega}$. After the sweep, all fermions are still polarized in a coherent superposition state of $|1\rangle$ and $|2\rangle$ and need several tens of milliseconds to decohere, as discussed in chapter 4 and in [106]. As the sample has decohered, evaporative cooling can proceed. Starting with an initial temperature of about $T/T_F = 0.3$, we reach $T/T_F = 0.05$.

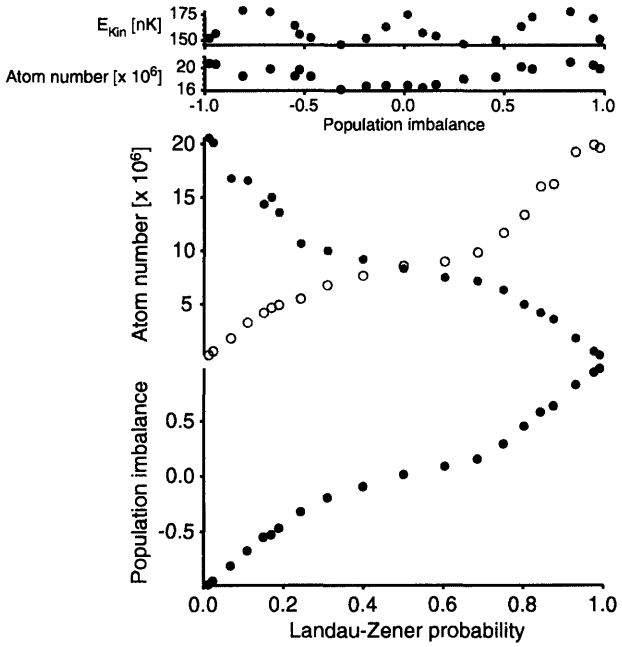

Figure 7-4: Creation of imbalanced Fermi mixtures. A faster-than-adiabatic Landau Zener RF sweep is used to transfer a fraction of atoms from state $|1\rangle$ into state $|2\rangle$. For a fixed final trap depth at the end of evaporation, the temperature varies only slightly with imbalance.

During evaporation, mostly majority atoms escape from the trap, as their Fermi energy is closer to the trap depth. Thus, evaporation will always reduce the imbalance in the cloud. Fig. 7-4 displays the final atom number as a function of the Landau-Zener probability. The dependence of the total atom number and temperature on the population imbalance is fairly small. It could be further minimized by adjusting the trap depth at the end of evaporation as a function of imbalance.

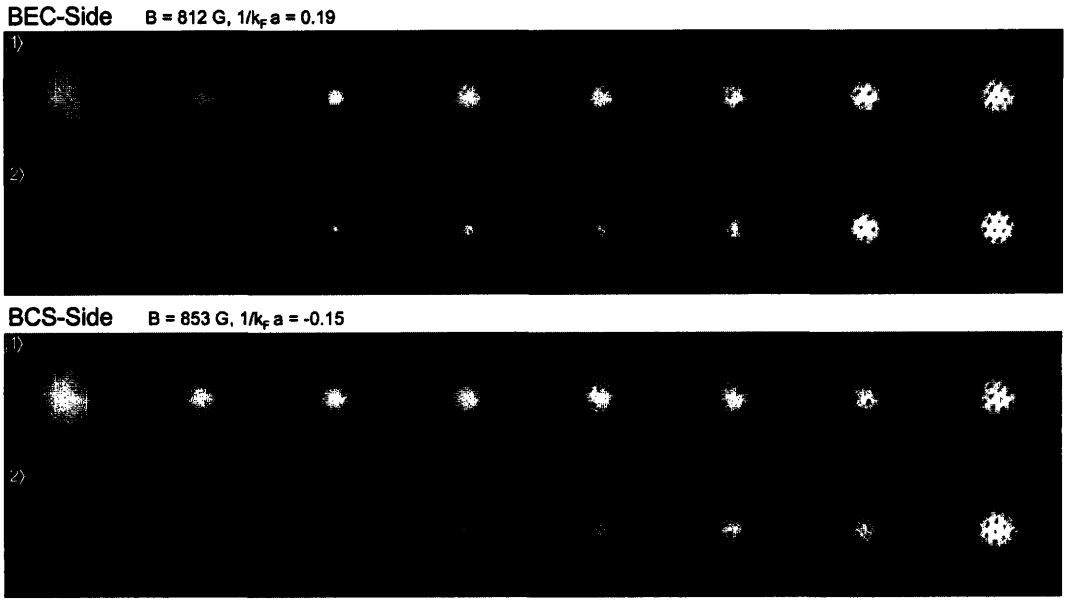

Figure 7-5: Superfluidity in an imbalanced fermion mixture. For the 812 G data, the population imbalance was (from left to right) 100%, 90%, 80%, 62%, 28%, 18%, 10% and 0%. For the 853 G data, the mismatch was 100%, 74%, 58%, 48%, 32%, 16%, 7% and 0%.

7.3.2 Rotating imbalanced mixtures: Vortices

After a strongly interacting, imbalanced spin mixture has been created, the cloud is set in rotation, equilibrates and is then imaged as described in chapter 6. Fig. 7-5 shows the resulting images, and Fig. 7-6 the number of vortices as a function of imbalance and interaction strength. Vortices are observed for a wide range of imbalances. Clearly, superfluidity in the strongly interacting Fermi gas is not constrained to a narrow region around the perfectly balanced spin-mixture, but instead superfluid flow is observed for large population asymmetries. Gradually, for decreasing interaction strength $1/k_F a$, the superfluid window closes around the optimal situation of an equal mixture. This is what we expect from the discussion of the Clogston limit above.

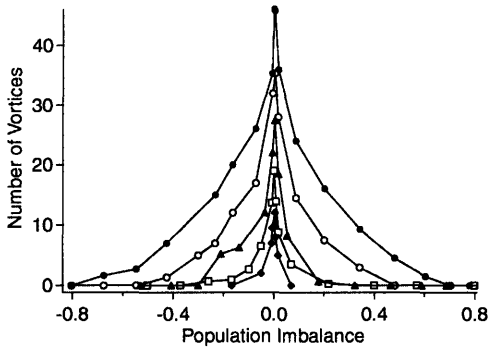

Figure 7-6: Number of vortices obtained in an imbalanced Fermi mixture. The curves, from top to bottom, correspond to decreasing interaction strength $1/k_F a = 0.2$ (BEC-side), -0.15, -0.3, -0.4, and -0.5 (BCS-side of the Feshbach resonance).

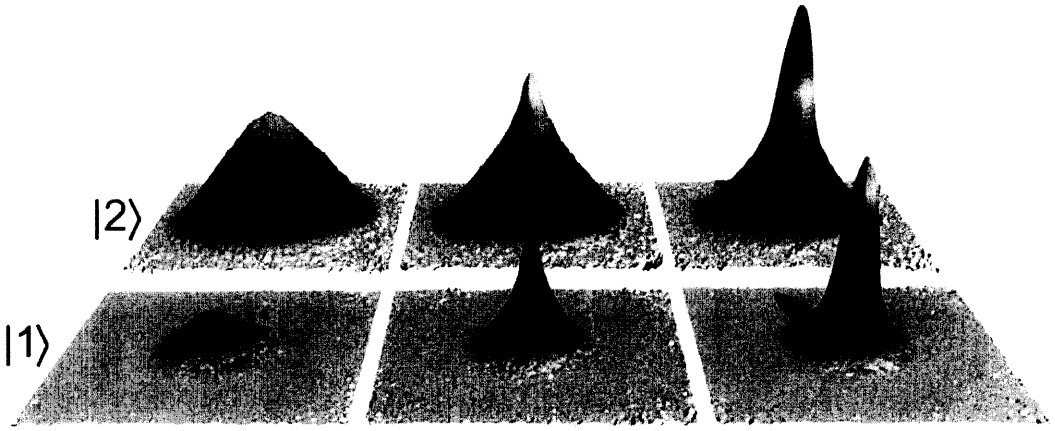

Figure 7-7: Fermion pair condensates and the Clogston limit of superfluidity in an imbalanced Fermi mixture. For high population imbalance ($\delta > \delta_c$), the gas is a normal mixture (left). At $\delta \lesssim \delta_c$, a condensate emerges in the clouds' center, which grows as the imbalance is further reduced (right). The images are obtained using the rapid ramp method, starting from resonance.

7.3.3 Condensate fraction

Vortices are a direct indicator for superfluid flow. However, close to the limit of superfluidity, the large normal cloud should quickly damp the rotation of the superfluid [107, 1, 265]. Therefore, the detection of vortices can only provide a lower bound for the size of the superfluid window. The methods of chapter 5 can be used to directly detect whether or not a condensate was present in the imbalanced clouds. A rapid ramp to the BEC-side, directly after release from the optical trap, stabilizes the fermion pairs and transforms the initial pair condensate on the BCS-side into a molecular condensate (see Fig. 7-7). Using this method has allowed to map out the regime of pair condensation as a function of population imbalance and demonstrate the Clogston limit of superfluidity.

Fig. 7-8a) shows the condensate fraction as a function of population imbalance for varying interaction strength. This directly displays the strong dependence of the superfluid window on $1/k_F a$. At a given interaction strength, there is a sharp threshold behavior at a certain critical imbalance, below which condensates are found. The critical imbalance determined from such data is shown in Fig. 7-3. On the BCS-side, it should closely follow the value of the superfluid gap Δ. The qualitative agreement with this expectation is excellent.

Fig. 7-8b) contrasts this quite dramatic dependence of the critical imbalance on the

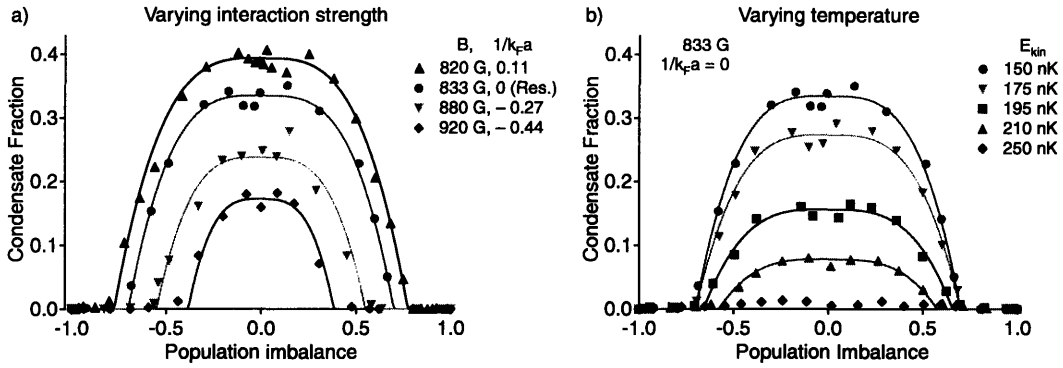

Figure 7-8: Superfluid window of imbalanced Fermi mixtures. The condensate fraction is shown as a function of population imbalance for a) varying interaction strength at the lowest temperature, and b) for varying temperature on resonance.

interaction strength with its *weak* dependence on temperature. While increasing the temperature reduces the condensate fraction substantially, it only affects the critical imbalance close to T_C. This is reminiscent of the weak dependence of the superfluid gap on temperature[5].

From Fig. 7-8a) we recognize a dramatic consequence of population imbalance. There is no longer a smooth crossover from the BEC- to the BCS-limit in the imbalanced case, in contrast to the case of equal mixtures studied in previous chapters. Rather, a phase transition occurs as the interaction strength is reduced below a critical value that depends on the interaction strength. In principle, it could well be that more than one phase transition occurs around the critical interaction, from a BCS-type superfluid to several forms of FFLO-type states, until finally the normal state is reached. If such intermediate superfluid states exist, they leave - at our present resolution - no distinct feature in the density profiles of the gas.

[5]For the BCS-gap $\Delta(T) \approx 1.74\,\Delta_0\sqrt{1-T/T_C}$ for $T_C - T \ll T_C$ and $\Delta(T) \approx \Delta_0 - \sqrt{2\pi\Delta_0 k_B T}\,e^{-\Delta_0/k_B T}$ for $T \ll T_C$ [89].

7.4 Direct observation of the phase transition, imbalanced case

The study of the condensate fraction has allowed us to establish the superfluid-to-normal phase diagram of Fig. 7-3. One of the most amazing results of the analysis that led to this phase diagram is clearly the prediction that the superfluid appears to phase separate from the normal cloud (see Fig. 7-2). This suggests that in striking contrast to the case of an equal mixture, one should be able to *directly observe* the superfluid phase transition in the density profile of the gas, without the need of poorly understood magnetic field ramps.

7.4.1 On resonance: Universality

We have indeed found this idea to be correct. Fig. 7-9 shows density profiles of an unequal mixture on resonance at an imbalance of about 60%. As the sample was cooled below a certain temperature, a central dense core appeared in the minority cloud. Even at our coldest temperatures, this core was observed only below a critical imbalance $\delta_c = 74(5)\%$, the same value that we have found before using the rapid ramp technique. It is thus natural to identify the central core with the fermion pair condensate.

A different imaging technique, a variant of phase-contrast imaging (explained below in section 7.5) was used to directly image the density *difference* as a function of temperature. According to our expectation of Fig. 7-2c), the density difference should rapidly drop to zero when crossing the boundary between the normal mixture and the superfluid core. Indeed, as we cool down the sample, we observe the appearance of a striking central depletion in the difference profiles, see Fig. 7-10. Naturally, this depletion emerges at the same temperature at which we observe the central dense core in the minority cloud (Fig. 7-9). In section 7.5 we will study whether the depletion is complete, that is, whether the central densities are indeed equal in the superfluid regime.

Apart from providing us with a direct method to detect the condensate, imbalanced mixtures also enable us to measure temperatures. A substance can only function as a reliable thermometer if it does not strongly interact with the sample to be measured. This explains the difficulty of assigning temperatures to the strongly interacting equal mixtures of chapter 5. In the case of imbalanced mixtures, atoms in the outer wings of the majority cloud are not in contact with minority atoms (see

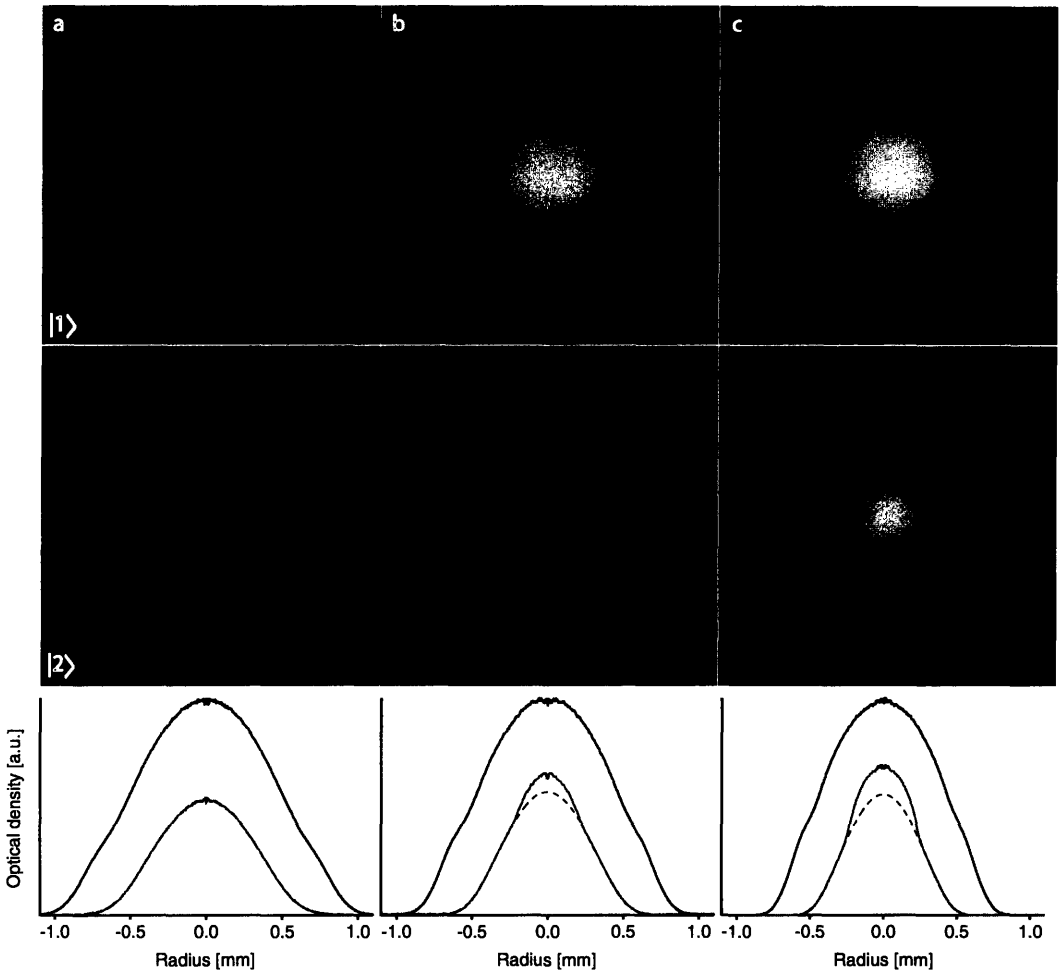

Figure 7-9: Direct observation of the superfluid phase transition in a resonantly interacting, imbalanced Fermi mixture. In contrast to the case of equal populations, the fermion pair condensate in an unequal mixture is clearly visible in the density profiles. This should be compared to the density profiles of an equal mixture, Fig. 5-11. The upper row shows majority clouds, the lower row minority clouds, for an imbalance of $\delta = 60\%$. All images were obtained after 11 ms of expansion. The dashed line is a fit to the wings of the minority cloud to a Thomas-Fermi profile, clearly missing the central feature. Temperature was varied by lowering the trapping power. It can be obtained from the ballistically expanding wings of the majority cloud. We have $T/T_F = 0.14$ (a), 0.09 (b) and 0.06 (c). Here, $k_B T_F$ is the Fermi temperature of an equal mixture containing the same total atom number.

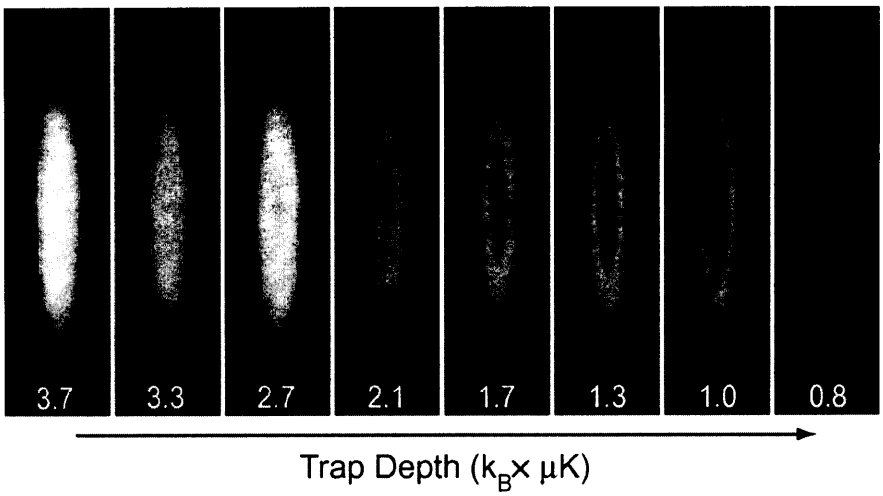

Figure 7-10: Direct observation of the superfluid phase transition via in-situ phase contrast imaging. At a critical temperature, a central depletion appears in the difference density, corresponding to the appearance of the condensate as observed in Fig. 7-9.

Fig. 7-9). They expand ballistically from our trap and can thus be used as a reliable thermometer. This has allowed us to measure the critical temperature for a given population imbalance (see Fig. 7-11). Future experiments can obtain the critical temperature as a function of imbalance and might thus - by extrapolation - lead to a reliable value even for the case of an equal mixture.

A mixed, unbalanced region on resonance

Fig. 7-9 shows that there exists a mixed region outside the condensate, where minority and majority spins coexist. This is a necessary consequence of the existence of the critical imbalance δ_c on resonance. Starting with a normal mixture at δ_c, the gas will not suddenly fully condense for slightly lower imbalance. This normal mixture above δ_c (or beyond the radius of the condensate at R_{SF}) is an intriguing state of matter: It is strongly (resonantly!) interacting, yet normal (as far as we know from the observation of condensates and vortices). Moreover, we find that the minority spin state in this mixed region is very well fit with a Thomas-Fermi profile of a non-interacting Fermi gas. Only the cloud radius shows that this is indeed a strongly interacting gas, as it is found to be smaller than that of an equivalent non-interacting cloud (we find $R_\downarrow/R_{\mathrm{TF}\downarrow} \approx 0.75$ at $\delta = \delta_c$). This might indicate that the strongly interacting Fermi gas behaves like a collection of non-interacting fermions with an effective mass. This

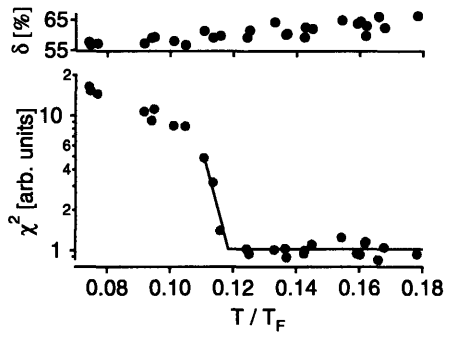

Figure 7-11: Critical temperature for an imbalanced Fermi mixture on resonance. The quality of a Thomas-Fermi fit, expressed as its χ^2-value, is plotted as a function of the reduced temperature T/T_F as determined from the majority cloud's ballistically expanding wings. A threshold fit (black line) gives the critical temperature for $\delta = 59\%$ as $T_C/T_F = 0.12$.

is the essence of Landau's Fermi liquid theory and the reason why other than pairing interactions between fermions can be neglected in BCS theory [215]. Here, the only role of interactions is to "dress" the "bare" fermions with an effective mass, the result being a reformulation of the interacting system in terms of weakly interacting quasi-particles. It is an important goal of future experiments to understand whether this idea still works in the strongly interacting regime on resonance.

Here, we will give an elegant argument independently found by F. Chevy [52] and Bulgac and Forbes [40] that shows how the different radii of the superfluid, the mixed region and the fully polarized cloud constrain the conditions for being in either of these three phases.

At unitarity, there are only two energy scales available, the chemical potentials $\mu_\uparrow$ and $\mu_\downarrow$ for the two species. Their ratio $\eta = \frac{\mu_\downarrow}{\mu_\uparrow}$ determines in which of the possible states the Fermi mixture is in. Clearly, for $\eta = 1$ we are in the superfluid state. As we reduce η, we will, according to our results, leave the superfluid state and enter the normal mixed state, say at a critical η_a. Then, upon further reduction of η, the system will eventually switch into the fully polarized state, say at η_b. The following considerations allow us to constrain these parameters.

Bounds for η_a and η_b

We start with the same analysis as for the Clogston limit in the weakly interacting case: We need to minimize the free energy density $\mathcal{F}$ of the two-species mixture, that is, find the state with maximum pressure $\mathcal{P} = -\mathcal{F}$. In the fully polarized state, the

pressure is (see Eq. 7.6)

$$\mathcal{P}_N = \frac{4}{15}\,\rho(1)\,\mu_\uparrow^{5/2} \tag{7.19}$$

Due to universality on resonance, the chemical potential μ of a fully paired superfluid state must be proportional to the Fermi energy, $\mu = \xi E_F = \xi\frac{\hbar^2}{2m}(6\pi^2 n)^{2/3}$. From $\mu = \frac{\partial\epsilon}{\partial n}$ it follows that the energy density in the superfluid state has the same form as that of a normal, two-component Fermi gas: $\epsilon(\mu_\uparrow, \mu_\downarrow) = \frac{3}{5}\,\mu_\uparrow\,n_\uparrow + \frac{3}{5}\,\mu_\downarrow\,n_\downarrow = \frac{6}{5}\,\mu\,n$, with $n = n_\uparrow = n_\downarrow$ and[6] $\mu = \frac{\mu_\uparrow+\mu_\downarrow}{2}$. The pressure $\mathcal{P}_S \equiv \mu_\uparrow\,n_\uparrow + \mu_\downarrow\,n_\downarrow - \epsilon(\mu_\uparrow, \mu_\downarrow) = \frac{4}{5}\mu n$ in the superfluid state is then

$$\mathcal{P}_S = \frac{4}{15}\,\rho(1)\,\frac{1}{(2\xi)^{3/2}}\,(\mu_\uparrow + \mu_\downarrow)^{5/2} \tag{7.20}$$

If there was *no* intermediate mixed phase, we would have a phase transition from the superfluid to the fully polarized normal state when their pressures become equal:

$$\begin{aligned} \mathcal{P}_N &= \mathcal{P}_S \\ \Rightarrow \mu_\downarrow &= ((2\xi)^{3/5} - 1)\,\mu_\uparrow \end{aligned} \tag{7.21}$$

The universal parameter ξ has been measured in experiments on equal mixtures [174, 26, 37, 139, 187], most simply by determining the cloud size, and calculated for example via Monte-Carlo calculations [43, 44, 17]. Our cloud size measurements yield $\xi = 0.47$ (see section 5.3), in close agreement with other determinations. This means that the superfluid-to-fully polarized normal transition would occur at $\eta_c = -0.04$. Since we observe the intermediate phase before the system becomes fully polarized, we must have $\eta_a > \eta_c$.

An upper bound for η_b, the transition from the mixed to the fully polarized region, can be obtained as follows. At η_b, we essentially have the situation of only one minority atom experiencing the interaction with the cloud of $N_\uparrow$ majority atoms. In the BCS-regime, this interaction would simply be the (attractive) mean-field-term $4\pi\hbar^2 a n_\uparrow/m$. On resonance it will be a universal number times the only energy scale left in this situation, $\mu_\uparrow$. We naturally expect this interaction to be still attractive, corresponding to some sort of "binding" of the minority particle to the majority Fermi sea. Two independent variational approaches by Chevy [52] and Bulgac and Forbes [40] result

[6]Note that this only depends on the average chemical potential μ, because the superfluid is not sensitive to the difference $\delta\mu$: The magnitization $\mathcal{M} = -\partial\epsilon/\partial\delta\mu = 0$ is zero in the BCS state.

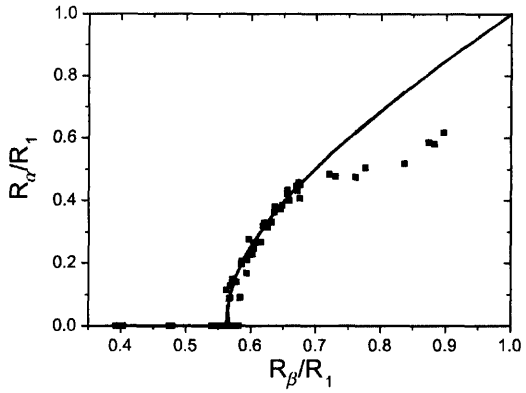

Figure 7-12: Constrained radii of the superfluid (R_α), the mixed (R_β) and the fully polarized phase (R_1) on resonance. The departure for larger minority clouds is likely due to the fact that for small population imbalance the superfluid did not have a very distinct boundary, which increased the uncertainty in determining R_α. Figure extracted from [52].

in the upper bounds for the "binding" energy $\mu_{b\downarrow}$:

$$\mu_{b\downarrow} \leq \begin{cases} -0.44\,\mu_{b\uparrow}, & \text{(Chevy)} \\ -0.50\,\mu_{b\uparrow}, & \text{(Bulgac and Forbes)} \end{cases} \tag{7.22}$$

Therefore we have $\eta_b \leq -0.50$.

Constraint from the measured cloud radii

In the case of a harmonic trap, the chemical potentials vary as given in Eq. 7.11. The transition from the superfluid to the mixed normal region will occur when

$$\frac{\mu_\downarrow^0 - \frac{1}{2}m\omega^2 R_{\mathrm{SF}}^2}{\mu_\uparrow^0 - \frac{1}{2}m\omega^2 R_{\mathrm{SF}}^2} = \eta_a \tag{7.23}$$

defining the radius of the superfluid R_{SF}. The transition from the mixed region to the fully polarized normal one occurs at a radius $R_\downarrow$, where the minority cloud vanishes:

$$\frac{\mu_\downarrow^0 - \frac{1}{2}m\omega^2 R_\downarrow^2}{\mu_\uparrow^0 - \frac{1}{2}m\omega^2 R_\downarrow^2} = \eta_b \tag{7.24}$$

Finally, one can note that the chemical potential $\mu_\uparrow^0$ of the majority spin state is simply given by the majority cloud radius, $\mu_\uparrow^0 = \frac{1}{2}m\omega^2 R_\uparrow^2$. These equations allow us

to eliminate both $\mu_\uparrow^0$ and $\mu_\downarrow^0$ and we obtain an equation for the radius of the superfluid core [52, 40]:

$$\frac{R_{\mathrm{SF}}}{R_\uparrow} = \sqrt{\frac{(R_\downarrow/R_\uparrow)^2 - q}{1-q}} \tag{7.25}$$

where $q = \frac{\eta_a - \eta_b}{1-\eta_b}$ is the value of $(R_\downarrow/R_\uparrow)^2$ at which the superfluid vanishes.

The comparison of Eq. 7.25 to our data [269] is reproduced from [52] in Fig. 7-12. Our data results in $q = 0.32$, from which Chevy deduces the following stringent bounds on η_a and η_b:

$$-0.04 < \quad \eta_a \quad < 0.02 \tag{7.26}$$

$$-0.55 < \quad \eta_b \quad < -0.50 \tag{7.27}$$

The parameter η_a has a meaningful interpretation: It is the ratio of the density discontinuities in the majority and minority clouds at the superfluid-to-normal transition[7],

$$\frac{\Delta n_\uparrow}{\Delta n_\downarrow} = -\eta_a \tag{7.28}$$

While the minority cloud clearly shows a sharp change in its density at the phase transition, the majority profiles do not feature a dramatic jump (see Fig. 7-9). We were able to see faint traces of the condensate in the majority density (see supplemental material in [269], reprinted in appendix I), but the smallness of the effect certainly speaks for a small value of η_a.

One should remark that the variational BCS approach (not including the correction due to Gorkov-Melikbarkhudarov) would predict a considerably smaller intermediate phase. The critical density imbalance beyond which no superfluid region persists in a uniform system would be $\approx 93\%$, corresponding to $\eta_a \approx 0.1$, as one can calculate using the results for the Clogston limit above. The energy needed to add a minority atom to a majority Fermi sea would be identically zero, $\eta_b = 0$, as interactions between atoms that do not form a Cooper pair are neglected. In contrast, the upper bounds found by Chevy and Bulgac and Forbes show that the minority atom is "bound" by an energy that is at least one half of the majority cloud's chemical potential. This nicely confirms the intuitive picture that the large spin up Fermi sea presents an attractive "mean-field" potential to a single minority atom.

[7] Due to universality, the pressure in both phases can be written as $P = f(\eta)\mu_\uparrow^{5/2}$. The densities are given by $n_\uparrow = \frac{\partial P}{\partial \mu_\uparrow} = f'(\eta)(-\frac{\mu_\downarrow}{\mu_\uparrow^2})\,\mu_\uparrow^{5/2} + \frac{5}{2}\frac{P}{\mu_\uparrow}$ and $n_\downarrow = \frac{\partial P}{\partial \mu_\downarrow} = f'(\eta)(\frac{1}{\mu_\uparrow})\,\mu_\uparrow^{5/2}$. The pressure and the chemical potentials are continuous across the transition, so $\Delta n_\uparrow = -\frac{\mu_\downarrow}{\mu_\uparrow}\,\Delta n_\downarrow$.

Concluding this section, we see how the simple measurement of cloud radii in the strongly interacting regime has allowed to extract viable information about the equation of state of the system. The general equation of state for the two-species mixture will read

$$\epsilon(\mu_\uparrow, \mu_\downarrow) = f(\eta) E_F \tag{7.29}$$

with an unknown *universal function* $f(\eta)$ that, hopefully, future studies will be able to determine.

7.4.2 On the BEC side: strongly interacting Bose-Fermi mixture

On the BEC-side, at $1/k_F a = 0.5$, we find several features that are qualitatively different from the resonance case.

1. At the lowest temperatures, the minority atoms are now essentially all part of the condensate. That is, there is practically no mixed region.

2. The majority spin species now also shows a dramatic signature of condensation.

A closer look on the resonance profiles reveals, however, that this latter distinction is only quantitative: There is indeed a very faint trace of the condensate in the majority distribution (see supplementary information in [269], reprinted in Appendix I).

Fig. 7-14 displays the condensate fraction as a function of the reduced temperature T/T_C, where T is determined as before from the non-interacting wings of the majority component, and T_C is the critical temperature of a non-interacting cloud of $N_\downarrow$ molecules. We see that interactions strongly reduce the critical temperature from the non-interacting value. The downshift by a factor of two is in accord with a mean-field model of condensates in the strongly interacting regime [35]. The cloud of excess atoms will act to further reduce the critical temperature.

Mean-field model

The situation on the BEC-side of the resonance resembles that of a strongly interacting mixture of bosons (the molecules) and fermions (the unpaired atoms of the majority species). Indeed, Pieri and Strinati [196] have shown that on the far BEC-side of the Feshbach resonance, where $k_F a \lesssim 1$, this view is indeed correct. What emerges is a mean-field description in which the condensed bosons repel the unpaired

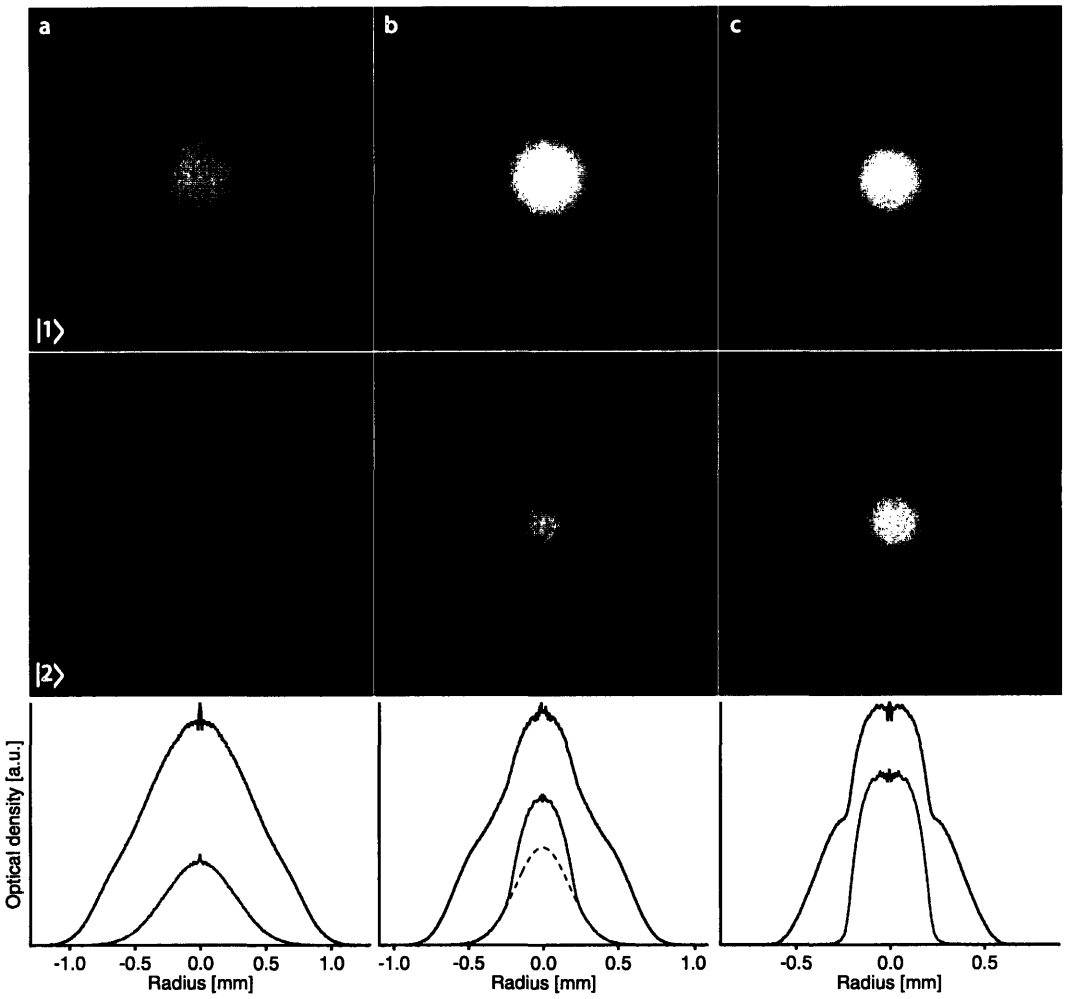

Figure 7-13: Phase transition in a strongly interacting atom-molecule mixture, at $B = 780$ G or $1/k_F a \approx 0.5$. Unlike on resonance, all minority particles are part of the condensate at low temperatures: there is essentially no mixed normal region. The reduced temperatures were $T/T_F = 0.2$ (a), $T/T_F = 0.12$ (b) and $T/T_F \leq 0.05$ (c). The noise in the center is an artefact of azimuthal averaging: the number of averaged pixels evidently increases with distance from the center.

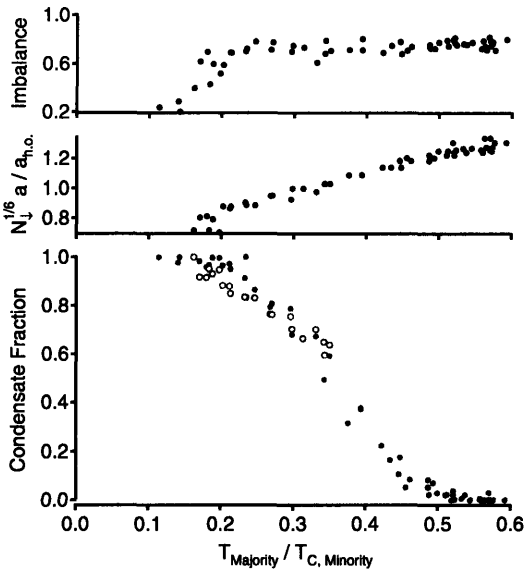

Figure 7-14: Condensate fraction of the molecular condensate (at $B = 780$ G) as a function of temperature. Strong interactions reduce the condensation temperature by a factor of two compared to the non-interacting value. The critical temperature is $T/T_F = 0.18$ for an imbalance of $\delta = 75\%$. $N_\downarrow^{1/6} a/a_{\text{h.o.}}$ is the gas parameter giving the interaction strength. In a weakly interacting atomic BEC, this number is typically on the order of 10^{-2}. The condensate fraction was determined using a simple bimodal fit, a gaussian plus a parabola (solid circles) or a fit that assumes full expulsion of the thermal cloud by the condensate (open circles).

fermions. For increasing interaction strength, the fermions are essentially fully expelled from the condensate. This form of phase separation has also been theoretically studied in "true" dilute Bose-Fermi mixtures, both in the trapped system [170] and in the bulk [253], and it certainly reminds of the phase separation between ^{3}He and ^{4}He mixtures [99] (only 6% of ^{3}He are soluble in ^{4}He at low temperatures).

We can quite easily "guess" the mean-field equations for this mixture, and refer the reader to the full derivation given in [196]. To start, we need to know the relevant scattering lengths for the system. The molecule-molecule scattering length was calculated by Petrov, Shlyapnikov and Salomon [193] by solving the four-body problem exactly. The result is $a_{BB} = 0.6a$, where a is the atom-atom scattering length. Thus, the molecules repel each other, as we had found in chapter 2 within the BCS variational approach. This, however, predicted the larger value[8] $a_{BB} = 2a$. The

[8]The reason is that the BCS variational approach neglects interactions between pairs, and three-body interactions between a fermion and a molecule.

fermion-boson scattering length $a_{\rm BF} = 1.18a$ was calculated almost half a century ago [228] but has so far not been verified experimentally.

At low temperature, all minority fermions will be paired with majority ones, and the resulting molecules will practically all be condensed. We thus have only two contributions, the molecular condensate $\psi(\mathbf{r})$ and the density of excess fermions $\delta n(\mathbf{r})$. The excess atoms experience the molecules as an additional external potential $\propto a_{\rm BF} |\psi(\mathbf{r})|^2$, so we have (see Eq. 2.28 in chapter 2)

$$\delta n(\mathbf{r}) = -\frac{1}{\lambda_{\rm dB}^3} \,\mathrm{PolyLog}\left(3/2, -e^{(\mu_\uparrow - V_{\rm ext}(\mathbf{r}) - \frac{3\pi\hbar^2 a_{\rm BF}}{m}|\psi(\mathbf{r})|^2)/k_B T}\right) \tag{7.30}$$

where $\mu_\uparrow$ is the chemical potential of the majority atoms. The molecules, in turn, feel the mean-field repulsion from the excess fermions, in addition to their own repulsive mean-field. The Gross-Pitaevskii equation for $\psi(\mathbf{r})$ thus reads

$$-\frac{\hbar^2\nabla^2}{2m_M}\psi(\mathbf{r}) + \left(2V_{\rm ext}(\mathbf{r}) + \frac{3\pi\hbar^2 a_{\rm BF}}{m}\delta n(\mathbf{r})\right)\psi(\mathbf{r}) + \frac{4\pi\hbar^2 a_{\rm BB}}{m_M}|\psi(\mathbf{r})|^2\psi(\mathbf{r}) = \mu_M\psi(\mathbf{r}) \tag{7.31}$$

with the mass $m_M = 2m$ of molecules. The factor 2 in front of $V_{\rm ext}$ simply signifies that each molecule experiences twice the potential felt by a single atom. The chemical potential for molecules μ_M in an equal mixture is $\mu_M = 2\mu + E_B$ with $E_B = \hbar^2/ma^2$ the molecular binding energy (see chapter 2). In the case of unequal mixtures, chemical equilibrium in the atom-molecule mixture requires $\mu_M = \mu_\uparrow + \mu_\downarrow + E_B$. The set of equations is closed by introducing the total density $n(\mathbf{r}) = 2|\psi(\mathbf{r})|^2 + \delta n(\mathbf{r})$ and requiring

$$N_\uparrow + N_\downarrow = \int d^3r\, n(\mathbf{r}) \tag{7.32}$$

$$N_\uparrow - N_\downarrow = \int d^3r\, \delta n(\mathbf{r}) \tag{7.33}$$

with the given number $N_\uparrow$ and $N_\downarrow$ of majority and minority atoms.

We can proceed further using the Thomas-Fermi approximation, neglecting the kinetic term in the Gross-Pitaevskii-equation. Also, we now work at zero temperature. The equations for $\psi(\mathbf{r})$ and $\delta n(\mathbf{r})$ become

$$|\psi(\mathbf{r})|^2 = \frac{m}{2\pi\hbar^2 a_{\rm BB}} \max\left(\mu_M - 2V_{\rm ext}(\mathbf{r}) - \frac{3\pi\hbar^2 a_{\rm BF}}{m}\delta n(\mathbf{r}), 0\right) \tag{7.34}$$

$$\delta n(\mathbf{r}) = \frac{1}{6\pi^2}\left(\frac{2m}{\hbar^2}\right)^{3/2} \max\left(\mu_\uparrow - V_{\rm ext}(\mathbf{r}) - \frac{3\pi\hbar^2 a_{\rm BF}}{m}|\psi(\mathbf{r})|^2, 0\right)^{3/2} \tag{7.35}$$

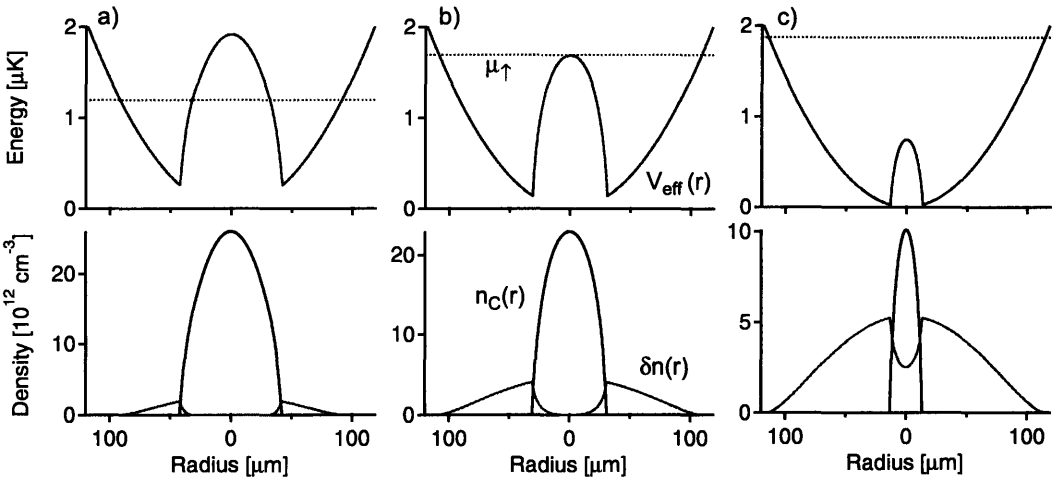

Figure 7-15: Effective potential and density of excess fermions in a Bose-Fermi mixture. The upper row shows the self-consistent effective potential $V_{\text{eff}}(r) = V_{\text{ext}}(r) + g_{\text{BF}}\,|\psi(r)|^2$ experienced by excess fermions in the presence of a molecular condensate with wavefunction $\psi(r)$. The dotted line gives the chemical potential $\mu_\uparrow$ of the majority spin species. The lower row shows the density of excess fermions $\delta n(r)$ and the condensate density $n_C(r) = |\psi(r)|^2$. The population imbalance δ was a) 20%, b) 70% and c) 99%, and the interaction strength $1/k_F a = 2$. Calculations are for a spherical trap with trapping frequency $\omega = 2\pi\,100\,\text{Hz}$ and a total number of 10^7 fermions.

These equations allow us to study several cases (see Fig. 7-15).

Small imbalance If the excess density is small, we can neglect the influence of the few excess atoms on the molecular condensate. The excess atoms, in turn, experience an effective "Mexican hat potential", the trapping potential plus the mean-field interaction from the condensate (see Fig. 7-15a):

$$V_{\text{eff}} = V_{\text{ext}}(\mathbf{r}) + \frac{g_{\text{BF}}}{g_{\text{BB}}}\max(\mu_M - 2V_{\text{ext}}(\mathbf{r}), 0) \tag{7.36}$$

with the couplings $g_{\text{BB}} = 2\pi\hbar^2 a_{\text{BB}}/m$ and $g_{\text{BF}} = 3\pi\hbar^2 a_{\text{BF}}/m$. The inverted potential from the condensate mean-field on the right always dominates the "bare" potential in the center, as $2g_{\text{BF}}/g_{\text{BB}} = 3a_{\text{BF}}/a_{\text{BB}} \approx 6 > 1$. This shows that the excess atoms will, for small imbalance, always reside in the wings of the condensate, never in the center. As the imbalance or the strength of the interactions are increased, the mean-field repulsion from the excess atoms starts to affect the condensate. Still, the effective potential retains its qualitative shape (see Fig. 7-15). Thus we arrive at the fact that

in the trapped case, there will always be an extended region in the phase diagram where an "unmagnetized" superfluid at *equal* spin densities is spatially separated from a mixed region.

A "magnetized superfluid" As the population imbalance is increased, or the interaction strength decreased, more and more excess atoms enter the condensate from the edge inwards. At the critical point where the chemical potential of majority atoms becomes large enough to overcome the condensate's mean-field repulsion at the trap center, $\mu_\uparrow = \frac{g_{BF}}{g_{BB}}\mu_M$, excess particles can penetrate all the way into the condensate (see Fig. 7-15b). The superfluid phase is "magnetized" throughout. In the language of the BCS-state, now the cost of having unpaired atoms inside the superfluid is outweighed by the gain in "Zeeman energy" $2h = \mu_\uparrow - \mu_\downarrow$ of changing a spin down (minority) into a spin up (majority) particle. Recall from chapter 2 that the role of the excitation gap on the BEC-side is played by $\sqrt{\mu^2 + \Delta^2}$. The fact that polarization of the superfluid is favorable means $h > \sqrt{\mu^2 + \Delta^2}$. This is indeed possible on the far BEC-side, as there is no Clogston limit anymore (see Fig. 7-3). One can note that $\sqrt{\mu^2 + \Delta^2} \to |\mu| + \frac{g_{BF}}{g_{BB}}\mu_M$ in the far BEC-limit (with the variational BCS-Ansatz, that leads however to the "wrong" values of g_{BF} and g_{BB}), and we recover the above criterion for $\mu_\uparrow$.

Strong interactions: complete phase separation For strong interactions, on the other hand, the condensate expels essentially all excess fermions. Phase separation between the superfluid and the normal region is thus complete and occurs for all imbalances. The situation now closely resembles our expectations for the BCS-side.

Fig. 7-16 summarizes these findings by plotting the central density of excess fermions $\delta n(0)$ as a function of imbalance and the interaction parameter $1/k_F a$. The equations Eqs. 7.34 and 7.35 were solved by iterative insertion of one density profile into the equation for the other, and adjusting at each step the value of the chemical potentials μ_M and $\mu_\uparrow$ to converge to the required particle number.

As pointed out by [196], the details of the density profiles - the maxima in the density of excess fermions, the critical imbalance / interaction where phase separation starts, etc. - depend on the value of the atom-molecule scattering length. Accurate measurements of the density profiles will allow to verify the 50 year old prediction $a_{BF} = 1.18$.

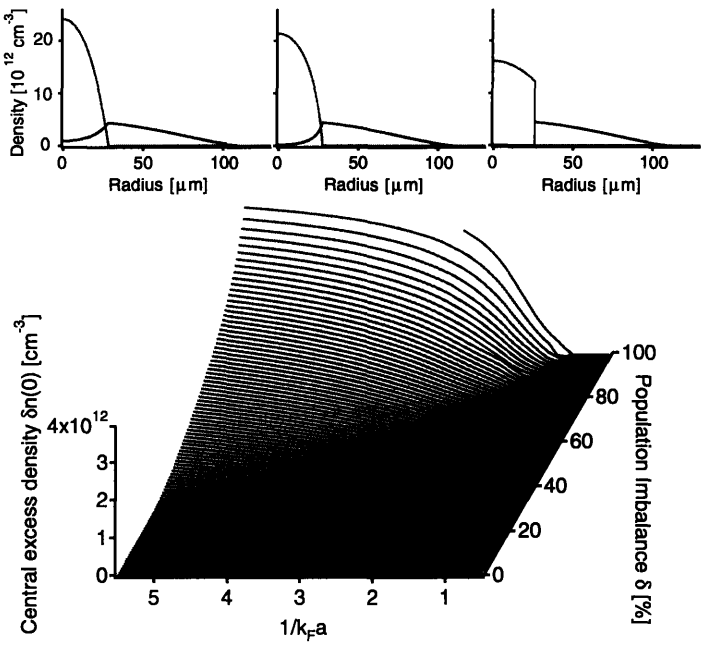

Figure 7-16: Phase diagram for the strongly interacting Bose-Fermi mixture in a harmonic trap at zero temperature. Shown is the density of excess fermions in the center of the trap. Excess fermions can enter the condensate either for large imbalance or fixed (non-zero) imbalance and weak interactions, above the critical line shown in black. Near a critical interaction around $1/k_F a = 1$, excess fermions are expelled from the condensate's center at all imbalances. The profiles on top show the case for $\delta = 80\%$ at varying interaction parameters, $1/k_F a = 3$ (left), 2 (middle) and 1 (right). Other parameters as in 7-15.

7.5 Observation of phase separation

In previous sections we have seen that both on the BCS, and on the BEC-side of the resonance, we would expect to observe phase separation in the sample. We define a phase separated state by the presence of a region in space where the spin densities have equal densities, and which is surrounded by a shell at unequal densities. Hints of phase separation were found by subtracting the column density profiles in Fig. 7-9 and finding a dip in the center of the difference distribution. Similar central depletions have been found in [187]. However, to distinguish a phase-separated state from a merely strongly interacting normal state that would show similar depletions [267], it is necessary to reconstruct the 3D density *difference*. In principle this can be achieved by subtracting the absorption pictures of the two spin species, and inverting the resulting profiles [267]. But forming the difference between two large and fluctuating

quantities leads to large fluctuations in the result. A method was needed to directly image the density difference. Phase contrast imaging provides such a method, as is discussed in the following.

7.5.1 Experimental method: Phase-contrast imaging

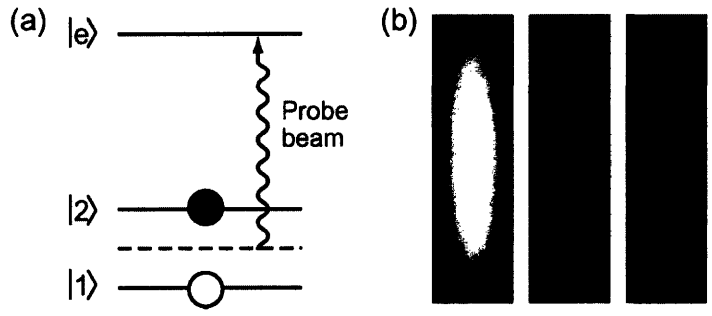

Figure 7-17: Phase contrast imaging for the observation of phase separation in an imbalanced Fermi mixture. a) The probe beam is tuned right in between the two resonance frequencies for atoms in states $|1\rangle$ and $|2\rangle$. The resulting phase shift is thus proportional to the difference in column densities. b) Phase contrast image of atoms in state $|1\rangle$ (left) and $|2\rangle$ (right) and that of an equal mixture of the two states (middle).

In order to directly measure the density *difference* distribution, we employ a variant of phase contrast imaging (see Fig. 7-17 and [232]). Light that is off-resonant with an atomic transition (detuning $|\delta|$ much larger than the linewidth Γ) experiences a phase shift $\phi(x,y) \propto \frac{1}{\delta}\int dz\, n(x,y,z)$ when passing through the atomic cloud with density $n(x,y,z)$. Atoms in states $|1\rangle$ and $|2\rangle$ have imaging resonances that are about 80 MHz apart. Thus, if a laser is detuned right in between those two imaging resonances, the phase shift due to atoms in state $|1\rangle$ will have the opposite sign of that due to atoms in $|2\rangle$. The total phase shift will be proportional to the *difference* of the column densities.

The phase information can be transformed into an intensity information by a standard homodyning technique. If E_i is electric field of the collimated incoming light, and E_f is the field after passing through the atoms, then $E_s = E_f - E_i = E_i(\, e^{i\phi} - 1)$ is the scattered light from the atoms (we neglect absorption in our description as $|\delta| \gg \Gamma$). The scattered light is imaged onto a CCD camera, where it interferes with the unscattered light E_i. This would give an intensity propotional to $|E_i + E_s|^2 \propto |1 + i\phi|^2 \propto 1 + \phi^2/2$ for small phase shifts ϕ. The dependence is quadratic and thus

weak. To increase the sensitivity to ϕ, the collimated light that misses the atoms is phase shifted by $\pi/2$ using a phase spot in the focus of a lens. The scattered, phase-shifted light from the atoms in the object plane will miss the phase spot. The intensity on the camera is now proportional to $\left|e^{i\pi/2} + i\phi\right|^2 \propto |1+\phi|^2 \propto 1 + 2\phi$. The signal is thus linear in ϕ and thus sensitive to small phase shifts.

7.5.2 In-situ profiles of the column density difference

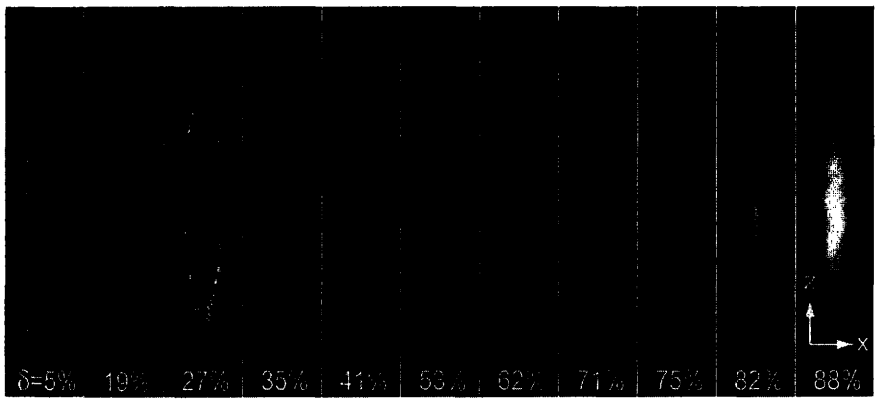

Figure 7-18: In situ imaging of an imbalanced Fermi mixture for various population imbalances. The profiles directly measure the column density difference of the two spin states. Below an imbalance of $\delta \leq 75\%$, a distinctive central depletion is observed and a shell structure emerges.

This new experimental tool has allowed us to directly probe the density difference in imbalanced Fermi mixtures in-situ (in the trap) (see Fig. 7-18). We observed how the depleted core region diminished for increasing imbalance and eventually vanished completely around an imbalance $\delta \approx 75\%$.

The 3D reconstruction of the density difference finally revealed that at low temperatures, the central depletion in the density difference actually results from a central core at equal densities, surrounded by a shell at unequal densities (see Fig. 7-19). The reconstruction is performed using an inverse Abel transformation. The only assumption entering this analysis is that of cylindrical symmetry of our trap, which we know from chapter 6 to be very well fulfilled. This allows us to check two further assumptions that are often made, namely the local density approximation (LDA) and the approximation of harmonic trapping [226, 125].

In local density approximation, the densities $n_{\uparrow,\downarrow}(r,z)$ and their difference can only depend on the value of the local potential $V(r,z) = \frac{1}{2}m\omega_r^2 r^2 + \frac{1}{2}m\omega_z^2 z^2$. That is,

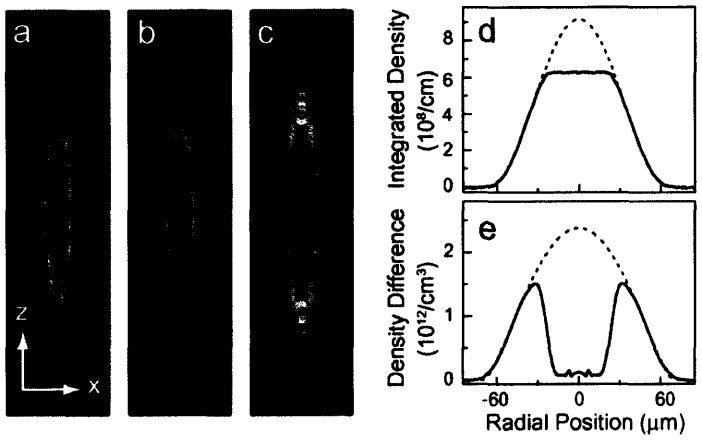

Figure 7-19: Reconstruction of 3D density profiles. Double integration results in a flat difference density profile, as expected from LDA when integrating over a hollow shell. The 3D reconstruction of the difference density profile shows an extended region of equal densities surrounded by a shell with unequal densities.

they are functions of $\lambda^2 r^2 + z^2$ only, where $\lambda = \omega_r/\omega_z$ is the aspect ratio of the trap. The border of the region of equal densities must likewise be defined by a certain value of the potential V, hence constant $\lambda^2 r^2 + z^2 \equiv R_{\rm core}^2$. Let us now calculate the *doubly* integrated difference profile

$$\Delta n_{\rm ax}(z) = \int dx\, dy\, \Delta n(\lambda^2(x^2+y^2)+z^2) = \frac{\pi}{\lambda^2}\int_0^\infty d(\rho^2)\, \Delta n(\rho^2+z^2) = \frac{\pi}{\lambda^2}\int_{z^2}^\infty du\, \Delta n(u) \tag{7.37}$$

Now if $|z| < R_{\rm core}$, then $\Delta n(u)$ is zero from $u = z^2$ up to $u = R_{\rm core}^2$. The doubly integrated density is thus *constant*:

$$\Delta n_{\rm ax}(|z| < R_{\rm core}) = \frac{\pi}{\lambda^2}\int_{R_{\rm core}^2}^\infty du\, \Delta n(u) \tag{7.38}$$

Indeed, when performing the double integration, we observed such a characteristic "flat top" distribution, indicating that LDA and harmonic trapping are good approximations.

7.5.3 Two regimes of phase separation

For the range of interaction parameters studied in the experiment [223] ($-0.4 \leq 1/k_F a \leq 0.6$), the observation of a central core with equal densities was correlated with the existence of a condensate after the rapid ramp to the BEC-side (see Fig. 7-

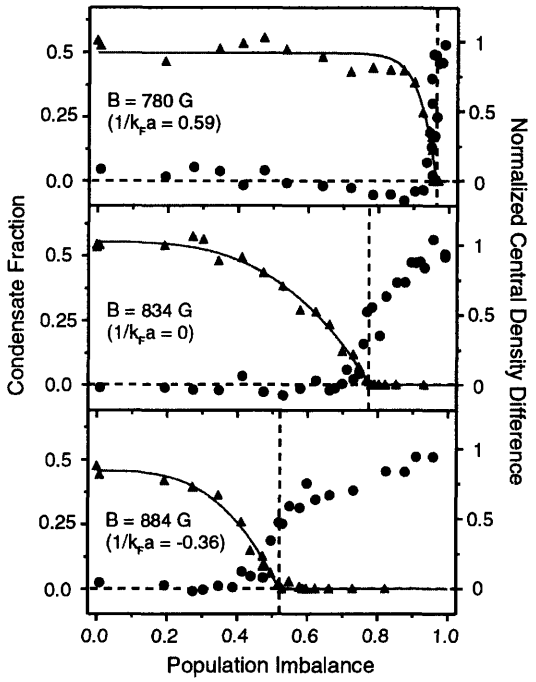

Figure 7-20: Correlating the condensate fraction with the observation of phase separation. Whenever a condensate is found after the rapid ramp, the in-situ densities of the two species are equal.

20). This shows that the physics on both sides of (but still close to) the Feshbach resonance is qualitatively the same, which does not surprise given the experience with equal mixtures.

However, there is an important qualitative difference between the BEC- and the BCS-regimes. On the BCS-side, it is always energetically favorable to place a new majority atom not inside the superfluid, but on top of the Fermi sea of excess atoms in the phase separated normal state. To reverse this situation, the "Zeeman" energy h would have to overcome the pairing gap Δ, but the Clogston limit occurs already before this can happen, at $h = \Delta/\sqrt{2}$. In the far-BEC-regime, on the other hand, we are dealing with a Bose-Fermi mixture of tightly bound molecules and unpaired atoms. Excess fermions can enter the molecular condensate without destroying it. While for small imbalance, the central region of the trap will still contain a superfluid at equal spin densities, at a certain imbalance excess atoms start to fill in the central region. This means that there will be a "magnetized superfluid" on the BEC-side of the imbalance phase diagram (see Fig. 7-21).

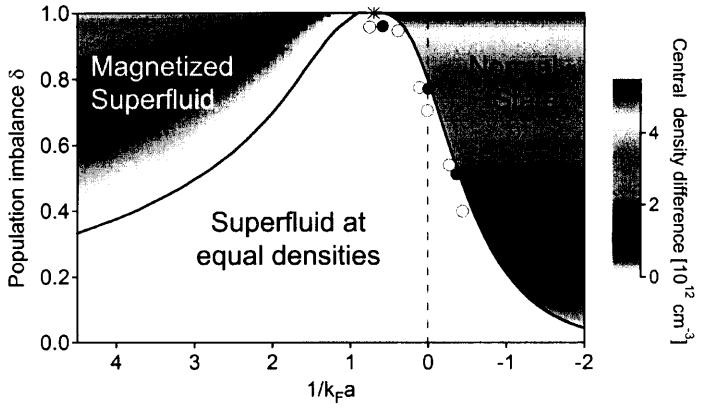

Figure 7-21: Phase diagram for trapped, strongly interacting, imbalanced Fermi mixtures. This shows the combined diagrams of Figs. 7-3 and 7-16, along with the data of [268] (empty circles) and [223] (full circles). The normal state density difference in the BCS-regime was calculated for a non-interacting mixture. This central density difference should sharply rise from zero on the BCS-side as the system turns normal. In contrast, on the BEC-side the density difference increases smoothly from zero, starting at some critical imbalance. The superfluid is *not* destroyed, and one obtains a "magnetized superfluid".

7.6 Outlook

The study of imbalanced Fermi mixtures has revealed a host of interesting effects. Their quantitative explanation presents a challenge to many-body theories, especially in the strongly interacting regime. Varying the spin imbalance led to new insight into the strongly interacting *normal* state above the critical imbalance. The critical polarization is itself an important number. It provides a measure for the stability of the superfluid state at equal densities, when compared to the strongly interacting normal state. On resonance, it is a universal number, of the same importance as the gap or the chemical potential of an equal mixture in units of the Fermi energy. In the BCS-limit, the critical polarization is linearly related to the pairing gap, with a universal coefficient (see Eq. 7.17). Future experiments can study the superfluid-normal mixture, as well as the mixed normal state in the trap for example by measuring their collective excitations, the damping of out-of-phase oscillations ("second sound"), the excitation spectrum via RF spectroscopy and the behavior under rotation. An exciting experiment would be to observe majority atoms trapped inside vortex cores. In principle, this should be possible using phase contrast imaging of a rotating mixture.

New forms of superfluidity? In all of the above, we only considered the normal state and the BCS state as possible "candidates" for the ground state of the imbalanced system. However, the BCS derivation does not include the possibility of forming Cooper pairs at finite center-of-mass momentum. In the balanced case, this can well be justified: As a system (without currents) turns superfluid, the growth rate of the zero-momentum pair population is largest [215]. By "mode-competition" these zero-momentum pairs completely dominate other possible populations. However, in the imbalanced case, Fulde, Ferrell [94] and Larkin and Ovchinnikov [146] have shown that there is indeed a state of lower energy than both the normal and the BCS-type superconducting state, which involves pairing of fermions at finite momenta. This superfluid state is expected to approximately occur between (slightly below) the Clogston limit $h = \frac{1}{\sqrt{2}}\Delta = 0.707\,\Delta$ and $h_{\mathrm{FFLO}} = 0.754\,\Delta$. While this state is favorable compared to the normal and BCS state, there is a host of other possible proposals for the ground state, involving more than one common Cooper pair momentum or states with deformed Fermi surfaces [46]. Unfortunately, the parameter space for these exotic states of superfluidity appears to be very small [221] (but see [169] for a more optimistic view). The trapping potential tunes h/μ quickly over the interesting range, and the FFLO-state might be obscured by surface effects at the superfluid-to-normal phase boundary.

Nevertheless, the study of imbalanced Fermi mixtures will necessarily improve our understanding of fermionic superfluidity in the strongly interacting regime, and will help us to decide on the features a full theory of Fermi gases must have.

Chapter 8

Conclusion

Not even three years ago the first Bose-Einstein condensates of molecules had been observed. The rapid developments, the quick succession of major experimental breakthroughs and new theoretical insights were and still are truly breathtaking. The amazing pace in the field of fermionic superfluids in atomic gases has its origins evidently in the (comparatively) long experience with the bosonic counterparts, Bose-Einstein condensates of atoms. While four and a half years had passed between the discovery of the first atomic BEC and the first observation of a vortex lattice in a condensate, it only took a third of that time for fermionic superfluids. By now the field has matured as experiments are in a position to address open questions of many-body physics. My colleagues and I have been fortunate to be able to contribute to this exciting field of physics. To conclude this thesis, let me shortly summarize what has been accomplished by our group, what questions still await an answer and in what directions we can go from here.

From the moment it became clear that molecules, formed out of two fermionic atoms, would not undergo fast vibrational decay close to a Feshbach resonance, the strategy in the search for fermionic superfluidity was evident: One should first produce a stable molecular condensate before entering the unknown realm of strong interactions. For this task, ^{6}Li turned out to be a "magic" substance, allowing molecular lifetimes of several tens of seconds close to resonance. Molecular BEC could thus be achieved by evaporating the gas at fixed interaction strength, much in the same way bosonic atoms are condensed. These condensates allow to explore the regime of strong interactions, where beyond mean-field corrections apply. Such effects are difficult to observe in atomic condensates, where quantum depletion is marginal ($\sim 1\%$) (at least in the bulk). One might worry that the fermionic nature of the molecular constituents might dominate beyond mean-field corrections expected

for point-like bosons. However, a diagrammatic expansion in the BEC-limit of the crossover shows [195], and Monte-Carlo calculations confirm [17], that the only effect of the fermionic constituents in this regime is to modify the scattering length for molecules into $a_M = 0.6a$. The study of strongly interacting molecules could thus confirm decade old predictions, for example the Lee-Yang correction for the equation of state for point-bosons [148]. Preliminary data on collective oscillations from the Innsbruck group indicates these corrections to be present and to have the expected value.

The next step in achieving fermionic superfluidity was to change the sign of the scattering length from repulsive to attractive and search for condensation of fermion pairs. In this regime binding is purely a many-body effect, as the molecular state has disappeared. The binding can be understood as arising from Pauli-blocking of possible scattering states, as in conventional Cooper pairing. However, the pairs in our experiments are likely never larger than the interparticle spacing, as $k_F|a| \gtrsim 1$ in all cases studied so far. This might explain why the transfer into tightly bound molecules is so efficient. This transfer allows to detect condensates on the attractive side of the Feshbach resonance, by effectively "mapping" the many-body wavefunction onto a thermally excited state containing a molecular condensate. We could confirm that the transfer occurred on a timescale short compared to the growth time of pair condensates, which gave an important piece of evidence that the fermion pair condensates were indeed formed before the transfer. This work also demonstrates the great potential given by the Feshbach resonance mechanism to study time-dependent and out-of-equilibrium situations. These are theoretically challenging problems, as the most widespread tool, the time-dependent Ginzburg-Landau equation, only works if the order parameter Δ varies so slowly that the system is always close to equilibrium [260].

The final goal of the experiments was evidently to prove superfluidity and phase coherence in atomic Fermi mixtures. Both these goals were simultaneously achieved by observing ordered vortex lattices in a rotating Fermi gas. These Abrikosov lattices are well-known from Type-II superconductors placed in a magnetic field. They have not yet been observed in Helium-3, the only other neutral fermionic superfluid. A future direction for the work on rotating Fermi gases can be the observation of a critical rotation frequency [251, 262], which is analogous to the critical magnetic field H_{c2} in Type-II superconductors. Another interesting topic is the non-trivial density profile of a vortex on the BCS-side of the resonance [143, 109, 116, 173, 158, 219]. On the BEC-side, the only microscopic scale is the healing length $\xi \propto 1/\sqrt{na}$ which

then necessarily sets the size of the vortex core. On the BCS-side, however, there are *two* length scales at zero temperature, the Fermi wavelength $\propto 1/k_F$ and the Pippard or BCS coherence length $\xi_0 = \hbar v_F/\pi\Delta \gg 1/k_F$. The vortex profile should show variation on the scale of ξ_0 and oscillations on the scale of the Fermi wavelength. To complicate things further, the vortex core size should also depend on temperature (the Kramer and Pesch effect) [143, 109, 116]. Furthermore, the density depletion due to the vortex core is strongly reduced when tuning the interaction towards the BCS-side [41, 134, 158, 219, 56]. One can relate this effect to the presence of quasi-particle bound states inside the vortex core [45, 219, 56]. Preparing imbalanced Fermi mixtures might allow the direct observation of these bound states as locations where the majority atoms reside preferentially [242].

In all of the above examples, we could be guided either by intuition borrowed from atomic BEC or from BCS superconductors. The last chapter of this thesis has described arguably the first experiment where truly new questions were addressed, that cannot be studied in this way in superconductors or other materials, namely the study of fermionic superfluidity with imbalanced spin populations. Superfluidity survived in a certain window of imbalance, a result that one could have guessed on the molecular side of the resonance, but that is less trivial on the BCS-side. Quite intriguing was the observation of direct signatures of the phase transition in the density profile, without any magnetic field ramps. A remarkable result was that in a resonantly interacting gas, superfluidity can be destroyed by a chemical potential mismatch. The nature of this strongly interacting "normal" state (as it appears) remains to be understood. Can it be described as a collection of quasi-particles with effective mass? A recent Monte-Carlo study indicates this to be the case [153]. However, Monte-Carlo methods have their limits when dealing with unequal Fermi mixtures because of the famous "sign-problem" in requiring the antisymmetry of the many-body wavefunction. Experiments might be able to determine the full equation of state for arbitrary density imbalance. An important question is whether a fermionic superfluid in three dimensions can exist (at zero temperature) at unequal densities. On the BEC-side, such a "magnetized" superfluid should clearly be observable. On the BCS-side, calculations indicate the FFLO-state to be the ground state of the system, in a certain window of parameters (see for example [65, 169, 221, 157]). The question is whether this parameter regime translates into a large enough region in real space for the novel state to be observable in experiments. As there is a multitude of candidate FFLO-like states with crystal-like distribution of Cooper pair momenta, it is not at all clear how such a state could be unambiguously observed.

Finally, let me attempt to give a brief outlook as to where atomic physics can help to answer burning questions in condensed matter, nuclear and astrophysics. As both bosonic and fermionic superfluids are now available, these gases can be applied to form model systems that simulate real materials. One of the most challenging and important problems is that of High-T_C superconductors, specifically the question whether d-wave Cooper pairs are contained in the Hubbard model, one of the most promising candidate hamiltonians for High-T_C materials. Fermionic atoms with repulsive interaction in optical lattices could potentially realize the Hubbard model. One of the first signatures to look for will be anti-ferromagnetic ordering of spin-up and spin-down atoms, a robust normal state one obtains when all lattice-sites are singly occupied. Experiments are being set up to study this important topic.

An important future subject will be the study of strongly interacting quantum mixtures of *different* atomic species. For example, a mixture of ^{6}Li and ^{40}K could be used to observe fermionic superfluidity of unequal particles, with unequal masses. This is yet another way to imbalance the chemical potentials of the two species, qualitatively different from the population imbalance studied in the preceding chapter. It will be intriguing to see how nature copes with this mass mismatch. One can go further and dream about studying superfluids with three different atoms or spin states, which would be a (simplified) analog of quark ("Color") superfluidity, where different quarks with different Fermi momenta form superfluid pairs.

Furthermore, the use of interspecies Feshbach resonances, like the ones discovered by our group [234], might provide a new road towards ultracold, heteronuclear ground state molecules. Such molecules would have a large electric dipole moment, very useful for a variety of applications. These range from measurements of fundamental constants [142] to the use of dipolar molecules as q-bits in a quantum computer [77]. For many-body physics, ultracold dipolar molecules would open the door to the study of quantum gases with strong *anisotropic* interactions [210].

About hundred years have passed since the first formation of a superfluid in 1908, and the discovery of superconductivity in 1911. After the discovery of Bose-Einstein condensation in dilute gases in 1995, atomic physics has been in fast-forward mode for ten years to "catch up" with condensed matter physics. We appear to finally be in the position to start solving open problems, using atoms, the building blocks of matter, as model systems for real materials. With ever more experimental and theoretical groups joining in for the excitement, we can look forward to new discoveries and insights in the years ahead. The last four years were certainly a thrill for me.

Appendix A

Spectroscopic Insensitivity to Cold Collisions in a Two-State Mixture of Fermions

This appendix contains a reprint of Ref. [266]: Martin W. Zwierlein, Zoran Hadzibabic, Subhadeep Gupta, and Wolfgang Ketterle, *Spectroscopic Insensitivity to Cold Collisions in a Two-State Mixture of Fermions*, Phys. Rev. Lett. **91**, 250404 (2003).

Spectroscopic Insensitivity to Cold Collisions in a Two-State Mixture of Fermions

Martin W. Zwierlein, Zoran Hadzibabic, Subhadeep Gupta, and Wolfgang Ketterle

Department of Physics, MIT-Harvard Center for Ultracold Atoms, and Research Laboratory of Electronics, MIT, Cambridge, Massachusetts 02139, USA

(Received 24 June 2003; published 19 December 2003)

We have experimentally demonstrated the absence of spectroscopic resonance shifts in a mixture of two interacting Fermi gases. This result is linked to observations in an ultracold gas of thermal bosons. There, the measured resonance shift due to interstate collisions is independent of the coherence in the system, and twice that expected from the equilibrium energy splitting between the two internal states in a fully decohered cloud. We give a simple theoretical explanation of these observations, which elucidates the effect of coherent radiation on an incoherent mixture of atoms.

DOI: 10.1103/PhysRevLett.91.250404 PACS numbers: 03.75.Ss, 05.30.Jp, 32.30.Bv, 34.20.Cf

The coherence properties of light and matter are intimately connected with the quantum statistics of the constituent particles. One quantitative measure of the coherence in a system is the two-particle correlation function at zero distance, $g^{(2)}$, which measures the probability that two particles are simultaneously detected. Intensity fluctuations in the incoherent light emitted by a light bulb lead to photon "bunching," making this probability twice higher than in the coherent light of a laser. Identical fermions on the other hand exhibit "antibunching," making such a probability zero.

Interactions in ultracold atomic gases crucially depend on the value of $g^{(2)}$ [1]. The reason is that s-wave scattering relies on particles overlapping in real space. The interaction energy in a many-body system is determined by coherent collisions, for which the outgoing and the incoming two-particle states are identical. Under this constraint, the two colliding particles can at most do two things—either preserve their momenta, or exchange them. We can thus distinguish four cases: (i) Two identical bosons in a thermal gas can collide in both ways, corresponding to $g^{(2)} = 2$. (ii) Two atoms in a Bose-Einstein condensate (BEC) have the same momenta and cannot undergo the exchange interaction. Here $g^{(2)} = 1$. (iii) Two distinguishable particles, fermions or bosons, also cannot exchange their momenta because that would make the outgoing state different from the incoming one. Again, $g^{(2)} = 1$. (iv) Two identical fermions cannot collide at all, so $g^{(2)} = 0$. In all cases, the mean-field energy of a particle with mass m is given by $g^{(2)}(4\pi\hbar^2/m)an$, where a is the s-wave scattering length, and n is the density of atoms it interacts with.

Mean field energies and therefore $g^{(2)}$ can be measured spectroscopically. In experiments on ultracold hydrogen, mean-field shifts of the $1S$-$2S$ two-photon transition were used to prove the existence of a BEC [2]. However, quantitative interpretation of the shifts led to a vivid theoretical discussion about the coherence related "factors of 2" [3–6]. More recently, Harber *et al.* performed Ramsey spectroscopy in a two-component, thermal gas of ^{87}Rb bosons to measure $g^{(2)}$ in the interstate collisional shift [7]. Their measurements yielded $g^{(2)} = 2$, independent of the degree of coherence between the two states. The spectroscopic results thus seemed to correspond to the case of all particles being in an identical coherent superposition of the two internal states, even though the binary mixture was partially decohered and should have had a mean-field energy corresponding to $1 < g^{(2)} < 2$. The authors commented on this mystery [8]: "it is a pleasure to note that a two-level system can still yield surprises, 75 years after the advent of quantum mechanics." The mystery can be formally resolved using a quantum Boltzmann equation [9–13].

Here, we experimentally address the relation between coherence and spectroscopic measurements in a binary mixture of ultracold *fermions*. We demonstrate that shifts of spectroscopic lines are absent even in a fully decohered binary mixture, in which the particles are distinguishable, and the many-body mean-field energy in the system has developed. We theoretically show that this is a direct consequence of the coherent nature of the radiofrequency (rf) *excitation*, which, in general, leads to a final state with $g^{(2)}$ different from the initial state.

Our calculation intuitively explains both our results for fermions, and the results for bosons of Ref. [7].

In a recent paper [14], we demonstrated the absence of mean-field "clock shifts" in a coherent two-state superposition of ^{6}Li fermions. In this case, rf spectroscopy was performed on a gas prepared purely in one internal state. Since an rf pulse acts as a rotation in the two-state Hilbert space, all the atoms stayed in an identical (superposition) state and could not interact. As long as the fermionic atoms were indistinguishable, $g^{(2)} = 0$, and the resonance was thus found to be unperturbed at $\nu_0 = (E_{12}/h)$, where E_{12} is the energy difference between the internal states $|1\rangle$ and $|2\rangle$.

However, once decoherence sets in, for example due to inhomogeneous magnetic fields across the cloud, the spatial overlap between atoms in different states grows and mean-field energy density builds up:

 © 2003 The American Physical Society

$$\mathcal{E}_{\rm int}(\mathbf{r}) = g^{(2)} V_{12} n_1(\mathbf{r})\, n_2(\mathbf{r}), \qquad V_{12} = \frac{4\pi\hbar^2}{m} a_{12}, \quad (1)$$

where n_1 and n_2 are the local densities of particles in states $|1\rangle$ and $|2\rangle$, and a_{12} is the interstate s-wave scattering length. Here decoherence means that off-diagonal matrix elements of the density matrix have vanished locally. As a result, everywhere in the sample, atoms are no longer in one pure state, but occupy two orthogonal states, and s-wave collisions are no longer suppressed by the Pauli principle. In a fully decohered cloud, we have a binary mixture of two distinct species of atoms, with a mean-field energy density $\mathcal{E}_{\rm int} = V_{12} n_1 n_2$. This interaction changes the equilibrium energy level of atoms in state $|1\rangle$ ($|2\rangle$) according to $\delta\mu_{1,2} = V_{12} n_{2,1}$. The difference in equilibrium mean-field energy of the two states is then

$$\Delta E_{\rm int} = \delta\mu_2 - \delta\mu_1 = V_{12}(n_1 - n_2). \quad (2)$$

This suggests [7,8,14] that in a decohering sample, the resonant frequency for population transfer between the two states gradually changes from $\nu_{12} = \nu_0$ to $\nu_{12} = \nu_0 + \frac{1}{h}\Delta E_{\rm int}$. Here, we show both experimentally and theoretically that this conclusion is wrong, and that the spectroscopic resonance frequency ν_{12} is always the unperturbed frequency ν_0.

Our experimental setup was described in [14,15]. About 10^7 fermionic ^{6}Li atoms were confined in an optical dipole trap at a temperature of 35 μK. The two-level system under consideration is formed by the two lowest ground state hyperfine levels, $|1\rangle$ and $|2\rangle$, corresponding to $|F, m_F\rangle = |1/2, 1/2\rangle$ and $|1/2, -1/2\rangle$ in the low field basis, respectively. A dc magnetic field of $B =$ 320 G was applied to the sample in order to tune the interstate scattering length a_{12} to a large value of $\sim -300 a_0$, where a_0 is the Bohr radius [14].

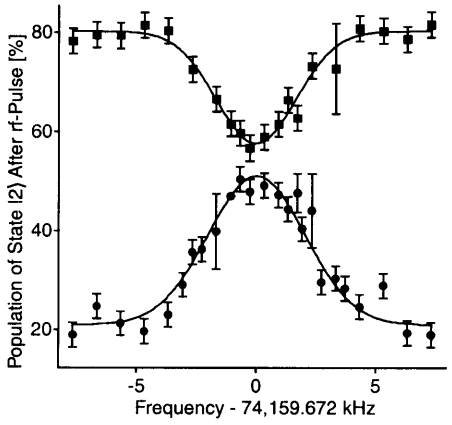

FIG. 1. Absence of mean-field shift of an rf transition in a binary Fermi system. The resonance curves were measured for fully decohered (80/20)% two-state mixtures of fermions. The measured frequency difference between the two lines is (34 ± 146) Hz, even though Eq. (2) would predict a splitting of 20 kHz.

We created a superposition of atoms in states $|1\rangle$ and $|2\rangle$ using a nonadiabatic rf sweep around the energy splitting of 74 MHz. As the sample decohered, efficient evaporative cooling set in, confirming a large elastic scattering length. After 1 sec, we were left with a fully decohered mixture at a mean density $n = 5 \times 10^{13}$ cm^{-3}. The rate of the rf sweep was adjusted so that after decoherence and cooling, 80% of the atoms were in state $|2\rangle$. The mean-field interaction should thus have increased the energy splitting of the two levels by $h\delta\nu = \delta\mu_2 - \delta\mu_1 = V_{12}(n_1 - n_2) \approx h \times 10$ kHz. Our experiments involving a third state [14] have confirmed the presence of such energy shifts, and prove that full decoherence has been reached.

Rabi spectroscopy in the interacting binary mixture was performed by applying 200 μs rf pulses of different frequencies, and recording the final populations in the two states by simultaneous absorption imaging (Fig. 1). In order to eliminate the systematic uncertainty in the value of ν_0, we performed a second experiment with the population ratios of states $|1\rangle$ and $|2\rangle$ reversed. According to Eq. (2), one would expect an opposite shift of the resonance.

Within our precision, no interaction shift of the resonance frequency was observed. Comparing the expected difference in mean-field shifts for the two experiments, $2\delta\nu = 20$ kHz, with the measured line separation of (34 ± 146) Hz, we arrive at an apparent value for $g^{(2)} =$ 0.002(7). This demonstrates the universal absence of a resonance shift in a very cold two-level Fermi gas, independent of the coherence in the system.

Evidently, rf spectroscopy does not measure the expected difference in thermodynamic chemical potentials for the two states. Experiments with thermal bosons have posed a similar puzzle [7]. Here we explain that this is a

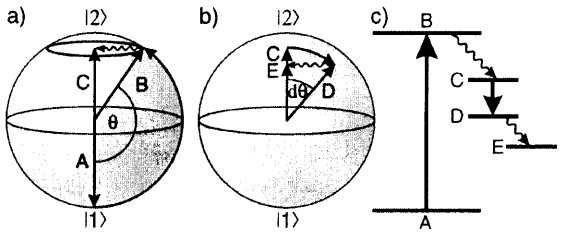

FIG. 2. Bloch sphere representation of rf transitions. (a) An rf pulse rotates a pure state A into B. The superposition state decoheres into a "ring" distribution, represented by its average, C. (b) A second rf pulse transforms the fully decohered state C into a partially coherent state D. The final state E is reached only after further decoherence. (c) Transfers $A \rightarrow B$ and $C \rightarrow D$ are coherent and reversible. $B \rightarrow C$ and $D \rightarrow E$ are irreversible.

direct consequence of the coherent nature of the rf excitation.

In Fig. 2, the average properties of the many-body state at a specific point $\mathbf{r}$ in the trap are described by the three coordinates of the local spin-1/2 Bloch vector $\mathbf{m}(\mathbf{r}) = m_z(\mathbf{r})\hat{\mathbf{e}}_z + \mathbf{m}_\perp(\mathbf{r})$. In the following, we omit the label $\mathbf{r}$. $m_z = [(n_2 - n_1)/2]$ represents the population difference in the two states, whereas the transverse component $\mathbf{m}_\perp$ is a measure of the coherence in the system. The length of the Bloch vector measures the purity of the average state and hence the entropy of the system. Fully decohered statistical mixtures do not have off-diagonal matrix elements of the density matrix and are represented by vectors with $\mathbf{m}_\perp = 0$, with state A being the special case of a pure state. In Fig. 2(a), state B is created by applying an rf pulse on a pure sample A. In this case, there is no interaction energy in the system during the rf pulse, and no frequency shift is expected [14]. State C is formed through subsequent decoherence of state B. States B and C have the same number of particles in $|1\rangle$ and $|2\rangle$, but in C the mean-field has fully developed.

Our experiment is performed on a C-like state [Fig. 2(b)]. Here we explain why Eq. (2) still does not give the correct resonance frequency for an infinitesimal transfer of atoms between $|1\rangle$ and $|2\rangle$. The key point is that even though the sample is fully decohered, the applied rf pulse reintroduces coherence into the system. According to Eq. (6) below, this will change the value of $g^{(2)}$. Let us consider two fully decohered states, C and E. Equation (2) correctly gives the energy of the transformation $C \rightarrow E$. However, these two states have different entropies, as indicated by Bloch vectors of different lengths. An rf pulse is a unitary transformation of the system, and must preserve entropy. The true effect of the rf pulse is thus to change the relative populations of $|1\rangle$ and $|2\rangle$ by tilting the Bloch vector away from the z axis, into state D. It is the energy of *this* transformation, $C \rightarrow D$, that needs to be calculated in order to find the correct resonant rf frequency.

In the case of fermions with short-range (delta function) interactions, we can prove very generally that the resonance frequency will always be ν_0, by showing that the interaction Hamiltonian is invariant under rotations on the Bloch sphere. The interstate s-wave interaction at point $\mathbf{r}$ is described by the second-quantized Hamiltonian density

$$H_{\text{int}}(\mathbf{r}) = V_{12}\psi_1^\dagger(\mathbf{r})\psi_2^\dagger(\mathbf{r})\psi_2(\mathbf{r})\psi_1(\mathbf{r}). \tag{3}$$

Under a general rotation, described by polar angles θ, ϕ, the field operators $\psi_{1,2}^\dagger$ transform according to:

$$\begin{aligned}\psi_{1\theta,\phi}^\dagger &= \cos\frac{\theta}{2}e^{-i\phi/2}\psi_1^\dagger + \sin\frac{\theta}{2}e^{i\phi/2}\psi_2^\dagger,\\ \psi_{2\theta,\phi}^\dagger &= -\sin\frac{\theta}{2}e^{-i\phi/2}\psi_1^\dagger + \cos\frac{\theta}{2}e^{i\phi/2}\psi_2^\dagger.\end{aligned} \tag{4}$$

Using the standard fermionic anticommutation relations ($\psi_1\psi_2 = -\psi_2\psi_1$, $\psi_1\psi_1 = 0$, etc.), it is easy to show that

$$H_{\text{int}}^{\theta,\phi} = V_{12}\psi_{1\theta,\phi}^\dagger\psi_{2\theta,\phi}^\dagger\psi_{2\theta,\phi}\psi_{1\theta,\phi} = H_{\text{int}}. \tag{5}$$

We therefore see that an rf-induced rotation on the Bloch sphere commutes with the interaction Hamiltonian, and hence does not change the energy of the many-body state. It is then obvious that the resonant frequency will always be ν_0, independent of the coherence of the system.

We now present a more general calculation of the mean-field frequency shifts, which holds for both fermions and bosons. To reduce complexity and concentrate on the only controversial case of interstate interactions, we consider a fictitious boson with no intrastate interactions ($a_{11} = a_{22} = 0$). The (local) mean-field expectation value of the Hamiltonian density in Eq. (3) is [16]

$$\begin{aligned}\mathcal{E}_{\text{int}}(\mathbf{r}) &= \langle H_{\text{int}}\rangle = V_{12}(n_1 n_2 + \epsilon n_{12}n_{21})\\ &\Rightarrow g^{(2)} = 1 + \epsilon\frac{n_{12}n_{21}}{n_1 n_2},\end{aligned} \tag{6}$$

where $n_1 = \langle\psi_1^\dagger\psi_1\rangle$ and $n_2 = \langle\psi_2^\dagger\psi_2\rangle$ are the local densities in the two states, we have introduced "coherences" $n_{12} = \langle\psi_1^\dagger\psi_2\rangle$ and $n_{21} = \langle\psi_2^\dagger\psi_1\rangle$, and $\epsilon = \pm 1$ for bosons/fermions. In a fully coherent sample $n_{12}n_{21} = n_1 n_2$ and $g^{(2)} = 1 + \epsilon$. As decoherence sets in, $g^{(2)}$ increases (decreases) from 0 (2) to 1 for fermions (bosons). For the most general case of a partially decohered sample, we can rewrite Eq. (6) in terms of the (local) Bloch vector, using $n_{1,2} = \frac{n}{2} \mp m_z$, $n_{12} = m_x + i m_y = n_{21}^*$, and $n_{12}n_{21} = m_x^2 + m_y^2 = m_\perp^2$, where n is the total particle density. This gives

$$\mathcal{E}_{\text{int}} = V_{12}\frac{n^2}{4} + \epsilon V_{12}|\mathbf{m}|^2 - (1+\epsilon)V_{12}m_z^2. \tag{7}$$

Two samples with the same numbers of atoms in states $|1\rangle$ and $|2\rangle$, but different levels of coherence, have the same m_z, but different $|\mathbf{m}_\perp|$ [e.g., states D and E in Fig. 2(b)]. Again we see that two such samples indeed have different interaction energies.

Now, let us evaluate the effect of coherence on the resonant rf frequency. A coherent rf excitation preserves entropy ($|\mathbf{m}| = \text{const}$), and the total density n. In an infinitesimal tilt of the Bloch vector, the density of atoms transferred from $|1\rangle$ to $|2\rangle$ is $dn_2 = -dn_1 = dm_z$. Therefore, the change of interaction energy per transferred particle, and thus the shift in the resonant frequency $\Delta\nu$, comes out to be

$$\Delta\nu = \frac{1}{h}\frac{\partial\mathcal{E}_{\text{int}}}{\partial m_z}\bigg|_{n,|m|} = \frac{1}{h}(1+\epsilon)V_{12}\,(n_1 - n_2). \tag{8}$$

In analogy with a spinning top which precesses in the gravitational field, the resonant frequency for an infinitesimal tilt of the Bloch vector is also equal to the frequency of its free precession. In the traditional language of atomic physics, this analogy just reiterates

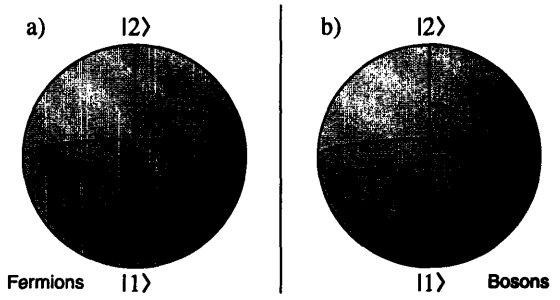

FIG. 3. Mean-field represented as effective magnetic field. (a) Fermions: The exchange and direct interaction add up to form a magnetic field aligned with the average spin ($V_{12} < 0$ in the drawing). The net torque vanishes and the Bloch vector $\mathbf{m}$ precesses at the unperturbed frequency ν_0. (b) Bosons: The exchange interaction has opposite sign to that in fermions. It exerts a torque on the average spin equal to the torque induced by the direct interaction, as can be seen by comparing the two cross products with $\mathbf{m}$. The Bloch vector thus precesses at ν_0 plus twice the frequency shift due to direct interaction.

that Rabi [14] and Ramsey [7] spectroscopy measure the same characteristic frequency of the system. The striking result is that in contrast to the interaction energy [Eqs. (6) and (7)], the precession of the Bloch vector, or equivalently the rf frequency shift [Eq. (8)], *does not* depend on the level of coherence in the sample. Remarkably, the final state may have a value of $g^{(2)}$ different from the initial state, such that the energy difference per transferred particle is *independent* of the initial $g^{(2)}$. Equation (8) explains both our measurements with fermions, and the experiment with thermal bosons of Ref. [7].

In order to further elucidate the role of coherences in the precession of the Bloch vector, we employ the interpretation of the mean-field energy as the interaction of the average spin with an effective magnetic field [12,13]. Using Eq. (7), we obtain $\mathcal{E}_{\rm int} = \text{const} - \frac{1}{2}\mathbf{B}_{\rm eff} \cdot \mathbf{m}$ [17] with

$$\mathbf{B}_{\rm eff} = 2V_{12}(m_z\hat{\mathbf{e}}_z - \epsilon\mathbf{m}_\perp). \tag{9}$$

In this picture, the precession of the spin due to interactions is driven by the torque $\mathbf{B}_{\rm eff} \times \mathbf{m}$. The magnetic field along the z axis is induced by the direct interaction, and has the same sign for fermions and bosons (Fig. 3). The transverse magnetic field comes from the exchange interaction, and has opposite signs for fermions and bosons. For fermions, $\mathbf{B}_{\rm eff}$ is parallel to $\mathbf{m}$ [Eq. (9)] and hence does not cause any precession. Equivalently, the direct and exchange interaction exert torques equal and opposite to each other. For bosons, the two contributions add up to yield exactly twice the precession frequency given by the direct interaction alone. During decoherence, the exerted torque shrinks in proportion to the decaying transverse spin. Therefore, the precession frequency remains constant, no matter how small the coherences are.

In conclusion, we have demonstrated the absence of the mean-field shift of rf transitions in a fully decohered, interacting binary mixture of fermions. This was explained by proving the invariance of the interaction energy under coherent Hilbert space rotations. This result is relevant for the potential use of a fermionic atom supplying the frequency standard in an atomic or optical clock, since it implies a robust elimination of the systematic errors due to density dependent frequency shifts. Previously, the absence of such clock shifts was explained by the absence of mean-field energy in a purely coherent superposition state [14]. Now we have shown that there is no spectroscopic shift even after decoherence has led to measurable mean-field energies. Further, we have presented a simple theoretical framework for calculating the precession frequency of the Bloch vector which describes an arbitrary spin state of either fermions or bosons. This resolves "the mystery of the Ramsey fringe that did not chirp" [8] with a simple and intuitive picture.

We thank Claudiu Stan and Christian Schunck for experimental assistance, and Michele Saba for critical reading of the manuscript. This work was supported by the NSF, ONR, ARO, and NASA.

[1] W. Ketterle and H.-J. Miesner, Phys. Rev. A **56**, 3291 (1997).
[2] D. G. Fried *et al.*, Phys. Rev. Lett. **81**, 3811 (1998).
[3] R. Côté and V. Kharchenko, Phys. Rev. Lett. **83**, 2100 (1999).
[4] M. Ö. Oktel and L. S. Levitov, Phys. Rev. Lett. **83**, 6 (1999).
[5] M. Ö. Oktel *et al.*, Phys. Rev. A **65**, 033617 (2002).
[6] C. J. Pethick and H. T. C. Stoof, Phys. Rev. A **64**, 013618 (2001).
[7] D. M. Harber *et al.*, Phys. Rev. A **66**, 053616 (2002).
[8] D. M. Harber *et al.* in *Proceedings of the XVIII International Conference on Atomic Physics*, edited by H. R. Sadeghpour, E. J. Heller, and D. E. Pritchard (World Scientific, Cambridge, Massachusetts, 2003), pp. 3–10.
[9] M. Ö. Oktel and L. S. Levitov, Phys. Rev. Lett. **88**, 230403 (2002).
[10] J. E. Williams, T. Nikuni, and C. W. Clark, Phys. Rev. Lett. **88**, 230405 (2002).
[11] A. S. Bradley and C. W. Gardiner, J. Phys. B **35**, 4299 (2002).
[12] J. N. Fuchs, D. M. Gangardt, and F. Laloë, Phys. Rev. Lett. **88**, 230404 (2002).
[13] J. N. Fuchs, D. M. Gangardt, and F. Laloë, Eur. Phys. J. D **25**, 57 (2003).
[14] S. Gupta *et al.*, Science **300**, 1723 (2003).
[15] Z. Hadzibabic *et al.*, Phys. Rev. Lett. **91**, 160401 (2003).
[16] A. L. Fetter and J. D. Walecka, *Quantum Theory of Many-Particle Systems* (Dover Publications, New York, 2003).
[17] The factor of 1/2 reflects the self-interaction.

Appendix B

Observation of Bose-Einstein Condensation of Molecules

This appendix contains a reprint of Ref. [271]: M.W. Zwierlein, C. A. Stan, C. H. Schunck, S.M. F. Raupach, S. Gupta, Z. Hadzibabic, and W. Ketterle, *Observation of Bose-Einstein Condensation of Molecules*, Phys. Rev. Lett. **91**, 250401 (2003).

Observation of Bose-Einstein Condensation of Molecules

M.W. Zwierlein, C. A. Stan, C. H. Schunck, S. M. F. Raupach, S. Gupta, Z. Hadzibabic, and W. Ketterle
Department of Physics, MIT–Harvard Center for Ultracold Atoms, and Research Laboratory of Electronics, MIT, Cambridge, Massachusetts 02139, USA
(Received 27 November 2003; published 15 December 2003)

We have observed Bose-Einstein condensation of molecules. When a spin mixture of fermionic ^{6}Li atoms was evaporatively cooled in an optical dipole trap near a Feshbach resonance, the atomic gas was converted into $^6Li_2$ molecules. Below 600 nK, a Bose-Einstein condensate of up to 900 000 molecules was identified by the sudden onset of a bimodal density distribution. This condensate realizes the limit of tightly bound fermion pairs in the crossover between BCS superfluidity and Bose-Einstein condensation.

DOI: 10.1103/PhysRevLett.91.250401 PACS numbers: 03.75.Ss, 05.30.Jp

Over the past few years, many different approaches have been used to cool and trap molecules [1,2]. One major goal has been the creation of molecular Bose-Einstein condensates, which could lead to advances in molecular spectroscopy, studies of collisions, and precision tests of fundamental symmetries.

Recently, a new technique for creating ultracold molecules led to major advances towards molecular Bose-Einstein condensation (BEC). Molecules were produced from ultracold atoms [3–9] near a Feshbach resonance [10], where a molecular state is resonant with the atomic state and molecules can form without heat release. These molecules are highly vibrationally excited and would usually undergo fast decay. However, in the case of fermionic atoms the molecules showed very long lifetimes [7–9,11]. This has been attributed to Pauli suppression of the vibrational quenching process, which couples a very weakly bound molecular state to much more tightly bound lower lying vibrational states [12]. We have now been able to cool such molecules to Bose-Einstein condensation.

This Bose-Einstein condensate represents one extreme of the crossover from Bose-Einstein condensation of tightly bound pairs (molecules) to BCS superfluidity of Cooper pairs, where fermions form delocalized pairs in momentum space [13].

In most of the recent experiments, molecules were formed by sweeping an external magnetic field through the Feshbach resonance, adiabatically converting atoms to molecules [3–6,8]. This atom-molecule coupling is a coherent two-body process [14].

In the case of ^{6}Li, experimental work indicated [7,9] and theoretical work predicted [15,16] that cooling the atoms at constant magnetic field would create an atom-molecule mixture in thermal equilibrium. In this case, the atoms and molecules are coupled by three-body recombination [17]. For temperatures lower than the binding energy of the molecular state, an almost pure molecular gas should form, and at even lower temperatures, a molecular Bose-Einstein condensate. This work demonstrates that this surprisingly simple method to create molecular condensates works. The success of this approach depends on a very favorable ratio of collisional rates for formation and decay of molecules which may be unique to ^{6}Li.

The goal of molecular BEC was reached in several steps. Using Feshbach resonances, atomic condensates were put into an atom-molecule superposition state [2]. Pure molecular gases made of bosonic atoms were created close to [6] or clearly in [4] the quantum-degenerate regime, but the effective heating time (of about 2 ms in Ref. [4]) was too short to reach equilibrium. Earlier this month, while this work was in progress, two papers were submitted. Reference [18] observed a quantum-degenerate gas of potassium molecules with an effective lifetime of 5 to 10 ms, sufficiently long to reach equilibrium in two dimensions and to form a quasi- or nonequilibrium condensate [19]. Reference [20] provided indirect evidence for a long-lived condensate of lithium molecules [21]. Here we observe the formation of a condensate by evaporative cooling of a molecular gas close to equilibrium.

The basic scheme of the experiment is similar to our earlier work when we identified two Feshbach resonances in lithium by monitoring the loss of trapped atoms due to three-body recombination as a function of the external magnetic field [22]. This process leads to ultracold molecules in the highest vibrational state below the continuum. However, no attempt was made to detect these molecules because until very recently [7,9] they were believed to decay rapidly.

Our experimental setup was described in Refs. [22,23]. After laser cooling and sympathetic cooling with sodium atoms in a magnetic trap, 35×10^6 lithium atoms in the $|F, m_F\rangle = |3/2, 3/2\rangle$ state were transferred into an optical trap formed by a single far detuned laser beam with up to 7 W of power at 1064 nm. The beam had a 20 μm waist and was aligned horizontally along the symmetry axis of the magnetic trap. This generated a 650 μK deep trapping potential with 15 kHz radial and 175 Hz axial trapping frequencies. They were determined with an accuracy of 10% by exciting dipolar oscillations with an atomic

 © 2003 The American Physical Society

sodium condensate and scaling them to lithium atoms using the ratios of polarizabilities and masses.

The ^{6}Li atoms were then transferred to the lowest energy state $|1\rangle$, using an adiabatic frequency sweep around the lithium hyperfine splitting of 228 MHz. dc magnetic fields of up to 1025 G could be applied, a range encompassing the $|1\rangle - |2\rangle$ Feshbach resonance [22,24,25], where $|2\rangle$ denotes the second lowest hyperfine state of ^{6}Li.

Most of our experiments were performed at a magnetic field of 770 G. This was below but still within the width of the broad Feshbach resonance. Here the atomic scattering length is positive corresponding to a stable weakly bound molecular state. Using rf-induced transitions near 80 MHz, an equal mixture of states $|1\rangle$ and $|2\rangle$ was prepared with a ratio of temperature T to Fermi temperature T_F around 0.3. The sample was cooled in 350 ms by ramping down the laser power of the optical trap to typically 10^{-3} of the maximum power resulting in a calculated trap depth for unbound atoms of 650 nK. The weakly bound molecules have twice the atomic polarizability. They experience the same trap frequencies and twice the trap depth as the lithium atoms. Therefore, we expect mainly atoms to be evaporated.

Atoms and molecules were detected by absorption imaging after ballistic expansion times of 1 to 30 ms. During the time of flight, the magnetic field was suddenly switched off, and atoms in both states were imaged simultaneously since the two optical transition frequencies are equal at zero field. Molecules were detected by first dissociating them by sweeping the magnetic field across the Feshbach resonance up to 925 G and then by imaging the resulting atoms at zero field. With the Feshbach sweep, molecules and residual atoms were imaged together. Without it, only the unbound atoms were detected after switching off the magnetic field. We have found that during the initial phase of the evaporative cooling the atomic population dominated. A significant molecule fraction formed around $T \sim 2\ \mu$K, and in the final phase of the cooling, no atoms could be discerned. The absorption images and profiles shown in Figs. 1 and 2 therefore represent purely molecular column densities.

When the laser power of the optical dipole trap was ramped down, the shrinking size of the cloud in absorption imaging signaled lower temperatures. Very abruptly, the smooth distribution changed to a bimodal distribution—the well-known 'smoking gun' of Bose-Einstein condensation [26,27] (Figs. 1 and 2). Because of a slight asymmetry of our trapping potential, the centers of the condensate and of the thermal cloud were shifted.

The phase transition could be identified by plotting the effective area of the cloud vs laser power P [Fig. 3(a)]. At the phase transition, there was an abrupt change in slope, whereas the temperature changed smoothly. For a classical gas, the area depends only on temperature and trap frequencies, which vary smoothly with P.

Quantitative information on temperature, total atom number, and condensate fraction was obtained by fitting

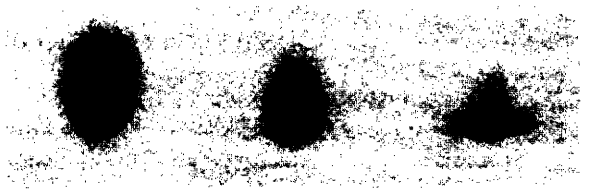

FIG. 1. Observation of Bose-Einstein condensation in a molecular gas. Shown are three single-shot absorption images after 6 ms of ballistic expansion for progressively lower temperatures (left to right). The appearance of a dark spot marks the onset of BEC. The field of view for each image is 1.4×1.4 mm^2. The long axis of the optical dipole trap was vertical in the image.

axial profiles (such as in Fig. 2) using a bimodal distribution: a Bose-Einstein distribution for the broad normal component and a Thomas-Fermi distribution for the narrow (condensate) component. Condensates containing up to 900 000 molecules and condensate fractions of up to 75% were obtained. The onset of BEC was observed at a temperature of 600 nK with 1.4×10^6 molecules. For an ideal gas with this number of molecules, the predicted BEC transition temperature $T_C = 0.94\,\hbar\bar{\omega}N^{1/3}/k_B$ is 650 nK, where $\bar{\omega}$ denotes the geometric mean of the three trapping frequencies. This agreement is fortuitous, given the uncertainty in the trap frequencies at low power [28].

The cooldown is characterized in Fig. 3. Axial temperatures were obtained from the spatial extent of the thermal cloud (the size stayed almost constant during the time of flight). The axial temperatures are in arbitrary

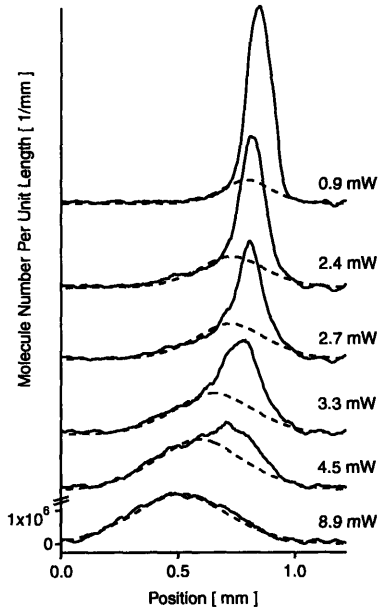

FIG. 2. Bimodality in the density distribution of a molecular gas. Shown are radially averaged profiles through absorption images such as those in Fig. 1, as a function of final laser power. The dashed lines are fits to the thermal clouds.

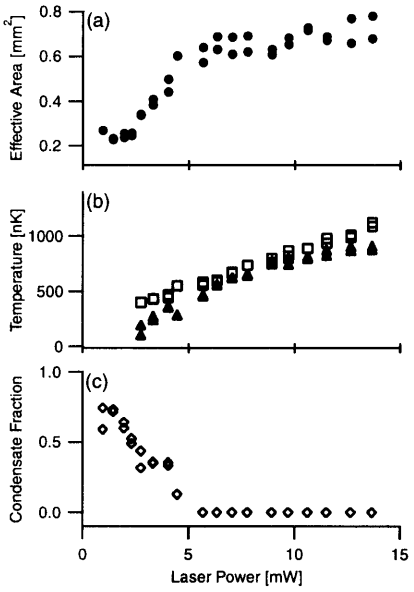

FIG. 3. Characterization of the phase transition. (a) The effective area is the integrated optical density divided by the peak optical density of the absorption images. The 'sudden shrinking' of the area coincides with the appearance of a bimodal density distribution and indicates the BEC phase transition. (b) The radial (squares) and axial (triangles) temperatures varied smoothly during the evaporation. The axial temperatures are in arbitrary units. (c) Condensate fraction. Below the critical temperature, the condensate fraction increased from zero to up to 75%.

units [28]. Absolute radial temperatures were obtained from the ballistic expansion. All of our temperature measurements are consistent with equilibration in three dimensions.

From the expansion of the largest condensates, we determined the mean-field energy μ to be 300 ± 100 nK. The peak density n of the condensate was obtained from the fit to be 7×10^{13} cm^{-3}. The relation $\mu = 4\pi\hbar^2 an/m$, where m is the molecular mass, implies a molecular scattering length of $a = 8$ nm with an uncertainty of $\pm 60\%$. These uncertainties were estimated from the discrepancy of fits done at different times of flight which were not fully consistent. This might reflect asymmetries and anharmonicities of the trapping potential which were not characterized.

It was predicted that the molecular scattering length a is 0.6 times the atomic scattering length a_a [12]. At our magnetic field of 770 G, the predicted value of a_a lies between 140 and 340 nm depending on the uncertain position of the Feshbach resonance between 810 and 850 G [25]. The discrepancy between the predicted and observed values of a needs further study.

The molecular gas decayed faster than extrapolated from Refs. [7,9]. Just above T_c, the thermal cloud had a peak density of 1×10^{13} cm^{-3} and an initial decay time of about 1 s. Condensate numbers decayed to one third after a hold time of 30 ms. Those short lifetimes may reflect leakage or heating in our optical dipole trap at low laser power. In the present experiments, the laser power was not stabilized. The lifetime of the thermal gas is much longer than estimated values of the axial trap period of 100 ms and of the collision time of 2 ms, which should lead to full equilibrium. Depending on how the condensate grew during the evaporative cooling, its lifetime may have been too short to develop phase coherence in the axial direction [19].

Using the experimentally determined scattering length, we find that the molecular cloud at T_c has a ratio of mean-free path to radius close to 10 and should show only negligible anisotropy during ballistic expansion [19]. Therefore, the onset of strongly anisotropic expansion is a distinguishing feature of the molecular condensate (Fig. 1).

The $^6Li_2$ molecules are extremely weakly bound. The molecular binding energy depends on the atomic scattering length a_a as $\hbar^2/ma_a^2$ [29]. For an assumed $a_a = 200$ nm the binding energy is 2 μK. The molecular state which causes the Feshbach resonance is the $X\,^1\Sigma_g^+$, $v = 38$ state. This state is tightly bound, but near the Feshbach resonance it is strongly mixed with the state of the colliding atoms, and the molecular wave function is spread out over an extension of order $a_a/2$ [29].

Direct evidence for the large size of the molecules was obtained by resonant imaging during ballistic expansion at high magnetic fields. At 770 G, molecules could be directly imaged using light in resonance with the atoms at the same field. The absorption was comparable to the zero-field absorption signal obtained after dissociating the molecules. This shows that the molecular bond is so weak that the absorption line is shifted from the atomic line by less than a linewidth Γ. The molecules are expected to absorb most strongly near the outer turning point R. The excited state potential is split by the resonant van der Waals interaction $\zeta\hbar\Gamma(\lambda\!\!\!^{-}/R)^3$, where $\lambda\!\!\!^{-}$ is the resonant wavelength divided by 2π and ζ is $\pm 3/4, \pm 3/2$ for different excited molecular states. The observed absorption signal implies a molecular size $R \geq 100$ nm. It is this huge size compared with the much smaller size of the molecule in lower vibrational states which, together with Fermi statistics, inhibits vibrational relaxation and leads to the long lifetimes [12].

Condensates were observed after evaporative cooling at various magnetic fields between 720 and 820 G. At the lower magnetic fields, the condensate expanded more slowly, consistent with the predictions of a smaller repulsive mean-field energy.

In future work, we plan to use the molecular BEC as the starting point for studying the BEC-BCS crossover [13]. By ramping up the magnetic field across the Feshbach resonance, the molecules are dissociated into fermionic atoms and the interaction between the atoms changes from repulsive to attractive, allowing for the formation of Cooper pairs. Starting with an almost pure

condensate and conserving entropy, a Fermi sea should form with temperatures well within the range where BCS type superfluidity has been predicted [30,31].

In conclusion, we have realized Bose-Einstein condensates of up to 900 000 molecules by evaporative cooling of a spin mixture of fermionic lithium atoms.

This work was supported by the NSF, ONR, ARO, and NASA. We thank A. Leanhardt for helpful comments. S. Raupach is grateful to the Dr. Jürgen Ulderup foundation for financial support.

Note added. In an optical trap with a slightly enlarged beam waist, we were recently able to hold molecular condensates for up to 400 ms (or three axial trapping periods) which should result in 3D equilibration. The $1/e$ decay time was about 200 ms.

[1] J. D. Weinstein, R. DeCarvalho, T. Guillet, B. Friedrich, and J. M. Doyle, Nature (London) **395**, 148 (1998); T. Takekoshi, B. M. Patterson, and R. J. Knize, Phys. Rev. Lett. **81**, 5105 (1998); R. Wynar, R. S. Freeland, D. J. Han, C. Ryu, and D. J. Heinzen, Science **287**, 1016 (2000); H. L. Bethlem, G. Berden, F. M. H. Crompvoets, R. T. Jongma, A. J. A. van Roij and G. Meijer, Nature (London) **406**, 491 (2000); C. Chin, A. J. Kerman, V. Vuletic, and S. Chu, Phys. Rev. Lett. **90**, 033201 (2003).

[2] E. A. Donley, N. R. Claussen, S. T. Thompson, and C. E. Wieman, Nature (London) **417**, 529 (2002).

[3] C. A. Regal, C. Ticknor, J. L. Bohn, and D. S. Jin, Nature (London) **424**, 47 (2003).

[4] K. Xu, T. Mukaiyama, J. R. Abo-Shaeer, J. K. Chin, D. E. Miller, and W. Ketterle, Phys. Rev. Lett. **91**, 210402 (2003).

[5] S. Dürr, T. Volz, A. Marte, and G. Rempe, e-print cond-mat/0307440.

[6] J. Herbig, T. Kraemer, M. Mark, T. Weber, C. Chin, H.-C. Nägerl, and R. Grimm, Science **301**, 1510 (2003).

[7] J. Cubizolles, T. Bourdel, S. J. J. M. F. Kokkelmans, G. V. Shlyapnikov, and C. Salomon, Phys. Rev. Lett. **91**, 240401 (2003).

[8] K. E. Strecker, G. B. Partridge, and R. G. Hulet, Phys. Rev. Lett. **91**, 080406 (2003).

[9] S. Jochim, M. Bartenstein, A. Altmeyer, G. Hendl, C. Chin, J. H. Denschlag, and R. Grimm, Phys. Rev. Lett. **91**, 240402 (2003).

[10] W. C. Stwalley, Phys. Rev. Lett. **37**, 1628 (1976); E. Tiesinga, B. J. Verhaar, and H. T. C. Stoof, Phys. Rev. A **47**, 4114 (1993); S. Inouye, M. R. Andrews, J. Stenger, H.-J. Miesner, D. M. Stamper-Kurn, and W. Ketterle, Nature (London) **392**, 151 (1998); P. Courteille, R. S. Freeland, D. J. Heinzen, F. A. van Abeelen, and B. J. Verhaar, Phys. Rev. Lett. **81**, 69 (1998).

[11] C. A. Regal, M. Greiner, and D. S. Jin, e-print cond-mat/0308606.

[12] D. S. Petrov, C. Salomon, and G. V. Shlyapnikov, e-print cond-mat/0309010.

[13] M. Randeria, in *Bose-Einstein Condensation*, edited by A. Griffin, D. Snoke, and S. Stringari (Cambridge University, Cambridge, 1995), pp. 355–392; H. T. C. Stoof, M. Houbiers, C. A. Sackett, and R. G. Hulet, Phys. Rev. Lett. **76**, 10 (1996); E. Timmermans, K. Furuya, P. W. Milonni, and A. K. Kerman, Phys. Lett. A **285**, 228 (2001); M. Holland, S. J. J. M. F. Kokkelmans, M. L. Chiofalo, and R. Walser, Phys. Rev. Lett. **87**, 120406 (2001); Y. Ohashi and A. Griffin, Phys. Rev. Lett. **89**, 130402 (2003).

[14] P. D. Drummond, K. V. Kheruntsyan, and H. He, Phys. Rev. Lett. **81**, 3055 (1998); P. Tommasini, E. Timmermans, M. Hussein, and A. Kerman, e-print cond-mat/9804015; F. A. van Abeelen and B. J. Verhaar, Phys. Rev. Lett. **83**, 1550 (1999); F. H. Mies, E. Tiesinga, and P. S. Julienne, Phys. Rev. A **61**, 022721 (2000).

[15] S. J. J. M. F. Kokkelmans, G. V. Shlyapnikov, and C. Salomon, e-print cond-mat/0308384.

[16] C. Chin and R. Grimm, e-print cond-mat/0309078.

[17] P. O. Fedichev, M. W. Reynolds, and G. V. Shlyapnikov, Phys. Rev. Lett. **77**, 2921 (1996); B. D. Esry, C. H. Greene, and H. Suno, Phys. Rev. A **65**, 010705 (2001); D. S. Petrov, Phys. Rev. A **67**, 010703 (2003).

[18] M. Greiner, C. A. Regal, and D. S. Jin, Nature (London) **426**, 537 (2003).

[19] I. Shvarchuck, C. Buggle, D. S. Petrov, K. Dieckmann, M. Zielonkowski, M. Kemmann, T. G. Tiecke, W. v. Klitzing, G. V. Shlyapnikov, and J. T. M. Walraven, Phys. Rev. Lett. **89**, 270404 (2002).

[20] S. Jochim, M. Bartenstein, A. Altmeyer, G. Hendl, S. Riedl, C. Chin, J. H. Denschlag, and R. Grimm, Science (to be published).

[21] This work inferred the presence of a condensate from the number of particles in a shallow trap and the magnetic field dependence of the loss rate consistent with mean-field effects. No observation of a phase transition or measurements of equilibration, temperature, or condensate fraction were reported.

[22] K. Dieckmann, C. A. Stan, S. Gupta, Z. Hadzibabic, C. H. Schunck, and W. Ketterle, Phys. Rev. Lett. **89**, 203201 (2002).

[23] Z. Hadzibabic, S. Gupta, C. A. Stan, C. H. Schunck, M. W. Zwierlein, K. Dieckmann, and W. Ketterle, Phys. Rev. Lett. **91**, 160401 (2003).

[24] T. Bourdel, J. Cubizolles, L. Khaykovich, K. M. F. Magalhães, S. J. J. M. F. Kokkelmans, G. V. Shlyapnikov, and C. Salomon, Phys. Rev. Lett. **91**, 020402 (2003).

[25] S. Gupta, Z. Hadzibabic, M. W. Zwierlein, C. A. Stan, K. Dieckmann, C. H. Schunck, E. G. M. v. Kempen, B. J. Verhaar, and W. Ketterle, Science **300**, 1723 (2003).

[26] M. H. Anderson, J. R. Ensher, M. R. Matthews, C. E. Wieman, and E. A. Cornell, Science **269**, 198 (1995).

[27] K. B. Davis, M.-O. Mewes, M. R. Andrews, N. J. van Druten, D. S. Durfee, D. M. Kurn, and W. Ketterle, Phys. Rev. Lett. **75**, 3969 (1995).

[28] The trap frequencies were scaled from measurements done at full power. The axial frequency was affected by small magnetic field curvatures which were negligible at high laser power.

[29] T. Köhler, T. Gasenzer, P. S. Julienne, and K. Burnett, Phys. Rev. Lett. **91**, 230401 (2003).

[30] L. D. Carr, G. V. Shlyapnikov, and Y. Castin, e-print cond-mat/0308306.

[31] J. N. Milstein, S. J. J. M. F. Kokkelmans, and M. J. Holland, Phys. Rev. A **66**, 043604 (2002).

Appendix C

Condensation of Pairs of Fermionic Atoms near a Feshbach Resonance

This appendix contains a reprint of Ref. [272]: M.W. Zwierlein, C. A. Stan, C. H. Schunck, S.M. F. Raupach, A. J. Kerman, and W. Ketterle, *Condensation of Pairs of Fermionic Atoms near a Feshbach Resonance*, Phys. Rev. Lett. **92**, 120403 (2004).

Condensation of Pairs of Fermionic Atoms near a Feshbach Resonance

M.W. Zwierlein, C. A. Stan, C. H. Schunck, S. M. F. Raupach, A. J. Kerman, and W. Ketterle
Department of Physics, MIT-Harvard Center for Ultracold Atoms, and Research Laboratory of Electronics, MIT, Cambridge, Massachusetts 02139, USA
(Received 1 March 2004; published 25 March 2004)

We have observed Bose-Einstein condensation of pairs of fermionic atoms in an ultracold ^{6}Li gas at magnetic fields above a Feshbach resonance, where no stable $^6Li_2$ molecules would exist in vacuum. We accurately determined the position of the resonance to be 822 ± 3 G. Molecular Bose-Einstein condensates were detected after a fast magnetic field ramp, which transferred pairs of atoms at close distances into bound molecules. Condensate fractions as high as 80% were obtained. The large condensate fractions are interpreted in terms of preexisting molecules which are quasistable even above the two-body Feshbach resonance due to the presence of the degenerate Fermi gas.

DOI: 10.1103/PhysRevLett.92.120403 PACS numbers: 03.75.Ss, 05.30.Fk

Ultracold atomic gases have become a medium to realize novel phenomena in condensed matter physics and test many-body theories in new regimes. The particle densities are 10^8 times lower than in solids, but at temperatures in the nanokelvin range, which are now routinely achieved, interactions and correlations become important. Of particular interest are pairing phenomena in fermionic gases, which have direct analogies to superconductivity [1].

The interactions which drive the pairing in these gases can be controlled using a Feshbach resonance [2], in which a molecular level is Zeeman tuned through zero binding energy using an external magnetic field. This provides an opportunity to experimentally probe what is known as the BCS-BEC crossover; as the strength of the effective attractive interaction between particles is increased a continuous transition from condensation of delocalized Cooper pairs to condensation of tightly bound bosonic molecules is predicted [3–6]. Whereas in the BCS limit the pairing is a strictly many-body effect [7], in the BEC limit a pair of fermions is bound even as an isolated molecule. A novel form of high-temperature superfluidity has been predicted to emerge in the crossover region [3–6]. Until recently, the observation of condensation phenomena in fermionic atomic gases was restricted to the extreme BEC limit, where several groups have observed Bose-Einstein condensation of diatomic molecules [8–11].

An important step was recently reported, in which condensation of atomic ^{40}K fermion pairs was observed on the BCS side of a Feshbach resonance [12]. It was argued that those pairs were not bound into molecules, but merely moved together in a correlated fashion, similar to Cooper pairs of electrons in a superconductor [13]. However, the exact nature of these pairs remained unclear. In this Letter, we apply similar techniques to ^{6}Li atoms, which have very different collisional properties [14], and observe the pair condensation phenomenon above a Feshbach resonance. In contrast to the previous work, where at most 15% of the atom pairs were condensed [12], condensate fractions of up to 80% were observed. We argue that such a high condensate fraction is unlikely for pairs which are long range, but rather it indicates a condensate of short-range atom pairs which are essentially molecular in character even on the BCS side of the resonance.

A simple argument supports this possibility. In the basic picture of a Feshbach resonance, a molecular state above the dissociation threshold has a finite lifetime, which becomes shorter as the energy of the state increases, as recently observed [15]. In the presence of the Fermi sea, its lifetime will be increased due to Pauli blocking. The molecular level will be populated until its energy becomes larger than twice the Fermi energy corresponding to the total number of atoms. The BCS-BEC crossover is expected to occur at this point, and not at the location of the two-body Feshbach resonance [5,6].

The basic setup of our experiment was described in [10]. By sympathetic cooling of ^{6}Li atoms with ^{23}Na in a magnetic trap, a degenerate gas of about 3×10^7 ^{6}Li fermions at $\sim 0.3 T/T_F$ was created. After transfer into an optical dipole trap (maximum power 9 W focused to an e^{-2} radius of 25 μm), an equal mixture of atoms in the lowest two hyperfine states $|1\rangle$ and $|2\rangle$ was prepared. The sample was evaporatively cooled at a magnetic field of 770 G using an exponential ramp-down (time scale $\sim$ 400 ms) of the optical trap to a final laser power of 15 mW. This created essentially pure Bose-Einstein condensates of up to 3×10^6 $^6Li_2$ molecules. The observed trap vibrational frequencies could be described by the following expression: $\nu_{\mathrm{rad}} \approx 115\ \mathrm{Hz}\ \sqrt{P}$, $\nu_{\mathrm{ax}} \approx 1.1\ \mathrm{Hz}\ \sqrt{P + 120B}$, where P is the optical power in mW, and B is the magnetic field in kG. The latter dependence arises from the residual axial curvature of the magnetic field. Considerable improvements over our previous setup [10] led to an improved e^{-1} condensate lifetime of 10 s at 770 G. Moreover, within the experimental uncertainty in the total number of molecules ($\sim$50%), mean-field

 © 2004 The American Physical Society

measurements were consistent with a molecule-molecule scattering length of $0.6a$, where a is the atomic scattering length [16,17].

Previously, the location of the ^{6}Li Feshbach resonance was determined either by observing a peak in the inelastic loss [18] or the interaction energy of a $|1\rangle - |2\rangle$ mixture [19]. A more accurate determination can be made by mapping out the onset of dissociation of the molecular state [12,15]. After releasing an almost pure molecular sample from the trap at 770 G, the magnetic field was linearly ramped up in 10 ms to a variable value. During that time, the particle density dropped by a factor of 1000. If the field crossed the resonance, molecules dissociated into atoms. These atoms were then imaged at zero field, where the remaining molecules were not detected [10]. The Feshbach resonance appeared as a sharp onset in the number of detected atoms (Fig. 1). The speed of the downward ramp to zero field had to be chosen carefully. Fast ramps could dissociate very weakly bound molecules [20], such that the Feshbach resonance appeared systematically shifted to lower fields. For too slow a ramp-down, on the other hand, we found that even for clouds as dilute as $\sim 3 \times 10^{10}$ cm^{-3} molecules were recreated, lowering the measured atomic fraction. However, when we varied the ramp rate over more than 3 orders of magnitude, we found a range of rates which gave identical thresholds at 822 ± 3 G (Fig. 1).

To produce samples in the crossover region, we started with an essentially pure Bose-Einstein condensate of molecules formed at 770 G. The laser power of the optical trap was increased in 500 ms from 15 to 25 mW in order to accommodate larger Fermi clouds above the resonance. In some experiments, we used a deeper trap with up to 150 mW of power; the additional compression was carried out after ramping in 500 ms to 900 G to avoid enhanced losses on the BEC side of the resonance. Once the final trap depth was reached, the magnetic field was ramped in 500 ms to values between 650 and 1025 G. The adiabaticity of this ramp was checked by ramping back to 770 G and observing an identical density profile and condensate fraction, similar to studies in Ref. [8]. At 1025 G, the total peak density of the spin mixture in the deepest trap was 3×10^{13} cm^{-3}, corresponding to a Fermi energy of 3.6 μK and inverse Fermi wave vector $k_F^{-1} \simeq 2000 a_0$, where a_0 denotes the Bohr radius.

To probe the gas, we released it from the trap, and after a variable delay τ_d of usually 40 μs, applied a rapid transfer technique [12]: the magnetic field was switched off exponentially to zero with an initial slew rate of 30 G/μs, which adiabatically converted pairs of atoms into deeply bound molecules at zero field [21]. As long as no collisions or other dynamics occur during this ramp, the velocity distribution of the resulting molecules then constitutes a probe of the atom pairs' center-of-mass motion before the measurement. After 3–6 ms time of flight at zero field, we dissociated the molecules with a 3 ms field pulse to 900 G and imaged the resulting atoms after 2 ms at zero field [10,22]. We could also selectively detect any remaining atoms by omitting the dissociation pulse, and we observed that for $\tau_d \leq 500$ μs, less than 10% of the sample consisted of atoms, independent of the initial magnetic field. At longer delay times, the atom-molecule conversion became less efficient due to the decreased density.

Typical absorption pictures of molecular clouds after the rapid transfer ramp are shown in Fig. 2 for different temperatures, clearly exhibiting a bimodal distribution. This is evidence for condensation of pairs of ^{6}Li atoms on the BCS side of the Feshbach resonance. The condensate fractions were extracted from images like these, using a Gaussian fit function for the "thermal" part and a

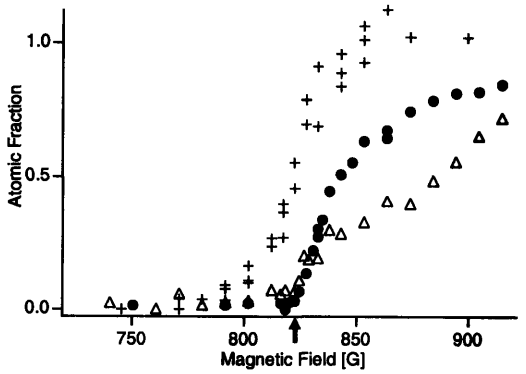

FIG. 1. Determination of the Feshbach resonance position. Shown is the onset of molecule dissociation when the magnetic field was slowly raised and then ramped down to zero field with a variable rate: Using a switch-off of the power supply at an initial rate of 30 G/μs (crosses), a linear ramp to zero field of 100 G/ms (circles), a linear ramp for 16 ms at 12.5 G/ms, followed by switch off (triangles). The identical threshold for the two lowest ramp rates determines the resonance position to be 822 ± 3 G, marked by an arrow.

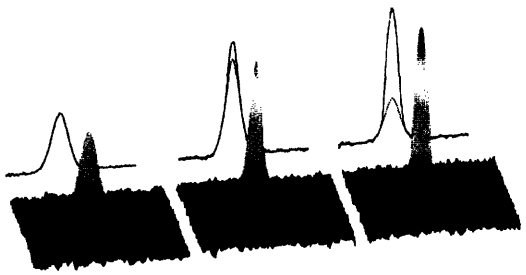

FIG. 2 (color online). Emergence of a Bose-Einstein condensate of atom pairs as the temperature was lowered. Shown are column densities (after 6 ms of time of flight) of the fermion mixture after a rapid transfer ramp from 900 G for three different initial temperatures $T/T_F \approx 0.2$, 0.1 and 0.05, together with their axially integrated radial density profiles. The dashed line is a Gaussian fit to the thermal component. Condensate fractions are 0.0, 0.1, and 0.6. Each cloud consists of about 2×10^6 molecules. The field of view is 3×3 mm.

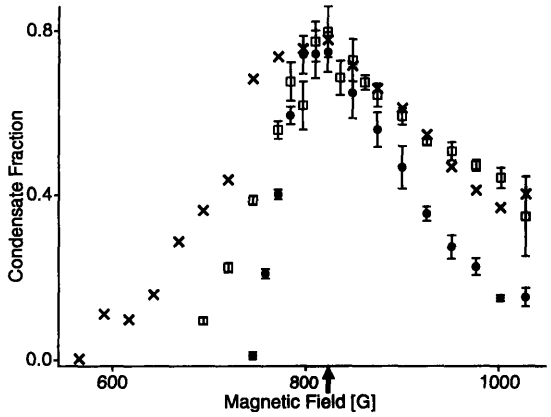

FIG. 3. Condensate fraction after the rapid transfer vs initial magnetic field, for different hold times at that field in the shallow trap ($P = 25$ mW). Crosses: 2 ms hold time, after 500 ms ramp to 1000 G and 4 ms ramp to the desired field; squares and circles: 100 ms and 10 s hold time, after 500 ms ramp from 770 G. The reduction of the condensate fraction for long hold times far on the left side of the resonance is probably due to the rapidly increasing inelastic losses for the more tightly bound molecules [20,23]. The lower condensate fraction at high field for long hold times is probably an effect of lower density since the number of atoms had decayed by a factor of 4 without change in temperature.

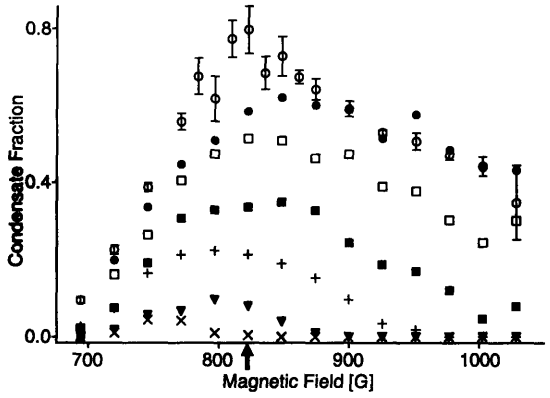

FIG. 4. Condensate fraction for different temperatures as a function of magnetic field. The temperature of the molecular cloud was varied by stopping the evaporative cooling earlier and applying parametric heating before ramping to the final magnetic field. Temperatures are parametrized by the molecular condensate fraction N_0/N at 820 G (open circles: 0.8; filled circles: 0.58; open squares: 0.51; filled squares: 0.34; "+": 0.21; triangles: 0.08; "×": <0.01). The lowest temperature was realized in the shallow trap ($P = 25$ mW); the higher temperatures required a deeper trap ($P = 150$ mW).

Thomas-Fermi profile for the "condensate." Figures 3–5 show the observed condensate fraction as a function of both magnetic field and temperature. The striking features of these data are the high condensate fraction of 80% near resonance, and the persistence of large condensate fractions on the BCS side of the resonance all the way to our maximum field of 1025 G. After 10 s hold time, this value was still as high as 20%. These observations were independent of whether the final magnetic field was approached starting with a Fermi sea or a molecular condensate. Note that for our peak densities, the strongly interacting region of $k_F|a| > 1$ extends from 710 G onward.

There is experimental evidence that the observed pair condensates existed before the sweep and were not produced during the sweep by collisions. First, the observed condensate fraction depended on the initial magnetic field. Second, the condensate fraction did not change when we varied the delay time τ_d (between release of the atoms from the trap and the magnetic field ramp) from 0 to 200 μs, although the density of the cloud changed by a factor of ~4 [25]. However, we cannot rule out with certainty that the momentum distribution of the pairs is modified by collisions during the ramp [26]. At our highest densities, it takes about 4 μs to take the molecules created during the ramp out of the strongly interacting region ($k_F|a| \geq 1$). A classical gas at the Fermi temperature would have a unitarity limited collision time comparable to the inverse of the Fermi energy divided by $\hbar$, which is about 2 μs. However, this may be affected by Pauli blocking for the atoms and bosonic stimulation for the molecules.

Assuming that collisions during the ramp can be neglected, it is still crucial to ask what exactly happens during the rapid transfer ramp, and what kind of pairs would likely be detected. A reasonable assumption is that atoms form molecules preferentially with their nearest neighbor, independent of the center-of-mass velocity of the pair. If, as our data show, a large fraction of the

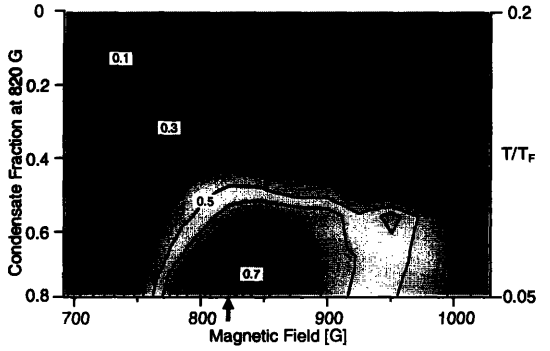

FIG. 5 (color online). Temperature and magnetic field ranges over which pair condensation was observed (using the same data as in Fig. 4). The right axis shows the range in T/T_F (measured at 1025 G) which was covered. For high degeneracies, fitting T/T_F was less reliable and we regard the condensate fraction as a superior "thermometer." Note that for an isentropic crossover from a BEC to a Fermi sea, T/T_F is approximately linearly related to the condensate fraction on the BEC side [24]. For our maximum densities the region where $k_F|a| \geq 1$ extends from about 710 G onward.

detected molecules are in a zero-momentum state after the fast transfer, this means that nearest neighbors had opposite momenta. If the distance between the fermions with opposite momenta making up each pair were comparable to or larger than the interatomic distance (as in long-range Cooper pairs) one would not expect to find high condensate fractions; on the contrary, the transfer into a tightly bound molecular state would randomly pick one of the nearest neighbors, resulting in a thermal molecule. We regard our observed high condensate fractions as evidence for the existence of condensed atomic pairs above the Feshbach resonance, which are smaller in size than the interatomic distance and, therefore, molecular in character. Their stability may be affected by Pauli blocking and mean-field effects, but their binding should be a two-body effect and not a many-body effect as in the case of Cooper pairs.

In conclusion, we have observed $^6Li_2$ molecular Bose-Einstein condensates after a fast downward magnetic field ramp starting with equilibrium samples at fields on either side of the broad ^{6}Li Feshbach resonance. Since there are no truly bound molecular states above the resonance, we tentatively interpret our results as a Bose-Einstein condensate of pairs of atoms which are molecular in character and stabilized by the existence of the Fermi sea. This condensate would drain particles from the Fermi sea and lead to a reduced atomic Fermi energy roughly equal to half the energy of the molecular level [5,6]. Indeed, both in Ref. [8] and in the present work, a reduction in the size of the cloud was observed as the Feshbach resonance was approached from above, which may be due to this effect. In agreement with theoretical predictions [6] we have observed pair condensation in the regime where $T/T_F < 0.2$ and $k_F|a| > 1$ (Fig. 5). The exact nature of the atom pairs remains to be elucidated; they could be related to virtual states or scattering resonances in the continuum; they may turn out to be the tight-binding limit of Cooper pairs. It is also possible that the pair condensate is a superposition state of molecules and Cooper pairs [4–6]. We regard the characterizing feature of the BCS-BEC crossover a qualitative change of the pairing phenomenon which has not yet been observed.

This work was supported by NSF, ONR, ARO, and NASA. We thank Walter Hofstetter, Michele Saba, and Zoran Hadzibabic for stimulating discussions. S. R. is grateful to the Dr. Jürgen Ulderup foundation for financial support.

[1] H. T. C. Stoof and M. Houbiers, in *Bose-Einstein Condensation in Atomic Gases, Proceedings of the International School of Physics Enrico Fermi, Course CXL*, edited by M. Inguscio, S. Stringari, and C. Wieman (IOS Press, Amsterdam, 1999), pp. 537–553.

[2] E. Tiesinga, B. J. Verhaar, and H. T. C. Stoof, Phys. Rev. A **47**, 4114 (1993); W. C. Stwalley, Phys. Rev. Lett. **37**, 1628 (1976); S. Inouye *et al.*, Nature (London) **392**, 151 (1998); P. Courteille *et al.*, Phys. Rev. Lett. **81**, 69 (1998).

[3] D. M. Eagles, Phys. Rev. **186**, 456 (1969); A. J. Leggett, in *Modern Trends in the Theory of Condensed Matter. Proceedings of the XVIth Karpacz Winter School of Theoretical Physics, Karpacz, Poland, 1980* (Springer-Verlag, Berlin, Karpacz, Poland, 1980), pp. 13–27; P. Nozières and S. Schmitt-Rink, J. Low Temp. Phys. **59**, 195 (1985).

[4] E. Timmermans *et al.*, Phys. Lett. A **285**, 228 (2001); M. Holland *et al.*, Phys. Rev. Lett. **87**, 120406 (2001); J. Stajic *et al.*, e-print cond-mat/0309329; A. Perali *et al.*, e-print cond-mat/0311309; R. Combescot, e-print cond-mat/0310583; J. Kinnunen, M. Rodriguez, and P. Törmä, e-print cond-mat/0401543.

[5] Y. Ohashi and A. Griffin, Phys. Rev. Lett. **89**, 130402 (2002).

[6] G. M. Falco and H. T. C. Stoof, e-print cond-mat/0402579.

[7] M. Houbiers *et al.*, Phys. Rev. A **56**, 4864 (1997).

[8] S. Jochim *et al.*, Science **302**, 2101 (2003); M. Bartenstein *et al.*, Phys. Rev. Lett. **92**, 120401 (2004).

[9] M. Greiner, C. A. Regal, and D. S. Jin, Nature (London) **426**, 537 (2003).

[10] M. W. Zwierlein *et al.*, Phys. Rev. Lett. **91**, 250401 (2003).

[11] T. Bourdel *et al.*, e-print cond-mat/0403091.

[12] C. A. Regal, M. Greiner, and D. S. Jin, Phys. Rev. Lett. **92**, 040403 (2004).

[13] NIST and University of Colorado at Boulder press release, January 28, 2004; http://www.nist.gov/public_affairs/releases/fermi_condensate.htm.

[14] M. Houbiers *et al.*, Phys. Rev. A **57**, R1497 (1998).

[15] T. Mukaiyama *et al.*, e-print cond-mat/0311558 [Phys. Rev. Lett.(to be published)].

[16] D. S. Petrov, C. Salomon, and G. V. Shlyapnikov, e-print cond-mat/0309010.

[17] The smaller value reported in our previous work [10] was based on an incorrect extrapolation of trap frequencies to 100 times lower power. The radial trap frequency was strongly influenced by multiple intensity maxima in the optical focus.

[18] K. Dieckmann *et al.*, Phys. Rev. Lett. **89**, 203201 (2002).

[19] T. Bourdel *et al.*, Phys. Rev. Lett. **91**, 020402 (2003).

[20] J. Cubizolles *et al.*, Phys. Rev. Lett. **91**, 240401 (2003).

[21] According to Fig. 1, this fast ramp can dissociate weakly bound molecules at low density, but at high density we observed an atom-molecule conversion $\geq 90\%$.

[22] At this point the cloud was sufficiently dilute that the final switch off of the field did not reconvert atoms into molecules.

[23] S. Jochim *et al.*, Phys. Rev. Lett. **91**, 240402 (2003).

[24] L. D. Carr, G. V. Shlyapnikov, and Y. Castin, e-print cond-mat/0308306 [Phys. Rev. Lett. (to be published)].

[25] The condensate peak broadened for longer τ_d and could not be reliably discerned after 200 μs.

[26] In the ^{40}K experiment, the ratio of the effective sweep rate through resonance and Fermi energy was similar [12].

Appendix D

Feshbach Resonances in Fermionic ^{6}Li

This appendix contains a reprint of Ref. [217]: C. H. Schunck, M. W. Zwierlein, C. A. Stan, S. M. F. Raupach, and W. Ketterle, A. Simoni, E. Tiesinga, C. J. Williams, and P. S. Julienne, *Feshbach resonances in fermionic ^6Li*, Phys. Rev. A **71**, 045601 (2004).

Feshbach resonances in fermionic ^{6}Li

C. H. Schunck, M. W. Zwierlein, C. A. Stan, S. M. F. Raupach, and W. Ketterle
Department of Physics, MIT-Harvard Center for Ultracold Atoms, and Research Laboratory of Electronics, MIT, Cambridge, Massachusetts 02139, USA

A. Simoni, E. Tiesinga, C. J. Williams, and P. S. Julienne
National Institute of Standards and Technology, 100 Bureau Drive stop 8423, Gaithersburg, Maryland 20899-8423, USA
(Received 14 July 2004; published 5 April 2005)

Feshbach resonances in ^{6}Li were experimentally studied and theoretically analyzed. In addition to two previously known s-wave resonances, three p-wave resonances were found. Four of these resonances are narrow and yield a precise value of the singlet scattering length. The position of the broad s-wave resonance near 83 mT is mostly sensitive to the triplet potential. It was previously determined in a molecule-dissociation experiment for which we, here, discuss systematic shifts.

DOI: 10.1103/PhysRevA.71.045601 PACS number(s): 03.75.Ss, 32.80.Pj, 34.50.Pi

Interactions in ultracold atomic gases can be magnetically tuned using Feshbach resonances [1]. A Feshbach resonance occurs when the energy of two colliding atoms is nearly degenerate to the energy of a bound molecular state. Tunable interactions have been used to explore novel phenomena in collisional and many-body physics. Recently, Feshbach resonances have been used to control pairing processes in ultracold fermionic gases. This led to the achievement of Bose-Einstein condensation (BEC) of molecules in ^{40}K [2] and ^{6}Li [3–5] and to the first studies of the BEC-BCS crossover, the continuous transition of fermion pairs from weakly bound molecules to long-range Cooper pairs [5–11].

Most experiments in ^{6}Li have been carried out in the vicinity of the s-wave Feshbach resonance near 830 G [5,7–11] (1 G=10^{-4} T). The quantitative interpretation of these experiments and the characterization of the BEC-BCS crossover require a precise knowledge of the resonance location. However, its determination is not trivial since the resonance width is extremely large and the line shape is strongly affected by many-body effects. In our previous work we determined the position of this resonance by the onset of molecule dissociation to be 822±3 G [8].

In this paper we report on a detailed study of Feshbach resonances in the two lowest hyperfine states of ^{6}Li with the goal of accurately characterizing the interaction potential of two ^{6}Li atoms. In addition to two previously known s-wave resonances, we find three p-wave resonances [12]. The positions of the p-wave resonances together with the location of the narrow s-wave resonance near 543 G are used for a precise determination of the singlet s-wave scattering length. These results, however, do not constrain the position of the broad resonance, which also depends on the triplet scattering length. An improved measurement of its location is presented and the magnitude and the origin of possible systematic errors are discussed.

The experimental setup has been described in Ref. [13]. Up to 4×10^7 quantum degenerate ^{6}Li atoms in the $|F,m_F\rangle = |3/2,3/2\rangle$ state were obtained in a magnetic trap by sympathetic cooling with ^{23}Na. The ^{6}Li atoms were then transferred into an optical dipole trap (ODT) formed by a focused 1064-nm laser beam with a maximum power of 9 W. In the optical trap a single radio-frequency sweep transferred the atoms to state $|1\rangle$ ($|F,m_F\rangle = |1/2,1/2\rangle$ at low field). A subsequent Landau-Zener sweep at an externally applied magnetic field of 565 G could then be used to either prepare the entire sample in state $|2\rangle$ ($|1/2,-1/2\rangle$ at low field) or create an equal mixture of atoms in states $|1\rangle$ and $|2\rangle$. Except for the measurement of the broad s-wave Feshbach resonance, all resonances were observed by monitoring magnetic-field-dependent atom losses. Atom numbers were obtained from absorption images taken at zero field. The externally applied field was calibrated by driving microwave transitions from state $|2\rangle$ to state $|5\rangle$ ($|3/2,1/2\rangle$ at low field) at several magnetic fields close to resonance positions and from state $|2\rangle$ to state $|3\rangle$ ($|3/2,-3/2\rangle$ at low field) at high magnetic fields around 800 G.

For spin-polarized samples either in state $|1\rangle$ or $|2\rangle$ s-wave scattering is forbidden by symmetry; therefore, the observed resonances occur in the p-wave channel. The same molecular state that is responsible for these two resonances also causes a p-wave resonance in the $|1\rangle+|2\rangle$ mixture. The three p-wave resonances were observed in clouds with typical temperatures $T\sim6$ μK and $T/T_F\simeq0.5-1.5$, where T_F is the Fermi temperature. Radial and axial trap frequencies were typically $\omega_r=2\pi\times1.0$ kHz and $\omega_a=2\pi\times6.9$ Hz.

The position of the p-wave resonance in the collision of a pair of state $|1\rangle$ atoms was determined by first ramping the magnetic field to approximately 5 G below the resonance. Using an additional power supply to precisely change the magnetic field within a 10 G range, the field was then switched in 1 ms to a test value $B_{\rm test}$. Here the atoms were kept for 200 ms before the field and the optical trap were switched off. Finally, atom number versus $B_{\rm test}$ was recorded. Resonantly enhanced losses due to inelastic three-body decay led to a Lorentzian shaped feature as shown in Fig. 1(a). Resonance positions and widths are summarized in Table I.

The same technique was used to determine the $|1\rangle+|2\rangle$ and $|2\rangle+|2\rangle$ p-wave resonances. The resonance line shapes are asymmetric (see Fig. 1), possibly due to threshold effects [14,15]. The splitting of a p-wave resonance due to spin-spin interactions [16] is for these resonances more than one order

 ©2005 The American Physical Society

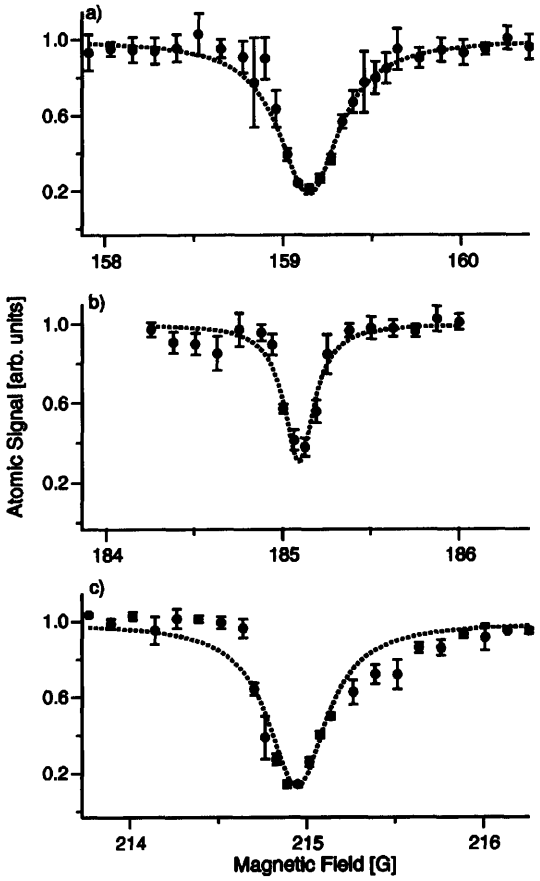

FIG. 1. p-wave resonances for $|1\rangle+|1\rangle$ (a), $|1\rangle+|2\rangle$ (b), and $|2\rangle+|2\rangle$ (c) collisions. Dashed lines are Lorentzian fits to the data. The results are summarized in Table I.

TABLE I. Position of the Feshbach resonances. Given are the experimentally and theoretically determined resonance locations B_{expt} and B_{theory}, respectively, and the measured resonance width. The uncertainties for the experimental data in the first four rows are dominated by magnetic field drifts between the measurement of the resonance and the field calibration for which we find an upper bound of 80 mG. For the $|1\rangle+|1\rangle$ resonance an additional drift was monitored. The statistical error of determining the line center and the estimated uncertainty due to asymmetric line shapes are negligible. The quoted linewidths are not corrected for source depletion due to atom loss. We estimate that this effect reduces the linewidths by 25%–40%. For the broad s-wave resonance (fifth row) only a range is given. See the text for a discussion.

States	Wave	B_{expt} [G]	B_{theory} [G]	Width [G]
$\|1\rangle+\|1\rangle$	p	159.14±0.14	159.15(4)	0.4
$\|1\rangle+\|2\rangle$	p	185.09±0.08	185.15(4)	0.2
$\|2\rangle+\|2\rangle$	p	214.94±0.08	214.90(4)	0.4
$\|1\rangle+\|2\rangle$	s	543.28±0.08	543.27(5)	0.4
$\|1\rangle+\|2\rangle$	s	822...834		

of magnitude smaller than the width and could not be discerned with our sensitivity.

The position of the s-wave resonance near 543 G in the $|1\rangle+|2\rangle$ mixture was determined as presented above in clouds with typical temperatures of 6 μK, but in a slightly deeper optical trap and with an extended holdtime of 2900 ms at B_{test}. The result of a fit to the Lorentzian lineshape is given in Table I. This s-wave resonance was first reported in [17] and calculated in [18].

To determine the position of the broad s-wave Feshbach resonance near 830 G a different method was required. The resonance was identified as the onset of molecular dissociation [6,8,19]. Molecules were first created on the repulsive (BEC) side of the Feshbach resonance and then dissociated into atoms when the magnetic field crossed the resonance. However, this method is subject to systematic shifts in the resonance position that depend on the molecular density and the speed of magnetic field ramps. To control the density-dependent shift, the molecular density was varied by using different parameters for the optical dipole trap and by performing the dissociation at different times of flight.

The starting point of the experiment was an almost pure $^6Li_2$ molecular BEC that was prepared at a magnetic field of about 780 G in the optical trap as described in Ref. [8]. The data shown in Fig. 2 were obtained by releasing the molecules from the optical trap at 780 G [20]. After 2 ms the field was ramped to a test value B_{test} in 14 ms. In these first 16 ms time of flight the peak molecular density dropped by three orders of magnitude to $n_{mol}=5\times10^9$ cm^{-3}. The magnetic field was held at B_{test} for another 5 ms before it was ramped down. The critical field ramp, which can alter the resonance position, is the initial phase of the magnetic field ramp down in which the molecules are still in the resonance region. Here, fast ramps can dissociate weakly bound molecules. However, we could only use a limited time of flight while maintaining a good signal-to-noise ratio. Therefore the field was ramped down in two steps: at an initial rate of 100 G/ms for 2 ms to leave the resonance region, followed by an exponential decay with time constant 30 G/μs which brought the field to zero in 3 ms. To better control the effects of the field ramp, the experiment was repeated for different initial switch off speeds. Finally, the sample was imaged with light which was resonant only with unbound atoms; the possible molecular transitions are far detuned from the atomic transition at zero field. By monitoring the atom number as a function of B_{test} the onset of molecule dissociation was observed. The data in Fig. 2 show the onset at 821±1 G. The slow approach of the atomic signal to unity reflects the time constant of dissociation and the possible reconversion of atoms into molecules during the magnetic field switch off. In our analysis only the onset of the atomic signal was evaluated.

We now consider the two sources of systematic errors mentioned above in more detail. Few-body collisions might dissociate molecules when their size, which near resonance is on the order of the scattering length between the constituent atoms [21], becomes comparable to the mean distance between the molecules, $a\sim n_{mol}^{-1/3}$. The scattering length near resonance is parametrized by $a=a_{bg}[1+\Delta B/(B-B_0)] \approx a_{bg}\Delta B/(B-B_0)$, where a_{bg} is the negative background scat-

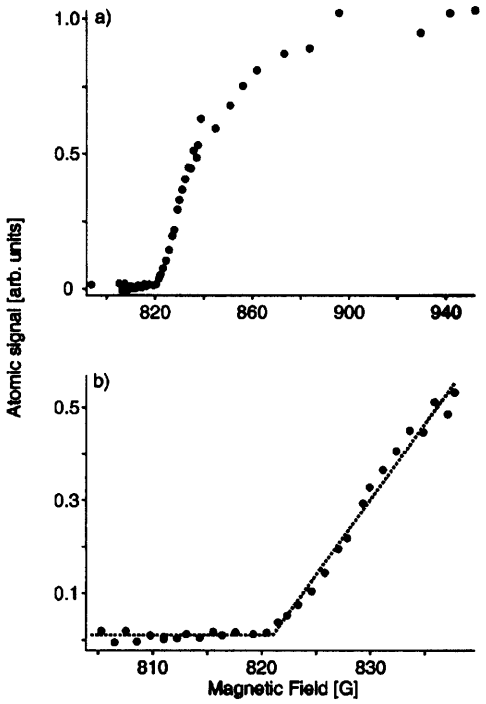

FIG. 2. Determination of the position of the broad s-wave Feshbach resonance. (a) Onset of dissociation of molecules into atoms at 821 ± 1 G. (b) The resonance position was obtained by fitting two lines to the data points near the threshold, one horizontal through the points showing no atomic signal and a second line following the initial rise in atom number. The intersection of the two lines gives the resonance position; the estimated uncertainty of this point is ±1 G.

tering length, B_0 is the resonance position, and ΔB is the resonance width. So molecule dissociation will become important at a magnetic field B for which $a_{bg}\Delta B/(B-B_0) \sim n_{mol}^{-1/3}$. For the broad resonance, this density-dependent, few-body effect is expected to shift the observed resonance position to lower magnetic fields.

The second systematic error is a density-independent, single-molecule effect. Switching off the magnetic field becomes nonadiabatic close to resonance and destroys very weakly bound molecules [22]. If a molecule with binding energy $\hbar\omega=\hbar^2/(ma^2)$ is forced to change its size faster than its oscillation frequency (i.e., if $\dot{a}/a \gg \omega$), the molecule may dissociate. With the magnetic field dependence of a given above, the rate $\dot{a}/a \sim \dot{B}/(B-B_0)$ becomes comparable to $\omega \sim (B-B_0)^2$ at a magnetic field that is shifted from the resonance location B_0 by $\Delta B=B-B_0 \sim \dot{B}^{1/3}$. This expression gives the scaling of the ramp-induced systematic error with the ramp speed $\dot{B}$.

To find the order of magnitude of these shifts we have determined the resonance locations for three different ramp rates at constant density and for three different densities at constant ramp rate.

At a molecular density of $n_{mol}=1.5\times10^{10}$ the resonance positions were measured at initial ramp speeds of 30 G/μs (fastest possible switch off), 100 G/ms (fastest externally controlled ramp), and 12.5 G/ms (controlled ramp). For the fastest switch off the onset of dissociation occurs at 793 ± 7 G, for the other two controlled ramps at 822 ± 3 G. Assuming that no density shifts affect these data, one can extrapolate to zero ramp speed based on the $(B-B_0)\propto\dot{B}^{1/3}$ dependence. In this way we find a resonance position of 825 ± 3 G.

For a fixed initial ramp speed of 100 G/ms the resonance locations were determined at densities of 5×10^9 cm^{-3}, 1.5×10^{10} cm^{-3}, and 1.2×10^{12} cm^{-3} to be 821 ± 1 G, 822 ± 3 G, and 800 ± 8 G, respectively. Here one can use the $(B-B_0)\propto n^{1/3}$ dependence to extrapolate to a resonance position of 825 ± 3 G, neglecting effects due to nonadiabatic magnetic field ramps.

Both systematic effects shift the maximum magnetic field value at which the molecules are stable to lower magnetic fields. In a simple picture, one would expect the total shift to be the larger of the two. However, if they are similar, as in our case, they may add or combine in a more complicated way. We have measured the threshold position at low density and slow ramp rates to be 822 ± 3 G and determined two shifts of 3 ± 3 G. Therefore, we expect the position of the Feshbach resonance to be between 822 and 834 G. A more accurate extrapolation requires measuring the dissociation threshold for more ramp speeds and densities. However, technical limitations in varying magnetic field ramp speeds and an unfavorable signal-to-noise ratio at lower densities precluded this.

All Feshbach resonances discussed in this paper are due to the $v=38$ vibrational state of the singlet potential with total electronic spin S equal to zero. The p-wave resonances have a total nuclear spin $I=1$, while the 543 G and broad s-wave resonances have $I=2$ and $I=0$, respectively.

The resonance locations are compared with results of scattering coupled-channel calculations. We locate the resonance from the maximum of the elastic cross section as a function of magnetic field. The collision energy is fixed at $E=k_BT$, where k_B is the Boltzmann constant and T is the experimental temperature. Our collision model, described in detail in Ref. [18], treats the singlet and triplet scattering lengths as adjustable parameters. The triplet state has a total electron spin equal to one. It turns out that all narrow resonances, which could be accurately located, are insensitive to the triplet scattering length. Only s- and p-waves are included in the calculation. Fitting the singlet scattering length a_S to the field locations given in the first four rows of Table I yields a very accurate value of $a_S=45.1591(16)a_0$, where $a_0=0.052\,917\,7$ nm. With this value, the resonance positions given in the third column of Table I were calculated at a collision energy equal to k_BT. The agreement with the experimental values is excellent. The location of the s-wave resonance is also in very good agreement with the determination of Ref. [23], 543.26(10) G.

Our theoretical uncertainties do not include contributions due to a thermal average. Moreover, there can be a discrepancy between the field values at which the observed three-body loss rate and the theoretical two-body elastic cross section are maximal. Experimental observations on ^{40}K [14] are

not conclusive about the magnitude of this shift, although they suggest it is well within the linewidth of the observed loss features. As an estimate of our possible systematic error, a shift in the resonance position δ(G) will give rise to a shift from our best a_S of $(-0.0365\delta)a_0$.

The broad resonance is caused by a hyperfine-induced mixing between a singlet vibrational level and an almost-bound virtual state of the triplet potential, a situation analyzed in [24,25]. It is the virtual state that gives rise to the large and negative triplet scattering length a_T of ^{6}Li. Mixing occurs for magnetic field values above 500 G. In fact, in absence of the hyperfine mixing, the resonance would occur around 550 G. The coupling shifts the resonance by a few hundred gauss. For typical Feshbach resonances, these shifts are no more than a few gauss. A consequence of the large shift is that the resonance location depends critically on the less well known triplet potential.

In conclusion, we have found three p-wave Feshbach resonances in ^{6}Li. Together with the narrow s-wave resonance they give a precise value of the singlet scattering length. The position of the broad resonance could not be constrained using the refined singlet potential. The determination of the position of the broad resonance via molecule dissociation is subject to systematic errors, which shift the onset of dissociation to lower magnetic fields.

The MIT research is supported by NSF, ONR, ARO, and NASA. S.R. acknowledges financial support from the Dr. Jürgen Ulderup Foundation.

[1] E. Tiesinga, B. J. Verhaar, and H. T. C. Stoof, Phys. Rev. A **47**, 4114 (1993); W. C. Stwalley, Phys. Rev. Lett. **37**, 1628 (1976); S. Inouye *et al.*, Nature (London) **392**, 151 (1998); P. Courteille *et al.*, Phys. Rev. Lett. **81**, 69 (1998).
[2] M. Greiner, C. A. Regal, and D. S. Jin, Nature (London) **426**, 537 (2003).
[3] S. Jochim *et al.*, Science **302**, 2101 (2003).
[4] M. W. Zwierlein *et al.*, Phys. Rev. Lett. **91**, 250401 (2003).
[5] T. Bourdel *et al.*, Phys. Rev. Lett. **93**, 050401 (2004).
[6] C. A. Regal, M. Greiner, and D. S. Jin, Phys. Rev. Lett. **92**, 040403 (2004).
[7] M. Bartenstein *et al.*, Phys. Rev. Lett. **92**, 120401 (2004).
[8] M. W. Zwierlein *et al.*, Phys. Rev. Lett. **92**, 120403 (2004).
[9] J. Kinast *et al.*, Phys. Rev. Lett. **92**, 150402 (2004).
[10] M. Bartenstein *et al.*, Phys. Rev. Lett. **92**, 203201 (2004).
[11] C. Chin *et al.*, Science **305**, 1128 (2004).
[12] We presented most of the results of the present paper at the KITP workshop in Santa Barbara, 2004. Similar results were independently obtained in Paris [15].
[13] Z. Hadzibabic *et al.*, Phys. Rev. Lett. **91**, 160401 (2003).
[14] C. A. Regal *et al.*, Phys. Rev. Lett. **90**, 053201 (2003).
[15] J. Zhang *et al.*, Phys. Rev. A **70**, 030702(R) (2004).
[16] C. Ticknor *et al.*, Phys. Rev. A **69**, 042712 (2004).
[17] K. Dieckmann *et al.*, Phys. Rev. Lett. **89**, 203201 (2002).
[18] K. M. O'Hara *et al.*, Phys. Rev. A **66**, 041401(R) (2002).
[19] T. Mukaiyama *et al.*, Phys. Rev. Lett. **92**, 180402 (2004).
[20] The ODT power was 36 mW, yielding trap frequencies of $\omega_r = 2\pi \times 690$ Hz radially and $\omega_a = 2\pi \times 12.5$ Hz axially. The axial frequency is mostly due to magnetic field curvature.
[21] T. Kohler *et al.*, Phys. Rev. Lett. **91**, 230401 (2003).
[22] J. Cubizolles *et al.*, Phys. Rev. Lett. **91**, 240401 (2003).
[23] K. E. Strecker, G. B. Partridge, and R. G. Hulet, Phys. Rev. Lett. **91**, 080406 (2003).
[24] B. Marcelis *et al.*, Phys. Rev. A **70**, 012701 (2004).
[25] E. G. M.v. Kempen, B. Marcelis, and S. J. J. M. F. Kokkelmans, Phys. Rev. A **70**, 050701(R) (2004).

Appendix E

Formation Dynamics of a Fermion Pair Condensate

This appendix contains a reprint of Ref. [270]: M.W. Zwierlein, C. H. Schunck, C. A. Stan, S. M. F. Raupach, and W. Ketterle, *Formation Dynamics of a Fermion Pair Condensate*, Phys. Rev. Lett. **94**, 180401 (2005).

Formation Dynamics of a Fermion Pair Condensate

M. W. Zwierlein, C. H. Schunck, C. A. Stan, S. M. F. Raupach, and W. Ketterle
Department of Physics, MIT-Harvard Center for Ultracold Atoms, and Research Laboratory of Electronics, MIT, Cambridge, Massachusetts 02139, USA
(Received 23 December 2004; published 9 May 2005)

The dynamics of pair condensate formation in a strongly interacting Fermi gas close to a Feshbach resonance was studied. We employed a phase-shift method in which the delayed response of the many-body system to a modulation of the interaction strength was recorded. The observable was the fraction of condensed molecules in the cloud after a rapid magnetic field ramp across the Feshbach resonance. The measured response time was slow compared to the rapid ramp, which provides final proof that the molecular condensates reflect the presence of fermion pair condensates before the ramp.

DOI: 10.1103/PhysRevLett.94.180401 PACS numbers: 03.75.Ss, 05.30.Fk

Atomic Fermi gases close to a Feshbach resonance [1] offer the unique possibility of studying many-body phenomena in a strongly interacting system with tunable interactions. Recently a major focus has been on condensates of pairs of fermionic atoms [2–8]. By changing the magnetic field, the interaction strength between atoms in two spin states can be varied. That way, condensates of either tightly bound molecules or of extended pairs of fermions can be created, whose size can become comparable or even larger than the interparticle spacing. The description of this so-called BEC-BCS crossover [9] is an active frontier in many-body physics with still controversial interpretations [10–13].

The control of interactions via magnetic fields does not only give access to very different physical regimes, it also allows one to apply a time-varying interaction strength [14,15] and to study the dynamics of a many-body system in novel ways. This was used in recent experiments in which molecular condensates were observed after a rapid field ramp from the BCS to the Bose-Einstein condensate (BEC) side of the Feshbach resonance [6,7]. It was argued that if the ramp time was faster than the formation time of a molecular condensate, its presence after the sweep necessarily reflected a preexisting condensate of fermion pairs. However, without access to that formation time, secondary evidence was gathered, namely, the invariance of the condensate fraction under variations of the sweep rate [6] or of the density immediately before the ramp [7]. This excluded simple models of the molecular condensate formation during the ramp, but left room for more sophisticated many-body effects. In particular, the time to cross the Feshbach resonance in these experiments was not faster than the unitarity limited collision time $\propto \hbar E_F^{-1}$, and therefore dynamics during the sweep could not be ruled out.

Here we present an experimental study of the formation dynamics of a fermion pair condensate on the BCS side of the Feshbach resonance [16]. We employ a novel phase-shift method, which records the delayed response of the many-body system to a modulation of the magnetic field that changes periodically its interaction strength. The observable is again the molecular condensate fraction after a rapid sweep to the BEC side of the Feshbach resonance. Its sensitivity to changes in the scattering length on the BCS side [6,7] arises through the dependence of the critical temperature for pair condensation on the interaction strength. By showing that the delayed response time of the molecular condensate fraction is long compared to the sweep times used in the present and previous experiments, we infer that the observed condensates could not have been created during the rapid transfer and thus must originate from preexisting fermion pair condensates. However, we do find evidence that condensed pairs are more likely to be transferred into molecules than thermal pairs. Therefore, in contrast to assumptions made in previous work [6,7], the molecular condensate fraction after the ramp may not equal the fraction of condensed atom pairs above resonance.

The experimental setup was the same as in our previous work [7]. A degenerate cloud of ^{6}Li, sympathetically cooled with ^{23}Na, was loaded into an optical dipole trap to access a broad Feshbach resonance at 834 G [17,18] between the two lowest hyperfine states of ^{6}Li, labeled $|1\rangle$ and $|2\rangle$. An equal mixture of these states was evaporatively cooled at 770 G using an exponential ramp-down of the optical trap to 15 mW. This resulted in an essentially pure Bose-Einstein condensate of 3×10^6 molecules. An upper limit for the temperature of the gas is $\frac{T}{T_F} < 0.2$, with the Fermi temperature T_F given by the zero-temperature, ideal gas relation $T_F = \hbar\omega(3N)^{1/3}$, $\omega/2\pi$ is the geometric mean of the trapping frequencies, and N is the total atom number. Next, the trap was recompressed to 25 mW (trap frequencies: $\nu_x = \nu_y = 580$ Hz, $\nu_z = 12.1$ Hz$\sqrt{0.2 + B}$ with the magnetic field B in kG) and the magnetic field was adiabatically increased in 500 ms to 1000 G, the starting point for the following experiments. Here, in the wings of the Feshbach resonance, the scattering length a was still sufficiently large and negative for the gas to be in the strongly interacting regime, with $k_F|a| = 1.6$ at a Fermi energy of $E_F = 2.0$ μK and a Fermi wave number $k_F = 1/2700a_0$. The temperature at this point could therefore not be reli-

 © 2005 The American Physical Society

ably determined, but is expected to be significantly lower than the one on the BEC side due to adiabatic cooling [19]. Subsequently, the magnetic field and thus the interaction strength in the gas were modulated at frequencies in the range of 100–500 Hz, and an amplitude of about 50 G [20]. At a variable time t after the start of the modulation, the fraction of condensed fermion pairs was recorded by time-of-flight analysis.

To identify fermionic condensates across the resonance region, we proceeded as in [6,7]. Immediately after the release of the cloud from the optical potential, the magnetic field was switched to zero field (initial ramp rate 30 G/μs), where further expansion of the cloud took place. This rapid ramp out of the resonance region transformed large fermion pairs into deeply bound molecules with high efficiency [21]. Figure 1 details the imaging procedure used to determine molecular condensate fractions and the number of unpaired atoms in each state after the ramp. In our previous work, we showed that the condensate fractions had a peak around the Feshbach resonance and fell off on either side [7]. Here, this dependence was exploited to observe the delayed response of the system to the magnetic field modulation on the BCS side.

Figure 2 shows the main result of this Letter: The condensate fraction in the molecular clouds after the rapid ramp did not follow the magnetic field modulation instantaneously, but lagged behind. At a Fermi energy of $E_F = 2\ \mu$K, the peak condensate fraction was delayed by $\tau_R = (500 \pm 100)\ \mu$s with respect to the magnetic field's closest approach to resonance [22]. This time scale was independent of the modulation frequency [compare Figs. 2 and 4(a), below]. This also rules out that our results are affected by the excitation of collective modes. τ_R equals 130 times the unitarity limited collision time, $\hbar E_F^{-1} = 3.8\ \mu$s. The rapid magnetic field ramp utilized here and in [7] traversed the Feshbach resonance in less than 10 μs, which is much smaller than τ_R.

This delay time can be interpreted as the relaxation time of the fermionic condensate. In a normal Fermi gas of N particles at temperatures much smaller than the Fermi temperature T_F, relaxation occurs through collisions between the thermally excited particles close to the Fermi surface, whose number scales as $N_{th} \simeq N\frac{k_BT}{E_F}$. The number of available scattering states again being proportional to $\frac{k_BT}{E_F}$, the relaxation time will be $\tau_R \simeq \hbar\frac{E_F}{(k_BT)^2}$. In general, if the Fermi surface is smeared out over an energy width ΔE, the relaxation time is $\simeq \hbar\frac{E_F}{(\Delta E)^2}$. This formula with $\Delta E = \Delta$ should apply also to the superfluid state [23] when the gap parameter Δ is rapidly changed to a much smaller value. Generally, one would expect ΔE to be the larger of Δ and k_BT. Using $\tau_R = 500\ \mu$s, we obtain the estimate $\Delta E = 0.1E_F$ which may set an upper bound for both temperature and pairing gaps.

A decay is superimposed to the periodic modulation of the condensate fraction. It could be caused by heating due to the nonadiabaticity of the process. Another source of heating could be the excitation of the cloud via the small accompanying variation of the magnetic field curvature.

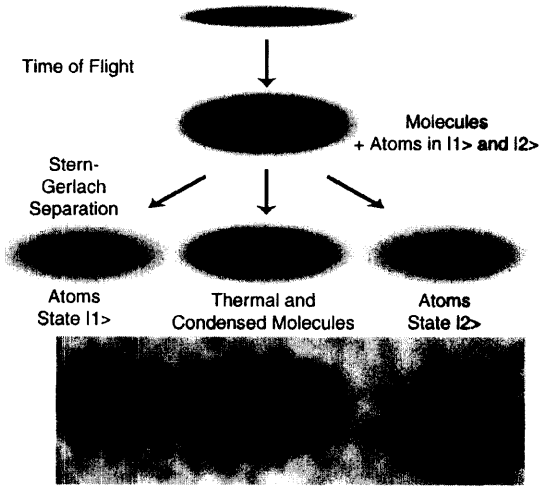

FIG. 1. Imaging of molecular condensates. The rapid ramp to zero field after release from the trap created a cloud containing both molecules and unpaired atoms. A Stern-Gerlach field gradient separated atoms (magnetic moment $\pm\frac{1}{3}\ \mu_B$ for states $|1\rangle$ and $|2\rangle$, respectively) from molecules, which are purely singlet at zero field. At the end of 5 ms of ballistic expansion, the molecules were dissociated in a fast ramp (in 3 ms to ~1200 G) across the Feshbach resonance. After another 2 ms expansion again at zero field, an absorption image of the separated clouds was taken. Condensate fractions were determined from the molecular cloud, and the numbers in each component were recorded. An absorption image is shown on the bottom, the field of view is 3 mm × 1 mm.

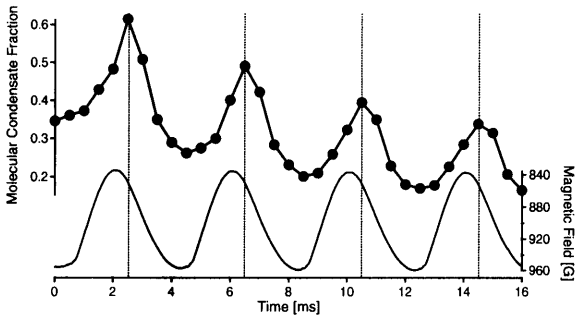

FIG. 2. Measurement of the relaxation time of fermionic pair condensates. Shown is the delayed response of the observed condensate fraction (data points and thick line to guide the eye) to a 250 Hz magnetic field modulation (thin line) on the BCS side of the Feshbach resonance at 834 G. The condensates were detected as described in Fig. 1. Three measurements per point were taken in random order, the size of the data points reflecting the standard deviation. The vertical lines indicate the points of maximum condensate fraction, which are delayed with respect to the times at which the magnetic field is closest to resonance.

Despite the decay of the condensate fraction, the relaxation time was constant for subsequent cycles of modulation, within the (limited) accuracy of our measurement.

In a compressed trap of $p = 150$ mW, at a 1.8 times higher Fermi energy of 3.6 μK, the measured delay time was $\tau_R \simeq (230 \pm 100)$ μs. BCS theory predicts that the relaxation time should scale with density like $\tau_R \propto E_F^{-1} e^{\pi/(k_F|a|)}$, giving $\tau_R \simeq 200$ μs for this experiment performed around 900 G. However, we regard this agreement with observation as fortuitous since BCS theory cannot be rigorously applied, and finite temperature effects may contribute to the relaxation.

We now discuss further observations regarding the efficiency of converting atoms into molecules. Since the relaxation time introduces some hysteresis, we observe the same condensate fraction at two different magnetic field values. Therefore, in contrast to equilibrium experiments [6,7], we can distinguish the dependence of the conversion efficiency on condensate fraction and magnetic field.

Figure 3 shows that the total number of detected atoms (in both the atom and the molecule channels) was modulated by the magnetic field. We assume that this instantaneous response reflects the two-body physics during the magnetic field sweep. In a simple two-state Landau-Zener model, the initial magnetic field and the sweep rate determine what fraction of the atoms appears as bound molecules. However, the total number of bound or unbound atoms should be constant in contrast to our observations. This is evidence for the presence of other molecular states (e.g., lower lying vibrational states) which are populated during the magnetic field sweep, and the population is larger for initial magnetic fields closer to the Feshbach resonance. Note that the determination of the condensate fraction is immune against those "disappeared" molecules, since the two-body physics does not depend on the center-of-mass motion of the atom pair.

We now look at the molecular fraction which we define as $1 - N_{\mathrm{atom}}/N_{\mathrm{total}}$, where N_{atom} is the number of atoms observed after the sweep and N_{total} the total number of atoms before the sweep (this definition includes the disappeared molecules) [24]. If the molecule fraction would follow the instantaneous magnetic field, it would again reflect the two-body physics during the sweep. Instead, we observe a delayed response in perfect correlation with the condensate fraction (Fig. 4). Since the delay time reflects the many-body physics of condensate formation, this is clear evidence that the molecule conversion efficiency depends on the initial many-body state.

One consistent explanation of these findings is that fermion pairs in the condensate are more completely transferred into tightly bound molecules than thermal pairs. With this assumption, we extrapolated the fitted line in Fig. 4(b) to a zero condensate fraction to obtain the transfer efficiency from thermal atom pairs into molecules (including the missing fraction) as $p_{\mathrm{th}} = 75\%$ [21]. Extrapolating towards the other limit, we do not expect any unpaired atoms after the ramp already for a condensate fraction of 80% [25], suggesting a transfer efficiency for condensed fermion pairs into molecules of $p_0 = 100\%$. This effect would lead to an overestimate of the fermionic condensate fraction before the sweep. Small condensate fractions could be overestimated by as much as $\frac{p_0 - p_{\mathrm{th}}}{p_{\mathrm{th}}} = 33\%$. The largest absolute error occurs for an initial pair condensate

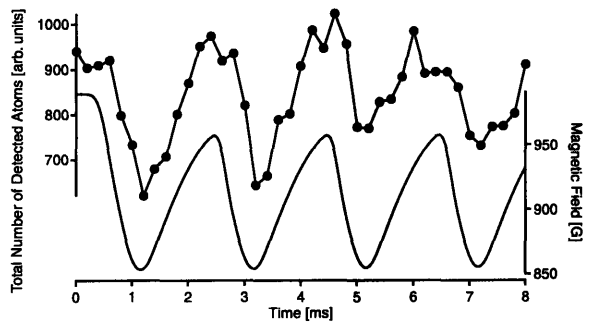

FIG. 3. Total number of detected atoms (unbound atoms and molecules) after the rapid ramp (same data set as in Fig. 4). It is modulated in phase with the magnetic field. For initial fields close to resonance, more atoms are "missing" after the rapid ramp.

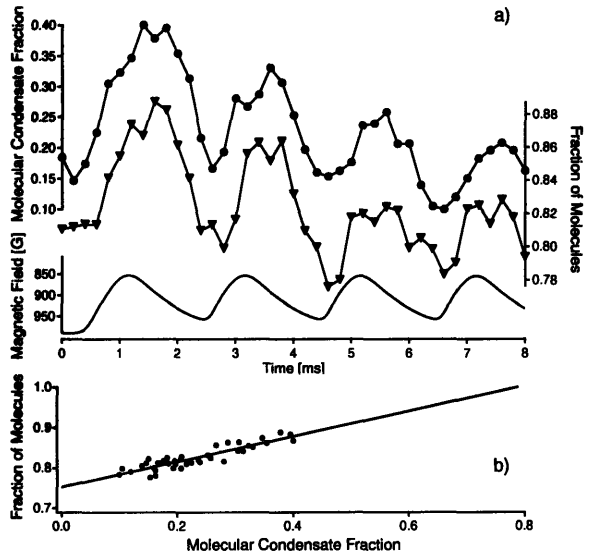

FIG. 4. Correlation between the observed condensate fraction and the molecular fraction. Shown are (a) the condensate fraction vs time during a 500 Hz field modulation (circles), the fraction of molecules (triangles) and the magnetic field. Unlike the total detected signal (Fig. 3), the molecular fraction is modulated not in phase with the magnetic field, but in complete correlation with the condensate fraction. (b) The molecular fraction vs the condensate fraction, together with a fitted line through the data.

fraction of $\frac{\sqrt{p_{th}}}{\sqrt{p_0}+\sqrt{p_{th}}} = 46\%$ and would be about 7% in our case.

This effect can have several possible origins: One is that the atomic separation in a condensed atom pair is smaller than that of two uncondensed atoms. Also, the presence of a large pair condensate increases the density of the cloud [26]. Finally, if there are incoherent processes involved during the rapid ramp, bosonic stimulation into the molecular condensate could play a role.

In conclusion, we have determined the intrinsic time scale for the growth of a fermion pair condensate by observing the delayed response of the system to a change in its interaction strength. For our trap parameters, the response was delayed by ≈ 500 μs. This time is far longer than the time spent within the resonance region during the conversion of fermion pairs into molecules. This provides final proof that the observed molecular condensates originated from condensates of pairs of fermions above the resonance. Regarding the two-body physics of the rapid transfer, we found that there is a missing fraction of particles after the ramp, presumably transferred into unobserved molecular states. We found evidence that condensed fermion pairs are more efficiently transformed into molecules than thermal pairs during the rapid ramp. Thus, the observed molecular condensate fractions tend to overestimate the initial fermion pair condensate fraction.

This work was supported by the NSF, ONR, ARO, and NASA. We thank Michele Saba for the critical reading of the manuscript. S. Raupach is grateful to the Dr. Jürgen Ulderup foundation for financial support.

[1] E. Tiesinga, B. J. Verhaar, and H. T. C. Stoof, Phys. Rev. A **47**, 4114 (1993); W. C. Stwalley, Phys. Rev. Lett. **37**, 1628 (1976); S. Inouye, M. R. Andrews, J. Stenger, H.-J. Miesner, D. M. Stamper-Kurn, and W. Ketterle, Nature (London) **392**, 151 (1998); P. Courteille, R. S. Freeland, D. J. Heinzen, F. A. van Abeelen, and B. J. Verhaar, Phys. Rev. Lett. **81**, 69 (1998).

[2] M. Greiner, C. A. Regal, and D. S. Jin, Nature (London) **426**, 537 (2003).

[3] S. Jochim, M. Bartenstein, A. Altmeyer, G. Hendl, S. Riedl, C. Chin, J. H. Denschlag, and R. Grimm, Science **302**, 2101 (2003).

[4] M. W. Zwierlein, C. A. Stan, C. H. Schunck, S. M. F. Raupach, S. Gupta, Z. Hadzibabic, and W. Ketterle, Phys. Rev. Lett. **91**, 250401 (2003).

[5] T. Bourdel, L. Khaykovich, J. Cubizolles, J. Zhang, F. Chevy, M. Teichmann, L. Tarruell, S. J. J. M. F. Kokkelmans, and C. Salomon, Phys. Rev. Lett. **93**, 050401 (2004).

[6] C. A. Regal, M. Greiner, and D. S. Jin, Phys. Rev. Lett. **92**, 040403 (2004).

[7] M. W. Zwierlein, C. A. Stan, C. H. Schunck, S. M. F. Raupach, A. J. Kerman, and W. Ketterle, Phys. Rev. Lett. **92**, 120403 (2004).

[8] J. Kinast, S. L. Hemmer, M. E. Gehm, A. Turlapov, and J. E. Thomas, Phys. Rev. Lett. **92**, 150402 (2004).

[9] D. M. Eagles, Phys. Rev. **186**, 456 (1969); A. J. Leggett, in *Modern Trends in the Theory of Condensed Matter, Proceedings of the XVIth Karpacz Winter School of Theoretical Physics, Karpacz, Poland, 1980* (Springer-Verlag, Berlin, Karpacz, Poland, 1980), pp. 13–27; P. Nozières and S. Schmitt-Rink, J. Low Temp. Phys. **59**, 195 (1985).

[10] G. M. Falco and H. T. C. Stoof, Phys. Rev. Lett. **92**, 130401 (2004).

[11] R. A. Barankov and L. S. Levitov, Phys. Rev. Lett. **93**, 130403 (2004).

[12] Roberto B. Diener and Tin-Lun Ho, cond-mat/0404517.

[13] S. Simonucci, P. Pieri, and G. C. Strinati, cond-mat/0407600.

[14] M. R. Matthews, D. S. Hall, D. S. Jin, J. R. Ensher, C. E. Wieman, E. A. Cornell, F. Dalfovo, C. Minniti, and S. Stringari, Phys. Rev. Lett. **81**, 243 (1998).

[15] M. Greiner, C. A. Regal, and D. S. Jin, Phys. Rev. Lett. **94**, 070403 (2005).

[16] We presented the main result of the present Letter at the KITP workshop in Santa Barbara, May 10–14, 2004.

[17] C. H. Schunck, M. W. Zwierlein, C. A. Stan, S. M. F. Raupach, W. Ketterle, A. Simoni, E. Tiesinga, C. J. Williams, and P. S. Julienne, Phys. Rev. A **71**, 045601 (2005).

[18] M. Bartenstein, A. Altmeyer, S. Riedl, R. Geursen, S. Jochim, C. Chin, J. H. Denschlag, R. Grimm, A. Simoni, E. Tiesinga, C. J. Williams, and P. S. Julienne, Phys. Rev. Lett. **94**, 103201 (2005).

[19] L. D. Carr, G. V. Shlyapnikov, and Y. Castin, Phys. Rev. Lett. **92**, 150404 (2004).

[20] The instantaneous magnetic field was determined by probing the atoms using a Zeeman-sensitive optical transition. For the 500 Hz modulation, the deduced field followed the modulation current with a time delay of (85 ± 5) μs and a reduced amplitude of 95% compared to the dc situation. This was due to induced eddy currents in the apparatus.

[21] The transfer probability depends on the ramp speed and on the density of the cloud. In a tighter trap with 150 mW of power we cannot discern any unpaired atoms after the ramp.

[22] This was far shorter than evaporation time scales, which were on the order of 100 ms.

[23] R. A. Barankov, L. S. Levitov, and B. Z. Spivak, Phys. Rev. Lett. **93**, 160401 (2004).

[24] N_{total} was determined in a different cycle of the experiment, for which the rapid ramp was omitted.

[25] Indeed, on resonance we observe almost pure condensates, and only a negligible amount of unpaired atoms after the ramp. Note that fitting routines, saturated absorption, and imaging noise all tend to underestimate condensate fractions.

[26] This is not true in the BCS regime, where the atomic density is independent of the presence of a condensate. Still, an additional overestimation of the condensate fraction comes from the fact that the condensed pairs are concentrated in the high density region of the cloud, where the conversion efficiency is higher. However, this does not affect the total molecular signal.

Appendix F

Vortices and Superfluidity in a Strongly Interacting Fermi Gas

This appendix contains a reprint of Ref. [265]: M. W. Zwierlein, J. R. Abo-Shaeer, A. Schirotzek, C. H. Schunck, and W. Ketterle *Vortices and Superfluidity in a Strongly Interacting Fermi Gas*, Nature **435**, 1047 (2005), (in Nature *Articles*).

ARTICLES

Vortices and superfluidity in a strongly interacting Fermi gas

M. W. Zwierlein[1], J. R. Abo-Shaeer[1]†, A. Schirotzek[1], C. H. Schunck[1] & W. Ketterle[1]

Quantum degenerate Fermi gases provide a remarkable opportunity to study strongly interacting fermions. In contrast to other Fermi systems, such as superconductors, neutron stars or the quark-gluon plasma of the early Universe, these gases have low densities and their interactions can be precisely controlled over an enormous range. Previous experiments with Fermi gases have revealed condensation of fermion pairs. Although these and other studies were consistent with predictions assuming superfluidity, proof of superfluid behaviour has been elusive. Here we report observations of vortex lattices in a strongly interacting, rotating Fermi gas that provide definitive evidence for superfluidity. The interaction and therefore the pairing strength between two ^{6}Li fermions near a Feshbach resonance can be controlled by an external magnetic field. This allows us to explore the crossover from a Bose-Einstein condensate of molecules to a Bardeen-Cooper-Schrieffer superfluid of loosely bound pairs. The crossover is associated with a new form of superfluidity that may provide insights into high-transition-temperature superconductors.

The first observations of Bose–Einstein condensates (BECs) of molecules consisting of loosely bound fermionic atoms[1–3] initiated a series of explorations[4–12] of the crossover between a BEC and a Bardeen–Cooper–Schrieffer (BCS) superfluid[13–15]. When an external magnetic field is varied across a Feshbach resonance, these molecules transform adiabatically into the Cooper pairs of a BCS superfluid. All physical properties are expected to vary smoothly throughout this crossover. For example, the size of fermion pair condensates smoothly increases from the BEC- to the BCS-side of the resonance, while the strength of the bond between two paired atoms smoothly decreases. The similar size and shape of normal and condensed gas clouds makes it difficult to detect condensation on the BCS-side. However, using a rapid magnetic field sweep back to the BEC-side, introduced by the Boulder group[4], pair condensation was observed[4,5,12]. Although Bose–Einstein condensation and superfluidity are intimately connected, they do not necessarily occur together. In lower dimensions, superfluidity occurs in the absence of Bose–Einstein condensation[16]. An ideal Bose gas or disordered three-dimensional system can have a condensate, but shows no superfluidity[16]. Phase fluctuations, which are probably present in short-lived condensates of fermionic pairs[1], can suppress superfluid behaviour.

Several ground-breaking studies in Fermi gases of hydrodynamic expansion[7,17], collective excitations[8,9], thermodynamic properties[11] and the binding energy of pairs[10] were suggestive of superfluid behaviour or were consistent with theoretical calculations predicting superfluidity, but did not provide unambiguous evidence. In the meantime, several theoretical papers[18–22] emphasized that the rotational properties of a gas of fermion pairs could directly reveal superfluidity in such systems.

Quantized vortices in a rotating gas provide conclusive evidence for superfluidity because they are a direct consequence of the existence of a macroscopic wavefunction that describes the superfluid. The velocity field of the superfluid is proportional to the gradient of the wavefunction's phase. In such a case, flow must be irrotational and angular momentum can enter the system only in the form of discrete line defects (vortices). In contrast, for a normal gas the lowest state of rotation corresponds to rigid body rotation. Metastable vortex patterns have been observed in classical inviscid fluids[23]. However, the final number and charge of the vortices depends chaotically on the initial conditions, in contrast to the regular vortex lattices that we have reproducibly observed. Furthermore, vortex patterns in classical fluids are only stable at extremely low viscosity (that is, for Reynolds numbers $>10^5$). For a Boltzmann gas rotating close to the trap frequency, the Reynolds number is approximately the cloud size divided by the mean free path, which does not exceed 10^3 in our case. Pauli blocking can only decrease the Reynolds number further.

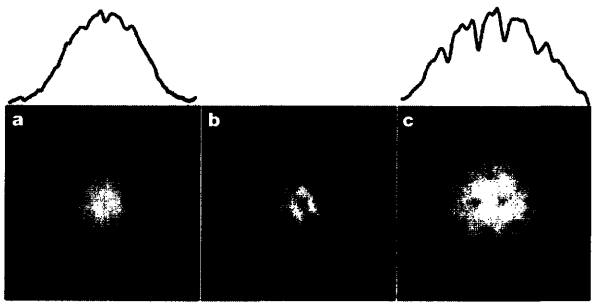

Figure 1 | Observation of a vortex lattice in a molecular condensate. **a**, Fixed field. Stirring for 800 ms, followed by 400 ms of equilibration, and imaging after 12 ms time-of-flight all took place at 766 G. The vortex core depletion of the integrated density profile is barely 10%, as indicated by the 5-μm-wide cut on top. **b**, Fourier filter applied to **a** to accentuate the vortex contrast. Spatial frequencies with an absolute value of about the inverse vortex core size were enhanced by a factor of four. **c**, Varying field. The vortex lattice was created at 766 G and imaged at 735 G following the procedure outlined in the text. The vortex core depletion is now about 35% (see 5-μm-wide cut on top). The field of view is 780 μm × 780 μm.

[1]Department of Physics, MIT-Harvard Center for Ultracold Atoms, and Research Laboratory of Electronics, MIT, Cambridge, Massachusetts 02139, USA. †Present address: Lawrence Berkeley National Laboratory, One Cyclotron Road, MS 88R0192, Berkeley, California 94720, USA.

© 2005 Nature Publishing Group

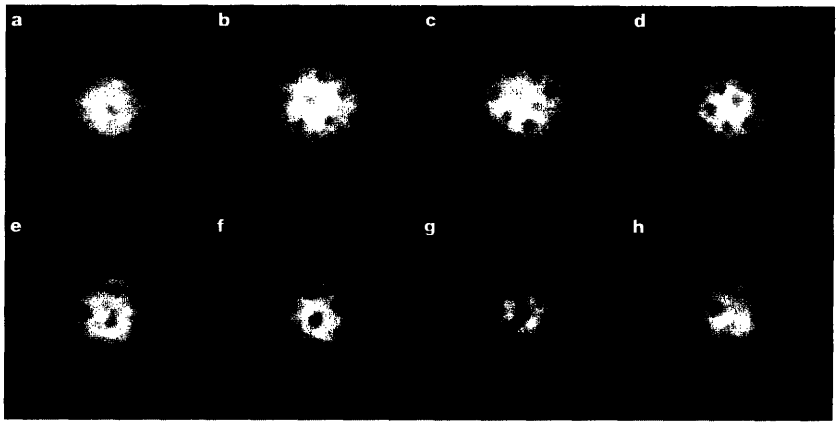

Figure 2 | Vortices in a strongly interacting gas of fermionic atoms on the BEC- and the BCS-side of the Feshbach resonance. At the given field, the cloud of lithium atoms was stirred for 300 ms (**a**) or 500 ms (**b–h**) followed by an equilibration time of 500 ms. After 2 ms of ballistic expansion, the magnetic field was ramped to 735 G for imaging (see text for details). The magnetic fields were 740 G (**a**), 766 G (**b**), 792 G (**c**), 812 G (**d**), 833 G (**e**), 843 G (**f**), 853 G (**g**) and 863 G (**h**). The field of view of each image is 880 μm × 880 μm.

Experimental procedure

To create a strongly interacting Fermi gas, spin-polarized fermionic ^{6}Li atoms were sympathetically cooled to degeneracy by ^{23}Na atoms in a magnetic trap[24]. The Fermi cloud was then loaded into an optical dipole trap, and an 875 G external magnetic field was applied. Here a 50%/50% spin mixture of the two lowest hyperfine states of ^{6}Li was prepared. Between these two states, labelled $|1\rangle$ and $|2\rangle$, there is a 300-G-wide Feshbach resonance located at 834 G (refs 25, 26). Evaporative cooling (achieved by reducing the laser power) accompanied by a magnetic field ramp to 766 G on the BEC-side of the resonance typically produced a BEC of 3×10^6 molecules[3].

Previous experiments studying the rotation of atomic BECs employed magnetic traps operating at low bias fields[27–31]. Because the Feshbach resonance in our system occurs between two high-field seeking states that cannot be trapped magnetically, an optical dipole trap operating at high magnetic bias fields was necessary. Our set-up employed a trapping beam with a $1/e^2$ radius of 123 μm (wavelength 1,064 nm), radially confining the gas with a trap frequency of 59 Hz at a power of 145 mW. Axial confinement with trap frequency $\nu_z = 23$ Hz was provided by an applied magnetic field curvature that decreased the radial trap frequency to $\nu_r = 57$ Hz. The aspect ratio of the trap was 2.5. In this trap, at a field of 766 G, condensates of 1×10^6 molecules (the typical number in our experiment after rotating the cloud) have Thomas–Fermi radii of about 45 μm radially and 110 μm axially, a peak molecular density of 2.6×10^{12} cm^{-3}, a chemical potential of about 200 nK, and a characteristic microscopic length scale of $1/k_F \approx 0.3$ μm. Here, the Fermi wavevector k_F is defined by the Fermi energy (E_F) of a non-interacting two-state mixture of ^{6}Li atoms of mass m with total atom number N in a harmonic trap of (geometric) mean frequency $\bar{\omega}$, $E_F = \hbar\bar{\omega}(3N)^{1/3} \equiv \hbar^2 k_F^2/2m$. Throughout this Article we will estimate the interaction parameter $1/k_F a$ using the average number of fermion pairs $N/2 = 1 \times 10^6$. Here, a is the scattering length between atoms in states $|1\rangle$ and $|2\rangle$. At a field of 766 G, $1/k_F a = 1.3$. Because this gas is strongly interacting, it is difficult to extract a temperature from the spatial profile. For weaker interactions (at 735 G) the condensate fraction was in excess of 80%, which would isentropically connect to an ideal Fermi gas[32] at $T/T_F = 0.07$. The BEC–BCS crossover ($1/k_F|a| < 1$) occurs in the region between 780 G and 925 G.

The trapped cloud was rotated about its long axis using a blue-detuned laser beam (wavelength 532 nm)[28,29,33]. A two-axis acousto-optic deflector generated a two-beam pattern (beam separation $d = 60$ μm, gaussian beam waist $w = 16$ μm) that was rotated symmetrically around the cloud at a variable angular frequency Ω. The two beams with 0.4 mW power each produced a repulsive potential of 125 nK for the ^{6}Li cloud, creating a strongly anisotropic potential. This method was first tested using a weakly interacting, atomic BEC of ^{23}Na in the stretched upper hyperfine state in an optical trap with $\nu_r = 60$ Hz, $\nu_z = 23$ Hz. Fully equilibrated lattices of up to 80 vortices were observed. The vortex number decayed with a 1/e lifetime of 4.2 ± 0.2 s, while the atom number decayed, owing to three-body losses and evaporation, with a lifetime of 8.8 ± 0.4 s. The roundness of the optical trap and its alignment with both the optical stirrer and the axes of the magnetic potential were critical. Any deviation from cylindrical symmetry owing to misalignment, optical aberrations, or gravity rapidly damped the rotation. The generation of vortices in sodium was comparatively forgiving, and had to be optimized before vortices in ^{6}Li$_2$ could be observed.

Observation of vortex lattices

In experiments with ^{6}Li close to the Feshbach resonance, the interaction strength between atoms in states $|1\rangle$ and $|2\rangle$ can be freely tuned via the magnetic field. Thus, it is possible to choose different magnetic fields to optimize the three steps involved in the creation of a vortex lattice: stirring of the cloud (for 800 ms at a typical stirring frequency of 45 Hz), the subsequent equilibration (typically 500 ms) and time-of-flight expansion for imaging. To stay close to the

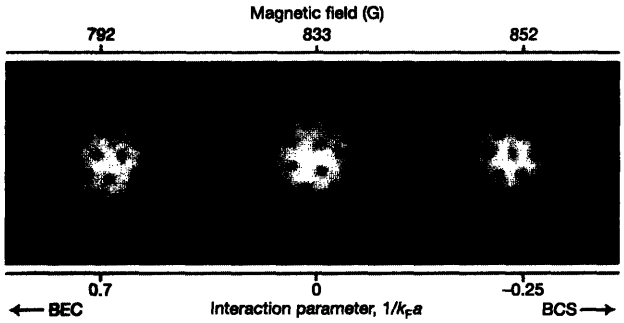

Figure 3 | Optimized vortex lattices in the BEC–BCS crossover. After a vortex lattice was created at 812 G, the field was ramped in 100 ms to 792 G (BEC-side), 833 G (resonance) and 853 G (BCS-side), where the cloud was held for 50 ms. After 2 ms of ballistic expansion, the magnetic field was ramped to 735 G for imaging (see text for details). The field of view of each image is 880 μm × 880 μm.

© 2005 Nature Publishing Group

analogous case of an atomic condensate, our search for vortices started on the BEC-side of the resonance, at a fixed magnetic field of 766 G. To image the cloud, the trapping beam was switched off and the cloud expanded in the residual magnetic potential. After 12 ms time-of-flight, a molecular absorption image along the axial direction was taken with light resonantly exciting atoms in state $|2\rangle$[3] (Fig. 1a). Although the contrast of the vortex cores was low, a regular lattice pattern containing about 25 vortices was visible (see Fourier filtered image in Fig. 1b). This establishes superfluidity for molecular condensates.

Subsequently, it was found that the contrast of the vortex cores could be enhanced by the following procedure: the magnetic field curvature was reduced by a factor of five during the first millisecond of time-of-flight. After 2 ms expansion at the initial field, the magnetic field was ramped down over 2 ms to 735 G. The cloud was imaged after an additional 9 ms of expansion at this field. Attempts to image at even lower fields did not enhance the contrast. Further improvements were achieved by forcing the cloud to expand faster by increasing the power of the optical trap by a factor of 4.5 during the last 2 ms of trapping (Fig. 1c). We suspect that owing to the residual magnetic field curvature, a faster expansion was superior to a longer time-of-flight.

Using this procedure, we observed vortices that were created not only on the BEC- but also the BCS-side of the Feshbach resonance, at magnetic fields between 740 G and 863 G (Fig. 2). On the BCS-side, isolated fermion pairs are unstable. As the cloud expands from the trap and the density decreases, the pairs will become more fragile and dissociate at a certain point in the time-of-flight. Information on the centre-of-mass wavefunction of the pairs, and hence the vortex contrast, will be gradually lost. The field ramp to the BEC-side during expansion protects the pairs by transforming them into stable molecules. At 853 G, this ramp could be delayed by 6 ms into ballistic expansion before the vortex contrast was lost. It is not clear why this ramp was found to be necessary already at 812 G, on the BEC-side of the resonance, where isolated fermion pairs are stable.

It is impossible for vortex lattices to form during ballistic expansion at the imaging field (735 G). We show below that the formation of vortex lattices even at the high density of the trapped cloud takes several hundred milliseconds. Furthermore, even if there was some unpredicted fast formation mechanism for vortices, they could not form a regular array with long-range order in a cloud that expands at the speed of sound of the trapped gas. The observation of vortex lattices on the BCS-side of the Feshbach resonance above 834 G demonstrates superfluidity of fermions at magnetic fields where they cannot form stable, isolated molecules.

The highest number of vortices (~40) was obtained by stirring at 766 G and then equilibrating close to resonance at 812 G ($1/k_Fa = 0.35$). We suspect that the violent nature of the stirring produced more heating near the Feshbach resonance where the pairs are loosely bound. On the other hand, fields closer to resonance were favourable for equilibration owing to suppression of vibrational relaxation. After preparing such a vortex lattice at 812 G, the magnetic field was ramped over 100 ms to a test field. After a hold time of 50 ms, the vortex lattice was imaged as discussed above (Fig. 3). Vortices were observed for test fields between 700 G ($1/k_Fa = 3.8$) and 954 G ($1/k_Fa = -1.2$) (Fig. 4).

The regularity of the lattice proves that all vortices have the same vorticity. From their number, the size of the cloud and the quantum of circulation $h/2m$ for each vortex, we can estimate the rotational frequency of the lattice. For an optimized stirring procedure, we find that it is close to the stirring frequency. This excludes a quantum of circulation of h/m or doubly charged vortices.

Formation and lifetime of vortex lattices

Before we found the detection scheme described above, we studied the formation and decay of the vortex lattices using a different procedure. The magnetic field was lowered to 735 G ($1/k_Fa = 2.3$) in the last 30 ms before expansion. Reduction of the magnetic field curvature by a factor of five took place during the last 5 ms before expansion, avoiding undesired compression of the cloud in the axial direction. As before, the trap was compressed by increasing the trapping power by a factor of 4.5 during the last 2 ms before the switch-off. Imaging was done after 12 ms expansion at 735 G.

When a superfluid is rotated, the creation of quantized vortices is energetically favoured only above a certain critical rotation frequency. In some cases, a higher rotational frequency is necessary to actually nucleate the vortices[34]. This occurs through a dynamic instability of surface excitations[33,35,36]. Figure 5 shows that vortices in the BEC region were created over a large range of stirring frequencies, as opposed to only near the quadrupole surface mode resonance[28,29]. Similar non-resonant behaviour was observed in atomic sodium condensates with small stirring beams[36]. The strong dependence of the observed stirring efficiency curve on the magnetic

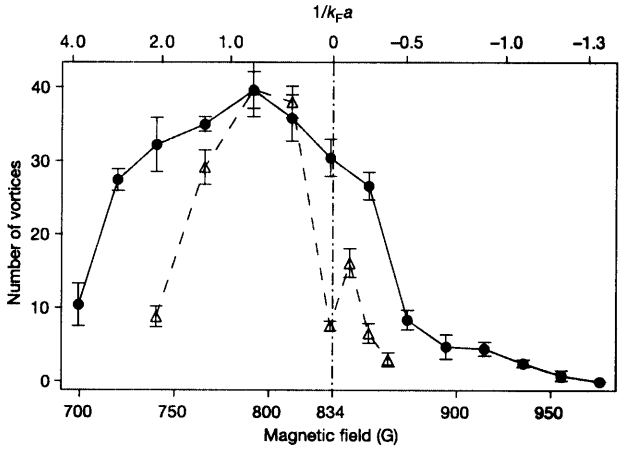

Figure 4 | Vortex number versus magnetic field and interaction strength in the BEC-BCS crossover. The open triangles show the number of vortices obtained after stirring and equilibration at the given, fixed magnetic field, as in Fig. 2. For the filled circles, a procedure similar to the one in Fig. 3 was used, where the vortex lattice was prepared at 812 G, and then the field was ramped to the test field. The position of the Feshbach resonance[26] is marked with the vertical dash-dotted line. The data points and error bars give the average and standard deviation of several measurements.

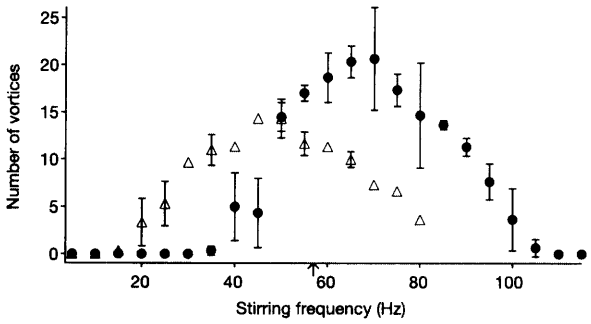

Figure 5 | Vortex number versus stirring frequency in the BEC region for different interaction strengths. Vortices were efficiently created over a broad range of stirring frequencies. The open triangles and filled circles correspond to stirring (for 800 ms) and equilibration (for 500 ms) at 766 G and 812 G, respectively. The data points and error bars (if larger than the symbol) show the average and standard deviation of three measurements. The radial trap frequency (57 Hz) is indicated by the small arrow on the horizontal axis.

© 2005 Nature Publishing Group

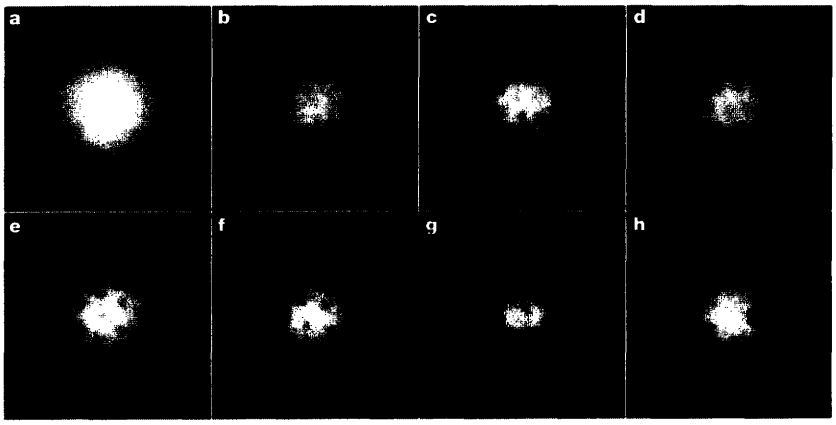

Figure 6 | Formation and decay of a vortex lattice in a fermion pair condensate on the BEC-side close to the Feshbach resonance. A molecular condensate, prepared at 766 G as shown in **a**, was stirred for 800 ms. The field was then ramped to 812 G in 20 ms for equilibration. At this field, $1/k_Fa = 0.35$, and the condensate was deep in the strongly interacting regime. To observe the vortex lattice, the field was ramped in 25 ms to 735 G ($1/k_Fa = 2.3$), where the condensate was released from the trap and imaged after 12 ms time-of-flight. The equilibration times after the end of the stirring were 40 ms (**b**), 240 ms (**c**), 390 ms (**d**), 790 ms (**e**), 1,140 ms (**f**), 1,240 ms (**g**) and 2,940 ms (**h**). Owing to stirring, evaporation and vibrational relaxation, the number of fermion pairs decayed from 3×10^6 (**a**) to 1×10^6 (**b–h**). The field of view of each image is 830 μm × 830 μm.

field strength could be related to the increase of the speed of sound in the condensate for stronger interactions, leading to a higher critical velocity.

Figure 6 shows the formation of a vortex lattice close to the Feshbach resonance, on the BEC-side at 812 G ($1/k_Fa = 0.35$). Immediately after stirring, the cloud was in a turbulent state (Fig. 6b). It took several hundred milliseconds for the vortices to fully crystallize into a lattice (Fig. 6c–e). The vortices arranged themselves in a hexagonal Abrikosov lattice to minimize their interaction energy[29,37]. Because the trap potential was not perfectly round (trap asymmetry $(\nu_x^2 - \nu_y^2)/(\nu_x^2 + \nu_y^2) \approx 0.03$), the vortex lattice slowly decayed on a timescale of several seconds (Fig. 6f–h). These observations are fully analogous to those already made in atomic BECs[29,35,38]. The formation time of several hundred milliseconds is in agreement with these experimental studies, as well as with a recent theoretical study on the vortex lattice formation in a strongly interacting Fermi gas[39]. Note that this timescale was found to be independent of temperature[38], and seems to represent an intrinsic timescale of superfluid hydrodynamics. The long formation time excludes the possibility that ordered vortex lattices can be created during the 30 ms field ramp to 735 G, used for imaging. This holds even more strongly for the imaging method described first, where the magnetic field was switched only in time-of-flight. We are not aware of any possible formation mechanism that could create regular vortex lattices during ballistic expansion.

In principle, the presence of vortices can be used to map out the superfluid regime as a function of temperature and interaction strength, even in regions where fermion pairs are much larger than the interparticle spacing and can no longer be detected by transforming them into stable molecules[4,5,12]. As a first step, the lifetime of the vortex lattice was studied at different magnetic fields and interaction strengths. After preparing a fully crystallized vortex lattice containing about 30 vortices in the BEC-region at 812 G, the magnetic field was ramped to a chosen point in the crossover. After a variable hold time, the cloud was imaged at 735 G as described above, and the remaining number of vortices was counted. The results of this measurement are summarized in Fig. 7. The longest lifetime, 3.4 s, was obtained for magnetic fields slightly below resonance, near 810 G ($1/k_Fa = 0.4$). Here, we observed four vortices even after 7 s. During this time the fluid at the vortex core (with characteristic size $1/k_F$) rotated more than 50,000 times, displaying truly superfluid behaviour. As expected, the lifetime was reduced at low magnetic fields where the molecules heat up owing to vibrational relaxation. In addition, and unexpectedly, a narrow dip in lifetime at approximately 831 G with a width of 8 G was observed. We speculate that this decrease in lifetime so close to resonance is caused by a coupling of the external motion of the loosely bound pairs to their internal motion, causing pair breaking or rotational excitation. Indeed, at 831 G, the binding energy for isolated molecules divided by h is about 35 Hz, comparable to the initial rotational frequency of the lattice. The reduced lifetime on the BCS-side could be caused by an increasing fraction of thermal fermion pairs[5,38] due to the decreasing critical temperature for superfluidity. In a two-fluid model, angular momentum is stored as a vortex lattice in the superfluid component. Friction is provided by the normal component, which increases as we move further away from resonance on the BCS-side. At 925 G ($1/k_Fa = -1.0$) the vortex lifetime was reduced to only 10 ms, with a large error bar indicating

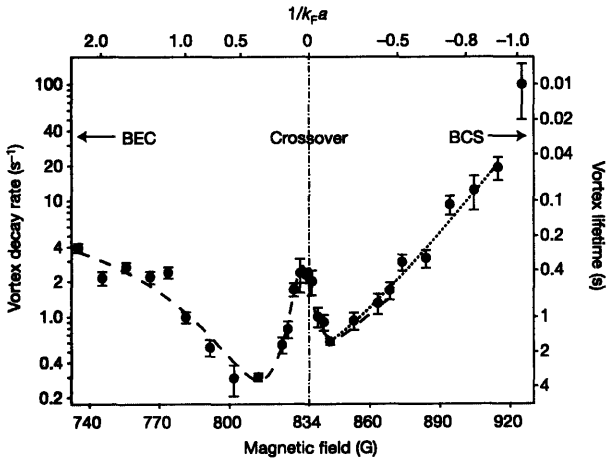

Figure 7 | Decay rate and lifetime of the vortex lattice versus magnetic field and interaction strength. The data points and error bars give the decay rate or lifetime and one standard deviation extracted from exponential fits to the vortex number decay. The dashed and dotted lines are gaussian and exponential fits to guide the eye, the dashed line including a lorentzian fit for the narrow feature near resonance. The position of the Feshbach resonance[26] is marked with the vertical dash-dotted line.

© 2005 Nature Publishing Group

strong fluctuations in the vortex number. Here we might be approaching the region where the superfluid-to-normal transition takes place.

Conclusions

We have detected long-lived vortex lattices in a strongly interacting Fermi gas over the entire BEC–BCS crossover region by imaging them after switching to lower magnetic fields during ballistic expansion. This provides the first direct signature of superfluidity in these systems. We expect that vortices in rotating Fermi gases will serve as an important starting point for future studies on superfluid dynamics.

Received 9 May; accepted 31 May 2005.

1. Greiner, M., Regal, C. A. & Jin, D. S. Emergence of a molecular Bose–Einstein condensate from a Fermi gas. *Nature* **426,** 537–540 (2003).
2. Jochim, S. *et al.* Bose-Einstein condensation of molecules. *Science* **302,** 2101–2103 (2003).
3. Zwierlein, M. W. *et al.* Observation of Bose-Einstein condensation of molecules. *Phys. Rev. Lett.* **91,** 250401 (2003).
4. Regal, C. A., Greiner, M. & Jin, D. S. Observation of resonance condensation of fermionic atom pairs. *Phys. Rev. Lett.* **92,** 040403 (2004).
5. Zwierlein, M. W. *et al.* Condensation of pairs of fermionic atoms near a Feshbach resonance. *Phys. Rev. Lett.* **92,** 120403 (2004).
6. Bartenstein, M. *et al.* Crossover from a molecular Bose-Einstein condensate to a degenerate Fermi gas. *Phys. Rev. Lett.* **92,** 120401 (2004).
7. Bourdel, T. *et al.* Experimental study of the BEC-BCS crossover region in lithium 6. *Phys. Rev. Lett.* **93,** 050401 (2004).
8. Kinast, J., Hemmer, S. L., Gehm, M. E., Turlapov, A. & Thomas, J. E. Evidence for superfluidity in a resonantly interacting Fermi gas. *Phys. Rev. Lett.* **92,** 150402 (2004).
9. Bartenstein, M. *et al.* Collective excitations of a degenerate gas at the BEC-BCS crossover. *Phys. Rev. Lett.* **92,** 203201 (2004).
10. Chin, C. *et al.* Observation of the pairing gap in a strongly interacting Fermi gas. *Science* **305,** 1128–1130 (2004).
11. Kinast, J. *et al.* Heat capacity of a strongly-interacting Fermi gas. *Science* **307,** 1296–1299 (2005).
12. Zwierlein, M. W., Schunck, C. H., Stan, C. A., Raupach, S. M. F. & Ketterle, W. Formation time of a fermion pair condensate. *Phys. Rev. Lett.* **94,** 180401 (2005).
13. Eagles, D. M. Possible pairing without superconductivity at low carrier concentrations in bulk and thin-film superconducting semiconductors. *Phys. Rev.* **186,** 456–463 (1969).
14. Leggett, A. J. in *Modern Trends in the Theory of Condensed Matter* (eds Pekalski, A. & Przystawa, J.) 13–27 (Proc. XVIth Karpacz Winter School of Theoretical Physics, Springer, Berlin, 1980).
15. Nozières, P. & Schmitt-Rink, S. Bose condensation in an attractive fermion gas: from weak to strong coupling superconductivity. *J. Low Temp. Phys.* **59,** 195–211 (1985).
16. Huang, K. in *Bose-Einstein Condensation* (eds Griffin, A., Snoke, D. W. & Stringari, S.) 31–50 (Cambridge Univ. Press, Cambridge, 1995).
17. O'Hara, K. M., Hemmer, S. L., Gehm, M. E., Granade, S. R. & Thomas, J. E. Observation of a strongly interacting degenerate Fermi gas of atoms. *Science* **298,** 2179–2182 (2002).
18. Rodriguez, M., Paraoanu, G.-S. & Törmä, P. Vortices in trapped superfluid Fermi gases. *Phys. Rev. Lett.* **87,** 100402 (2001).
19. Bruun, G. M. & Viverit, L. Vortex state in superfluid trapped Fermi gases at zero temperature. *Phys. Rev. A* **64,** 063606 (2001).
20. Pitaevskii, L. & Stringari, S. The quest for superfluidity in Fermi gases. *Science* **298,** 2144–2146 (2002).
21. Cozzini, M. & Stringari, S. Fermi gases in slowly rotating traps: superfluid versus collisional hydrodynamics. *Phys. Rev. Lett.* **91,** 070401 (2002).
22. Bulgac, A. & Yu, Y. Vortex state in a strongly coupled dilute atomic fermionic superfluid. *Phys. Rev. Lett.* **91,** 190404 (2003).
23. Schecter, D. A., Dubin, D. H. E., Fine, K. S. & Driscoll, C. F. Vortex crystals from 2D Euler flow: Experiment and simulation. *Phys. Fluids* **11,** 905–914 (1999).
24. Hadzibabic, Z. *et al.* Fifty-fold improvement in the number of quantum degenerate fermionic atoms. *Phys. Rev. Lett.* **91,** 160401 (2003).
25. Dieckmann, K. *et al.* Decay of ultracold fermionic lithium gas near a Feshbach resonance. *Phys. Rev. Lett.* **89,** 203201 (2002).
26. Bartenstein, M. *et al.* Precise determination of ^{6}Li cold collision parameters by radio-frequency spectroscopy on weakly bound molecules. *Phys. Rev. Lett.* **94,** 103201 (2004).
27. Matthews, M. R. *et al.* Vortices in a Bose-Einstein condensate. *Phys. Rev. Lett.* **83,** 2498–2501 (1999).
28. Madison, K. W., Chevy, F., Wohlleben, W. & Dalibard, J. Vortex formation in a stirred Bose-Einstein condensate. *Phys. Rev. Lett.* **84,** 806–809 (2000).
29. Abo-Shaeer, J. R., Raman, C., Vogels, J. M. & Ketterle, W. Observation of vortex lattices in Bose-Einstein condensates. *Science* **292,** 476–479 (2001).
30. Haljan, P. C., Coddington, I., Engels, P. & Cornell, E. A. Driving Bose-Einstein-condensate vorticity with a rotating normal cloud. *Phys. Rev. Lett.* **87,** 210403 (2001).
31. Hodby, E., Hechenblaikner, G., Hopkins, S. A., Maragò, O. M. & Foot, C. J. Vortex nucleation in Bose-Einstein condensates in an oblate, purely magnetic potential. *Phys. Rev. Lett.* **88,** 010405 (2002).
32. Carr, L. D., Shlyapnikov, G. V. & Castin, Y. Achieving a BCS transition in an atomic Fermi gas. *Phys. Rev. Lett.* **92,** 150404 (2004).
33. Onofrio, R. *et al.* Surface excitations in a Bose-Einstein condensate. *Phys. Rev. Lett.* **84,** 810–813 (2000).
34. Anglin, J. R. Local vortex generation and the surface mode spectrum of large Bose-Einstein condensates. *Phys. Rev. Lett.* **87,** 240401 (2001).
35. Madison, K. W., Chevy, F., Bretin, V. & Dalibard, J. Stationary states of a rotating Bose-Einstein condensate: routes to vortex nucleation. *Phys. Rev. Lett.* **86,** 4443–4446 (2001).
36. Raman, C., Abo-Shaeer, J. R., Vogels, J. M., Xu, K. & Ketterle, W. Vortex nucleation in a stirred Bose-Einstein condensate. *Phys. Rev. Lett.* **87,** 210402 (2001).
37. Madison, K. W., Chevy, F., Wohlleben, W. & Dalibard, J. Vortices in a stirred Bose-Einstein condensate. *J. Mod. Opt.* **47,** 2715–2723 (2000).
38. Abo-Shaeer, J. R., Raman, C. & Ketterle, W. Formation and decay of vortex lattices in Bose-Einstein condensates at finite temperatures. *Phys. Rev. Lett.* **88,** 070409 (2002).
39. Tonini, G. & Castin, Y. Formation of a vortex lattice in a rotating BCS Fermi gas. Preprint at (http://arxiv.org/cond-mat/0504612) (2005).

Acknowledgements We thank P. Zarth for experimental assistance and C. Stan for contributions in the early stages of the experiment. We also acknowledge discussions with the participants of the OCTS conference in Ohio, and thank J. Anglin, Z. Hadzibabic, D. Kleppner and A. Leanhardt for a critical reading of the manuscript. This work was supported by the NSF, ONR, ARO and NASA.

Author Information Reprints and permissions information is available at npg.nature.com/reprintsandpermissions. The authors declare no competing financial interests. Correspondence and requests for materials should be addressed to M.W.Z. (zwierlei@mit.edu).

© 2005 Nature Publishing Group

Appendix G

Superfluid Expansion of a Rotating Fermi Gas

This appendix contains the preprint Ref. [216]: C. H. Schunck, M. W. Zwierlein, A. Schirotzek, and W. Ketterle, *Superfluid Expansion of a Rotating Fermi Gas*, preprint cond-mat/0607298.

Superfluid Expansion of a Rotating Fermi Gas

C.H. Schunck, M.W. Zwierlein, A. Schirotzek, and W. Ketterle
Department of Physics, MIT-Harvard Center for Ultracold Atoms, and Research Laboratory of Electronics, MIT, Cambridge, MA 02139
(Dated: October 5, 2006)

We study the expansion of a rotating, superfluid Fermi gas. The presence and absence of vortices in the rotating gas is used to distinguish superfluid and normal parts of the expanding cloud. We find that the superfluid pairs survive during the expansion until the density decreases below a critical value. Our observation of superfluid flow in the expanding gas at $1/k_F a = 0$ extends the range where fermionic superfluidity has been studied to densities of 1.2×10^{11} cm^{-3}, about an order of magnitude lower than any previous study.

PACS numbers: 03.75.Ss, 03.75.Hh, 05.70.Fh

Ultracold atomic gases have been used to create novel quantum many-body systems ranging from Bose-Einstein condensates and Mott insulators in optical lattices to high-temperature superfluids of strongly interacting fermions. These systems offer a high degree of control over physical parameters including interaction strength and density. Many important features in these gases have a spatial scale too small to be resolved while the gas is trapped. A standard technique to reveal this physics is to switch off the confining potential and release the gas from the trap. A non-interacting gas expands ballistically and the expansion reveals its momentum distribution. The expansion dynamics of an interacting gas is modified by the effect of collisions. This can result in classical hydrodynamic flow and in this case the expansion serves as a (not necessarily linear) magnifying glass for the trapped state. In contrast to classical hydrodynamics, superfluid hydrodynamic flow does not rely on collisions. When a weakly interacting Bose-Einstein-Condensate (BEC) is released from an anisotropic trapping potential, superfluid hydrodynamics leads to an inversion of the aspect ratio, often regarded as a hallmark of Bose-Einstein condensation [1].

The expansion dynamics of strongly interacting Fermi gases has been the subject of a longstanding debate. For a weakly interacting ultracold Fermi gas anisotropic expansion has been proposed as a probe for superfluidity, analogous to the case of weakly interacting BECs [2]. Anisotropic expansion has been experimentally observed in strongly interacting Fermi gases [3–5]. In this case, however, the inversion of the aspect ratio can occur due to collisions between the expanding atoms even if they were initially at zero temperature [6, 7]. So far experiments have not been able to discriminate between superfluid and collisional hydrodynamics in expansion and indeed one would expect both effects to contribute: In the BCS-regime, the superfluid transition temperature T_C depends exponentially on the density. Starting at $T < T_C$, the superfluid gas first expands according to superfluid hydrodynamics. As the density drops, T approaches T_C and superfluidity cannot be maintained. From this point on, the gas should expand according to collisional hydrodynamics or enter a regime intermediate between collisional hydrodynamic and collisionless expansion.

In this paper we study the expansion of a superfluid Fermi gas, in the regime where pairing is purely a many-body effect. We have observed superfluid flow even after 5 ms of expansion, when the cloud size had increased by more than a factor of 4 and the peak density had dropped by a factor of 17 compared to the in-trap values.

Superfluidity in Fermi gases has previously been established through the observation of vortex lattices [8, 9]. To detect vortices in a rotating fermion pair condensate the pairs are transferred into stable molecules by sweeping an external magnetic field across a Feshbach resonance shortly after the gas is released from the trap. Vortices can be observed only when the gas is still a superfluid at the moment of the magnetic field sweep [10]. At the final magnetic field (on the BEC side of the Feshbach resonance) the interactions are much weaker. Therefore the vortex core has higher contrast and is larger than near resonance. If the gas is no longer superfluid at the time of the field ramp, we expect the vortex core to fill in quickly and disappear. The observed vortex cores therefore serve as markers for the regions which are superfluid at the time of the magnetic field ramp.

Our experimental setup has been described earlier [11, 12]. ^{6}Li fermion pair condensates containing 5×10^6 fermions were created in an optical dipole trap at a magnetic field of 812 G. This is on the BEC-side of a Feshbach resonance at $B_0 = 834$ G. At magnetic fields below (above) B_0, on the BEC (BCS) side, the scattering length a is positive (negative) and a nearby molecular bound state exists (does not exist). The radial and axial trapping frequencies were $\omega_r = 2\pi \times 120$ Hz and $\omega_a = 2\pi \times 23$ Hz, respectively. To observe vortices as a probe of superfluid flow, the gas was set in rotation: two blue-detuned laser beams were rotated symmetrically around the cloud for 1 s at an angular frequency of $2\pi \times 80$ Hz [8]. We allowed 500 ms of equilibration before the magnetic field was ramped (in 500 ms) to several probe fields on the

FIG. 1: Superfluid expansion of a strongly interacting rotating Fermi gas. Shown are absorption images for different expansion times on the BCS-side of the Feshbach resonance at 910 G (0.0, 1.0, 2.0, 3.0, 3.5, 4.0, and 4.5 ms) and 960 G (0.0, 0.5, 1.0, 1.5, 2.0, 2.5, and 3 ms), before the magnetic field was ramped to the BEC-side for further expansion. The vortices served as markers for the superfluid parts of the cloud. Superfluidity survived the expansion for several milliseconds and was gradually lost from the low density edges of the cloud towards its center. Compared to 910 G ($a = -7200\ a_0$), superfluidity decayed faster at 960 G ($a = -5000\ a_0$) due to the reduced interaction strength. The total expansion time remained constant [14]. The field of view of each image is 1.2 mm × 1.2 mm.

BCS side of the resonance. Finally, we studied the expansion of the rotating superfluid: The gas was released from the optical trap and expanded at the probe field for a variable "BCS-expansion" time $t_{\rm BCS}$, that was increased in 500 μs steps. To transfer the remaining fermion pairs into stable molecules the magnetic field was then lowered in 400 μs to 680 G [13]. Here, the cloud was given several milliseconds of "BEC-expansion". For absorption imaging the magnetic field was raised to 730 G in 500 μs before the last 2 ms of time-of-flight. For most of the data the total time-of-flight was chosen to be 11 ms [14]. An absorption image of the gas was obtained separately at $t_{\rm BCS}$ to determine the peak density and the peak Fermi momenta k_F before the magnetic field sweep.

Fig. 1 shows absorption images taken as outlined above for seven different BCS-expansion times at both 910 G and 960 G. The presence of vortices proves that superfluid fermion pairs survived in the expanding gas for several milliseconds. As the density of the gas dropped during the BCS-expansion the vortices were gradually lost from the low density edges of the cloud towards its center. After 4.5 ms time-of-flight at 910 G and 3 ms at 960 G all of the vortices had decayed. If we regard the number of vortices as an indicator of the superfluid fraction of the gas, we can draw the "phase diagram" of Fig. 2. Here the number of vortices is shown as a function of the inverse scattering length $1/a$ and the inverse peak Fermi momentum $1/k_F$. As $1/k_F$ increases at a given magnetic field, corresponding to the decrease in density during time-of-flight, vortices are lost. The reduction in the number of vortices for decreasing $|a|$ reflects the decrease of the superfluid fraction for smaller attractive interactions at a given temperature. In addition, the increase in the normal fraction leads to higher damping of the remaining vortex number [8]. Most importantly, however, we see that vortices are lost earlier in time-of-flight as the interactions are reduced.

At all magnetic fields, we find that the peak interaction strength at the point where all vortices were lost is about constant, $k_F a \sim -0.8$ (see Fig. 3). As shown in Fig. 1 the loss of vortices occurred gradually and the surviving vortices were located within a circle of decreasing radius. We assume that the critical value of $k_F a$ for which superfluidity was lost, was first reached at the edge of the cloud and subsequently further inward. However, we were not able to confirm this picture quantitatively without a model that describes how the shape of the cloud and the bimodality develop during and after the magnetic field sweep.

It is remarkable that the observation of superfluidity and fermion pair condensation for *trapped* gases has also been limited to values of $k_F|a|$ larger than 1 [8, 12, 17]. This suggests that the underlying reason for this limitation is the same for a trapped and an expanding gas. One obvious scenario for the decay of the vortex lattice during expansion is the breakdown of superfluidity due to finite temperature when a critical interaction strength is reached. As the density decreases, T_C/T_F drops while T/T_F remains constant (since the phase space density $n \times T^{-3/2}$ is invariant during expansion). Therefore T_C eventually becomes smaller than T everywhere in the cloud and superfluidity is lost. The critical interaction strength can be estimated by equating $1 \equiv T/T_C = (T/T_F)(T_F/T_C) = 1.76(T/T_F)(E_F/\Delta)$. Here $\Delta = (2/e)^{7/3} E_F \exp(-\pi/2k_F|a|)$ is the pairing gap in the BCS limit (valid for $k_F|a| \lesssim 1$) [18], where the peak Fermi energy $E_F = \hbar^2 {k_F}^2/2m$ and k_F are density dependent. For an estimate of our lowest tempera-

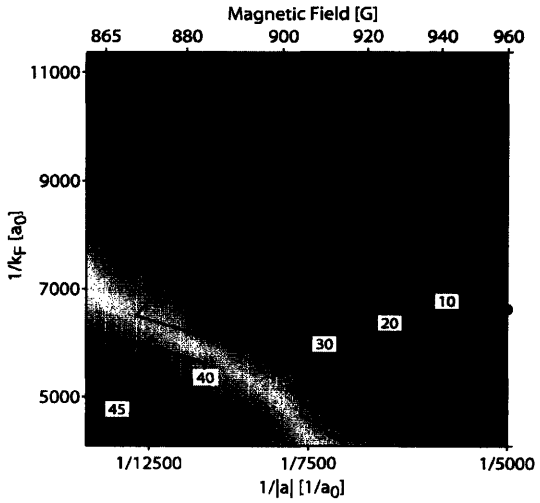

FIG. 2: (color online) "Phase diagram" of an expanding, rotating Fermi gas: At a given magnetic field the number of vortices served as a measure for the size of the superfluid region in the gas. The number of vortices is plotted versus $1/k_F$ and $1/|a|$. The contour plot was created from a total of 53 data points. In this diagram lines of constant $k_F a$ correspond to hyperbolas. The vortices decayed when the density (increasing $1/k_F$) or the scattering length (increasing $1/|a|$) was reduced. For weaker interactions, at smaller scattering lengths $|a|$, vortices were lost already at higher densities. The four data points shown mark the breakdown of superfluidity and are the same as the squares in Fig. 3.

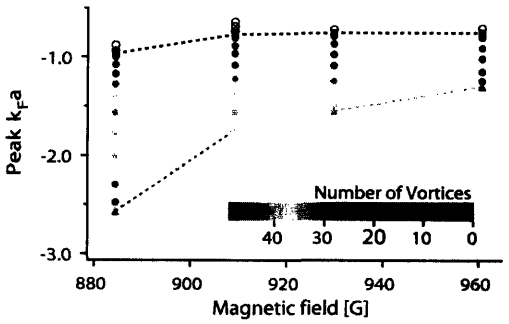

FIG. 3: (color online) The peak interaction strength during superfluid expansion. Starting at a peak $k_F a$ in the optical trap (triangles) vortices survived up to a critical peak $k_F a$ of -0.8 +/- 0.1 (squares), almost independent of the magnetic field (scattering length). Filled circles correspond to partially superfluid, open circles to normal clouds. The observed number of vortices is color coded. The critical $k_F a$ was obtained for each magnetic field separately by taking the average of the peak k_F of the last partially superfluid and the first completely normal cloud. The error in $k_F a$ is about 10% and dominated by the systematic error in the atom number.

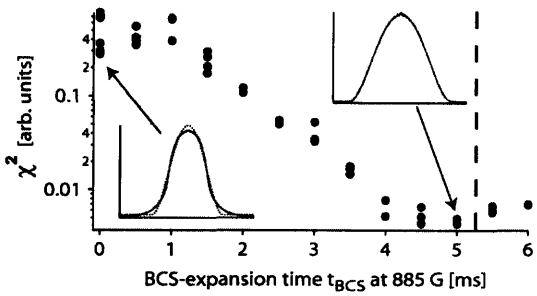

FIG. 4: Disappearance of bimodality. Zero temperature Thomas-Fermi profiles (dotted) were fit to the density profiles (solid) obtained after BCS-expansion at 885 G and subsequent BEC-expansion at 680 G. The χ^2 of the fit was monitored as a function of the BCS-expansion time $t_{\rm BCS}$. A high χ^2 indicates a bimodal density distribution. Vortices were still observed after 5 ms of expansion (indicated by the dashed line in the figure) while the bimodality had already disappeared (for χ^2 values smaller than 0.01 bimodality cannot be discerned). Hence, the absence of bimodality does not imply the absence of superfluidity.

tures of $T/T_F = 0.05$ [19] this gives $k_F a = -0.9$ close to the observed value. This finite-temperature scenario implies that the superfluid state evolves adiabatically during expansion, which is plausible: Even when the critical $k_F a$ is reached, the pair binding energy still changes at a slower rate, $\dot{\Delta}/\Delta$, than the rate at which the pairs can respond to this change, $\Delta/\hbar$ [20]. For weakly interacting BECs, the decay of vortex lattices at finite temperature was studied theoretically in [21], and remarkably similar structures are found.

In analogy to the critical magnetic field H_{c2} in type-II superconductors, superfluidity can also break down in response to rapid rotation [22, 23]. Superfluidity is quenched when the vortex core size becomes comparable to the separation between the vortices. Both the critical temperature as well as the vortex core size in the BCS limit depend exponentially on $k_F a$ and therefore the effects of rotation might not be negligible. In [23], however, it was found that superfluidity should be stable in the strongly interacting regime ($k_F|a| \gtrsim 1.0$) at all rotation frequencies.

Another explanation for the loss of vortices is a possible failure of the transfer of correlated fermion pairs into molecules since the size of the fermion pairs increases with decreasing density. When the fermion pair size becomes larger than the interparticle spacing, molecules might be formed out of uncorrelated nearest neighbors rather than out of correlated pairs. The magnetic field sweep then destroys the coherent many-body wavefunction.

Vortices [8, 9] and bimodal density distributions [12, 17] have been used as indicators for superfluidity and

FIG. 5: Loss of vortex contrast on resonance at 834 G. Shown are absorption images after a fixed total time-of-flight, but for different expansion times on resonance (2, 2.5, 3, 3.5, 4, 5, and 6 ms) before the magnetic field was swept to the BEC-side for further expansion. A gradual loss of the vortex contrast from about 15% (after 2 ms of expansion on resonance) to 3% (after 5 ms) was observed across the whole cloud. The field of view of each image is 1.2 mm $\times$1.2 mm.

pair condensation, respectively. If a fermion pair condensate is transferred to the BEC side before its interaction energy has been converted into kinetic energy, it continues to expand with the drastically reduced mean-field energy of a molecular BEC at 680 G. This results in a clear separation of condensate and thermal cloud after further BEC-expansion. If the transfer of fermion pairs into molecules is delayed after releasing the gas from the trap, the fermion pair condensate initially expands just like the normal part of the cloud. This eventually leads to a loss of bimodality in the density profiles after the transfer. We can now study how the two indicators, vortices and bimodality, are related in this experiment. For short BCS-expansion $t_{\rm BCS}$ our data showed bimodality as well as vortices. However, the bimodality was gradually lost and could not be discerned after a longer BCS-expansion although vortices were still visible (see Fig. 4 for details). The absence of bimodality therefore does not indicate a breakdown of superfluidity.

So far we have studied the expansion of the gas on the BCS side of the Feshbach resonance. On the BEC side and on resonance, T_C is proportional to T_F so that T/T_C is constant during expansion. Therefore, one would not expect to observe a breakdown of superfluidity in expansion. Fig. 5 shows absorption images that were obtained after an initial expansion of the cloud on resonance at 834 G. In contrast to the situation on the BCS-side of the resonance no vortices were lost. Instead, the vortex contrast decreased uniformly across the cloud for longer expansion times. Vortices have been detected at total densities as low as 1.2×10^{11} cm^{-3} in the wings of the expanded cloud. Here the critical temperature T_C of approximately $0.2\,T_F$ [15, 16] was below 20 nK ($k_B T_F$ is the local Fermi energy). We believe that the decrease in the vortex contrast is due to the low density of the gas after long BCS-expansion: after the magnetic field sweep the vortex cores cannot adjust quickly enough to the high contrast and large size they would have in equilibrium on the BEC-side. This reduction of contrast limited our study of the breakdown of superfluidity to magnetic fields above 880 G.

In conclusion we have shown that superfluid pairs can survive during the expansion of a strongly interacting Fermi gas. This is the first observation of non-equilibrium superfluid flow in such systems. It has allowed us to observe fermionic superfluidity at total densities as low as 1.2×10^{11} cm^{-3}. Our results show that future experiments with expanding, superfluid Fermi gases can be carried out in situ, i.e. without magnetic field sweeps to the BEC side. An intriguing question is whether fermion pairs expanding from two clouds can coherently interfere.

We thank Gretchen Campbell for a critical reading of the manuscript. This work was supported by the NSF, ONR, and NASA.

[1] W. Ketterle et al., in "Bose-Einstein Condensation in Atomic Gases", IOS Press, Amsterdam, 1999 pp. 67–176.
[2] C. Menotti et al., Phys. Rev. Lett. **89**, 250402 (2002).
[3] K. M. O'Hara et al., Science **298**, 2179 (2002).
[4] C. A. Regal et al. Phys. Rev. Lett. **90**, 230404 (2003).
[5] T. Bourdel et al., Phys. Rev. Lett. **91**, 020402 (2003).
[6] S. Gupta et al., Phys. Rev. Lett. **92**, 100401 (2004).
[7] B. Jackson et al., Europhys. Lett. **67**, 524 (2004).
[8] M. W. Zwierlein et al., Nature **435**, 1047 (2005).
[9] M. W. Zwierlein et al., Science **311**, 492 (2006).
[10] The sweep time is much faster than the formation time of a vortex lattice in the trap, which is several hundred milliseconds. Detection of vortices after the ramp therefore proves their presence before the ramp [8].
[11] Z. Hadzibabic et al., Phys. Rev. Lett. **91**, 160401 (2003).
[12] M. W. Zwierlein et al., Phys. Rev. Lett. **92**, 120403 (2004).
[13] The ramp time was 200 μs for the data taken at 834, 865 and 885 G. We have checked that the rate of the magnetic field sweep to 680 G had no influence on the number of observed vortices within our measurement accuracy.
[14] To increase the visibility of the vortices for $t_{\rm BCS} = 0$ and 500 μs the total time-of-flight was increased to up to 15 ms and/or the power of the optical trap was increased by a factor of 4.5 during the last 2 ms of trapping [8].
[15] A. Bulgac et al., Phys. Rev. Lett. **96**, 090404 (2006).
[16] E. Burovski et al., Phys. Rev. Lett. **96**, 160402 (2006).
[17] C. A. Regal et al., Phys. Rev. Lett. **92**, 040403 (2004).
[18] L. P. Gor'kov et al., Sov. Phys. JETP **13**, 1018 (1961).
[19] M. W. Zwierlein et al., Nature **442**, 54 (2005).

[20] We find $\frac{\hbar\dot{\Delta}}{\Delta^2} = \frac{\hbar}{\Delta} \times \frac{\dot{n}}{n} \times \left(\frac{2}{3} + \frac{\pi}{6k_F|a|}\right)$. Since the gas expands to a very good approximation only radially, we assume that the density varies as $n(t) = n_0/(1+\omega_r^2 t^2)$, and obtain $\left|\frac{\hbar\dot{\Delta}}{\Delta^2}\right| = \frac{\hbar}{\Delta}\frac{2\omega_r^2 t}{1+\omega_r^2 t^2}\left(\frac{2}{3} + \frac{\pi}{6k_F|a|}\right)$. For the experimental parameters when the vortices in the center of the cloud are lost we find that $\hbar\dot{\Delta}/\Delta^2 \leq 0.4$.

[21] S. Kragset et al., preprint, cond-mat/0604416.

[22] M. Y. Veillette et al., preprint, cond-mat/0607775.

[23] H. Zhai et al., preprint, cond-mat/0608233.

Appendix H

Fermionic Superfluidity with Imbalanced Spin Populations

This appendix contains a reprint of Ref. [268]: Martin W. Zwierlein, André Schirotzek, Christian H. Schunck, and Wolfgang Ketterle, *Fermionic Superfluidity with Imbalanced Spin Populations*, Science **311**, 492 (2006), published online on Science *Express* on 21 December, 2005 (10.1126/science.1122318) (in Science *Research Articles*).

Fermionic Superfluidity with Imbalanced Spin Populations

Martin W. Zwierlein,* André Schirotzek, Christian H. Schunck, Wolfgang Ketterle

We established superfluidity in a two-state mixture of ultracold fermionic atoms with imbalanced state populations. This study relates to the long-standing debate about the nature of the superfluid state in Fermi systems. Indicators for superfluidity were condensates of fermion pairs and vortices in rotating clouds. For strong interactions, near a Feshbach resonance, superfluidity was observed for a broad range of population imbalances. We mapped out the superfluid regime as a function of interaction strength and population imbalance and characterized the quantum phase transition to the normal state, known as the Pauli limit of superfluidity.

Fermionic superfluidity, whether it occurs in superconductors, helium-3, or inside a neutron star, requires pairing of fermions, particles with half-integer spin. In an equal mixture of two states of fermions ("spin up" and "spin down"), pairing can be complete and the entire system will become superfluid. When the two populations of fermions are unequal, however, not every particle can find a partner, raising the question of whether superfluidity can persist in response to such a population imbalance. This problem arises in many different fields of physics—for example, in the study of superfluidity of quarks in the dense matter of the early universe, where charge neutrality and differing masses impose unequal quark densities. In superconductors, an applied magnetic field could in principle imbalance the densities of spin up and spin down electrons. As first discussed by Clogston in 1962 (*1*), there exists an upper limit for this magnetic field, beyond which superconductivity with equal spin densities will break down. Fulde and Ferrell (*2*), and independently Larkin and Ovchinnikov (*3*), proposed a more stable configuration of the superconductor that allows for unequal densities, the FFLO or LOFF state containing nonzero-momentum Cooper pairs. The true ground state of imbalanced fermionic superfluids has been the subject of debate for decades (*4*, *5*), and experimental studies are highly desirable. However, superconductors are charged fermionic superfluids, and imbalancing the electron densities by applying magnetic fields is hindered by the Meissner effect. The fields are either fully shielded from the superconductor, or they enter in the form of quantized flux lines or vortices. Only in special materials can these effects be suppressed, such as in heavy-fermion superconductors (*6*–*8*) or in quasi–two-dimensional (2D) organic superconductors (*6*). In the neutral superfluid helium-3, one can mismatch the Fermi surfaces by a magnetic field and thus destroy interspin pairing. However, superfluidity persists due to (p-wave) pairing between equal spins (*9*).

Fermionic superfluids of atom pairs. The recently discovered fermionic superfluids in ultracold atomic gases (*10*–*19*) provide an exciting new possibility of exploring unequal mixtures of fermions, because populations in two hyperfine states of the fermionic atom can be freely chosen. In addition, the (s-wave) interactions between two atoms in different states and the binding energy of atom pairs can be tuned via Feshbach resonances. In equal mixtures of fermions, this tunability gives access to the crossover from a Bose-Einstein Condensate (BEC) of molecules to a Bardeen-Cooper-Schrieffer (BCS) superfluid of loosely bound pairs (*13*–*19*). At zero temperature, this crossover is smooth (*20*–*22*), the system stays

Department of Physics, Massachusetts Institute of Technology (MIT)–Harvard Center for Ultracold Atoms, and Research Laboratory of Electronics, MIT, Cambridge, MA 02139, USA.

*To whom correspondence should be addressed. E-mail: zwierlei@mit.edu

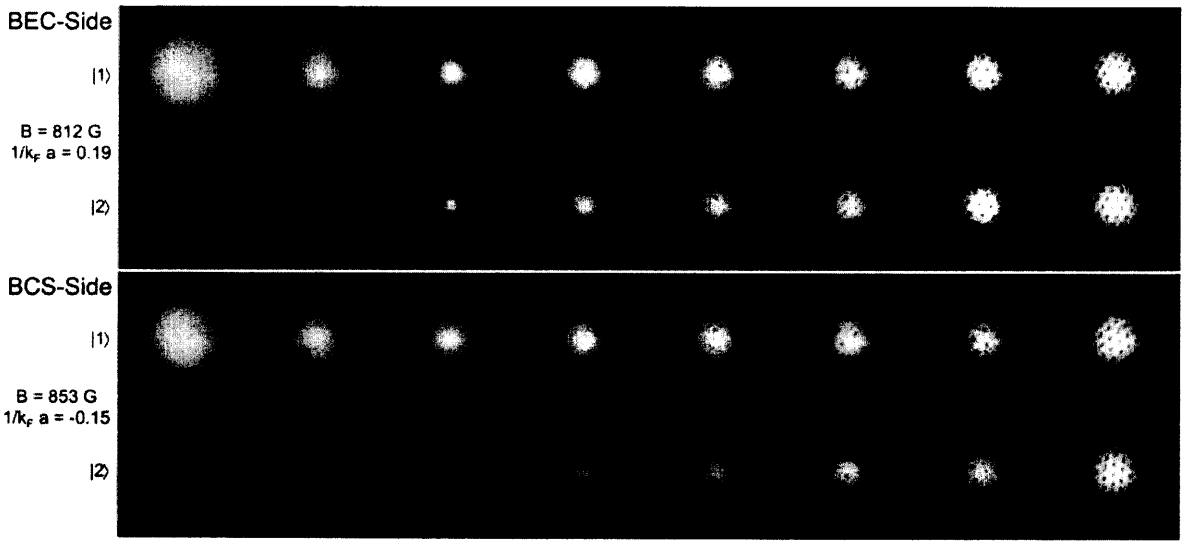

Fig. 1. Superfluidity in a strongly interacting Fermi gas with imbalanced populations. The upper (lower) pair of rows shows clouds prepared at 812 G, on the BEC side (853 G, BCS side), where $1/k_F a = 0.2$ ($1/k_F a = -0.15$). In each pair of rows, the upper image shows state $|1\rangle$, the lower one state $|2\rangle$. For the 812-G data, the population imbalance $\delta = (N_2 - N_1)/(N_1 + N_2)$ between N_1 atoms in state $|1\rangle$ and N_2 in state $|2\rangle$ was (from left to right) 100, 90, 80, 62, 28, 18, 10, and 0%. For the 853-G data, the imbalance was 100, 74, 58, 48, 32, 16, 7, and 0%. For different values of δ, the total number of atoms varied only within 20% around $N = 7 \times 10^6$, with the exception of the end points $\delta = 100\%$ ($N = 1 \times 10^7$) and $\delta = 0\%$ ($N = 1.2 \times 10^7$). The field of view of each image is 1.4 mm by 1.4 mm.

superfluid even for arbitrarily weak interactions, and no phase transition occurs. In the case of unequal mixtures, the phase diagram is predicted to be much richer (*23*–*28*). In the molecular limit of tight binding, all fermions in the less populated spin state will pair up with atoms in the other state. The resulting molecular condensate will spatially coexist with the remaining Fermi sea of unpaired atoms. As the repulsive interaction between atoms and molecules is increased, the condensate will start to expel unpaired atoms, leading to a phase separation of the superfluid from the normal phase (*24*–*26*, *29*, *30*). This picture is expected to extend into the BCS limit of weakly bound pairs, where the pairing gap Δ prevents unpaired atoms from entering the BCS superfluid (*24*–*26*, *31*). As the binding energy and hence the pairing gap is further reduced, Δ will eventually become small compared to the chemical potential difference $\delta\mu = \mu_2 - \mu_1$ between the two spin states, allowing unpaired excess atoms to enter the superfluid region. Close to this point, superfluidity will cease to exist. In the weakly interacting BCS limit, the pairing gap is exponentially small compared to the Fermi energy; hence, an exponentially small population imbalance can destroy superfluidity.

This superfluid-to-normal transition is an example of a quantum phase transition, which occurs even at zero temperature, when all thermal fluctuations are frozen out and only quantum fluctuations prevail. It can also be driven by increasing the mismatch in chemical potentials between the two spin states to the critical value of $\delta\mu \approx \Delta$, inducing collapse into the normal state. In this context the phase transition is known as the Pauli or Clogston limit of superfluidity (*1*). However, its exact nature—whether there is one or several first- and/or second-order transitions—remains the subject of debate (*6*, *27*, *28*).

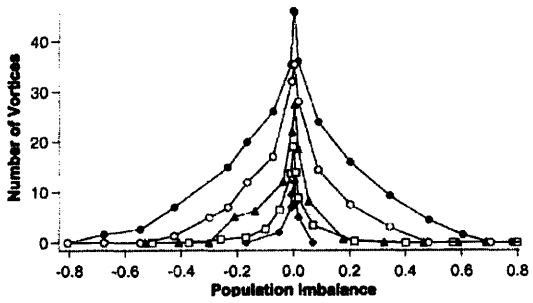

Fig. 2. Vortex number versus population imbalance for different interaction strengths. Results are shown for 812 G or $1/k_Fa = 0.2$ (●), 853 G ($1/k_Fa = -0.15$, ○), 874 G ($1/k_Fa = -0.3$, ▲), 896 G ($1/k_Fa = -0.4$, □), and 917 G ($1/k_Fa = -0.5$, ♦).

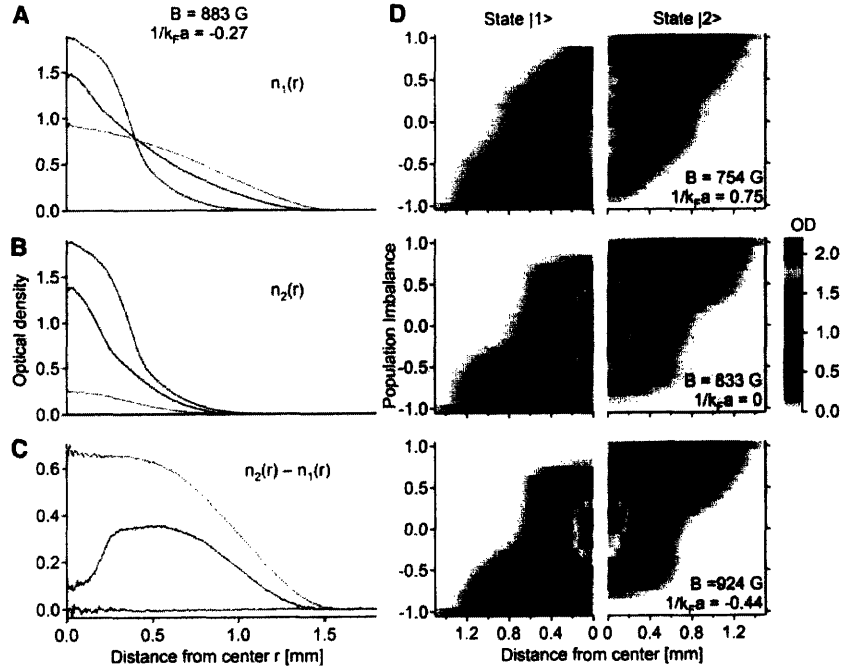

Fig. 3. Radial density profiles of the two components of a strongly interacting Fermi gas mixture with unequal populations. The profiles are azimuthal averages of the axially integrated density. (**A** and **B**) Profiles of the component in state $|1\rangle$ and $|2\rangle$, respectively, originating from 883 G ($1/k_Fa = -0.27$). The imaging procedure, as detailed in the text and in (*32*), involves a magnetic-field sweep and ballistic expansion. The population imbalance was $\delta = 0\%$ (red), $\delta = 46\%$ (blue), and $\delta = 86\%$ (green). (**C**) Difference between the distributions in state $|1\rangle$ and $|2\rangle$. The total number of atoms was $N = 2.3 \times 10^7$. The clear dip in the blue curve caused by the pair condensate indicates phase separation of the superfluid from the normal gas. (**D**) Color-coded profiles of clouds prepared at three different interaction strengths. The condensate is clearly visible as the dense central part surrounded by unpaired fermions or uncondensed molecules. Spin-polarized clouds ($\delta = \pm 100\%$) are not in thermal equilibrium, owing to Pauli suppression of collisions. OD, optical density.

For the study of vortices and superfluid flow as a function of population imbalance, the spin mixture was set in rotation on the BEC side, using two laser beams that rotated symmetrically around the cloud (*19*, *32*). Starting with either a rotating or a nonrotating cloud, we then varied the interaction strength by ramping the magnetic field B to several values around the Feshbach resonance. To image the fermion pair condensates, the cloud was released from the optical trap and the binding energy of the pairs was increased by switching the magnetic field to the BEC side, far away from resonance (*13*, *14*, *19*, *32*). This revealed the center-of-mass wave function of the pairs and thus, for rotating clouds, the eventual presence of vortices.

Figure 1 shows images of the two spin states for varying population imbalance, originating from the BEC side ($B < 834$ G) and from the BCS side ($B > 834$ G) of the resonance. Starting with a pure Fermi sea in state $|1\rangle$, we see how gradually, for increasing numbers in the second spin state $|2\rangle$, first a normal (uncondensed) cloud of fermion pairs emerges, then a condensate peak appears within the normal cloud (see also Fig. 3, A and B). The condensate can be clearly distinguished in the minority cloud as the dense

Imbalanced spin populations. As the starting point of our experiments, we prepared a degenerate Fermi gas of spin-polarized ^{6}Li atoms, using methods of laser cooling, sympathetic cooling by sodium atoms, and optical trapping (*32*). A radiofrequency sweep with an adjustable sweep rate created a variable spin mixture of the two lowest hyperfine states, labeled $|1\rangle$ and $|2\rangle$. Interactions between these two states are strongly enhanced around a 300-G-wide Feshbach resonance located at $B_0 = 834$ G. At lower values of the magnetic-bias field B, two isolated fermions can bind into a stable molecule (BEC side), whereas at higher values fermion pairs can exist only in the stabilizing presence of the surrounding gas (BCS side). The interaction is described by the parameter $1/k_Fa$, where a is the scattering length and k_F is defined as the Fermi momentum of a noninteracting, equal spin mixture.

central region (appearing as white in the image) surrounded by the lower density normal component (appearing as gray). As the condensate size increases and the friction due to the normal component decreases, vortices appear in the rotating cloud, a direct and unambiguous signature of superfluid flow. As expected, the largest condensates with the largest number of vortices are obtained for an equal mixture. However, superfluidity in the strongly interacting Fermi gas is clearly not constrained to a narrow region around the perfectly balanced spin mixture, but is observed for large population asymmetries.

Figures 1 and 2 summarize our findings for rotating spin mixtures and displays the number of detected vortices versus the population imbalance between the two spin states. The vortex number measures qualitatively how deep the system is in the superfluid phase: The higher the nonsuperfluid fraction, the faster the condensate's rotation will damp given the nonvanishing anisotropy $[(\omega_x - \omega_y)/(\omega_x + \omega_y) \approx 1.5\%]$ of our trap (*19*, *33*, *34*). Figure 2 therefore shows the shrinking of the superfluid region with decreasing interaction strength on the BCS side, closing in on the optimal situation of equal populations.

The fraction of condensed fermion pairs. Close to the breakdown of superfluidity, vortices are strongly damped and difficult to observe. Therefore, the presence of vortices provides only a lower bound on the size of the superfluid window. A more detailed map of the superfluid phase as a function of interaction strength and temperature was obtained from a study of condensate fractions, determined from cloud profiles such as those shown in Fig. 3. Throughout the whole crossover region, pair condensation occurred for a broad range of population imbalances. As expected, this range was even wider than that obtained from the observation of vortices.

An intriguing property of the superfluid state with imbalanced populations is the clear depletion in the excess fermions of the majority component (Fig. 3C). The profiles in Fig. 3 present the axially integrated density; hence, the true depletion in the 3D density is even stronger. The condensate seems to repel the excess fermions. This feature was observed after expansion at 690 G, where interactions are still strong (initially $1/k_F a \approx 2.0$). The expansion, at least in the region around the condensate, is hydrodynamic and should proceed as a scaling transformation (*35*, *36*). Therefore, the depletion observed in expansion hints at spatial phase separation of the superfluid from the normal state. This effect was observed throughout the resonance region, and on resonance even when no magnetic field ramps were performed during expansion. After submission of our work, depletion of excess fermions in the center of the trap was reported (*37*). However, to distinguish a phase-separated state with equal densities in the superfluid region from more exotic states allowing unequal densities, a careful analysis of the 3D density, reconstructed from the integrated optical densities, will be necessary.

We did not observe (by simultaneously imaging along the long and short axis) a modulation in the condensate density as would be predicted for the FFLO state (*23*, *38*, *39*). However, this state is predicted to be favored only in a narrow region of parameter space and might have escaped our attention.

The condensate fraction was determined from the minority component, which in all cases is very well fit by a Gaussian for thermal molecules and unpaired atoms, plus a Thomas-Fermi profile for the condensate (fig. S2) (*32*). Figure 4 shows the condensate fraction obtained for varying population difference and temperature, and for several magnetic fields (i.e., interaction strengths) around resonance. The data for 754 G, on the BEC side of the resonance, show condensation over almost the entire range of population imbalance. As the interaction strength is increased toward resonance, the condensate fraction for equal mixtures grows (*14*). However, for large population asymmetries, the condensate disappears. The window of condensation shrinks further as we cross the resonance and move to the BCS side (Fig. 4, 833 to 924 G).

The temperature varied with number imbalance, as indicated in the insets of Fig. 4. The temperature maximum for equal mixtures at 754 G is likely due to the greater energy release when more deeply bound molecules were formed and explains the smaller condensate fraction for equal mixtures found at this field. For higher fields, the temperature changes much less with the spin composition (*32*). The observed critical population imbalance was only weakly dependent on temperature. This may reflect the fact that well below the critical temperature for superfluidity, the pairing gap is only weakly dependent on temperature (*40*). The critical imbalance at our coldest temperatures will thus essentially coincide with its value at zero temperature.

On resonance, where the scattering length a diverges, the system is in the unitary regime (*41*), where the only remaining energy scales of the system are the Fermi energies $E_{F,1}$ and $E_{F,2}$ of the two spin components (*42*). The breakdown of

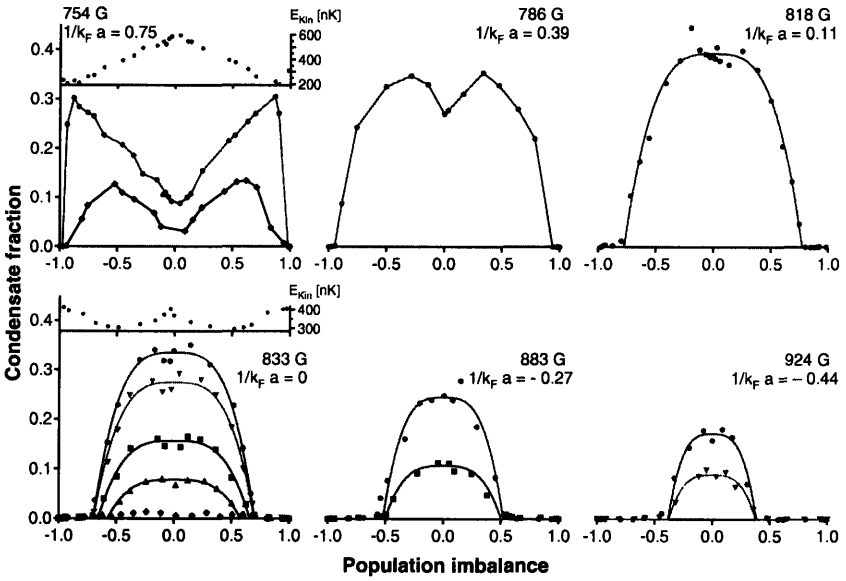

Fig. 4. Condensate fraction versus population imbalance for several temperatures and interaction strengths. The total number of atoms $N = 2.3 \times 10^7$ is constant to within 20% for all data points ($T_F = 1.9$ μK for an equal mixture) (*32*). For a given population imbalance, the uppermost curves for different magnetic fields are approximately isentropically connected. The different symbols correspond to different evaporation ramps. The average radial kinetic energy per molecule of thermal clouds in the minority component serves as an indicator for temperature and is shown in the insets for 754 G (upper) and 833 G (lower) for the coldest data. On resonance, for a population asymmetry of 50%, we measure an energy of $k_B \times 300$ nK (circles) (k_B is the Boltzmann constant), 345 nK (inverted triangles), 390 nK (squares), 420 nK (triangles), and 505 nK (diamonds). The critical population imbalance δ_c for the breakdown of condensation at 754 G is about $\delta_c^{754} \approx 96\%$, and at 786 G it is $\delta_c^{786} \approx 95\%$. For the data at higher magnetic fields, we determine δ_c through a threshold fit to the first three data points with nonzero condensate fraction for each sign of asymmetry. Although we could have used any reasonable threshold function, empirically, it was found that the function $n_c(1 - |\delta/\delta_c|^{3.3})$ (n_c = maximum condensate fraction) provided a good fit to all data points. Therefore, it was used for the threshold fits and is shown as a guide to the eye.

superfluidity occurs for a certain universal ratio of these two or equivalently, in a harmonic trap, for a certain critical population imbalance. We determine this universal number to be $\delta_c \approx \pm 70(3)\%$ for our approximately harmonic trapping potential. In (*37*), depletion of excess fermions was reported up to an imbalance of 85% and was interpreted as indirect evidence for superfluidity. However, superfluidity was not directly observed, and our data show that the system is normal at this imbalance.

The critical imbalance δ_c corresponds to a Fermi energy difference $\delta E_F = E_{F,2} - E_{F,1} = [(1 + \delta_c)^{1/3} - (1 - \delta_c)^{1/3}]E_F = 0.53(3)E_F$, where E_F is the Fermi energy of an equal mixture of noninteracting fermions. The standard BCS state is predicted (*1*) to break down for a critical chemical-potential difference $\delta\mu = \sqrt{2}\,\Delta$. On resonance, however, Monte-Carlo studies predict (*24*) the superfluid breakdown to occur when $\delta\mu = 2.0(1)\Delta = 1.0(1)E_F$. Only in the weakly interacting regime do the chemical potentials equal the Fermi energies. Quantitative agreement with the Monte-Carlo study would require that $\delta\mu \approx 2\delta E_F$. This is not unreasonable given that interactions will reduce the chemical potential of the minority component. In a preliminary analysis, we indeed find close agreement with theory.

Figure 5 summarizes our findings, showing the critical mismatch in Fermi energies for which we observed the breakdown of superfluidity as well as the pairing gap Δ versus the interaction parameter $1/k_F a$. Far on the BEC side of the resonance, the superfluid is very robust with respect to population imbalance. Here, pairing is dominantly a two-body process: The smallest cloud of atoms in state $|1\rangle$ will fully pair with atoms in state $|2\rangle$ and condense at sufficiently low temperatures. On the BCS side of the resonance, however, pairing is purely a many-body effect and depends on the density of the two Fermi clouds. As the density of the minority component becomes smaller, the net energy gain from forming a pair condensate will decrease. Even at zero temperature, this eventually leads to the breakdown of superfluidity and the quantum phase transition to the normal state. We have experimentally confirmed the qualitative picture that fermionic superfluidity breaks down when the difference in chemical potentials between the two species becomes larger than the pairing gap.

Concluding remarks and outlook. We have observed superfluidity with imbalanced spin populations. Contrary to expectations for the weakly interacting case, superfluidity in the resonant region is extremely stable against population imbalance. As the asymmetry is increased, we observe the quantum phase transition to the normal state, known as the Pauli limit of superfluidity. Our observation opens up intriguing possibilities for further studies on Fermi systems with mismatched Fermi surfaces. One important aspect concerns the density distribution in the superfluid regime. Standard BCS theory allows only equal spin densities, which would entail complete phase separation of the superfluid from the normal density. More exotic solutions (*6*) allow superfluidity also with imbalanced densities, most notably the FFLO state. A more detailed scan of the parameter space and precise measurements of spatial profiles might resolve the long-standing question of the true ground state. Equally fascinating is the nature of the strongly correlated normal state slightly below resonance. For sufficient population imbalance, we have the remarkable situation in which bosonic molecules, stable even in isolation, do not condense at zero temperature, owing to the presence of the Fermi sea.

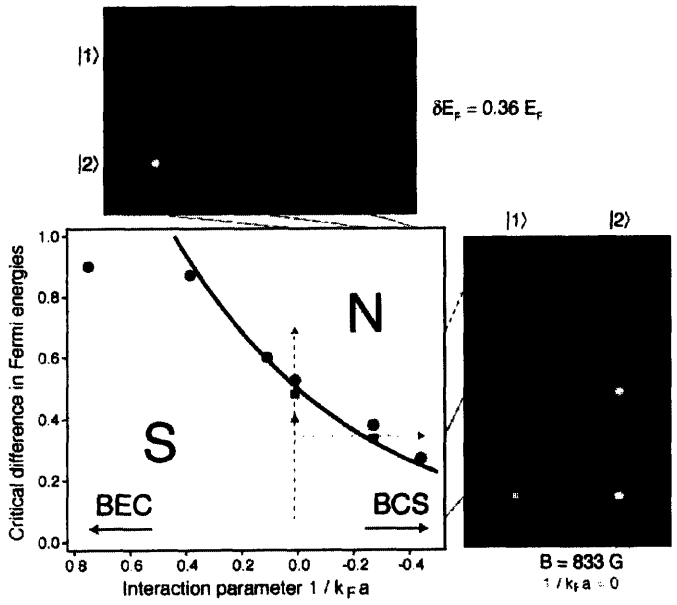

Fig. 5. Critical difference in Fermi energies δE_F between the two spin states for which the superfluid-to-normal transition is observed. δE_F for each interaction strength and temperature is obtained from the critical population imbalance determined in Fig. 3 using $\delta E_F/E_F = (1 + \delta_c)^{1/3} - (1 - \delta_c)^{1/3}$. The symbols are defined in Fig. 3. The line shows the expected variation of the pairing gap Δ, where the value on resonance has been taken from (*24*) and the exponential behavior in the BCS regime, $\Delta \sim e^{-\pi/2k_F|a|}$, was assumed. Although the trend of δE_F is expected to follow that of Δ, the close agreement is coincidental. Representative density profiles illustrate the quantum phase transition for fixed interaction and for fixed population imbalance along the dashed lines.

References and Notes

1. A. M. Clogston, *Phys. Rev. Lett.* **9**, 266 (1962).
2. P. Fulde, R. A. Ferrell, *Phys. Rev.* **135**, A550 (1964).
3. A. J. Larkin, Y. N. Ovchinnikov, *Zh. Eksp. Teor. Fiz.* **47**, 1136 (1964) [*Sov. Phys. JETP* **20**, 762 (1965)].
4. G. Sarma, *J. Phys. Chem. Solids* **24**, 1029 (1963).
5. W. V. Liu, F. Wilczek, *Phys. Rev. Lett.* **90**, 047002 (2003).
6. R. Casalbuoni, G. Nardulli, *Rev. Mod. Phys.* **76**, 263 (2004).
7. H. A. Radovan *et al.*, *Nature* **425**, 51 (2003).
8. A. Bianchi, R. Movshovich, C. Capan, P. G. Pagliuso, J. L. Sarrao, *Phys. Rev. Lett.* **91**, 187004 (2003).
9. D. Vollhardt, P. Wölfle, *The Superfluid Phases of Helium 3* (Taylor & Francis, London, 1990).
10. C. A. Regal, C. Ticknor, J. L. Bohn, D. S. Jin, *Nature* **424**, 47 (2003).
11. S. Jochim *et al.*, *Science* **302**, 2101 (2003).
12. M. W. Zwierlein *et al.*, *Phys. Rev. Lett.* **91**, 250401 (2003).
13. C. A. Regal, M. Greiner, D. S. Jin, *Phys. Rev. Lett.* **92**, 040403 (2004).
14. M. W. Zwierlein *et al.*, *Phys. Rev. Lett.* **92**, 120403 (2004).
15. T. Bourdel *et al.*, *Phys. Rev. Lett.* **93**, 050401 (2004).
16. J. Kinast, S. L. Hemmer, M. E. Gehm, A. Turlapov, J. E. Thomas, *Phys. Rev. Lett.* **92**, 150402 (2004).
17. C. Chin *et al.*, *Science* **305**, 1128 (2004).
18. G. B. Partridge, K. E. Strecker, R. I. Kamar, M. W. Jack, R. G. Hulet, *Phys. Rev. Lett.* **95**, 020404 (2005).
19. M. W. Zwierlein, J. R. Abo-Shaeer, A. Schirotzek, C. H. Schunck, W. Ketterle, *Nature* **435**, 1047 (2005).
20. D. M. Eagles, *Phys. Rev.* **186**, 456 (1969).
21. A. J. Leggett, in *Modern Trends in the Theory of Condensed Matter. Proceedings of the XVIth Karpacz Winter School of Theoretical Physics, Karpacz, Poland, 1980* (Springer-Verlag, Berlin, Karpacz, Poland, 1980), pp. 13–27.
22. P. Nozières, S. Schmitt-Rink, *J. Low Temp. Phys.* **59**, 195 (1985).
23. A. Sedrakian, J. Mur-Petit, A. Polls, H. Müther, *Phys. Rev. A.* **72**, 013613 (2005).
24. J. Carlson, S. Reddy, *Phys. Rev. Lett.* **95**, 060401 (2005).
25. C.-H. Pao, S.-T. Wu, S.-K. Yip, preprint available at http://xxx.lanl.gov/abs/cond-mat/0506437.
26. D. E. Sheehy, L. Radzihovsky, preprint available at http://xxx.lanl.gov/abs/cond-mat/0508430.
27. D. T. Son, M. A. Stephanov, preprint available at http://xxx.lanl.gov/abs/cond-mat/0507586.
28. K. Yang, preprint available at http://xxx.lanl.gov/abs/cond-mat/0508484.
29. L. Viverit, C. J. Pethick, H. Smith, *Phys. Rev. A.* **61**, 053605 (2000).
30. S. Powell, S. Sachdev, H. P. Büchler, *Phys. Rev. B* **72**, 024534 (2005).
31. P. F. Bedaque, H. Caldas, G. Rupak, *Phys. Rev. Lett.* **91**, 247002 (2003).

32. Materials and methods are available as supporting material on *Science* Online.
33. J. R. Abo-Shaeer, C. Raman, W. Ketterle, *Phys. Rev. Lett.* **88**, 070409 (2002).
34. D. Guéry-Odelin, *Phys. Rev. A.* **62**, 033607 (2000).
35. Y. Kagan, E. L. Surkov, G. V. Shlyapnikov, *Phys. Rev. A.* **55**, R18 (1997).
36. C. Menotti, P. Pedri, S. Stringari, *Phys. Rev. Lett.* **89**, 250402 (2002).
37. G. B. Partridge, W. Li, R. I. Kamar, Y.-a. Liao, R. G. Hulet, *Science*, **311**, 503 (2006); published online 22 December 2005 (10.1126/science.1122876).
38. T. Mizushima, K. Machida, M. Ichioka, *Phys. Rev. Lett.* **94**, 060404 (2005).
39. P. Castorina, M. Grasso, M. Oertel, M. Urban, D. Zappalà, *Phys. Rev. A.* **72**, 025601 (2005).
40. A. A. Abrikosov, L. P. Gorkov, I. E. Dzyaloshinski, *Methods of Quantum Field Theory in Statistical Physics* (Dover, New York, 1975).
41. G. Bertsch, INT Workshop on Effective Field Theory in Nuclear Physics (Seattle, WA, February 1999).
42. T. D. Cohen, *Phys. Rev. Lett.* **95**, 120403 (2005).
43. We thank G. Campbell for critical reading of the manuscript and X.-G. Wen, E. Demler, and S. Sachdev for stimulating discussions. This work was supported by the NSF, Office of Naval Research, Army Research Office, and NASA.

Supporting Online Material

www.sciencemag.org/cgi/content/full/1122318/DC1
Materials and Methods
Figs. S1 and S2
References and Notes

7 November 2005; accepted 14 December 2005
Published online 22 December 2005;
10.1126/science.1122318
Include this information when citing this paper.

Community Genomics Among Stratified Microbial Assemblages in the Ocean's Interior

Edward F. DeLong,[1]* Christina M. Preston,[2] Tracy Mincer,[1] Virginia Rich,[1] Steven J. Hallam,[1] Niels-Ulrik Frigaard,[1] Asuncion Martinez,[1] Matthew B. Sullivan,[1] Robert Edwards,[3] Beltran Rodriguez Brito,[3] Sallie W. Chisholm,[1] David M. Karl[4]

Microbial life predominates in the ocean, yet little is known about its genomic variability, especially along the depth continuum. We report here genomic analyses of planktonic microbial communities in the North Pacific Subtropical Gyre, from the ocean's surface to near–sea floor depths. Sequence variation in microbial community genes reflected vertical zonation of taxonomic groups, functional gene repertoires, and metabolic potential. The distributional patterns of microbial genes suggested depth-variable community trends in carbon and energy metabolism, attachment and motility, gene mobility, and host-viral interactions. Comparative genomic analyses of stratified microbial communities have the potential to provide significant insight into higher-order community organization and dynamics.

Microbial plankton are centrally involved in fluxes of energy and matter in the sea, yet their vertical distribution and functional variability in the ocean's interior is still only poorly known. In contrast, the vertical zonation of eukaryotic phytoplankton and zooplankton in the ocean's water column has been well documented for over a century (*1*). In the photic zone, steep gradients of light quality and intensity, temperature, and macronutrient and trace-metal concentrations all influence species distributions in the water column (*2*). At greater depths, low temperature, increasing hydrostatic pressure, the disappearance of light, and dwindling energy supplies largely determine vertical stratification of oceanic biota.

For a few prokaryotic groups, vertical distributions and depth-variable physiological properties are becoming known. Genotypic and phenotypic properties of stratified *Prochlorococcus* "ecotypes" for example, are suggestive of depth-variable adaptation to light intensity and nutrient availability (*3*–*5*). In the abyss, the vertical zonation of deep-sea piezophilic bacteria can be explained in part by their obligate growth requirement for elevated hydrostatic pressures (*6*). In addition, recent cultivation-independent (*7*–*15*) surveys have shown vertical zonation patterns among specific groups of planktonic *Bacteria*, *Archaea*, and *Eukarya*. Despite recent progress however, a comprehensive description of the biological properties and vertical distributions of planktonic microbial species is far from complete.

Cultivation-independent genomic surveys represent a potentially useful approach for characterizing natural microbial assemblages (*16*, *17*). "Shotgun" sequencing and whole genome assembly from mixed microbial assemblages has been attempted in several environments, with varying success (*18*, *19*). In addition, Tringe *et al.* (*20*) compared shotgun sequences of several disparate microbial assemblages to identify community-specific patterns in gene distributions. Metabolic reconstruction has also been attempted with environmental genomic approaches (*21*). Nevertheless, integrated genomic surveys of microbial communities along well-defined environmental gradients (such as the ocean's water column) have not been reported.

To provide genomic perspective on microbial biology in the ocean's vertical dimension, we cloned large [~36 kilobase pairs (kbp)] DNA fragments from microbial communities at different depths in the North Pacific Subtropical Gyre (NPSG) at the open-ocean time-series station ALOHA (*22*). The vertical distribution of microbial genes from the ocean's surface to abyssal depths was determined by shotgun sequencing of fosmid clone termini. Applying identical collection, cloning, and sequencing strategies at seven depths (ranging from 10 m to 4000 m), we archived large-insert genomic libraries from each depth-stratified microbial community. Bidirectional DNA sequencing of fosmid clones (~10,000 sequences per depth) and comparative sequence analyses were used to identify taxa, genes, and metabolic pathways that characterized vertically stratified microbial assemblages in the water column.

Study Site and Sampling Strategy

Our sampling site, Hawaii Ocean Time-series (HOT) station ALOHA (22°45' N, 158°W), represents one of the most comprehensively characterized sites in the global ocean and has been a focal point for time series–oriented oceanographic studies since 1988 (*22*). HOT investigators have produced high-quality spatial and time-series measurements of the defining physical, chemical, and biological oceanographic parameters from surface waters to the seafloor. These detailed spatial and temporal datasets present unique opportunities for placing microbial genomic depth profiles into appropriate oceanographic context (*22*–*24*) and leverage these data to formulate meaningful ecological hypotheses. Sample depths were selected, on the basis of well-defined physical, chemical, and biotic characteristics, to represent discrete zones in the water column (Tables 1 and 2, Fig. 1; figs. S1 and S2). Specifically, seawater samples from the upper euphotic zone (10 m and 70 m), the base of the chlorophyll maximum (130 m), below the base of the euphotic zone (200 m), well below the upper mesopelagic (500 m), in the core of the dissolved oxygen minimum layer (770 m), and in the deep abyss, 750 m above the seafloor (4000 m), were collected for preparing microbial community DNA libraries (Tables 1 and 2, Fig. 1; figs. S1 and S2).

The depth variability of gene distributions was examined by random, bidirectional end-sequencing of ~5000 fosmids from each depth, yielding ~64 Mbp of DNA sequence total from the 4.5 Gbp archive (Table 1). This represents raw sequence coverage of about 5 (1.8 Mbp sized) genome equivalents per depth. Because we surveyed ~180 Mbp of cloned DNA (5000 clones by

[1]Massachusetts Institute of Technology, Cambridge, MA 02139, USA. [2]Monterey Bay Aquarium Research Institute, Moss Landing, CA 95064, USA. [3]San Diego State University, San Diego, CA 92182, USA. [4]University of Hawaii Honolulu, HI 96822, USA.

*To whom correspondence should be addressed. E-mail: delong@mit.edu

Fermionic Superfluidity with Imbalanced Spin Populations

Martin W. Zwierlein, André Schirotzek, Christian H. Schunck, Wolfgang Ketterle

Materials and Methods

Creation of ultracold imbalanced spin mixtures. To map out the superfluid regime as a function of population imbalance, we use two complementary techniques: the detection of vortices in a rotating cloud (*S1*) and the determination of the fraction of condensed fermion pairs in non-rotating mixtures (*S2–S4*). The two experimental methods require slightly different procedures for imaging the pair condensate wavefunction after release from the trap. To determine the fraction of condensed vs uncondensed pairs, the condensate must separate well from the thermal cloud and should therefore remain small. For the detection of rotating clouds, the condensate should expand to a large size in order to magnify the vortices. In the following, we give the parameters used to determine the condensate fraction (experiment B) in parentheses after those used for vortex detection (experiment A).

In the first stage of the experiment, fermionic ^{6}Li atoms were sympathetically cooled to degeneracy by ^{23}Na atoms in a magnetic trap (*S5*). The ultracold cloud was subsequently loaded into an optical dipole trap (waist $w \approx 120\,\mu$m) at a maximum trap depth of about 8 μK. At a magnetic bias field of 875 G, a variable spin-mixture of the two lowest hyperfine states (labelled $|1\rangle$ and $|2\rangle$) was created via a Landau-Zener radiofrequency sweep with an adjustable sweep rate. The spin mixture was evaporatively cooled further by lowering the trap depth to 1.6 μK resulting in radial and axial trap frequencies of $\nu_r = 110$ Hz and $\nu_a = 23$ Hz, respectively. At the same time, the magnetic field was ramped to about 815 G, which is on the BEC-side close to the Feshbach resonance at 834 G (*S6*), and deep in the strongly interacting regime. The rather moderate evaporation still leaves room for thermal molecules in an equal mixture, but was chosen to efficiently cool highly asymmetric mixtures, avoiding spilling of large Fermi clouds. This ensured that the total number of atoms was approximately constant and independent of the asymmetry between the two spin states (see Fig. S1).

For the vortex experiment, we set the spin mixture in rotation using two blue-detuned laser beams (wavelength 532 nm) rotated symmetrically around the cloud at angular frequency $\Omega = 2\pi\,70$ Hz) (*S1*). After 800 ms of stirring, the rotating cloud was left to equilibrate for several hundred ms (*S7*).

Tuning the interactions and imaging the cloud. Starting with either the rotating or the non-rotating cloud, we varied the interaction strength between the two spin states in the gas by ramping the magnetic field in 100 ms (experiment B: 500 ms) to several values around the Feshbach resonance (for the condensate fraction experiment B, the trap depth was simultaneously increased to 4 μK (ν_r = 192 Hz)). After 50 ms (B: 100 ms) of hold time, an image of the cloud was taken following the procedure outlined in (*S1*): After releasing the cloud from the optical trap the binding energy of fermion pairs was rapidly increased by ramping the magnetic field within 2 ms (B: 200 μs) to 690 G, in the far wings of the resonance on the BEC side. Here, fermion pairs were stable throughout further expansion. After a total of 11 ms (B: 14 ms) of expansion (in the remaining magnetic saddle-point potential) an image of either state $|1\rangle$ or state $|2\rangle$ was taken. In experiment A on vortices, the clouds were imaged at 690 G. For the condensate fraction data (B), the magnetic field was suddenly switched to 800 G right before imaging. At this field the molecules absorb the probe light with the same strength as free atoms (reduced to 75% at 690 G). The images revealed the center-of-mass wavefunction of the pairs and, for rotating clouds, eventually the presence of vortices. For the condensate fraction experiment, the 200 μs fast ramp to the BEC-side immediately after release from the trap ensured that even large condensates separated well from the normal, uncondensed component. A rapid ramp to zero field would result in an even better separation (*S3, S4*), but we found that field sweeps into regions far outside the resonance cause loss of observed atoms (*S4*). Since the ramp was fast compared to the radial trapping period, the size of the expanded condensate was mostly governed by the residual mean-field interaction at 690 G, where $a = 1400\,a_0$. This expanded size was actually smaller than that of a condensate released from equilibrium at 690 G, because of the lower mean-field energy before expansion.

The described approach to detect fermion pair condensates originating from the BCS-side was theoretically discussed by several authors (*S8–S12*). In some cases (*S8, S10, S11*) even quantitative agreement with experiments (*S2, S3*) was reached. It is reasonable to assume that condensed fermion pairs on the BCS-side can transform into zero-momentum molecules, as long as their original pair size is smaller than the interparticle spacing. Experimentally, our group showed that the formation dynamics of these condensates is slow compared to the time needed to cross resonance in the rapid ramp (*S4*), excluding growth of the condensate during the ramp. The ramp employed in our present work does not result in loss of atoms, previously encountered for ramps to zero field (*S4*). The condensate fraction is thus a direct measure of the superfluid component in the mixture.

Determining the condensate fraction. Fig. S2 shows typical optical density profiles originating from resonance. Azimuthal averaging resulted in very good signal-to-noise in the optical density, with relative fluctuations of 10^{-3}. The total signal fluctuated from shot-to-shot by about 5%, due to frequency fluctuations of the imaging laser, but the profile's shape was not affected. Imperfections in the polarization of the light, stray light etc. tend to systematically lower the optical density. Indeed, the total signal obtained by imaging with circularly polarized light along the magnetic field axis was 20% smaller than the (more robust) number obtained from imaging perpendicular to the magnetic field axis. The latter coincided with the total number of atoms, which was calibrated by measuring the trap frequencies and the Fermi radius of almost perfectly spin-polarized degenerate Fermi clouds (a pure spin-polarized Fermi gas would not reach thermal equilibrium due to Pauli suppression of collisions).

The profile of the minority component was very well fit by a bimodal fit, consisting of a gaussian $e^{-r^2/2R_{\rm th}^2}$ plus a Thomas-Fermi-profile of the form $(1-x^2)^{3/2}$ for the condensate. The standard deviation in the condensate fraction for three measurements taken over the course of an hour was 1%, while the standard deviation of the population imbalance was 3%. A more refined fitting function, accounting for depletion of the thermal cloud in the presence of the condensate, increased the condensate fraction by at most 10% (for a condensate fraction of 50%), without changing the quality of the fit (see Fig. S2).

The highest condensate fractions of 40% were limited by the chosen evaporation ramp, which avoided spilling of large Fermi clouds but did not result in the coldest attainable temperatures for equal mixtures (see Fig. S1). Essentially pure condensates, with no appreciable thermal component, were achieved in equal mixtures by evaporating to a lower final trap depth. For asymmetric mixtures, such a ramp strongly reduces the population imbalance by preferentially removing unpaired atoms.

Thermometry in the strongly interacting regime. The width of the expanded thermal molecular cloud $R_{\rm th}$ after the rapid ramp to the BEC-side provides an upper limit for the system's temperature (see Fig. S1). The average radial kinetic energy per molecule in the thermal cloud is given by $E_{\rm kin} = 2mR_{\rm th}^2/t^2$, where m is the mass of a lithium atom and t is the expansion time. A standard correction was applied to this formula accounting for the cloud's expansion in the harmonic saddle-point potential. For a non-interacting cloud, $E_{\rm kin}/k_B$ equals the temperature of the gas, where k_B is Boltzmann's constant. Interactions increase $E_{\rm kin}$. Note, however, that the mixture immediately after the rapid ramp to the BEC-side is more dilute than an equilibrium sample at 690 G, due to the large initial size of the Fermi gas on the BCS-side. $E_{\rm kin}/k_B$ should therefore be a good estimate of the system's temperature. Indeed, for equal mixtures on resonance, a condensate was observed when $E_{\rm kin}/E_F$ (E_F is the Fermi energy of an equal mixture) was lowered from 0.34 (diamonds in Fig. 4, 833 G) to 0.28 (triangles in Fig. 4). This is close to the predictions $T_{\rm C}/T_{\rm F} = 0.29$ (*S13*), $T_{\rm C}/T_{\rm F} = 0.31$ (*S14*) and $T_{\rm C}/T_{\rm F} = 0.3$ (*S15*) for the ratio of the critical temperature of superfluidity on resonance and the Fermi temperature $T_{\rm F} = E_{\rm F}/k_B$.

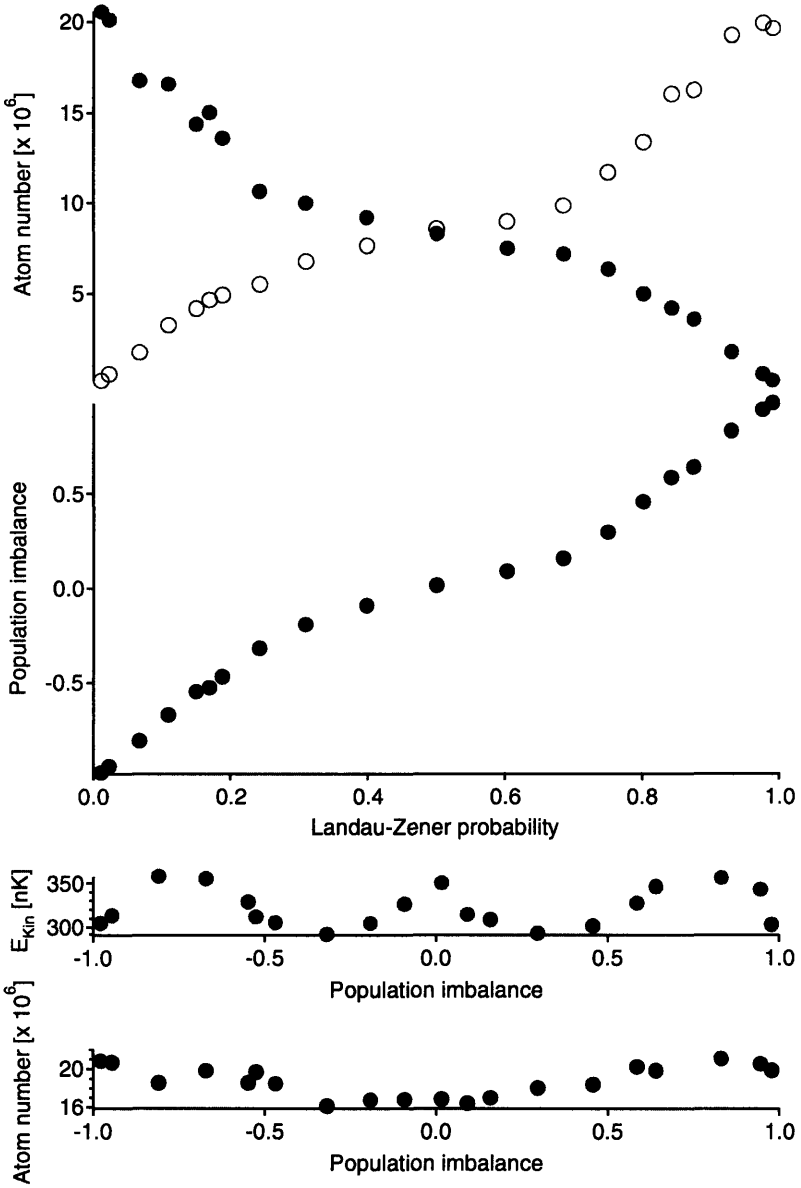

Figure 1: Upper two panels: Dependence of the spin populations after evaporation and their imbalance as a function of the rate of the radiofrequency sweep applied to control the spin populations at full trap depth. These sweeps are characterized by their Landau-Zener transfer probability. Lower panels: Dependence of the average radial kinetic energy and the total number of atoms in the mixture as a function of population imbalance. The clouds originate from 883 G (BCS-side, see Fig. 4). Red closed circles: Atoms in state $|1\rangle$. Open blue circles: Atoms in state $|2\rangle$. The data-points are averages of three measurements taken over the course of one hour.

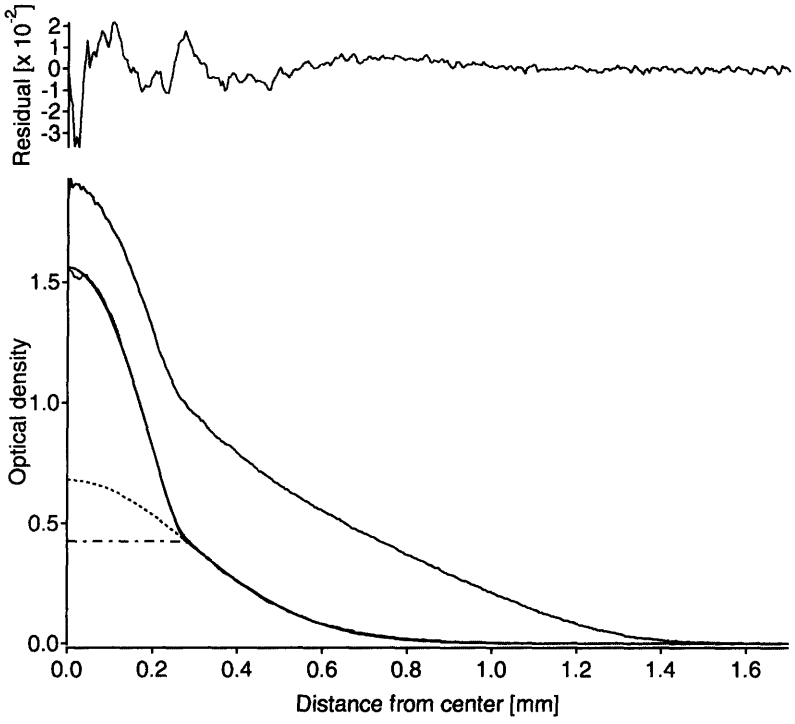

Figure 2: Radial density profiles of an unequal spin mixture originating from resonance. The density profile of the minority component (red curve) was fit using two different models for the thermal cloud: the non-interacting case (gaussian, dotted line) and the strongly interacting case of a thermal cloud that is fully separated from the condensate (leading to a flat distribution in the axially integrated profile at points where there is a condensate, dash-dotted line). The two fits are indistinguishable on the scale of this graph. The residual of the gaussian plus Thomas-Fermi-fit after subtraction of the original profile is shown on top.

References and Notes

S1. M. W. Zwierlein, J. R. Abo-Shaeer, A. Schirotzek, C. H. Schunck, W. Ketterle, *Nature* **435**, 1047 (2005).

S2. C. A. Regal, M. Greiner, D. S. Jin, *Phys. Rev. Lett.* **92**, 040403 (2004).

S3. M. W. Zwierlein, *et al.*, *Phys. Rev. Lett.* **92**, 120403 (2004).

S4. M. W. Zwierlein, C. H. Schunck, C. A. Stan, S. M. F. Raupach, W. Ketterle, *Phys. Rev. Lett.* **94**, 180401 (2005).

S5. Z. Hadzibabic, *et al.*, *Phys. Rev. Lett.* **91**, 160401 (2003).

S6. M. Bartenstein, *et al.*, *Phys. Rev. Lett.* **94**, 103201 (2004).

S7. Note that due to damping in our not perfectly round trap, the mixture will rotate at a speed lower than Ω. The vortex number in an equal mixture around 875 G (BCS-side) decayed with a time constant of 3 s. Asymmetric spin mixtures should spin down faster, due to the increased friction exerted by the non-superfluid component.

S8. T.-L. Ho. Preprint cond-mat/0404517.

S9. A. V. Avdeenkov, J. L. Bohn, *Phys. Rev. A* **71**, 023609 (2005).

S10. A. Perali, P. Pieri, G. C. Strinati, *Phys. Rev. Lett.* **95**, 010407 (2005).

S11. L. Salasnich, N. Manini, A. Parola, *Phys. Rev. A* **72**, 023621 (2005).

S12. E. Altman, A. Vishwanath, *Phys. Rev. Lett.* **95**, 110404 (2005).

S13. J. Kinast, *et al.*, *Science* **307**, 1296 (2005).

S14. A. Perali, P. Pieri, L. Pisani, G. C. Strinati, *Phys. Rev. Lett.* **92**, 220404 (2004).

S15. G. M. Bruun, H. Smith, *Phys. Rev. A* **72**, 043605 (2005).

Appendix I

Direct Observation of the Superfluid Phase Transition in Ultracold Fermi Gases

This appendix contains a reprint of Ref. [269]: Martin W. Zwierlein, Christian H. Schunck, André Schirotzek, and Wolfgang Ketterle, *Direct Observation of the Superfluid Phase Transition in Ultracold Fermi Gases*, Nature 442, 54-58 (2006)

LETTERS

Direct observation of the superfluid phase transition in ultracold Fermi gases

Martin W. Zwierlein[1], Christian H. Schunck[1], André Schirotzek[1] & Wolfgang Ketterle[1]

Phase transitions are dramatic phenomena: water freezes into ice, atomic spins spontaneously align in a magnet, and liquid helium becomes superfluid. Sometimes, such a drastic change in behaviour is accompanied by a visible change in appearance. The hallmark of Bose–Einstein condensation and superfluidity in trapped, weakly interacting Bose gases is the sudden formation of a dense central core inside a thermal cloud[1–7]. However, in strongly interacting gases—such as the recently observed fermionic superfluids[8]—there is no longer a clear separation between the superfluid and the normal parts of the cloud. The detection of fermion pair condensates has required magnetic field sweeps[9–11] into the weakly interacting regime, and the quantitative description of these sweeps presents a major theoretical challenge. Here we report the direct observation of the superfluid phase transition in a strongly interacting gas of ^{6}Li fermions, through sudden changes in the shape of the clouds—in complete analogy to the case of weakly interacting Bose gases. By preparing unequal mixtures of the two spin components involved in the pairing[12,13], we greatly enhance the contrast between the superfluid core and the normal component. Furthermore, the distribution of non-interacting excess atoms serves as a direct and reliable thermometer. Even in the normal state, strong interactions significantly deform the density profile of the majority spin component. We show that it is these interactions that drive the normal-to-superfluid transition at the critical population imbalance of 70 ± 5 per cent (ref. 12).

The dramatic signature of Bose–Einstein condensation in weakly interacting gases in atom traps derives from a natural hierarchy of energy scales: the critical temperature for condensation, $T_C \propto n^{2/3}$ at particle density n, is much larger than the chemical potential (divided by the Boltzmann constant k_B) of a pure condensate, $\mu \propto na$, which measures the interaction strength between particles (a is the scattering length). Hence, for weak (repulsive) interactions ($a > 0$, $na^3 \ll 1$), the condensate is clearly distinguished from the cloud of uncondensed particles through its smaller size and higher density. However, as the interactions are increased, for example by tuning a using a Feshbach resonance, this hierarchy of energy scales breaks down, as μ can now become comparable to $k_B T_C$. In Fermi gases with weak attractive interaction ($a < 0$, $n|a|^3 \ll 1$), the chemical potential is given by the Fermi energy E_F and will even far exceed the superfluid transition temperature $k_B T_C \propto E_F e^{-\pi/2k_F|a|}$ (where $k_F \propto n^{1/3}$ is the Fermi wave vector). Both the normal and the condensed cloud will here be of the same size and shape, dependent only on E_F and the trapping potential.

The phase transition from the normal to the superfluid state, although dramatic in its consequences, is thus not revealed by a major change in the appearance of the gas. Indeed, in strongly interacting Fermi gases no deviation from a normal cloud's shape has so far been detected, either in the unitary regime, where a diverges, or on the attractive Bardeen–Cooper–Schrieffer (BCS) side of a Feshbach resonance. Theoretical works predicted small 'kinks'[14–16] or other slight deviations[17] in the density profiles of the gas in the superfluid regime, but after line-of-sight integration these effects have so far been too small to be observable. Condensates could only be observed via rapid magnetic field ramps to the Bose–Einstein condensate (BEC) side ($a > 0$) of the Feshbach resonance, performed during expansion[9,10]. This suddenly reduced the condensate's chemical potential, and let the thermal fraction grow beyond the condensate size. A similar ramp was used to detect vortices on resonance and on the BCS side in the demonstration of fermionic superfluidity[8]. However, these magnetic field ramps are difficult to model theoretically, and a satisfactory quantitative comparison of, for example, the condensate fraction with experiments has not been accomplished[18–21].

In this work we demonstrate that the normal-to-superfluid phase transition in a strongly interacting Fermi gas can be directly observed in absorption profiles, without the need for any magnetic field ramps. As in the case of weakly interacting BECs, preparation, expansion and detection of the sample all take place at the same, fixed magnetic field and scattering length. As for BECs, the phase transition is observed as a sudden change in the shape of the cloud during time-of-flight expansion, when the trap depth is decreased below a critical value. To clearly distinguish the superfluid from the normal component, we break the number symmetry between spin-up (majority atom number, $N_\uparrow$) and spin-down (minority atom number, $N_\downarrow$) and produce an unequal mixture of fermions (imbalance parameter $\delta = (N_\uparrow - N_\downarrow)/(N_\uparrow + N_\downarrow)$). Standard BCS superfluidity requires equal densities of the two spin components. Hence, when cooled below the phase transition the cloud should show a sudden onset of a superfluid region of equal densities. Indeed, below a critical temperature, we observe how the density distribution of the minority component becomes bimodal.

Breaking the symmetry in atom numbers thus produces a direct and striking signature of the superfluid phase transition[22–24]. A similar situation has been encountered in Bose–Einstein condensation, where breaking the symmetry of a spherical trap resulted in dramatic anisotropic expansion of the condensate, now a hallmark of the BEC phase transition.

Figure 1 shows column density profiles of the two imbalanced spin states for different points along the evaporation path corresponding to different temperatures, and for three magnetic fields that correspond to the BEC side, exact resonance and the BCS side of the resonance. For large final trap depths (upper panels in Fig. 1), the smaller cloud has the expected shape of a normal, non-superfluid gas: it is very well fitted using a single, finite temperature Thomas–Fermi-profile (with central optical density, radius and the fugacity as independent fit-parameters). However, below a critical trap depth, a second, denser feature appears in the centre of the minority component (lower panels in Fig. 1). This onset of bimodality occurs very suddenly as the trap depth is lowered, as can be seen from Fig. 2: Around the critical point, the atom number (Fig. 2a) and population

[1]Department of Physics, MIT-Harvard Center for Ultracold Atoms, and Research Laboratory of Electronics, MIT, Cambridge, Massachusetts 02139, USA.

© 2006 Nature Publishing Group

imbalance (Fig. 2b) are practically constant, and the temperature (Fig. 2c) varies in a smooth linear way with the trap depth. In contrast, below the critical trap depth, the shape of the smaller cloud starts to deviate drastically from the Thomas–Fermi distribution of a normal gas, as quantified in Fig. 2d. This sudden increase in the standard deviation of a fit to a single-component fitting function is a standard way of identifying the BEC phase transition in a model-independent way[2].

Figure 2e displays the fact that below the critical trap depth a new, third radius is required to describe the two clouds. As we will see below, the appearance of this central feature coincides with the appearance of the fermion pair condensate in experiments involving the magnetic field ramp technique[10–12]. It is this condensate that contains the superfluid vortices in refs 8 and 12. We are thus naturally led to interpret the central core as the condensate of fermion pairs, and the outer wings as the normal, uncondensed part of the cloud. This constitutes, to our knowledge, the first direct observation of the normal-to-superfluid phase transition in resonantly interacting Fermi gases on resonance and on the BCS side (that is, without a magnetic field sweep that so far cannot be quantitatively accounted for).

Already at high temperatures, above the phase transition, the larger cloud's profile is strongly deformed in the presence of the smaller cloud, a direct signature of interaction. Indeed, on resonance the cloud size of the minority component is significantly smaller than that of a non-interacting sample with the same number of atoms (see Fig. 2e). At the phase transition, the outer radii of the clouds do not change abruptly. This demonstrates that interactions, not superfluidity, are the main mechanism behind the reduced cloud size of an interacting Fermi gas.

On the BEC side, the condensate is clearly visible in the larger cloud. On resonance, however, the condensate is not easily discernible in the larger component's profiles at the scale of Fig. 1. Nevertheless, we have found a very faint but reproducible trace of the condensate when analysing the curvature of these column density profiles (see Supplementary Fig. S1). On resonance and on the BCS side, the onset of bimodality in the smaller cloud can be clearly observed for imbalances larger than ~20% (but below a certain critical imbalance, see below), for which the condensate is small compared to the minority cloud size. With increasing magnetic field on the BCS side (that is, with decreasing interaction strength), the bimodality becomes less pronounced and is not clearly discerned beyond 853 G (interaction parameter $1/k_F a < -0.15$).

Thermometry of strongly interacting Fermi gases has always been a major difficulty in experiments on strongly interacting fermions[25]. A thermometer can only be reliable if the working substance is not affected by the sample to be measured. In equal mixtures of fermions, the two overlapping atomic clouds are strongly interacting throughout. Temperatures determined from a non-interacting Thomas–Fermi fit to these clouds need calibration based on approximate theoretical calculations[25]. In addition, as will be reported elsewhere, we find that those fits do not describe the profiles of a partially superfluid Fermi gas as well as they do in the normal state, in agreement with theory[14–17]. In the case of imbalanced mixtures, the wings of the larger component, where the spin-down species are absent, are non-interacting and thus serve as a direct thermometer (see Fig. 2c). For an imbalance of $\delta = 75 \pm 3\%$ we determine the critical temperature for the phase transition on the BEC side at $1/k_F a = 0.46$ to be $T/T_F = 0.18(3)$ ($k_B T_F = \hbar\omega(3(N_\uparrow + N_\downarrow))^{1/3} \equiv \hbar^2 k_F^2/2m$ is the Fermi energy of a non-interacting, equal mixture with the same total number of fermions $N_\uparrow + N_\downarrow$, $\omega/2\pi$ is the

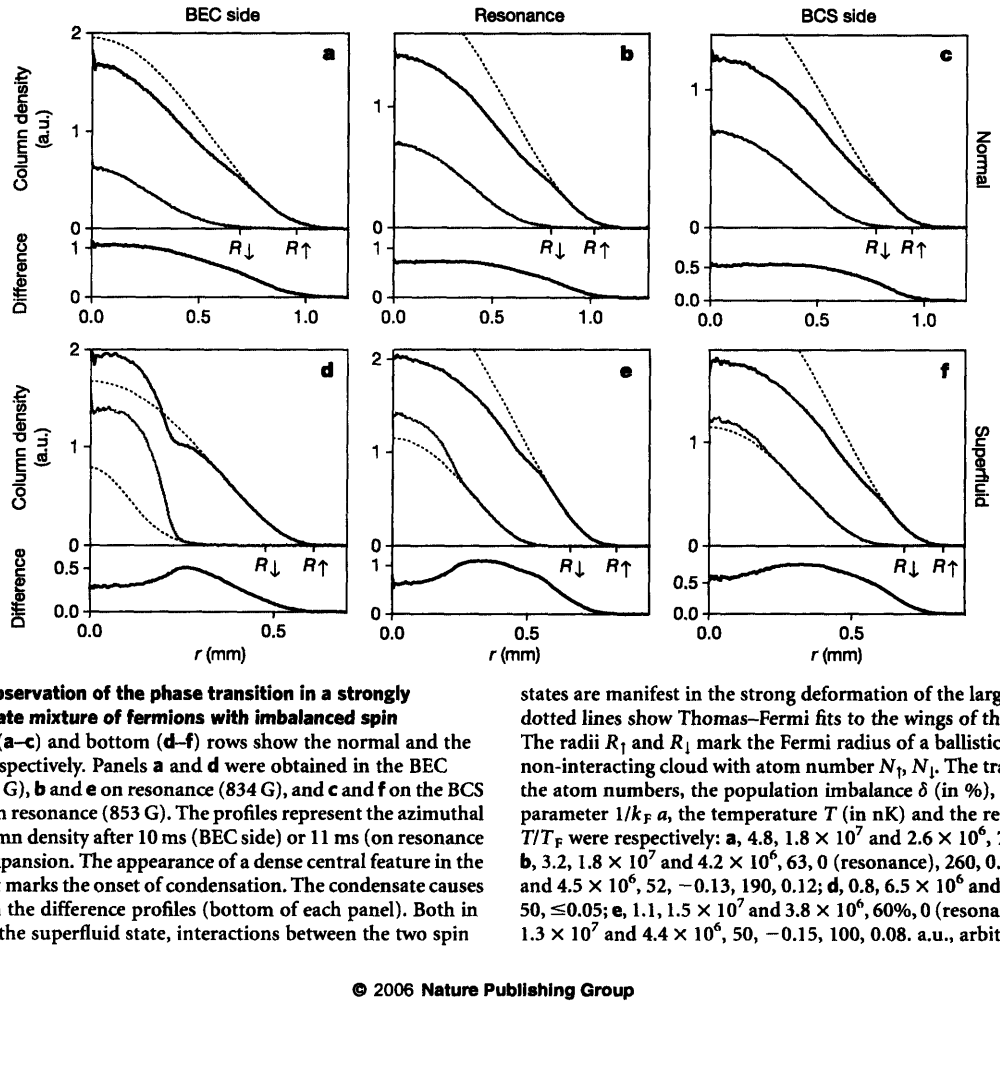

Figure 1 | Direct observation of the phase transition in a strongly interacting two-state mixture of fermions with imbalanced spin populations. Top (**a–c**) and bottom (**d–f**) rows show the normal and the superfluid state, respectively. Panels **a** and **d** were obtained in the BEC regime (at $B = 781$ G), **b** and **e** on resonance (834 G), and **c** and **f** on the BCS side of the Feshbach resonance (853 G). The profiles represent the azimuthal average of the column density after 10 ms (BEC side) or 11 ms (on resonance and BCS side) of expansion. The appearance of a dense central feature in the smaller component marks the onset of condensation. The condensate causes a clear depletion in the difference profiles (bottom of each panel). Both in the normal and in the superfluid state, interactions between the two spin states are manifest in the strong deformation of the larger component. The dotted lines show Thomas–Fermi fits to the wings of the column density. The radii $R_\uparrow$ and $R_\downarrow$ mark the Fermi radius of a ballistically expanding, non-interacting cloud with atom number $N_\uparrow$, $N_\downarrow$. The trap depth U (in μK), the atom numbers, the population imbalance δ (in %), the interaction parameter $1/k_F a$, the temperature T (in nK) and the reduced temperature T/T_F were respectively: **a**, 4.8, 1.8×10^7 and 2.6×10^6, 75, 0.42, 350, 0.20; **b**, 3.2, 1.8×10^7 and 4.2×10^6, 63, 0 (resonance), 260, 0.15; **c**, 2.5, 1.5×10^7 and 4.5×10^6, 52, −0.13, 190, 0.12; **d**, 0.8, 6.5×10^6 and 1.5×10^6, 62, 0.67, 50, ≤0.05; **e**, 1.1, 1.5×10^7 and 3.8×10^6, 60%, 0 (resonance), 70, 0.06; **f**, 1.2, 1.3×10^7 and 4.4×10^6, 50, −0.15, 100, 0.08. a.u., arbitrary units.

© 2006 Nature Publishing Group

geometric mean of the trapping frequencies, and m is the mass of ^{6}Li). This corresponds to $T/T_{C,\downarrow} = 0.55(9)$ when comparing the temperature to the critical temperature $T_{C,\downarrow}$ for Bose condensation in a non-interacting gas with $N_\downarrow$ bosons. The reduction in the critical temperature is a direct consequence of strong repulsive interactions between the molecules. On resonance, at $\delta = 59 \pm 3\%$, we find $T/T_F = 0.12(2)$, and on the BCS side ($1/k_F a = -0.14$) for $\delta = 53 \pm 3\%$ we obtain $T/T_F = 0.11(2)$. These are, to our knowledge, the first directly measured and reliable temperatures for the superfluid transition in strongly interacting Fermi gases. They may serve as a checkpoint for theoretical models.

We note that the critical temperature will in general depend on the population imbalance. For example, for large enough imbalance on resonance or on the BCS side, no condensate will form even at zero temperature[12], as we discuss below. Here, the critical temperature for superfluidity will be zero.

An important qualitative difference distinguishes the BEC side from resonance at the lowest temperatures. On the BEC side, the gas consists of only two parts—the superfluid core surrounded by a fully polarized degenerate Fermi gas of the excess species. On resonance and on the BCS side, however, there exists a third region, a normal state in which both species are mixed. Several recent theories describe

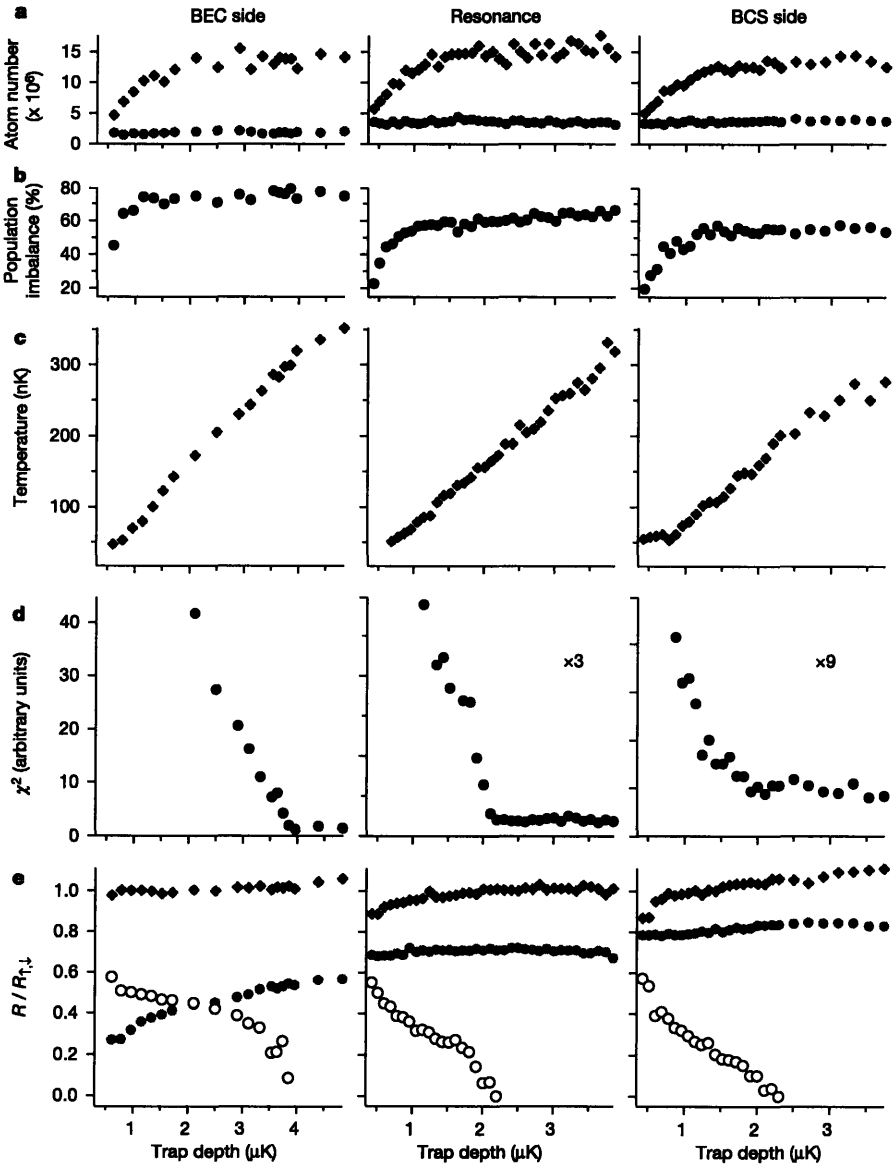

Figure 2 | Characterization of the phase transition. **a**–**e**, The data characterize the evolution of the fermion mixture as the cloud is evaporatively cooled by lowering the trap depth. The chosen magnetic fields are identical to those in Fig. 1. Data obtained from the majority (minority) cloud are shown as diamonds (circles). **a**, The atom number; **b**, the population imbalance between the two spin states; and **c**, the temperature of the spin mixture as determined from the non-interacting wings of the larger cloud's profile. **d**, A finite temperature Fermi–Dirac (for resonance and the BCS side) or gaussian (for the BEC side) distribution is fitted to the minority cloud; the phase transition is marked by a sudden increase in χ^2 as the condensate starts to appear. **e**, Outer radii of the majority and minority cloud (for the minority cloud on the BEC side, thermal cloud radius; all other cases, Thomas–Fermi radius) as well as the condensate radius (open circles), defined as the position of the 'kink' in the minority profile (see Fig. 1). The majority (minority and condensate) cloud size is normalized by the Fermi radius $R_\uparrow$ ($R_\downarrow$) of a non-interacting cloud with $N_\uparrow$ ($N_\downarrow$) atoms, and adjusted for ballistic (hydrodynamic) expansion. Note that the imbalance decreases during evaporation because the larger majority cloud incurs stronger evaporative losses. For the data, three (BEC and resonance) to five (BCS) independent measurements were averaged.

© 2006 Nature Publishing Group

density profiles of imbalanced Fermi mixtures[26–32]. Mean-field theories that neglect interactions in the normal cloud and between the normal and condensed cloud are only in qualitative agreement with our results. Descriptions that exclude the mixed region or find superfluidity on resonance at all population imbalances are ruled out by our observations.

To elucidate the origin of the clear separation between condensate and normal components, we varied the population imbalance at our coldest temperatures and on resonance. Figure 3b shows several resulting profiles after 11 ms expansion from the trap. For large imbalances, $\delta > 70\%$, the minority cloud is not bimodal and well fitted by a (unconstrained) Thomas–Fermi profile. At a critical imbalance of $\delta \approx 70\%$, the condensate appears and then grows further as the imbalance is reduced (for the cloud radii, see Supplementary Fig. S2).

To characterize the appearance of the condensate for imbalances around $\delta = 70\%$, a Thomas–Fermi profile is fitted to the wings of the minority cloud. The fraction of atoms not contained in this fit is a measure of the condensate fraction (see Fig. 3). We find a critical imbalance of $\delta_c = 70(5)\%$ above which the condensate disappears. This agrees with our previous work[12], where we employed a rapid ramp method to the BEC side to extract the condensate fraction. We observed the quantum phase transition from the superfluid to the normal state as a critical population imbalance of $\delta_c = 70\%$ was exceeded. This strongly suggests that the bimodality observed here directly in the minority component, and the bimodality observed in molecular clouds after a magnetic field sweep, are signatures of the same phase transition.

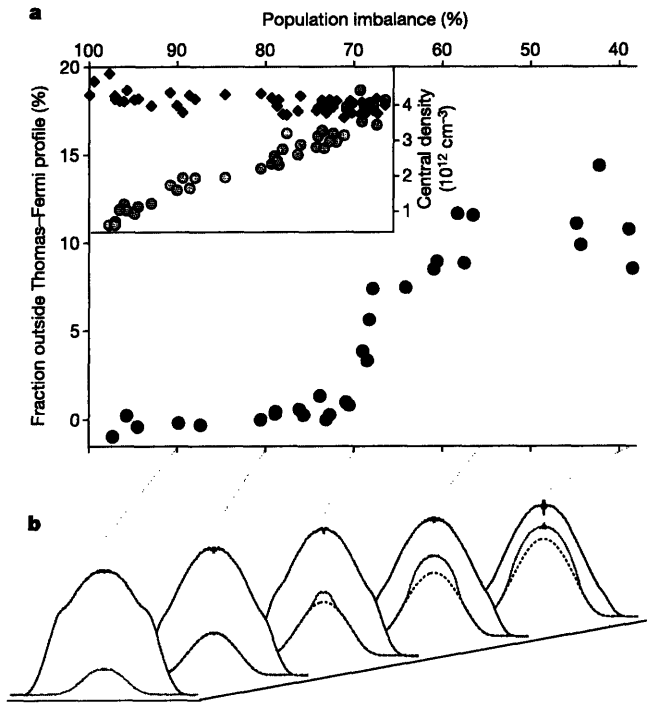

Figure 3 | Quantum phase transition to superfluidity for decreasing population imbalance. **a**, Main panel, the 'condensate fraction' of excess minority atoms, not contained in the Thomas–Fermi fit, versus population imbalance on resonance. **b**, Column density profiles of majority (blue) and minority (red) clouds, azimuthally averaged, for varying population imbalance. The condensate is clearly visible in the minority component as the dense central feature on top of the normal background (finite-temperature Thomas–Fermi fit, dotted lines). Below the critical imbalance $\delta_c = 70\%$, the condensate starts to form. The inset in **a** shows the central densities of the larger (black diamonds) and smaller (grey circles) cloud in the normal state above δ_c. This demonstrates that here the central densities are unequal, suppressing superfluidity. The densities were calculated from the central optical density and the fitted size of the clouds, assuming local density approximation and adjusting for ballistic (hydrodynamic) expansion of the outer radii of majority (minority) clouds. The data points for the condensate fraction show the average of several independent measurements.

The transition at δ_c is known as the Clogston limit of superfluidity[12,33], and occurs when the chemical potential difference $\delta\mu$ becomes larger than a constant times the (local) superfluid gap $\Delta(\mathbf{r})$ (see Supplementary Information). Here we present a simple picture for the character of this phase transition in a harmonic trap. Thomas–Fermi fits for the normal clouds beyond δ_c allow a simple estimate of the central three-dimensional density of the gas (with an estimated accuracy of 20% for the relative density difference), shown in the inset of Fig. 3. For large imbalances, we find that the three-dimensional densities differ significantly, as is expected for two weakly interacting Fermi clouds. As the imbalance is reduced towards the critical δ_c, the central densities approach each other and become approximately equal around δ_c. This is a direct consequence of strong interactions in the normal state. In a non-interacting Fermi mixture with an imbalance of δ_c, the central densities would differ by a factor of 2.4.

This observation now offers an intriguing insight into the nature of a fermionic superfluid on resonance or on the BCS side. Already in the normal state above T_C or beyond $\delta = \delta_c$, interactions between the two spin states are strong. Indeed, this is directly seen in the deformation of the majority cloud due to the presence of the minority species (see Figs 1, 3). However, here these interactions are not strong enough to let the central densities of the two clouds become comparable. At the critical imbalance the Clogston criterion $\delta\mu = c\Delta(\mathbf{r} = 0)$ is fulfilled in the centre of the trap (here, c is a constant that equals $\sqrt{2}$ in the BCS limit[33]). For smaller imbalance, a central superfluid region can form: the condensate. Its borders are defined by $\delta\mu < c\Delta(\mathbf{r})$. The simple density estimate in Fig. 3 suggests that in this region, the two clouds will have equal densities, although more refined techniques to measure small density differences have to be developed to finally settle this question. Outside the superfluid region there is still a normal state with unequal densities of minority and majority components. The discontinuity in the clouds' densities at the normal-to-superfluid phase boundary gives rise to the visible kink in the column density profiles. Such a density discontinuity is characteristic of a first-order phase transition.

Interestingly, most of the 'work' needed to build the superfluid state has already been done in the normal component by decreasing the density difference. Consequently, the critical population difference needed to form the superfluid is largely determined by the interactions in the normal gas.

In conclusion, we have observed the normal-to-superfluid phase transition through the direct observation of condensation in an imbalanced Fermi mixture—on the BEC side, on the BCS side, and right on the Feshbach resonance. Unequal mixtures offer a direct method of thermometry by analysing the non-interacting wings of the majority species. Strong interactions are already visible in the normal cloud as marked deformations of the majority profile. It is these interactions in the normal gas that squeeze the two components and eventually, at the critical imbalance, let them reach almost equal densities in the centre, aiding the formation of the superfluid. Our method of direct detection of the condensate is a powerful new tool to characterize the superfluid phase transition. At the current level of precision, the appearance of a condensate after magnetic field sweeps and the direct observation of the central dense core occur together, and indicate the normal-to-superfluid phase transition. An intriguing question is whether further phases are possible, including a more exotic superfluid state with unequal densities. Several theories predict that the Fulde–Ferrell–Larkin–Ovchinnikov state, a superfluid state with oscillating order parameter, should be present for imbalanced spin populations[24,26,28].

© 2006 Nature Publishing Group

METHODS

Experimental procedure. Our experimental setup is described in previous publications[8,12]. A spin-polarized cloud of ^{6}Li fermions is cooled to degeneracy using a combination of laser cooling and sympathetic cooling with sodium atoms in a magnetic trap. After transfer into an optical trap, a variable spin mixture of the lowest two hyperfine states, labelled $|\uparrow\rangle$ and $|\downarrow\rangle$, is prepared at a magnetic bias field of 875 G. Interactions between the two spin states can be freely tuned via a 300-G-wide Feshbach resonance located at $B_0 = 834$ G. At fields below B_0, two-body physics supports a stable molecular bound state (BEC side), while at higher fields (BCS side), no such bound state exists for two isolated atoms. Our trap combines a magnetic saddle potential with a weakly focused (waist $w \approx 120\,\mu$m) infrared laser beam (wavelength $\lambda = 1{,}064$ nm), leading to a harmonic axial confinement with oscillation frequency of $\nu_z = 22.8(0.2)$ Hz and a gaussian radial potential with variable trapping frequency ν_r in the central harmonic region. The trap depth U is related to ν_r and ν_z by:

$$U = \frac{1}{4}m(2\pi\nu_r)^2 w^2\left(1 - \frac{\nu_z^2}{2\nu_r^2}\ln\left(\frac{2\left(\nu_r^2 + \nu_z^2/2\right)}{\nu_z^2}\right)\right).$$

The initial degeneracy of the spin mixture is about $T/T_F \approx 0.3$. The strongly interacting gas is further cooled by decreasing the laser power of the optical trap over several seconds and evaporating the most energetic particles. During the first few seconds, the magnetic field is adiabatically ramped to a chosen final field in the resonance region where the last stage of the evaporation (shown in Fig. 2) takes place. For detection, the optical trap is switched off and the gas expands in the remaining magnetic saddle-point potential. After a variable time-of-flight, an absorption image of atoms either in state $|\uparrow\rangle$ or $|\downarrow\rangle$ is taken along the axial direction of the trap (the direction of the optical trapping beam). The cloud's radial symmetry allows for azimuthal averaging of the resulting column densities, leading to low-noise profiles[12].

For preparing clouds at the coldest temperatures (as shown in Fig. 3) with varying population imbalance, the spin mixture is evaporated down to a trap depth of 1 μK over several seconds on resonance, after which the trap depth is increased again to 1.4 μK for more harmonic confinement (trap frequencies: $\nu_r = 115(10)$ Hz and $\nu_z = 22.8(0.2)$ Hz). The temperature of the gas is determined to be $T/T_F \leq 0.06$ for all $\delta > 15\%$, and appears to smoothly rise to $T/T_F = 0.11$ for an equal mixture, although thermometry in the interacting wings is problematic. The total atom number was 1.5×10^7 and constant to within 15% for all values of δ.

Errors. The error in the critical temperature T_C/T_F for the phase transition is dominated by the uncertainty in the atom number entering the determination of T_F, which we estimate to be 30% (ref. 12). For T_F we use the harmonic approximation for the radially gaussian trapping potential, with the measured trapping frequencies reflecting the average curvature of the gaussian potential. The phase transition is observed above $U = 2\,\mu$K, where anharmonicities contribute only 3% to the error in T_F. Note that anharmonicities do not affect the temperature measurement performed on the majority wings: ballistic expansion of non-interacting atoms reveals their momentum distribution, regardless of the shape of the trap.

Received 6 March; accepted 23 May 2006.

1. Anderson, M. H., Ensher, J. R., Matthews, M. R., Wieman, C. E. & Cornell, E. A. Observation of Bose-Einstein condensation in a dilute atomic vapor. *Science* **269**, 198–201 (1995).
2. Davis, K. B. *et al.* Bose-Einstein condensation in a gas of sodium atoms. *Phys. Rev. Lett.* **75**, 3969–3973 (1995).
3. Greiner, M., Regal, C. A. & Jin, D. S. Emergence of a molecular Bose-Einstein condensate from a Fermi gas. *Nature* **426**, 537–540 (2003).
4. Zwierlein, M. W. *et al.* Observation of Bose-Einstein condensation of molecules. *Phys. Rev. Lett.* **91**, 250401 (2003).
5. Bartenstein, M. *et al.* Crossover from a molecular Bose-Einstein condensate to a degenerate Fermi gas. *Phys. Rev. Lett.* **92**, 120401 (2004).
6. Bourdel, T. *et al.* Experimental study of the BEC-BCS crossover region in lithium 6. *Phys. Rev. Lett.* **93**, 050401 (2004).
7. Partridge, G. B., Strecker, K. E., Kamar, R. I., Jack, M. W. & Hulet, R. G. Molecular probe of pairing in the BEC-BCS crossover. *Phys. Rev. Lett.* **95**, 020404 (2005).
8. Zwierlein, M. W., Abo-Shaeer, J. R., Schirotzek, A., Schunck, C. H. & Ketterle, W. Vortices and superfluidity in a strongly interacting Fermi gas. *Nature* **435**, 1047–1051 (2005).
9. Regal, C. A., Greiner, M. & Jin, D. S. Observation of resonance condensation of fermionic atom pairs. *Phys. Rev. Lett.* **92**, 040403 (2004).
10. Zwierlein, M. W. *et al.* Condensation of pairs of fermionic atoms near a Feshbach resonance. *Phys. Rev. Lett.* **92**, 120403 (2004).
11. Zwierlein, M. W., Schunck, C. H., Stan, C. A., Raupach, S. M. F. & Ketterle, W. Formation dynamics of a fermion pair condensate. *Phys. Rev. Lett.* **94**, 180401 (2005).
12. Zwierlein, M. W., Schirotzek, A., Schunck, C. H. & Ketterle, W. Fermionic superfluidity with imbalanced spin populations. *Science* **311**, 492–496 (2006). Published online 21 December 2005 (doi:10.1126/science.1122318).
13. Partridge, G. B., Li, W., Kamar, R. I., Liao, Y. & Hulet, R. G. Pairing and phase separation in a polarized Fermi gas. *Science* **311**, 503–505 (2006). Published online 21 December 2005 (doi:10.1126/science.1122876).
14. Chiofalo, M. L., Kokkelmans, S. J. J. M. F., Milstein, J. N. & Holland, M. J. Signatures of resonance superfluidity in a quantum Fermi gas. *Phys. Rev. Lett.* **88**, 090402 (2002).
15. Ho, T.-L. Universal thermodynamics of degenerate quantum gases in the unitarity limit. *Phys. Rev. Lett.* **92**, 090402 (2004).
16. Perali, A., Pieri, P., Pisani, L. & Strinati, G. C. BCS-BEC crossover at finite temperature for superfluid trapped Fermi atoms. *Phys. Rev. Lett.* **92**, 220404 (2004).
17. Stajic, J., Chen, Q. & Levin, K. Density profiles of strongly interacting trapped Fermi gases. *Phys. Rev. Lett.* **94**, 060401 (2005).
18. Diener, R. B. & Ho, T.-L. Projecting fermion pair condensates into molecular condensates. Preprint at ⟨http://arxiv.org/cond-mat/0404517⟩ (2004).
19. Perali, A., Pieri, P. & Strinati, G. C. Extracting the condensate density from projection experiments with Fermi gases. *Phys. Rev. Lett.* **95**, 010407 (2005).
20. Altman, E. & Vishwanath, A. Dynamic projection on Feshbach molecules: A probe of pairing and phase fluctuations. *Phys. Rev. Lett.* **95**, 110404 (2005).
21. Chen, Q., Regal, C. A., Greiner, M., Jin, D. S. & Levin, K. Understanding the superfluid phase diagram in trapped Fermi gases. *Phys. Rev. A* **73**, 041603 (2006).
22. Bedaque, P. F., Caldas, H. & Rupak, G. Phase separation in asymmetrical fermion superfluids. *Phys. Rev. Lett.* **91**, 247002 (2003).
23. Caldas, H. Cold asymmetrical fermion superfluids. *Phys. Rev. A* **69**, 063602 (2004).
24. Sheehy, D. E. & Radzihovsky, L. BEC-BCS crossover in "magnetized" Feshbach-resonantly paired superfluids. *Phys. Rev. Lett.* **96**, 060401 (2006).
25. Kinast, J. *et al.* Heat capacity of a strongly-interacting Fermi gas. *Science* **307**, 1296–1299 (2005).
26. Mizushima, T., Machida, K. & Ichioka, M. Direct imaging of spatially modulated superfluid phases in atomic fermion systems. *Phys. Rev. Lett.* **94**, 060404 (2005).
27. Pieri, P. & Strinati, G. C. Trapped fermions with density imbalance in the Bose-Einstein condensate limit. *Phys. Rev. Lett.* **96**, 150404 (2006).
28. Kinnunen, J., Jensen, L. M. & Törmä, P. Strongly interacting Fermi gases with density imbalance. *Phys. Rev. Lett.* **96**, 110403 (2006).
29. De Silva, T. N. & Mueller, E. J. Profiles of near-resonant population-imbalanced trapped Fermi gases. *Phys. Rev. A* **73**, 051602(R) (2006).
30. Yi, W. & Duan, L.-M. Trapped fermions across a Feshbach resonance with population imbalance. *Phys. Rev. A* **73**, 031604(R) (2006).
31. Chevy, F. Density profile of a trapped strongly interacting Fermi gas with unbalanced spin populations. *Phys. Rev. Lett.* **96**, 130401 (2006).
32. Haque, M. & Stoof, H. T. C. Pairing of a trapped resonantly-interacting fermion mixture with unequal spin populations. Preprint at ⟨http://arxiv.org/cond-mat/0601321⟩ (2006).
33. Clogston, A. M. Upper limit for the critical field in hard superconductors. *Phys. Rev. Lett.* **9**, 266–267 (1962).

Supplementary Information is linked to the online version of the paper at www.nature.com/nature.

Acknowledgements We thank the participants of the Aspen winter conference on strongly interacting fermions for discussions. This work was supported by the NSF, ONR and NASA.

Author Information Reprints and permissions information is available at npg.nature.com/reprintsandpermissions. The authors declare no competing financial interests. Correspondence and requests for materials should be addressed to M.W.Z. (zwierlei@mit.edu).

© 2006 Nature Publishing Group

Direct Observation of the Superfluid Phase Transition in Ultracold Fermi Gases

Martin W. Zwierlein, Christian H. Schunck, André Schirotzek, and Wolfgang Ketterle

Supplementary Information

Supplementary Figures

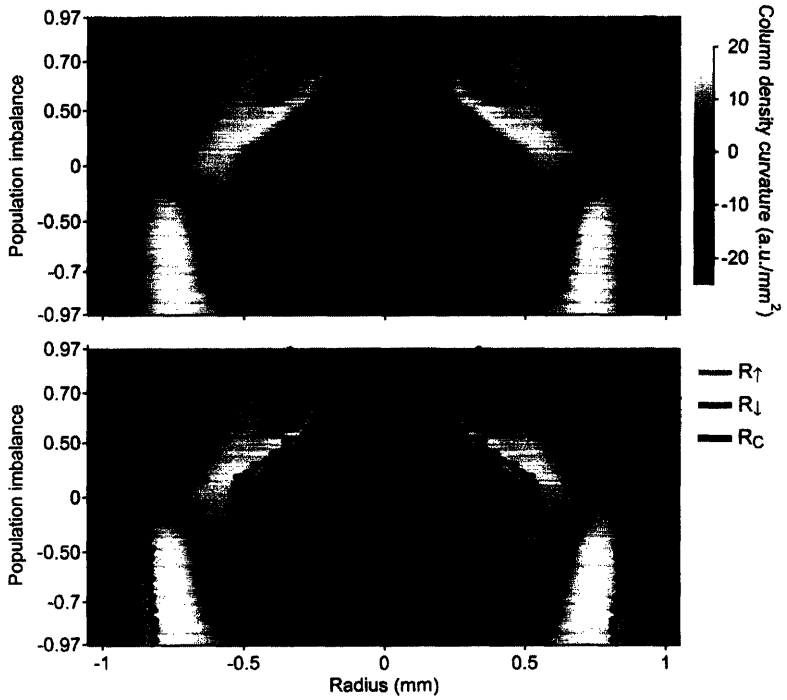

Supplementary Figure 1: (Color online) Signatures of the condensate on resonance in the spatial profiles. The curvature of the observed column density is encoded in shades of gray with white (black) corresponding to positive (negative) curvature. The outer radii of the two components and the condensate radius are shown as an overlay in the lower panel. As a direct consequence of strong interactions, the minority component causes a pronounced bulge in the majority density that is reflected in the rapid variation of the profile's curvature. The condensate is clearly visible in the minority component ($\delta > 0$), but also leaves a faint trace in the majority component ($\delta < 0$). The image was composed out of 216 individual azimuthally averaged column density profiles, smoothed to reduce technical noise. Data close to the cloud's center suffer from larger noise due to the lower number of averaged points. The central feature of about 50μm width is an artefact of smoothing in this region of increased noise.

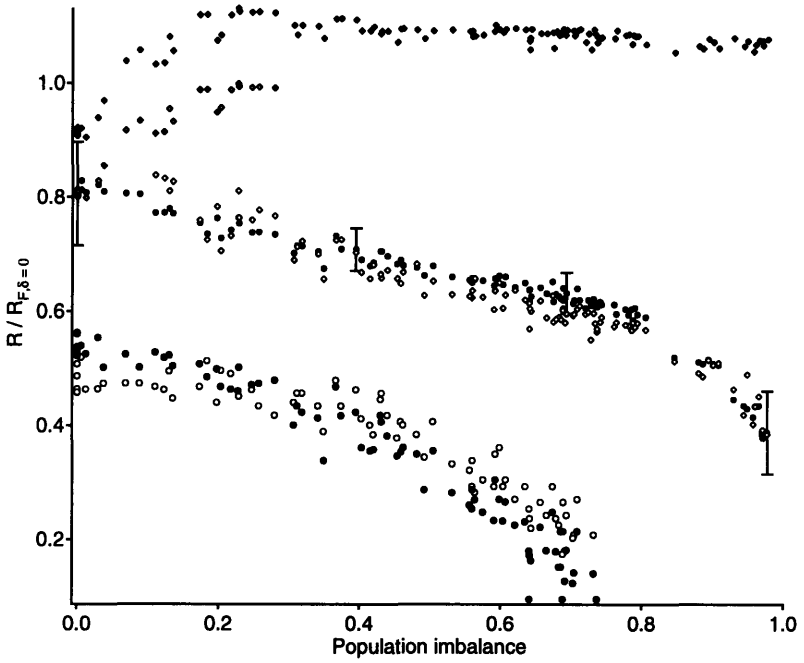

Supplementary Figure 2: Outer radii of the two cloud profiles and condensate radius versus population imbalance. Data obtained from the majority (minority) cloud are shown as diamonds (circles). The outer radii of the clouds (black) are determined from Thomas-Fermi fits to the profiles' wings, where the results of a zero-temperature and a finite temperature fit were averaged. For the minority cloud, the representative error bars indicate the difference between these two results. The position of the "bulge" in the majority profile (white diamonds) naturally follows the outer minority radius. The condensate radius is defined as the position of the "kink" in the minority profiles. It was obtained by a) fitting an increasing portion of the minority wings until a significant increase in χ^2 was observed (grey circles), and b) the position of the minimum in the profile's derivative (white circles). All sizes are scaled by the Fermi-radius of a non-interacting equal mixture. The minority radii were adjusted for the observed hydrodynamic expansion (expansion factor 11.0). The non-interacting wings of the majority cloud expand ballistically (expansion factor 9.7), as long as they are found a factor $11/9.7 = 1.13$ further out than the minority radius. For small imbalances ($\delta < 20\%$), also the majority wing's expansion will be affected by collisions. The grey diamonds give the majority cloud's outer radius if hydrodynamic expansion is assumed.

Supplementary Methods

Hydrodynamic vs. ballistic expansion

A non-interacting cloud of atoms simply expands ballistically from a trap. However, strongly interacting equal Fermi mixtures, above and below the phase transition, are collisionally dense and therefore expand according to hydrodynamic scaling laws [1–3]. These scaling laws only depend on the equation of state of the gas, $\epsilon \propto n^\gamma$, with $\gamma = 1$ for the BEC-side, $\gamma = 2/3$ for resonance (a direct consequence of unitarity) and $\gamma = 2/3$ for the BCS-side, away from resonance. In an unequal spin mixture of fermions, the expansion does not follow a simple scaling law. The minority cloud is always in contact with majority atoms and thus strongly interacting throughout the expansion, which is therefore hydrodynamic. The excess atoms in the wings of the larger cloud are non-interacting and will expand ballistically, as we have checked experimentally. The absorption images after expansion are taken along the axial direction of the trap (the direction of the optical trapping beam). In order to compare the expanded cloud sizes to the in-trap Fermi radii of non-interacting clouds (see Fig. 2 and Fig. S2 below) we scale the majority cloud with the ballistic factor for the radial direction

$$\sqrt{\cosh^2\left(2\pi\nu_z t/\sqrt{2}\right) + (\sqrt{2}\nu_r/\nu_z)^2 \sinh^2\left(2\pi\nu_z t/\sqrt{2}\right)},$$

where t is the expansion time and $\nu_z/\sqrt{2}$ gives the radial anti-trapping curvature of the magnetic saddle-point potential. The scaling factor for the hydrodynamic expansion of an equal mixture is given by the solution to a differential equation [2,3]. A priori, the minority cloud in unequal mixtures could expand with a different scaling, since the equation of state now depends on *two* densities. However, by imaging the cloud in trap and at different times during expansion, we found that the minority cloud's expansion is very well described by the scaling law for an equal mixture. In particular, the aspect ratio of the minority cloud did not change as a function of population imbalance (within our experimental error of 5%), and was equal to that of a balanced mixture.

For the data on resonance in Figs. 3, S1 and S2, which were obtained after 11 ms expansion out of a trap with radial (axial) frequency of $\nu_r = 113(10)$ Hz ($\nu_z = 22.8(0.2)$ Hz), the ballistic (hydrodynamic) expansion factor for the radial direction is 9.7 (11.0).

Supplementary Discussion

Signature of the condensate

Fig. S1 demonstrates that on resonance, the condensate is visible not only in the minority component, but also in the larger cloud as a small change in the profile's curvature. In the condensate region, the majority profile is slightly depleted when compared to the shape of a normal Fermi cloud. This effect is still significant on the BCS-side (see Fig. 1): Although here, the condensate is less visible in the smaller component than on resonance, the larger cloud's central depletion still produces a clear dip in the difference profile.

Radii in the unequal Fermi mixture

Fig. S2 shows the outer radii of the majority and minority cloud, together with the condensate radius (on resonance, for the deepest evaporation compatible with constant total atom number versus imbalance). As was the case for the phase transition at finite temperature, the outer cloud sizes change smoothly with imbalance. No drastic change is seen at the critical population imbalance. The radii are obtained by fitting the profiles' wings to the Thomas-Fermi expression for the radial column density $n(r)$:

$$n(r) = n_0 \frac{\mathrm{Li}_2\left(-\lambda^{1-r^2/R^2}\right)}{\mathrm{Li}_2\left(-\lambda\right)},$$

with the central column density n_0, the fugacity λ and the Thomas-Fermi radius R as the free parameters. $\mathrm{Li}_2(x)$ is the Dilogarithm. The zero-temperature expression reduces to $n(r) = n_0(1 - r^2/R^2)^2$.

Lower and upper bounds for the critical chemical potential difference at δ_c

For the clouds at the critical imbalance δ_c, we now want to extract a lower and upper bound for the difference in chemical potentials $\delta\mu_c$ of the majority and minority component. This difference allows us to conclude that BCS-type superfluidity with imbalanced densities is not possible.

The chemical potential difference $\delta\mu \equiv 2h = (\mu_\uparrow - \mu_\downarrow)$ measures the energy cost, relative to $\mu = (\mu_\uparrow + \mu_\downarrow)/2$, to add a particle to the cloud of excess fermions. Δ, the pairing gap, is the energy cost for this additional majority particle to enter the superfluid. Both the critical temperature T_C and the critical chemical potential difference $\delta\mu_c$ provide a measure of the superfluid gap: The superfluid can be either destroyed by raising the temperature or by increasing the population imbalance. If $h_c \equiv \delta\mu_c/2 < \Delta$, excess atoms will always stay outside the superfluid, in the phase separated normal state. For $h_c > \Delta$, excess atoms can enter the superfluid for $h_c > h > \Delta$. Hence, superfluidity with unequal densities, if allowed via $h_c > \Delta$, would be favored at large population imbalance, contrary to the interpretation in [4], where such a state was proposed for small population imbalance. A recent Monte-Carlo calculation [5] for the Clogston limit on resonance gives $h_c = 1.00(5)\Delta = 0.50(5)E_F$ and can thus not decide on the question of superfluidity with imbalanced densities.

We can attempt to extract the chemical potential from the cloud sizes $R_{\uparrow,\downarrow}$ - taking into account hydrodynamic expansion for the minority cloud and ballistic expansion for the excess fermions. For the majority cloud, we find $\mu_{c,\uparrow} = 1/2\, m\omega_r^2 R_\uparrow^2 = 1.21(6)E_F$. For the minority cloud, we find $1/2\, m\omega_r^2 R_\downarrow^2 = 0.39(10)E_F$. Throughout the smaller cloud, minority atoms are always strongly attracted by majority atoms. This strong attractive interaction likely reduces their chemical potential from the above upper limit. The difference of the chemical potentials $\delta\mu_c \equiv 2h_c$ is thus given by $h_c = (\mu_{c,\uparrow} - \mu_{c,\downarrow})/2 \geq 0.41(6)E_F = 0.51\mu$, our lower bound. Another condition on h_c concerns whether the normal state can be mixed, $h_c < \mu$, (minority and majority atoms in the same spatial region) or whether the normal state is always completely polarized $h_c > \mu$. Our observation of the mixed region in Fig. 1 immediately results in $h_c < \mu$, the upper bound.

On resonance, $\Delta = 1.16\mu$ in BCS-theory, while a recent Monte-Carlo study [5] obtains $\Delta = 1.2\mu$. If $\Delta > \mu$ holds true, our finding of the upper bound on h_c would imply $h_c < \Delta$ and hence would exclude a superfluid with unequal spin densities (at least on the basis of BCS-theory, see [6] for a recent suggestion which goes beyond BCS).

Supplementary Notes

1. O'Hara, K. M., Hemmer, S. L., Gehm, M. E., Granade, S. R. & Thomas, J. E. Observation of a strongly interacting degenerate fermi gas of atoms. *Science* **298**, 2179 (2002).

2. Menotti, C., Pedri, P. & Stringari, S. Expansion of an Interacting Fermi gas. *Phys. Rev. Lett.* **89**, 250402 (2002).

3. Castin, Y. Exact scaling transform for a unitary quantum gas in a time dependent harmonic potential. *Comptes Rendus Physique* **5**, 407–410 (2004).

4. Partridge, G. B., Li, W., Kamar, R. I., a. Liao, Y. & Hulet, R. G. Pairing and Phase Separation in a Polarized Fermi Gas. *Science* **311**, 503 (2006). Published online 21 December 2005 (10.1126/science.1122876).

5. Carlson, J. & Reddy, S. Asymmetric Two-Component Fermion Systems in Strong Coupling. *Phys. Rev. Lett.* **95**, 060401 (2005).

6. Ho, T.-L. & Zhai, H. Homogeneous Fermion Superfluid with Unequal Spin Populations. Preprint at <http://arxiv.org/cond-mat/0602568> (2006).

Appendix J

Observation of Phase Separation in a Strongly Interacting Imbalanced Fermi Gas

This appendix contains a reprint of Ref. [223]: Y. Shin, M. W. Zwierlein, C. H. Schunck, A. Schirotzek, and W. Ketterle, *Observation of Phase Separation in a Strongly Interacting Imbalanced Fermi Gas*, Phys. Rev. Lett. **97**, 030401 (2006).

Observation of Phase Separation in a Strongly Interacting Imbalanced Fermi Gas

Y. Shin,* M. W. Zwierlein, C. H. Schunck, A. Schirotzek, and W. Ketterle

Department of Physics, MIT-Harvard Center for Ultracold Atoms, and Research Laboratory of Electronics, Massachusetts Institute of Technology, Cambridge, Massachusetts, 02139, USA

(Received 15 June 2006; published 18 July 2006; corrected 21 July 2006)

We have observed phase separation between the superfluid and the normal component in a strongly interacting Fermi gas with imbalanced spin populations. The *in situ* distribution of the density difference between two trapped spin components is obtained using phase-contrast imaging and 3D image reconstruction. A shell structure is clearly identified where the superfluid region of equal densities is surrounded by a normal gas of unequal densities. The phase transition induces a dramatic change in the density profiles as excess fermions are expelled from the superfluid.

DOI: 10.1103/PhysRevLett.97.030401 PACS numbers: 03.75.Ss, 03.75.Hh, 05.70.Fh

Cooper pairing is the underlying mechanism for the Bardeen-Cooper-Schrieffer (BCS) superfluid state of an equal mixture of two fermionic gases. An interesting situation arises when the two components have unequal populations. Does the imbalance quench superfluidity, does it lead to phase separation between a balanced and an imbalanced region, or does it give rise to new forms of superfluidity? A search for exotic superfluid states is promising in imbalanced mixtures, since the imbalance destabilizes BCS-type s-wave pairing, which is usually the strongest pairing mechanism [1–4]. Recently, this problem has been experimentally addressed in ultracold atomic Fermi clouds with controlled population imbalances [5–7]. Superfluidity was observed in a strongly interacting regime with a broad range of imbalances, and the Clogston limit of superfluidity [8] was characterized [5,7].

The phase separation scenario suggests that unpaired fermions are spatially separated from a BCS superfluid of equal densities due to the pairing gap in the superfluid region [9–11]. In our previous experiments [5,7], we observed a strong central depletion in the difference profiles of expanding clouds indicating that excess atoms are expelled from the superfluid region. Reference [6] reports depletion of excess atoms at the trap center. None of these experiments answered the questions of whether the densities of the two spin components are *equal* in the *superfluid* region and whether phase separation or rather distortions of the cloud due to interactions have occurred [12,13].

Here we report the direct observation of phase separation between the superfluid and the normal region in a strongly interacting Fermi gas with imbalanced spin populations. The density difference between the two spin components is directly measured *in situ* using a special phase-contrast imaging technique and 3D image reconstruction. We clearly identify a shell structure in an imbalanced Fermi gas where the superfluid region of equal densities is surrounded by a normal gas of unequal densities. This phase separation is observed throughout the strongly interacting regime near a Feshbach resonance. Furthermore, we characterize the normal-to-superfluid phase transition of an imbalanced Fermi mixture using *in situ* phase-contrast imaging. The onset of superfluidity induces a dramatic change in the density profiles as excess fermions are expelled from the superfluid.

A degenerate Fermi gas of spin-polarized ^{6}Li atoms was prepared in an optical trap after laser cooling and sympathetic cooling with sodium atoms [14,15]. The population imbalance δ of the two lowest hyperfine states $|1\rangle$ and $|2\rangle$ was adjusted with a radio-frequency sweep [5]. Here $\delta \equiv (N_1 - N_2)/(N_1 + N_2)$, where N_1 and N_2 are the atom numbers in $|1\rangle$ and $|2\rangle$, respectively. Interactions between these two states were strongly enhanced near a broad Feshbach resonance at $B_0 = 834$ G. The final evaporative cooling was performed at $B = 780$ G by lowering the trap depth. Subsequently, the interaction strength was adiabatically changed to a target value by adjusting the value of the magnetic-bias field B with a ramp speed of ≤ 0.4 G/ms. For typical conditions, the total atom number was $N_t = N_1 + N_2 \approx 1 \times 10^7$ and the radial (axial) trap frequency was $f_r = 130$ Hz ($f_z = 23$ Hz).

The condensate fraction in the imbalanced Fermi mixture was determined via the rapid transfer technique [16,17]. Immediately after turning off the trap, the magnetic field was quickly ramped to $B = 690$ G ($1/k_F a \approx 2.6$, where k_F is defined as the Fermi momentum of a noninteracting equal mixture with the same total atom number and a is the scattering length) in approximately 130 μs. The density profile of the expanding minority cloud was fit by a Gaussian for normal components (thermal molecules and unpaired atoms) and a Thomas-Fermi (TF) profile for the condensate [18].

The density difference between the two components was directly measured using a phase-contrast imaging technique (Fig. 1). In this imaging scheme, the signs of the phase shifts due to the presence of atoms in each state are opposite so that the resulting phase signal is proportional to the density difference n_d of the two states [19]. This technique allows us to directly image the *in situ* distribution of the density difference $n_d(\vec{r})$ and avoid the shortcoming of previous studies [5–7] where two images were subtracted from each other.

 © 2006 The American Physical Society

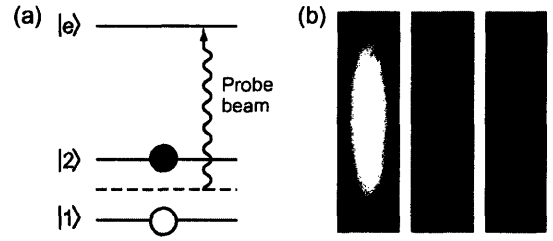

FIG. 1. Phase-contrast imaging of the density difference of two spin states. (a) The probe beam is tuned to the red for the $|1\rangle \rightarrow |e\rangle$ transition and to the blue for the $|2\rangle \rightarrow |e\rangle$ transition. The resulting optical signal in the phase-contrast image is proportional to the density difference $n_d \equiv n_1 - n_2$, where n_1 and n_2 are the densities of the states $|1\rangle$ and $|2\rangle$, respectively. (b) Phase-contrast images of trapped atomic clouds in state $|1\rangle$ (left) and state $|2\rangle$ (right) and of an equal mixture of the two states (middle).

For a partially superfluid imbalanced mixture, a shell structure was observed in the *in situ* phase-contrast image (Fig. 2). Since the image shows the column density difference (the 3D density difference integrated along the y direction of the imaging beam), the observed depletion in the center indicates a 3D shell structure with even stronger depletion in the central region. The size of this inner core decreases for increasing imbalance, and the core shows a distinctive boundary until it disappears for large imbalance. We observe this shell structure even for very small imbalances, down to 5(3)%, which excludes a homogeneous superfluid state at this low imbalance, contrary to the conclusions in Ref. [6].

The reconstructed 3D profile of the density difference shows that the two components in the core region have equal densities. We reconstruct 3D profiles from the 2D distributions $\tilde{n}_d(x, z)$ of the column density difference using the inverse Abel transformation (Fig. 3) [20]. The reconstruction does not depend on the validity of the local density approximation (LDA) or a harmonic approximation for the trapping potential [12,21,22] and assumes only cylindrical symmetry of the trap. The two transverse trap frequencies are equal to better than 2% [15]. A 1D profile obtained by integrating $\tilde{n}_d$ along the axial direction [Fig. 3(d)] shows a flattop distribution, which is the expected outcome for a shell structure with an empty inner region in a harmonic trap and assuming LDA.

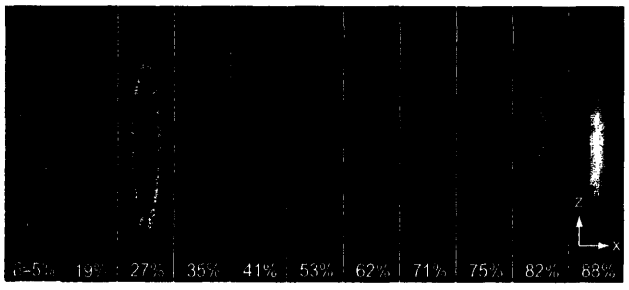

FIG. 2. *In situ* direct imaging of trapped Fermi gases for various population imbalance δ. The integrated 2D distributions of the density difference $\tilde{n}_d(x, z) \equiv \int n_d(\vec{r})dy$ were measured using phase-contrast imaging at $B = 834$ G for total atom number $N_t \approx 1 \times 10^7$. For $\delta \leq 75\%$, a distinctive core was observed showing the shell structure of the cloud. The field of view for each image is 160 μm $\times$ 800 μm. The three leftmost images are displayed with different contrast levels for clarity. The image with $\delta = 5(3)\%$ was taken for $N_t \approx 1.7 \times 10^7$.

The presence of a core region with equal densities for the two components was correlated with the presence of a pair condensate. The density difference at the center n_{d0} along with the condensate fraction is shown as a function of the imbalance δ in Fig. 4. As shown, there is a critical imbalance δ_c where superfluidity breaks down due to large imbalance [5,7]. In the superfluid region, i.e., $\delta < \delta_c$, n_{d0} vanishes, and for $\delta > \delta_c$, n_{d0} rapidly increases with a sudden jump around $\delta \approx \delta_c$. We observe a similar behavior throughout the strongly interacting regime near the Feshbach resonance, $-0.4 < 1/k_F a < 0.6$. This observation clearly demonstrates that for this range of interactions a paired superfluid is spatially separated from a normal component of unequal densities.

The shell structure is characterized by the radius of the majority component, the radial position R_p of the peak in $n_d(\vec{r})$, the size R_c of the region where n_d is depleted, and the "visibility" α of the core region (Fig. 5). The sudden drop of α around $\delta \approx \delta_c$ results from the sudden jump of n_{d0}. The comparison between R_p and R_c shows that the boundary layer between the superfluid and the normal region is rather thin. It has been suggested that the detailed shape of profiles in the intermediate region could be used to identify exotic states such as the Fulde-Ferrell-Larkin-Ovchinnikov state [23–25]. This will be a subject of future research.

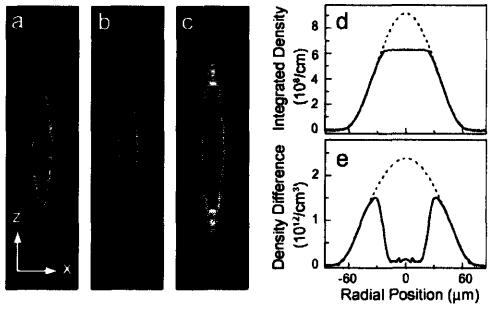

FIG. 3. Reconstruction of 3D distributions from their integrated 2D distributions. (a) An integrated 2D distribution $\tilde{n}_d$ with $\delta = 58\%$ at $B = 834$ G. (b) A less noisy distribution was obtained by averaging four quadrants with respect to the central dashed lines in (a). (d) The 1D profile obtained by integrating the averaged distribution along the z direction shows the "flattop" feature. (c) The 2D cut $n_d(x, y = 0, z)$ of the 3D distribution $n_d(\vec{r})$ was reconstructed by applying the inverse Abel transformation to (b). (e) The radial profile of the central section of the reconstructed 3D distribution in the xy plane. The dashed lines in (d) and (e) are fits to the profiles' wings using a TF distribution.

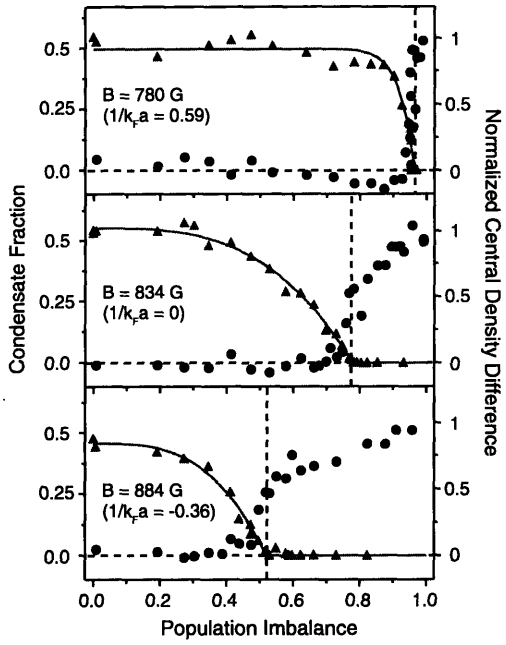

FIG. 4 (color online). Phase separation in a strongly interacting Fermi gas. Normalized central density difference η (black circles) and condensate fraction (red triangles) as functions of imbalance δ for various interaction strengths at our lowest temperatures ($T \lesssim 0.06T_F$). $\eta \equiv n_{d0}/n_0$, where n_{d0} was measured as the average over the central region of 7 μm $\times$ 40 μm in a 2D cut of the 3D distribution [Fig. 3(c)] and $n_0 = 3.3 \times 10^{12}$ cm^{-3} is the calculated central density of a fully polarized Fermi gas with $N_t = 1 \times 10^7$. The condensate fraction was determined from the minority component (see the text). The solid line is a fit for the condensate fraction to a threshold function $\propto (1 - |\delta/\delta_c|^n)$. The critical imbalances δ_c indicated by the vertical dashed lines were 96% (exponent $n = 21$), 77% ($n = 3.1$), and 51% ($n = 3.4$) for $B = 780$ G, $B = 834$ G, and $B = 884$ G, respectively.

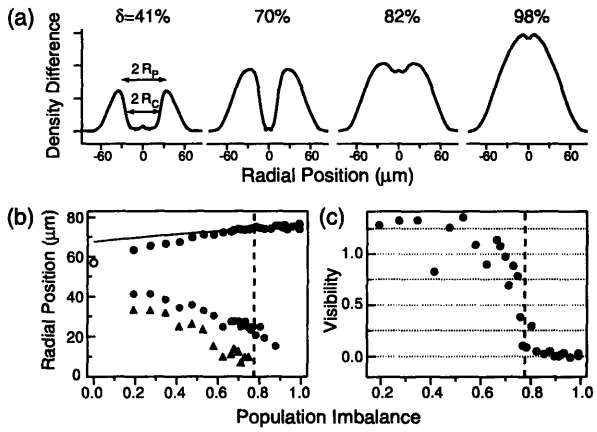

FIG. 5 (color online). Characterization of the shell structure. (a) Reconstructed 3D radial profiles at $B = 834$ G. (b) Radius of the majority component R (black circles), peak position of the density difference R_p (red circles), and radius of the empty core R_c (blue triangles) as a function of population imbalance δ. R was determined from the profiles' wings using a fit to a zero-temperature TF distribution. The solid line indicates the TF radius of the majority component in an ideal noninteracting case. R at $\delta = 0$ (open circle) was measured from an image taken with a probe frequency preferentially tuned to one component. R_c is defined as the position of the half-peak value in the empty core region for $\delta < \delta_c$. (c) Visibility of the core region is defined as $\alpha \equiv (n_d(R_p) - n_{d0})/(n_d(R_p) + n_{d0})$. For low δ, $n_d(R_p)$ is small, and small fluctuations of n_{d0} around zero lead to large fluctuations in α.

The superfluid requires equal central densities in the strongly interacting regime at our coldest temperatures. A normal imbalanced Fermi mixture will have unequal densities. Thus, one should expect that a visible change in the density difference occurs as the temperature is lowered across the normal-to-superfluid phase transition [7,9]. *In situ* phase-contrast images of a cloud at various temperatures are shown in Fig. 6. The temperature T of the cloud is controlled with the final value of the trap depth in the evaporation process. The shell structure appears and becomes prominent when T decreases below a certain critical value. This shell structure gives rise to the bimodal density profile of the minority component that we observed after expansion from the trap in our recent work [7]. Here we show via *in situ* measurements that the onset of superfluidity is accompanied by a pronounced change in the spatial density difference.

The phase transition is characterized in Fig. 7. As T is lowered, n_{d0} gradually decreases from its plateau value and the condensate fraction starts to increase. From the point of condensation (condensate fraction >1%) and deformation of the minority clouds [χ^2 in Fig. 7(b)], we determine the critical temperature $T_c = 0.13(2)T_F$ for the imbalance of $\delta = 56(3)\%$. $T_F = 1.7$ μK is the Fermi temperature of a noninteracting equal mixture with the same total atom number. The rise in χ^2, the drop in n_{d0}, and the onset of

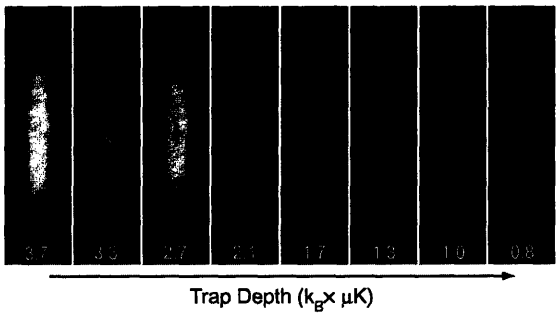

FIG. 6. Emergence of phase separation in an imbalanced Fermi gas. The temperature of the cloud was controlled by varying the final value of the trap depth U_f in the evaporation process. Phase-contrast images were taken after adiabatically ramping the trap depth up to $k_B \times 3.7$ μK ($f_r = 192$ Hz). The whole evaporation and imaging process was performed at $B = 834$ G ($N_t \approx 1.7 \times 10^7$, $\delta \approx 56\%$). The field of view for each image is 160 μm $\times$ 940 μm. The vertical and the horizontal scale of the images differ by a factor of 1.5.

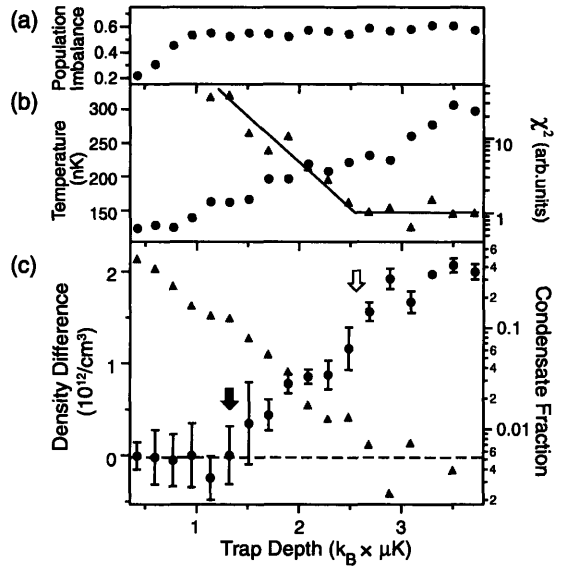

FIG. 7 (color online). Phase transition in an imbalanced Fermi gas. The phase transition shown in Fig. 6 was characterized by measuring (a) population imbalance δ, (b) temperature T (black circles), χ^2 for fitting the minority cloud with a finite temperature Fermi-Dirac distribution (red triangles), (c) central density difference n_{d0} (black circles), and condensate fraction (red triangles). The solid line is a guide to the eye for χ^2. δ decreased mainly due to loss in the majority component, which was reduced by 14% between $U_f/k_B = 3$ and 1 μK and more rapidly below 1 μK. The number of minority atoms was almost constant ($N_2 \approx 3.7 \times 10^6$). T was determined from the noninteracting outer region of the majority cloud after 10 ms of ballistic expansion [7]. T and n_{d0} are averaged values of three independent measurements. The open (solid) arrow in (c) indicates the position for T_c (T^*). See the text for the definitions of T_c and T^*.

condensation are all observed at about the same temperature. Better statistics are needed to address the question of whether some weak expulsion of majority atoms from the center occurs already slightly above T_c.

Below a certain temperature T^*, n_{d0} reaches zero while the condensate fraction is still increasing, implying that the superfluid region of equal densities continues to expand spatially with decreasing T (see Fig. 6). Full phase separation does not occur until this temperature $T^* < T_c$ is reached. We interpret the state between T^* and T_c as a superfluid of pairs coexisting with polarized quasiparticle excitations. This is expected, since at finite temperatures the BCS state of an equal mixture can accommodate excess atoms as fermionic quasiparticle excitations [23,26–28]. There is a finite energy cost given by the pairing gap $\Delta(T)$ for those quasiparticles to exist in the superfluid. The assumption that excess atoms should have thermal energy $k_B T > \Delta(T)$ to penetrate the superfluid region suggests the relation between T^* and $\Delta(T)$ to be $k_B T^* \approx \Delta(T^*)$. From our experimental results, $T^* \approx 0.09 T_F$ and $\Delta(T^*) \approx h \times$ 3.3 kHz.

In conclusion, we have observed phase separation of the superfluid and the normal component in a strongly interacting imbalanced Fermi gas. The shell structure consisting of a superfluid core of equal densities surrounded by a normal component of unequal densities was clearly identified using *in situ* phase-contrast imaging and 3D image reconstruction. The technique is a new method to measure the *in situ* density distribution, allowing direct comparison with theoretical predictions.

We thank G. Campbell for critical reading of the manuscript. This work was supported by the NSF, ONR, and NASA.

*Electronic address: yishin@mit.edu

[1] P. Fulde and R. A. Ferrell, Phys. Rev. **135**, A550 (1964).
[2] A. I. Larkin and Y. N. Ovchinnikov, Zh. Eksp. Teor. Fiz. **47**, 1136 (1964) [Sov. Phys. JETP **20**, 762 (1965)].
[3] G. Sarma, J. Phys. Chem. Solids **24**, 1029 (1963).
[4] W. V. Liu and F. Wilczek, Phys. Rev. Lett. **90**, 047002 (2003).
[5] M. W. Zwierlein *et al.*, Science **311**, 492 (2006).
[6] G. B. Partridge *et al.*, Science **311**, 503 (2006).
[7] M. W. Zwierlein *et al.*, Nature (London) **442**, 54 (2006).
[8] A. M. Clogston, Phys. Rev. Lett. **9**, 266 (1962).
[9] P. F. Bedaque *et al.*, Phys. Rev. Lett. **91**, 247002 (2003).
[10] J. Carlson and S. Reddy, Phys. Rev. Lett. **95**, 060401 (2005).
[11] D. E. Sheehy and L. Radzihovsky, Phys. Rev. Lett. **96**, 060401 (2006).
[12] M. W. Zwierlein and W. Ketterle, cond-mat/0603489.
[13] G. B. Partridge *et al.*, cond-mat/0605581. Partridge *et al.* state that their observations are consistent with phase separation, but that they do not prove phase separation and do not rule out other redistributions of atoms.
[14] Z. Hadzibabic *et al.*, Phys. Rev. Lett. **91**, 160401 (2003).
[15] M. W. Zwierlein *et al.*, Nature (London) **435**, 1047 (2005).
[16] C. A. Regal *et al.*, Phys. Rev. Lett. **92**, 040403 (2004).
[17] M. W. Zwierlein *et al.*, Phys. Rev. Lett. **92**, 120403 (2004).
[18] This underestimates the "true" condensate fraction since the bimodal distribution used for fitting does not account for the repulsion between the condensate and the normal components.
[19] The probe frequency was detuned by about 3 MHz from the exact center between the two resonance frequencies (frequency difference ~80 MHz, natural linewidth $\Gamma =$ 6 MHz) in order to compensate the effect of absorption, zeroing the optical signal in an equal mixture (Fig. 1).
[20] R. N. Bracewell, *The Fourier Transform and Its Applications* (McGraw-Hill, New York, 1986).
[21] T. N. De Silva and E. J. Mueller, Phys. Rev. A **73**, 051602(R) (2006).
[22] A. Imambekov *et al.*, cond-mat/0604423.
[23] W. Yi and L.-M. Duan, Phys. Rev. A **73**, 031604(R) (2006).
[24] T. Mizushima *et al.*, Phys. Rev. Lett. **94**, 060404 (2005).
[25] K. Machida *et al.*, cond-mat/0604339.
[26] C.-C. Chien *et al.*, cond-mat/0605039.
[27] J.-P. Martikainen, Phys. Rev. A **74**, 013602 (2006).
[28] M. M. Parish *et al.*, cond-mat/0605744.

Bibliography

[1] J. R. Abo-Shaeer, C. Raman, and W. Ketterle. Formation and decay of vortex lattices in Bose-Einstein condensates at finite temperatures. *Phys. Rev. Lett.*, 88:070409, 2002.

[2] J. R. Abo-Shaeer, C. Raman, J. M. Vogels, and W. Ketterle. Observation of vortex lattices in Bose-Einstein condensates. *Science*, 292:476–479, 2001.

[3] E. R. I. Abraham, W. I. McAlexander, J. M. Gerton, R. G. Hulet, R. Côté, and A. Dalgarno. Triplet s-wave resonance in ^{6}Li collisions and scattering lengths of ^{6}Li and ^{7}Li. *Phys. Rev. A*, 55:R3299, 1997.

[4] A. A. Abrikosov. On the magnetic properties of superconductors of the second group. *Sov. Phys. JETP*, 5:1174, 1957. Zh. Eksp. Teor. Fiz. 32, p. 1442(1957).

[5] A. A. Abrikosov, L. P. Gorkov, and I. E. Dzyaloshinski. *Methods of Quantum Field Theory in Statistical Physics.* Dover Publications, New York, 1975.

[6] V. K. Akkineni, D. M. Ceperley, and N. Trivedi. Pairing and superfluid properties of dilute fermion gases at unitarity. Preprint cond-mat/0608154.

[7] M. Alford, J. Berges, and K. Rajagopal. Gapless color superconductivity. *Phys. Rev. Lett.*, 84:598, 2000.

[8] J. F. Allen and A. D. Misener. Flow of liquid helium II. *Nature*, 141:75, 1938.

[9] M. Alpar and D. Pines. in The Lives of the Neutron Star: Conference Proceedings, edited by M. Alpar and J. van Paradijs (Kluwer Academic, Dordrecht, 1995).

[10] E. Altman and A. Vishwanath. Dynamic projection on Feshbach molecules: A probe of pairing and phase fluctuations. *Phys. Rev. Lett.*, 95:110404, 2005.

[11] B. P. Anderson, P. C. Haljan, C. E. Wieman, and E. A. Cornell. Vortex precession in Bose-Einstein condensates: Observations with filled and empty cores. *Phys. Rev. Lett.*, 85:2857, 2000.

[12] M. H. Anderson, J. R. Ensher, M. R. Matthews, C. E. Wieman, and E. A. Cornell. Observation of Bose-Einstein condensation in a dilute atomic vapor. *Science*, 269:198–201, 1995.

[13] M. R. Andrews, C. G. Townsend, H.-J. Miesner, D. S. Durfee, D. M. Kurn, and W. Ketterle. Observation of interference between two Bose-Einstein condensates. *Science*, 275:637–641, 1997.

[14] J. R. Anglin. Local vortex generation and the surface mode spectrum of large Bose-Einstein condensates. *Phys. Rev. Lett.*, 87:240401–4, 2001.

[15] J. R. Anglin and W. Ketterle. Bose-Einstein condensation of atomic gases. *Nature*, 416:211, 2002.

[16] J. R. Anglin and W. H. Zurek. Vortices in the wake of rapid Bose-Einstein condensation. *Phys. Rev. Lett.*, 83:1707, 1999.

[17] G. E. Astrakharchik, J. Boronat, J. Casulleras, and S. Giorgini. Equation of state of a Fermi gas in the BEC-BCS crossover: A Quantum Monte-Carlo study. *Phys. Rev. Lett.*, 93:200404, 2004.

[18] G. E. Astrakharchik, J. Boronat, J. Casulleras, and S. Giorgini. Momentum distribution and condensate fraction of a fermion gas in the BCS-BEC crossover. *Phys. Rev. Lett.*, 95:230405, 2005.

[19] S. Aubin, S. Myrskog, M. H. T. Extavour, L. J. LeBlanc, D. McKay, A. Stummer, and J. H. Thywissen. Rapid sympathetic cooling to Fermi degeneracy on a chip. *Nature Physics*, 2:384–387, 2006.

[20] A. V. Avdeenkov and J. L. Bohn. Pair wave functions in atomic Fermi condensates. *Phys. Rev. A*, 71:023609, 2005.

[21] R. A. Barankov and L. S. Levitov. Atom-molecule coexistence and collective dynamics near a Feshbach resonance of cold fermions. *Phys. Rev. Lett.*, 93:130403, 2004.

[22] J. Bardeen. Two-fluid model of superconductivity. *Phys. Rev. Lett.*, 1:399–400, 1958.

[23] J. Bardeen, L. N. Cooper, and J. R. Schrieffer. Theory of superconductivity. *Phys. Rev.*, 108:1175, 1957.

[24] M. Bartenstein, A. Altmeyer, S. Riedl, R. Geursen, S. Jochim, C. Chin, J. Hecker Denschlag, R. Grimm, A. Simoni, E. Tiesinga, C. J. Williams, and P. S. Julienne. Precise determination of ^{6}Li cold collision parameters by radio-frequency spectroscopy on weakly bound molecules. *Phys. Rev. Lett.*, 94:103201, 2004.

[25] M. Bartenstein, A. Altmeyer, S. Riedl, S. Jochim, C. Chin, J. Hecker Denschlag, and R. Grimm. Collective excitations of a degenerate gas at the BEC-BCS crossover. *Phys. Rev. Lett.*, 92:203201, 2004.

[26] M. Bartenstein, A. Altmeyer, S. Riedl, S. Jochim, C. Chin, J. Hecker Denschlag, and R. Grimm. Crossover from a molecular Bose-Einstein condensate to a degenerate Fermi gas. *Phys. Rev. Lett.*, 92:120401, 2004.

[27] H. P. Büchler, P. Zoller, and W. Zwerger. Spectroscopy of superfluid pairing in atomic Fermi gases. *Phys. Rev. Lett.*, 93:080401, 2004.

[28] P. F. Bedaque, H. Caldas, and G. Rupak. Phase separation in asymmetrical fermion superfluids. *Phys. Rev. Lett.*, 91:247002, 2003.

[29] J. G. Bednorz and K. A. Müller. Possible high-T_c superconductivity in the Ba-La-Cu-O system. *Z. Phys. B*, 64:189, 1986.

[30] A. Bianchi, R. Movshovich, C. Capan, P. G. Pagliuso, and J. L. Sarrao. Possible Fulde-Ferrell-Larkin-Ovchinnikov superconducting state in $CeCoIn_5$. *Phys. Rev. Lett.*, 91:187004, 2003.

[31] I. Bloch. Ultracold quantum gases in optical lattices. *Nature Physics*, 1:23, 2005.

[32] N. N. Bogoliubov. On the theory of superfluidity. *J. Phys. (USSR)*, 11:23, 1947.

[33] N. N. Bogoliubov. On a new method in the theory of superconductivity. *Nuovo Cimento*, 7:794, 1958.

[34] S. N. Bose. Plancks Gesetz und Lichtquantenhypothese. *Z. Phys.*, 26:178, 1924.

[35] T. Bourdel. *Gaz de Fermi en interaction forte : Du condensat de molécules aux paires de Cooper*. PhD thesis, Laboratoire Kastler Brossel, Ecole Normale Supérieure, 24 rue Lhomond, 75231 Paris 05, France, 2004.

[36] T. Bourdel, J. Cubizolles, L. Khaykovich, K. M. F. Magalhes, S. J. J. M. F. Kokkelmans, G. V. Shlyapnikov, and C. Salomon. Measurement of the interaction energy near a Feshbach resonance in a ^{6}Li Fermi gas. *Phys. Rev. Lett.*, 91:020402, 2003.

[37] T. Bourdel, L. Khaykovich, J. Cubizolles, J. Zhang, F. Chevy, M. Teichmann, L. Tarruell, S. J. J. M. F. Kokkelmans, and C. Salomon. Experimental study of the BEC-BCS crossover region in lithium 6. *Phys. Rev. Lett.*, 93:050401, 2004.

[38] A. Bulgac. Specific heat of a fermionic atomic cloud in the unitary regime. *Phys. Rev. Lett.*, 95:140403, 2005.

[39] A. Bulgac, J. E. Drut, and P. Magierski. Spin 1/2 fermions in the unitary regime at finite temperature. *Phys. Rev. Lett.*, 96:090404, 2006.

[40] A. Bulgac and M. M. Forbes. Zero temperature thermodynamics of asymmetric Fermi gases at unitarity. Preprint cond-mat/0606043.

[41] A. Bulgac and Y. Yu. The vortex state in a strongly coupled dilute atomic fermionic superfluid. *Phys. Rev. Lett.*, 91:190404, 2003.

[42] E. Burovski, N. Prokof'ev, B. Svistunov, and M. Troyer. Critical temperature and thermodynamics of attractive fermions at unitarity. *Phys. Rev. Lett.*, 96:160402, 2006.

[43] J. Carlson, S.-Y. Chang, V. R. Pandharipande, and K. E. Schmidt. Superfluid Fermi gases with large scattering length. *Phys. Rev. Lett.*, 91:050401, 2003.

[44] J. Carlson and S. Reddy. Asymmetric two-component fermion systems in strong coupling. *Phys. Rev. Lett.*, 95:060401, 2005.

[45] C. Caroli, P. G. d. Gennes, and J. Matricon. Bound fermion states on a vortex line in a type II superconductor. *Phys. Lett.*, 9:307, 1964.

[46] R. Casalbuoni and G. Nardulli. Inhomogeneous superconductivity in condensed matter and QCD. *Rev. Mod. Phys.*, 76:263, 2004. and references therein.

[47] Y. Castin. Exact scaling transform for a unitary quantum gas in a time dependent harmonic potential. *Comptes Rendus Physique*, 5:407–410, 2004.

[48] Y. Castin and R. Dum. Bose-Einstein condensation in time dependent traps. *Phys. Rev. Lett.*, 77:5315–5319, 1996.

[49] P. Castorina, M. Grasso, M. Oertel, M. Urban, and D. Zappal. Nonstandard pairing in asymmetric trapped Fermi gases. *Phys. Rev. A*, 72:025601, 2005.

[50] Q. Chen, Y. He, C.-C. Chien, and K. Levin. Stability conditions and phase diagrams for two component Fermi gases with population imbalance. Preprint cond-mat/0608454.

[51] Q. Chen, C. A. Regal, M. Greiner, D. S. Jin, and K. Levin. Understanding the superfluid phase diagram in trapped Fermi gases. *Phys. Rev. A*, 73:041601, 2006.

[52] F. Chevy. Universal phase diagram of a strongly interacting Fermi gas with unbalanced spin populations. Preprint cond-mat/0605751.

[53] F. Chevy. Density profile of a trapped strongly interacting Fermi gas with unbalanced spin populations. *Phys. Rev. Lett.*, 96:130401, 2006.

[54] F. Chevy, K. Madison, V. Bretin, and J. Dalibard. Formation of quantized vortices in a gaseous Bose-Einstein condensate. In S. Atutov, K. Kalabrese, and L. Moi, editors, *Proceedings of Trapped particles and fundamental physics Workshop, Les Houches, 2001,*, Les Houches, 2001.

[55] C.-C. Chien, Q. Chen, Y. He, and K. Levin. Finite temperature effects in trapped Fermi gases with population imbalance. *Phys. Rev. A*, 74:021602(R), 2006.

[56] C.-C. Chien, Y. He, Q. Chen, and K. Levin. Ground-state description of a single vortex in an atomic Fermi gas: From BCS to Bose–Einstein condensation. *Phys. Rev. A*, 73:041603, 2006.

[57] A. Chikkatur. *Colliding and Moving Bose-Einstein Condensates: Studies of superfluidity and optical tweezers for condensate transport.* PhD thesis, Massachusetts Institute of Technology, 2002.

[58] A. P. Chikkatur, A. Görlitz, D. M. Stamper-Kurn, S. Inouye, S. Gupta, and W. Ketterle. Suppression and enhancement of impurity scattering in a Bose-Einstein condensate. *Phys. Rev. Lett.*, 85:483–486, 2000.

[59] C. Chin, M. Bartenstein, A. Altmeyer, S. Riedl, S. Jochim, J. Hecker Denschlag, and R. Grimm. Observation of the pairing gap in a strongly interacting Fermi gas. *Science*, 305:1128, 2004.

[60] S. Chu. The manipulation of neutral particles. *Rev. Mod. Phys.*, 70:685, 1998.

[61] A. M. Clogston. Upper limit for the critical field in hard superconductors. *Phys. Rev. Lett.*, 9:266, 1962.

[62] T. D. Cohen. Phase separation and an upper bound for a generalized superfluid gap for cold Fermi fluids in the unitary regime. *Phys. Rev. Lett.*, 95:120403, 2005.

[63] C. N. Cohen-Tannoudji. Manipulating atoms with photons. *Rev. Mod. Phys.*, 70:707, 1998.

[64] R. Combescot, M. Y. Kagan, and S. Stringari. Collective mode of homogeneous superfluid Fermi gases in the BEC-BCS crossover. Preprint cond-mat/0607493.

[65] R. Combescot and C. Mora. The low-temperature Fulde-Ferrell-Larkin-Ovchinnikov phases in 3 dimensions. *Europhys. Lett.*, 68:79, 2004.

[66] L. N. Cooper. Bound electron pairs in a degenerate Fermi gas. *Phys. Rev.*, 104:1189–1190, 1956.

[67] E. A. Cornell and C. E. Wieman. Nobel lecture: Bose-Einstein condensation in a dilute gas, the first 70 years and some recent experiments. *Rev. Mod. Phys.*, 74:875, 2002.

[68] P. Courteille, R. S. Freeland, D. J. Heinzen, F. A. van Abeelen, and B. J. Verhaar. Observation of a Feshbach resonance in cold atom scattering. *Phys. Rev. Lett.*, 81:69–72, 1998.

[69] J. Cubizolles, T. Bourdel, S. J. J. M. F. Kokkelmans, G. V. Shlyapnikov, and C. Salomon. Production of long-lived ultracold Li_2 molecules from a Fermi gas. *Phys. Rev. Lett.*, 91:240401, 2003.

[70] F. Dalfovo and S. Stringari. Shape deformations and angular-momentum transfer in trapped Bose-Einstein condensates. *Phys. Rev. A*, 63:011601–4, 2001.

[71] J. C. Davis, J. D. Close, R. Zieve, and R. E. Packard. Observation of quantized circulation in superfluid ^{3}He-B. *Phys. Rev. Lett.*, 66:329, 1991.

[72] K. B. Davis, M.-O. Mewes, M. R. Andrews, N. J. van Druten, D. S. Durfee, D. M. Kurn, and W. Ketterle. Bose-Einstein condensation in a gas of sodium atoms. *Phys. Rev. Lett.*, 75:3969–3973, 1995.

[73] K. B. Davis, M.-O. Mewes, M. A. Joffe, M. R. Andrews, and W. Ketterle. Evaporative cooling of sodium atoms. *Phys. Rev. Lett.*, 74:5202–5205, 1995.

[74] C. A. R. Sá de Melo, M. Randeria, and J. R. Engelbrecht. Crossover from BCS to Bose superconductivity: Transition temperature and time-dependent Ginzburg-Landau theory. *Phys. Rev. Lett.*, 71:3202, 1993.

[75] B. S. Deaver and W. M. Fairbank. Experimental evidence for quantized flux in superconducting cylinders. *Phys. Rev. Lett.*, 7:43, 1961.

[76] B. DeMarco and D. S. Jin. Onset of Fermi degeneracy in a trapped atomic gas. *Science*, 285:1703–1706, 1999.

[77] D. DeMille. Quantum computation with trapped polar molecules. *Phys. Rev. Lett.*, 88:067901, 2002.

[78] K. Dieckmann, C. A. Stan, S. Gupta, Z. Hadzibabic, C. Schunck, and W. Ketterle. Decay of an ultracold fermionic lithium gas near a Feshbach resonance. *Phys. Rev. Lett.*, 89:203201, 2002.

[79] R. B. Diener and T.-L. Ho. Projecting fermion pair condensates into molecular condensates. Preprint cond-mat/0404517.

[80] R. Doll and M. Näbauer. Experimental proof of magnetic flux quantization in a superconducting ring. *Phys. Rev. Lett.*, 7:51, 1961.

[81] E. A. Donley, N. R. Claussen, S. T. Thompson, and C. E. Wieman. Atom-molecule coherence in a BoseEinstein condensate. *Nature*, 417:529, 2002.

[82] R. J. Donnelly. *Quantized vortices in helium II.* Cambridge University Press, Cambridge, 1991.

[83] M. Drechsler and W. Zwerger. Crossover from BCS-superconductivity to Bose-condensation. *Annalen der Physik*, 504:15–23, 1992.

[84] S. Dürr, T. Volz, A. Marte, and G. Rempe. Observation of molecules produced from a Bose-Einstein condensate. *Phys. Rev. Lett.*, 92:020406, 2004.

[85] D. M. Eagles. Possible pairing without superconductivity at low carrier concentrations in bulk and thin-film superconducting semiconductors. *Phys. Rev.*, 186:456, 1969.

[86] A. Einstein. Quantentheorie des einatomigen idealen Gases. *Sitzungsberichte der preussischen Akademie der Wissenschaften*, Bericht 22:261–267, 1924.

[87] P. Engels, I. Coddington, P. C. Haljan, and E. A. Cornell. Nonequilibrium effects of anisotropic compression applied to vortex lattices in Bose-Einstein condensates. *Phys. Rev. Lett.*, 89:100403, 2002.

[88] P. O. Fedichev and A. E. Muryshev. Equilibrium properties and dissipative dynamics of vortex arrays in trapped Bose-condensed gases. *Phys. Rev. A*, 65:061601, 2002.

[89] A. L. Fetter and A. A. Svidzinsky. Vortices in a trapped dilute Bose-Einstein condensate. *J. Phys.: Condens. Matter*, 13:R135–R194, 2001.

[90] A. L. Fetter and J. D. Walecka. *Quantum Theory of Many-Particle Systems.* McGraw-Hill, New York, 1971. reprint appeared as Dover Edition in Dover Publications, Inc., Mineola, N.Y. (2003).

[91] R. P. Feynman. Atomic theory of liquid helium near absolute zero. *Phys. Rev.*, 91:1301, 1953.

[92] R. P. Feynman. Atomic theory of the two-fluid model of liquid helium. *Phys. Rev.*, 94:262, 1954.

[93] H. Fröhlich. Theory of the superconducting state. I. the ground state at the absolute zero of temperature. *Phys. Rev.*, 79:845, 1950.

[94] P. Fulde and R. A. Ferrell. Superconductivity in a strong spin-exchange field. *Phys. Rev.*, 135:A550, 1964.

[95] M. E. Gehm, S. L. Hemmer, K. M. O'Hara, and J. E. Thomas. Unitarity-limited elastic collision rate in a harmonically trapped Fermi gas. *Phys. Rev. A*, 68:011603(R), 2003.

[96] F. Gerbier, A. Widera, S. Folling, O. Mandel, T. Gericke, and I. Bloch. Phase coherence of an atomic mott insulator. *Phys. Rev. Lett.*, 95:050404, 2005.

[97] J. Goldwin, S. Inouye, M. L. Olsen, B. Newman, B. D. DePaola, and D. S. Jin. Measurement of the interaction strength in a Bose-Fermi mixture with ^{87}Rb and ^{40}K. *Phys. Rev. A*, 70:021601, 2004.

[98] L. P. Gorkov and T. K. Melik-Barkhudarov. Contribution to the theory of superfluidity in an imperfect Fermi gas. *Zh. Eskp. Theor. Fiz.*, 40:1452, 1961.

[99] E. H. Graf, D. M. Lee, and J. D. Reppy. Phase separation and the superfluid transition in liquid ^{3}He-^{4}He mixtures. *Phys. Rev. Lett.*, 19:417 LP – 419, 1967.

[100] S. R. Granade, M. E. Gehm, K. M. O'Hara, and J. E. Thomas. All-optical production of a degenerate Fermi gas. *Phys. Rev. Lett.*, 88:120405, 2002.

[101] M. Greiner, O. Mandel, T. Esslinger, T. W. Hänsch, and I. Bloch. Quantum phase transition from a superfluid to a mott insulator in a gas of ultracold atoms. *Nature*, 415:39–44, 2002.

[102] M. Greiner, C. A. Regal, and D. S. Jin. Emergence of a molecular Bose-Einstein condensate from a Fermi gas. *Nature*, 426:537, 2003.

[103] Z.-C. Gu, G. Warner, and F. Zhou. Fermion pairing with population imbalance: energy landscape and phase separation in a constrained Hilbert subspace. Preprint condmat/0603091.

[104] S. Gupta. *Experiments with Degenerate Bose and Fermi Gases.* PhD thesis, Massachusetts Institute of Technology, 2003.

[105] S. Gupta, Z. Hadzibabic, J. R. Anglin, and W. Ketterle. Collisions in zero temperature Fermi gases. *Phys. Rev. Lett.*, 92:100401, 2004.

[106] S. Gupta, Z. Hadzibabic, M. W. Zwierlein, C. A. Stan, K. Dieckmann, C. H. Schunck, E. G. M. v. Kempen, B. J. Verhaar, and W. Ketterle. Rf spectroscopy of ultracold fermions. *Science*, 300:1723–1726, 2003.

[107] D. Guéry-Odelin. Spinning up and down a boltzmann gas. *Phys. Rev. A*, 62:033607, 2000.

[108] D. Guéry-Odelin and S. Stringari. Scissors mode and superfluidity of a trapped Bose-Einstein condensed gas. *Phys. Rev. Lett.*, 83:4452–4455, 1999.

[109] F. Gygi and M. Schlüter. Self-consistent electronic structure of a vortex line in a type-II superconductor. *Phys. Rev. B*, 43:7609 LP – 7621, 1991.

[110] Z. Hadzibabic. *Studies of a Quantum Degenerate Fermionic Lithium Gas.* PhD thesis, Massachusetts Institute of Technology, 2003.

[111] Z. Hadzibabic, S. Gupta, C. A. Stan, C. H. Schunck, M. W. Zwierlein, K. Dieckmann, and W. Ketterle. Fifty-fold improvement in the number of quantum degenerate fermionic atoms. *Phys. Rev. Lett.*, 91:160401, 2003.

[112] Z. Hadzibabic, C. A. Stan, K. Dieckmann, S. Gupta, M. W. Zwierlein, A. Görlitz, and W. Ketterle. Two species mixture of quantum degenerate Bose and Fermi gases. *Phys. Rev. Lett.*, 88:160401, 2002.

[113] P. C. Haljan, I. Coddington, P. Engels, and E. A. Cornell. Driving Bose-Einstein-condensate vorticity with a rotating normal cloud. *Phys. Rev. Lett.*, 87:210403–4, 2001.

[114] M. Haque and H. T. C. Stoof. Pairing of a trapped resonantly-interacting fermion mixture with unequal spin populations. *Phys. Rev. A*, 74:011602, 2006.

[115] R. Haussmann. *Self-consistent Quantum Field Theory and Bosonization for Strongly Correlated Electron Systems.* Springer Verlag, Berlin, 1999.

[116] N. Hayashi, T. Isoshima, M. Ichioka, and K. Machida. Low-lying quasiparticle excitations around a vortex core in quantum limit. *Phys. Rev. Lett.*, 80:2921, 1998.

[117] J. Herbig, T. Kraemer, M. Mark, T. Weber, C. Chin, H.-C. Nägerl, and R. Grimm. Preparation of a pure molecular quantum gas. *Science*, 301:1510, 2003.

[118] H. F. Hess. Evaporative cooling of magnetically trapped and compressed spin-polarized hydrogen. *Phys. Rev. B*, 34:3476, 1986.

[119] T.-L. Ho. Universal thermodynamics of degenerate quantum gases in the unitarity limit. *Phys. Rev. Lett.*, 92:090402, 2004.

[120] E. Hodby, G. Hechenblaikner, S. A. Hopkins, O. M. Maragò, and C. J. Foot. Vortex nucleation in Bose-Einstein condensates in an oblate, purely magnetic potential. *Phys. Rev. Lett.*, 88:010405–4, 2002.

[121] E. Hodby, S. T. Thompson, C. A. Regal, M. Greiner, A. C. Wilson, D. S. Jin, E. A. Cornell, and C. E. Wieman. Production efficiency of ultracold Feshbach molecules in bosonic and fermionic systems. *Phys. Rev. Lett.*, 94:120402, 2005.

[122] M. Holland, S. J. J. M. F. Kokkelmans, M. L. Chiofalo, and R. Walser. Resonance superfluidity in a quantum degenerate Fermi gas. *Phys. Rev. Lett.*, 87:120406, 2001.

[123] M. Holland, C. Menotti, and L. Viverit. The role of boson-fermion correlations in the resonance theory of superfluids. Preprint cond-mat/0404234.

[124] M. Houbiers, H. T. C. Stoof, W. I. McAlexander, and R. G. Hulet. Elastic and inelastic collisions of ^{6}Li atoms in magnetic and optical traps. *Phys. Rev. A*, 57:R1497, 1998.

[125] A. Imambekov, C. J. Bolech, M. Lukin, and E. Demler. Breakdown of the local density approximation in interacting systems of cold fermions in strongly anisotropic traps. Preprint cond-mat/0604423.

[126] S. Inouye, M. R. Andrews, J. Stenger, H.-J. Miesner, D. M. Stamper-Kurn, and W. Ketterle. Observation of Feshbach resonances in a Bose-Einstein condensate. *Nature*, 392:151–154, 1998.

[127] M. Iskin and C. A. R. Sá de Melo. Two-species fermion mixtures with population imbalance. accepted by PRL, Preprint cond-mat/0604184.

[128] S. Jochim, M. Bartenstein, A. Altmeyer, G. Hendl, C. Chin, J. Hecker Denschlag, and R. Grimm. Pure gas of optically trapped molecules created from fermionic atoms. *Phys. Rev. Lett.*, 91:240402, 2003.

[129] S. Jochim, M. Bartenstein, A. Altmeyer, G. Hendl, S. Riedl, C. Chin, J. Hecker Denschlag, and R. Grimm. Bose-Einstein condensation of molecules. *Science*, 302:2101, 2003.

[130] S. Jochim, M. Bartenstein, G. Hendl, J. Hecker Denschlag, R. Grimm, A. Mosk, and M. Weidemüller. Magnetic field control of elastic scattering in a cold gas of fermionic lithium atoms. *Phys. Rev. Lett.*, 89:273202, 2002.

[131] Y. Kagan, E. L. Surkov, and G. V. Shlyapnikov. Evolution of a Bose gas under variations of the confining potential. *Phys. Rev. A*, 54:R1753–R1756, 1996.

[132] P. Kapitza. Viscosity of liquid helium below the λ-point. *Nature*, 141:74, 1938.

[133] M. A. Kasevich. Coherence with atoms. *Science*, 298:1363, 2002.

[134] Y. Kawaguchi and T. Ohmi. Vortex state in a superfluid Fermi gas near a Feshbach resonance. Preprint cond-mat/0411018.

[135] W. Ketterle. Gordon Conference on Atomic Physics, Tilton School, June 28, 2005.

[136] W. Ketterle. Les prix nobel 2001. pages 118–154. The Nobel Foundation, Stockholm, 2002. reprinted in Rev. Mod. Phys. 74, 1131-1151 (2002).

[137] M. Köhl, H. Moritz, T. Stöferle, K. Günter, and T. Esslinger. Fermionic atoms in a three dimensional optical lattice: Observing Fermi surfaces, dynamics, and interactions. *Phys. Rev. Lett.*, 94:080403, 2005.

[138] J. Kinast, S. L. Hemmer, M. E. Gehm, A. Turlapov, and J. E. Thomas. Evidence for superfluidity in a resonantly interacting Fermi gas. *Phys. Rev. Lett.*, 92:150402, 2004.

[139] J. Kinast, A. Turlapov, J. E. Thomas, Q. Chen, J. Stajic, and K. Levin. Heat capacity of a strongly-interacting Fermi gas. *Science*, 307:1296–1299, 2005.

[140] J. Kinnunen, L. M. Jensen, and P. Törmä. Strongly interacting Fermi gases with density imbalance. *Phys. Rev. Lett.*, 96:110403, 2006.

[141] T. Koehler, K. Goral, and P. S. Julienne. Production of cold molecules via magnetically tunable Feshbach resonances. Preprint cond-mat/0601420.

[142] M. G. Kozlov and L. N. Labzowsky. Parity violation effects in diatomics. *J. Phys. B*, 28:1933, 1995.

[143] L. Kramer and W. Pesch. Core structure and low-energy spectrum of isolated vortex lines in clean superconductors at $T \ll T_C$. *Z. Phys.*, 269:59, 1974.

[144] L. D. Landau. On the theory of superfluidity. *Phys. Rev.*, series 2, 75:1949, 1949.

[145] L. D. Landau and E. M. Lifshitz. *Quantum Mechanics: Non-Relativistic Theory.* Pergamon Press, New York, 1977.

[146] A. J. Larkin and Y. N. Ovchinnikov. Inhomogeneous state of superconductors. *Zh. Eksp. Teor. Fiz.*, 47:1136, 1964. [Sov. Phys. JETP 20, 762 (1965)].

[147] P. A. Lee, N. Nagaosa, and X.-G. Wen. Doping a mott insulator: Physics of high-temperature superconductivity. *Rev. Mod. Phys.*, 78:17, 2006.

[148] T. D. Lee and C. N. Yang. Many-body problem in quantum mechanics and quantum statistical mechanics. *Phys. Rev.*, 105:1119, 1957.

[149] A. J. Leggett. Diatomic molecules and Cooper pairs. In *Modern Trends in the Theory of Condensed Matter. Proceedings of the XVIth Karpacz Winter School of Theoretical Physics, Karpacz, Poland, 1980,*, pages 13–27, Karpacz, Poland, 1980. Springer-Verlag, Berlin.

[150] A. J. Leggett. Superfluidity. *Rev. Mod. Phys.*, 71:S318, 1999.

[151] W. V. Liu and F. Wilczek. Interior gap superfluidity. *Phys. Rev. Lett.*, 90:047002, 2003.

[152] X.-J. Liu and H. Hu. BCS-BEC crossover in an asymmetric two-component Fermi gas. *Europhys. Lett.*, 75:364, 2006.

[153] C. Lobo, A. Recati, S. Giorgini, and S. Stringari. Normal state of a polarized Fermi gas at unitarity. Preprint cond-mat/0607730.

[154] T. Loftus, C. A. Regal, C. Ticknor, J. L. Bohn, and D. S. Jin. Resonant control of elastic collisions in an optically trapped Fermi gas of atoms. *Phys. Rev. Lett.*, 88:173201, 2002.

[155] F. London. Electromagnetic equations of the superconductor. *Proc. Roy. Soc. London, Ser. A*, A152:24, 1935.

[156] F. London. *Superfluids, Vol. II.* Dover, New York, 1964.

[157] K. Machida, T. Mizushima, and M. Ichioka. Generic phase diagram of fermion superfluids with population imbalance. *Phys. Rev. Lett.*, 97:120407, 2006.

[158] M. Machida and T. Koyama. Structure of a quantized vortex near the BCS-BEC crossover in an atomic Fermi gas. *Phys. Rev. Lett.*, 94:140401, 2005.

[159] K. W. Madison, F. Chevy, V. Bretin, and J. Dalibard. Stationary states of a rotating Bose-Einstein condensate: Routes to vortex nucleation. *Phys. Rev. Lett.*, 86:4443–4446, 2001.

[160] K. W. Madison, F. Chevy, W. Wohlleben, and J. Dalibard. Vortex formation in a stirred Bose-Einstein condensate. *Phys. Rev. Lett.*, 84:806–809, 2000.

[161] O. M. Maragò, S. A. Hopkins, J. Arlt, E. Hodby, G. Hechenblaikner, and C. J. Foot. Observation of the scissors mode and evidence for superfluidity of a trapped Bose-Einstein condensed gas. *Phys. Rev. Lett.*, 84:2056–2059, 2000.

[162] B. Marcelis, E. G. M. v. Kempen, B. J. Verhaar, and S. J. J. M. F. Kokkelmans. Feshbach resonances with large background scattering length: Interplay with open-channel resonances. *Phys. Rev. A*, 70:012701, 2004.

[163] M. Marini, F. Pistolesi, and G. C. Strinati. Evolution from BCS superconductivity to Bose condensation: analytic results for the crossover in three dimensions. *European Physical Journal B*, 1:151–159, 1998.

[164] M. R. Matthews, B. P. Anderson, P. C. Haljan, D. S. Hall, C. E. Wieman, and E. A. Cornell. Vortices in a Bose-Einstein condensate. *Phys. Rev. Lett.*, 83:2498–2501, 1999.

[165] E. Maxwell. Isotope effect in the superconductivity of mercury. *Phys. Rev.*, 78:477, 1950.

[166] W. Meissner and R. Ochsenfeld. Ein neuer Effekt bei Eintritt der Supraleitfähigkeit. *Naturwissenschaften*, 21:787, 1933.

[167] C. Menotti, P. Pedri, and S. Stringari. Expansion of an interacting Fermi gas. *Phys. Rev. Lett.*, 89:250402, 2002.

[168] F. H. Mies, E. Tiesinga, and P. S. Julienne. Manipulation of Feshbach resonances in ultracold atomic collisions using time-dependent magnetic fields. *Phys. Rev. A*, 61:022721, 2000.

[169] T. Mizushima, K. Machida, and M. Ichioka. Direct imaging of spatially modulated superfluid phases in atomic fermion systems. *Phys. Rev. Lett.*, 94:060404, 2005.

[170] K. Mølmer. Bose condensates and Fermi gases at zero temperature. *Phys. Rev. Lett.*, 80:1804, 1998.

[171] T. Mukaiyama, J. R. Abo-Shaeer, K. Xu, J. K. Chin, and W. Ketterle. Dissociation and decay of ultracold sodium molecules. *Phys. Rev. Lett.*, 92:180402, 2004.

[172] P. Nozières and S. Schmitt-Rink. Bose condensation in an attractive fermion gas: from weak to strong coupling superconductivity. *J. Low Temp. Phys.*, 59:195–211, 1985.

[173] N. Nygaard, G. M. Bruun, C. W. Clark, and D. L. Feder. Microscopic structure of a vortex line in a dilute superfluid Fermi gas. *Phys. Rev. Lett.*, 90:210402, 2003.

[174] K. M. O'Hara, S. L. Hemmer, M. E. Gehm, S. R. Granade, and J. E. Thomas. Observation of a strongly interacting degenerate Fermi gas of atoms. *Science*, 298:2179, 2002.

[175] K. M. O'Hara, S. L. Hemmer, S. R. Granade, M. E. Gehm, J. E. Thomas, V.Venturi, E. Tiesinga, and C. J. Williams. Measurement of the zero crossing in a Feshbach resonance of fermionic ^{6}Li. *Phys. Rev. A*, 66:041401(R), 2002.

[176] Y. Ohashi and A. Griffin. Superfluidity and collective modes in a uniform gas of Fermi atoms with a Feshbach resonance. *Phys. Rev. A*, 67:063612–24, 2003.

[177] K. Onnes. Investigations into the properties of substances at low temperatures, which have led, amongst other things, to the preparation of liquid helium. Nobel lecture, December 13 in Nobel Lectures, Physics 1901-1921, Elsevier Publishing Company, Amsterdam, 1967.

[178] R. Onofrio, D. S. Durfee, C. Raman, M. Köhl, C. E. Kuklewicz, and W. Ketterle. Surface excitations in a Bose-Einstein condensate. *Phys. Rev. Lett.*, 84:810–813, 2000.

[179] R. Onofrio, C. Raman, J. M. Vogels, J. R. Abo-Shaeer, A. P. Chikkatur, and W. Ketterle. Observation of superfluid flow in a Bose-Einstein condensed gas. *Phys. Rev. Lett.*, 85:2228–2231, 2000.

[180] L. Onsager. Discussion remark. (spontaneous magnetisation of the two-dimensional ising model). *Nuovo Cimento (Suppl)*, 6:261–262, 1949.

[181] G. Ortiz and J. Dukelsky. BCS-to-BEC crossover from the exact BCS solution. *Phys. Rev. A*, 72:043611, 2005.

[182] D. D. Osheroff, W. J. Gully, R. C. Richardson, and D. M. Lee. New magnetic phenomena in liquid ^{3}He below 3 mK. *Phys. Rev. Lett.*, 29:1621, 1972.

[183] D. D. Osheroff, R. C. Richardson, and D. M. Lee. Evidence for a new phase of solid ^{3}He. *Phys. Rev. Lett.*, 28:885–888, 1972.

[184] C. Ospelkaus, S. Ospelkaus, K. Sengstock, and K. Bongs. Interaction-driven dynamics of ^{40}K / ^{87}Rb Fermi-Bose gas mixtures in the large particle number limit. *Phys. Rev. Lett.*, 96:020401, 2006.

[185] C.-H. Pao, S.-T. Wu, and S.-K. Yip. Superfluid stability in BEC-BCS crossover. *Phys. Rev. B*, 73:132506, 2006.

[186] M. M. Parish, F. M. Marchetti, A. Lamacraft, and B. D. Simons. Finite temperature phase diagram of a polarised Fermi condensate. Preprint cond-mat/0605744.

[187] G. B. Partridge, W. Li, R. I. Kamar, Y. a. Liao, and R. G. Hulet. Pairing and phase separation in a polarized Fermi gas. *Science*, 311:503, 2006. published online 21 December 2005 (10.1126/science.1122876).

[188] G. B. Partridge, K. E. Strecker, R. I. Kamar, M. W. Jack, and R. G. Hulet. Molecular probe of pairing in the BEC-BCS crossover. *Phys. Rev. Lett.*, 95:020404, 2005.

[189] W. Pauli. The connection between spin and statistics. *Phys. Rev.*, 58:716, 1940.

[190] A. Perali, P. Pieri, L. Pisani, and G. C. Strinati. BCS-BEC crossover at finite temperature for superfluid trapped Fermi atoms. *Phys. Rev. Lett.*, 92:220404, 2004.

[191] A. Perali, P. Pieri, and G. C. Strinati. Extracting the condensate density from projection experiments with Fermi gases. *Phys. Rev. Lett.*, 95:010407, 2005.

[192] D. S. Petrov. Three-body problem in Fermi gases with short-range interparticle interaction. *Phys. Rev. A*, 67:010703, 2003.

[193] D. S. Petrov, C. Salomon, and G. V. Shlyapnikov. Weakly bound dimers of fermionic atoms. *Phys. Rev. Lett.*, 93:090404, 2004.

[194] W. D. Phillips. Laser cooling and trapping of neutral atoms. *Rev. Mod. Phys.*, 70:721, 1998.

[195] P. Pieri and G. C. Strinati. Strong-coupling limit in the evolution from BCS superconductivity to Bose-Einstein condensation. *Phys. Rev. B*, 61:15370 LP – 15381, 2000.

[196] P. Pieri and G. C. Strinati. Trapped fermions with density imbalance in the Bose-Einstein condensate limit. *Phys. Rev. Lett.*, 96:150404, 2006.

[197] F. Pistolesi and G. C. Strinati. Evolution from BCS superconductivity to Bose condensation: Role of the parameter $k_F\xi$. *Phys. Rev. B*, 49:6356 LP – 6359, 1994.

[198] H. A. Radovan, N. A. Fortune, T. P. Murphy, S. T. Hannahs, E. C. Palm, S. W. Tozer, and D. Hall. Magnetic enhancement of superconductivity from electron spin domains. *Nature*, 425:51–55, 2003.

[199] C. Raman, J. R. Abo-Shaeer, J. M. Vogels, K. Xu, and W. Ketterle. Vortex nucleation in a stirred Bose-Einstein condensate. *Phys. Rev. Lett.*, 87:210402, 2001.

[200] C. Raman, M. Köhl, R. Onofrio, D. S. Durfee, C. E. Kuklewicz, Z. Hadzibabic, and W. Ketterle. Evidence for a critical velocity in a Bose-Einstein condensed gas. *Phys. Rev. Lett.*, 83:2502–2505, 1999.

[201] M. Randeria, J.-M. Duan, and L.-Y. Shieh. Bound states, Cooper pairing, and Bose condensation in two dimensions. *Phys. Rev. Lett.*, 62:981 LP – 984, 1989.

[202] C. A. Regal, M. Greiner, and D. S. Jin. Lifetime of molecule-atom mixtures near a Feshbach resonance in ^{40}K. *Phys. Rev. Lett.*, 92:083201, 2004.

[203] C. A. Regal, M. Greiner, and D. S. Jin. Observation of resonance condensation of fermionic atom pairs. *Phys. Rev. Lett.*, 92:040403, 2004.

[204] C. A. Regal and D. S. Jin. Measurement of positive and negative scattering lengths in a Fermi gas of atoms. *Phys. Rev. Lett.*, 90:230404, 2003.

[205] C. A. Regal, C. Ticknor, J. L. Bohn, and D. S. Jin. Creation of ultracold molecules from a Fermi gas of atoms. *Nature*, 424:47, 2003.

[206] C. A. Reynolds, B. Serin, W. H. Wright, and L. B. Nesbitt. Superconductivity of isotopes of mercury. *Phys. Rev.*, 78:487, 1950.

[207] G. Roati, F. Riboli, G. Modugno, and M. Inguscio. Fermi-Bose quantum degenerate ^{40}K - ^{87}Rb mixture with attractive interaction. *Phys. Rev. Lett.*, 89:150403, 2002.

[208] S. L. Rolston and W. D. Phillips. Non-linear and quantum atom optics. *Nature*, 416:219, 2002.

[209] L. Salasnich, N. Manini, and A. Parola. Condensate fraction of a Fermi gas in the BCS-BEC crossover. *Phys. Rev. A*, 72:023621, 2005.

[210] L. Santos, G. V. Shlyapnikov, P. Zoller, and M. Lewenstein. Bose-Einstein condensation in trapped dipolar gases. *Phys. Rev. Lett.*, 85:1791, 2000.

[211] G. Sarma. On the influence of a uniform exchange field acting on the spins of the conduction electrons in a superconductor. *J. Phys. Chem. Solids*, 24:1029, 1963.

[212] N. V. Sarma. Direct evidence for the laminar and flux line models of mixed state in type II superconductors. *Phys. Lett. A*, 25:315, 1967.

[213] M. R. Schafroth. Remarks on the Meissner effect. *Phys. Rev.*, 111:72, 1958.

[214] F. Schreck, L. Khaykovich, K. L. Corwin, G. Ferrari, T. Bourdel, J. Cubizolles, and C. Salomon. Quasipure Bose-Einstein condensate immersed in a Fermi sea. *Phys. Rev. Lett.*, 87:080403, 2001.

[215] J. R. Schrieffer. *Theory of Superconductivity.* Westview Press, Boulder, Colorado, 1999.

[216] C. H. Schunck, M. W. Zwierlein, A. Schirotzek, and W. Ketterle. Superfluid expansion of a rotating Fermi gas. Preprint cond-mat/0607298.

[217] C. H. Schunck, M. W. Zwierlein, C. A. Stan, S. M. F. Raupach, W. Ketterle, A. Simoni, E. Tiesinga, C. J. Williams, and P. S. Julienne. Feshbach resonances in fermionic lithium-6. *Phys. Rev. A*, 71:045601, 2004.

[218] A. Sedrakian, J. Mur-Petit, A. Polls, and H. Müther. Pairing in a two-component ultracold Fermi gas: Phases with broken-space symmetries. *Phys. Rev. A*, 72:013613, 2005.

[219] R. Sensarma, M. Randeria, and T.-L. Ho. Vortices in superfluid Fermi gases through the BEC to BCS crossover. *Phys. Rev. Lett.*, 96:090403, 2006.

[220] D. E. Sheehy and L. Radzihovsky. BEC-BCS crossover, phase transitions and phase separation in polarized resonantly-paired superfluids. Preprint cond-mat/0607803.

[221] D. E. Sheehy and L. Radzihovsky. BEC-BCS crossover in magnetized Feshbach-resonantly paired superfluids. *Phys. Rev. Lett.*, 96:060401, 2006.

[222] Y. Shin, M. Saba, M. Vengalattore, T. A. Pasquini, C. Sanner, A. E. Leanhardt, M. Prentiss, D. E. Pritchard, and W. Ketterle. Dynamical instability of a doubly quantized vortex in a Bose-Einstein condensate. *Phys. Rev. Lett.*, 93:160406, 2004.

[223] Y. Shin, M. W. Zwierlein, C. H. Schunck, A. Schirotzek, and W. Ketterle. Observation of phase separation in a strongly interacting imbalanced Fermi gas. *Phys. Rev. Lett.*, 97:030401, 2006.

[224] I. Shvarchuck, C. Buggle, D. S. Petrov, K. Dieckmann, M. Zielonkowski, M. Kemmann, T. G. Tiecke, W. v. Klitzing, G. V. Shlyapnikov, and J. T. M. Walraven. Bose-Einstein condensation into nonequilibrium states studied by condensate focusing. *Phys. Rev. Lett.*, 89:270404, 2002.

[225] C. Silber, S. Günther, C. Marzok, B. Deh, P. W. Courteille, and C. Zimmermann. Quantum-degenerate mixture of fermionic lithium and bosonic rubidium gases. *Phys. Rev. Lett.*, 95:170408, 2005.

[226] T. N. De Silva and E. J. Mueller. Profiles of near-resonant population-imbalanced trapped Fermi gases. *Phys. Rev. A*, 73:051602(R), 2006.

[227] S. Simonucci, P. Pieri, and G. C. Strinati. Broad versus narrow Fano-Feshbach resonances in the BCS-BEC crossover with trapped Fermi atom. *Europhys. Lett.*, 69:713, 2005.

[228] G. V. Skorniakov and K. A. Ter-Martirosian. Three-body problem for short-range forces, I, scattering of low-energy neutrons by deuterons. *JETP Lett.*, 4:648, 1957.

[229] D. T. Son and M. A. Stephanov. Phase diagram of cold polarized Fermi gas. *Phys. Rev. A*, 74:013614, 2006.

[230] J. Stajic, Q. Chen, and K. Levin. Density profiles of strongly interacting trapped Fermi gases. *Phys. Rev. Lett.*, 94:060401, 2005.

[231] J. Stajic, J. N. Milstein, Q. Chen, M. L. Chiofalo, M. J. Holland, and K. Levin. Nature of superfluidity in ultracold Fermi gases near Feshbach resonances. *Phys. Rev. A*, 69:063610, 2004.

[232] D. M. Stamper-Kurn. *Peeking and poking at a new quantum fluid: Studies of gaseous Bose-Einstein condensates in magnetic and optical traps.* PhD thesis, Massachusetts Institute of Technology, 1999.

[233] C. A. Stan. *Experiments with Interacting Bose and Fermi Gases.* PhD thesis, Massachusetts Institute of Technology, 2005.

[234] C. A. Stan, M. W. Zwierlein, C. H. Schunck, S. M. F. Raupach, and W. Ketterle. Observation of Feshbach resonances between two different atomic species. *Phys. Rev. Lett.*, 93:143001, 2004.

[235] J. Stenger, S. Inouye, M. R. Andrews, H.-J. Miesner, D. M. Stamper-Kurn, and W. Ketterle. Strongly enhanced inelastic collisions in a Bose-Einstein condensate near Feshbach resonances. *Phys. Rev. Lett.*, 82:2422–2425, 1999.

[236] S. Stintzing and W. Zwerger. Ginzburg-Landau theory of superconductors with short coherence length. *Phys. Rev. B*, 56:9004 LP – 9014, 1997.

[237] H. T. C. Stoof, M. Houbiers, C. A. Sackett, and R. G. Hulet. Superfluidity of spin-polarized ^{6}Li. *Phys. Rev. Lett.*, 76:10 LP – 13, 1996.

[238] R. F. Streater and A. S. Wightman. *PCT, Spin and Statistics, and All That.* Benjamin/Cummings, Reading, Mass., 1964.

[239] K. E. Strecker, G. B. Partridge, and R. G. Hulet. Conversion of an atomic Fermi gas to a long-lived molecular Bose gas. *Phys. Rev. Lett.*, 91:080406, 2003.

[240] S. Stringari. Collective excitations of a trapped Bose-condensed gas. *Phys. Rev. Lett.*, 77:2360–2363, 1996.

[241] W. C. Stwalley. Stability of spin-aligned hydrogen at low temperatures and high magnetic fields: New field-dependent scattering resonances and predissociations. *Phys. Rev. Lett.*, 37:1628, 1976.

[242] M. Takahashi, T. Mizushima, M. Ichioka, and K. Machida. Vortex core structure in neutral fermion superfluids with population imbalance. Preprint cond-mat/0607147.

[243] E. Tiesinga, B. J. Verhaar, and H. T. C. Stoof. Threshold and resonance phenomena in ultracold ground-state collisions. *Phys. Rev. A*, 47:4114–4122, 1993.

[244] L. Tisza. Transport phenomena in helium II. *Nature*, 141:913, 1938.

[245] G. Tonini, F. Werner, and Y. Castin. Formation of a vortex lattice in a rotating BCS Fermi gas. *Eur. Phys. J. D*, 39:283, 2006.

[246] H. Träuble and U. Essmann. The direct observation of individual flux lines in type II superconductors. *Phys. Lett.*, 24A:526, 1967.

[247] A. G. Truscott, K. E. Strecker, W. I. McAlexander, G. B. Partridge, and R. G. Hulet. Observation of Fermi pressure in a gas of trapped atoms. *Science*, 291:2570–2572, 2001.

[248] E. G. M. v. Kempen, B. Marcelis, and S. J. J. M. F. Kokkelmans. Formation of fermionic molecules via interisotope Feshbach resonances. *Phys. Rev. A*, 70:050701(R), 2004.

[249] J. Valatin. Comments on the theory of superconductivity. *Nuovo Cimento*, 7:843, 1958.

[250] F. A. van Abeelen and B. J. Verhaar. Time-dependent Feshbach resonance scattering and anomalous decay of a Na Bose-Einstein condensate. *Phys. Rev. Lett.*, 83:1550–1553, 1999.

[251] M. Y. Veillette, D. E. Sheehy, L. Radzihovsky, and V. Gurarie. Superfluid transition in a rotating resonantly-interacting Fermi gas. Preprint cond-mat/0607775.

[252] W. F. Vinen. Detection of single quanta of circulation in rotating helium II. *Nature*, 181:1524, 1958.

[253] L. Viverit, C. J. Pethick, and H. Smith. Zero-temperature phase diagram of binary boson-fermion mixtures. *Phys. Rev. A*, 61:053605, 2000.

[254] K. Xu, Y. Liu, D. E. Miller, J. K. Chin, W. Setiawan, and W. Ketterle. Observation of strong quantum depletion in a gaseous Bose-Einstein condensate. *Phys. Rev. Lett.*, 96:180405, 2006.

[255] K. Xu, T. Mukaiyama, J. R. Abo-Shaeer, J. K. Chin, D. E. Miller, and W. Ketterle. Formation of quantum-degenerate sodium molecules. *Phys. Rev. Lett.*, 91:210402, 2003.

[256] K. Yang. Quantum liquid crystal phases in fermionic superfluids with pairing between fermion species of unequal densities. Preprint cond-mat/0508484.

[257] E. J. Yarmchuk, M. J. V. Gordon, and R. E. Packard. Observation of stationary vortex arrays in rotating superfluid helium. *Phys. Rev. Lett.*, 43:214, 1979.

[258] W. Yi and L.-M. Duan. Trapped fermions across a Feshbach resonance with population imbalance. *Phys. Rev. A*, 73:031604(R), 2006.

[259] V. A. Yurovsky, A. Ben-Reuven, P. S. Julienne, and C. J. Williams. Atom loss from Bose-Einstein condensates due to Feshbach resonance. *Phys. Rev. A*, 60:R765–R768, 1999.

[260] E. A. Yuzbashyan, B. L. Altshuler, V. B. Kuznetsov, and V. Z. Enolskii. Nonequilibrium Cooper pairing in the nonadiabatic regime. *Phys. Rev. B*, 72:220503, 2005.

[261] P. Zarth. private communication.

[262] H. Zhai and T.-L. Ho. Critical rotating frequency for superfluid fermionic gases across Feshbach resonance. Preprint cond-mat/0608233.

[263] O. N. Zhuravlev, A. E. Muryshev, and P. O. Fedichev. Dissipative dynamics of vortex arrays in anisotropic traps. *Phys. Rev. A*, 64:053601, 2001.

[264] M. W. Zwierlein. Cooling and trapping a Bose-Fermi mixture of dilute atomic gases. Stage de Recherche, Magistère Interuniversitaire de Physique, Paris, weblink: http://cua.mit.edu/ketterle_group/experimental_setup/BEC_I/theses/stage_martin.pdf.

[265] M. W. Zwierlein, J. R. Abo-Shaeer, A. Schirotzek, C. H. Schunck, and W. Ketterle. Vortices and superfluidity in a strongly interacting Fermi gas. *Nature*, 435:1047–1051, 2005.

[266] M. W. Zwierlein, Z. Hadzibabic, S. Gupta, and W. Ketterle. Spectroscopic insensitivity to cold collisions in a two-state mixture of fermions. *Phys. Rev. Lett.*, 91:250404, 2003.

[267] M. W. Zwierlein and W. Ketterle. Comment on pairing and phase separation in a polarized Fermi gas by G. B. Partridge, W. Li, R. I. Kamar, Y. Liao, R. G. Hulet, Science 311, 503 (2006). *Science*, 314:54a, 2006. www.sciencemag.org/cgi/content/full/314/5796/54a.

[268] M. W. Zwierlein, A. Schirotzek, C. H. Schunck, and W. Ketterle. Fermionic superfluidity with imbalanced spin populations. *Science*, 311:492–496, 2006. Published online on Science Express 22 December 2005 (10.1126/science.1122318).

[269] M. W. Zwierlein, C. H. Schunck, A. Schirotzek, and W. Ketterle. Direct observation of the superfluid phase transition in ultracold Fermi gases. *Nature*, 442:54–58, 2006.

[270] M. W. Zwierlein, C. H. Schunck, C. A. Stan, S. M. F. Raupach, and W. Ketterle. Formation dynamics of a fermion pair condensate. *Phys. Rev. Lett.*, 94:180401, 2005.

[271] M. W. Zwierlein, C. A. Stan, C. H. Schunck, S. M. F. Raupach, S. Gupta, Z. Hadzibabic, and W. Ketterle. Observation of Bose-Einstein condensation of molecules. *Phys. Rev. Lett.*, 91:250401, 2003.

[272] M. W. Zwierlein, C. A. Stan, C. H. Schunck, S. M. F. Raupach, A. J. Kerman, and W. Ketterle. Condensation of pairs of fermionic atoms near a Feshbach resonance. *Phys. Rev. Lett.*, 92:120403, 2004.

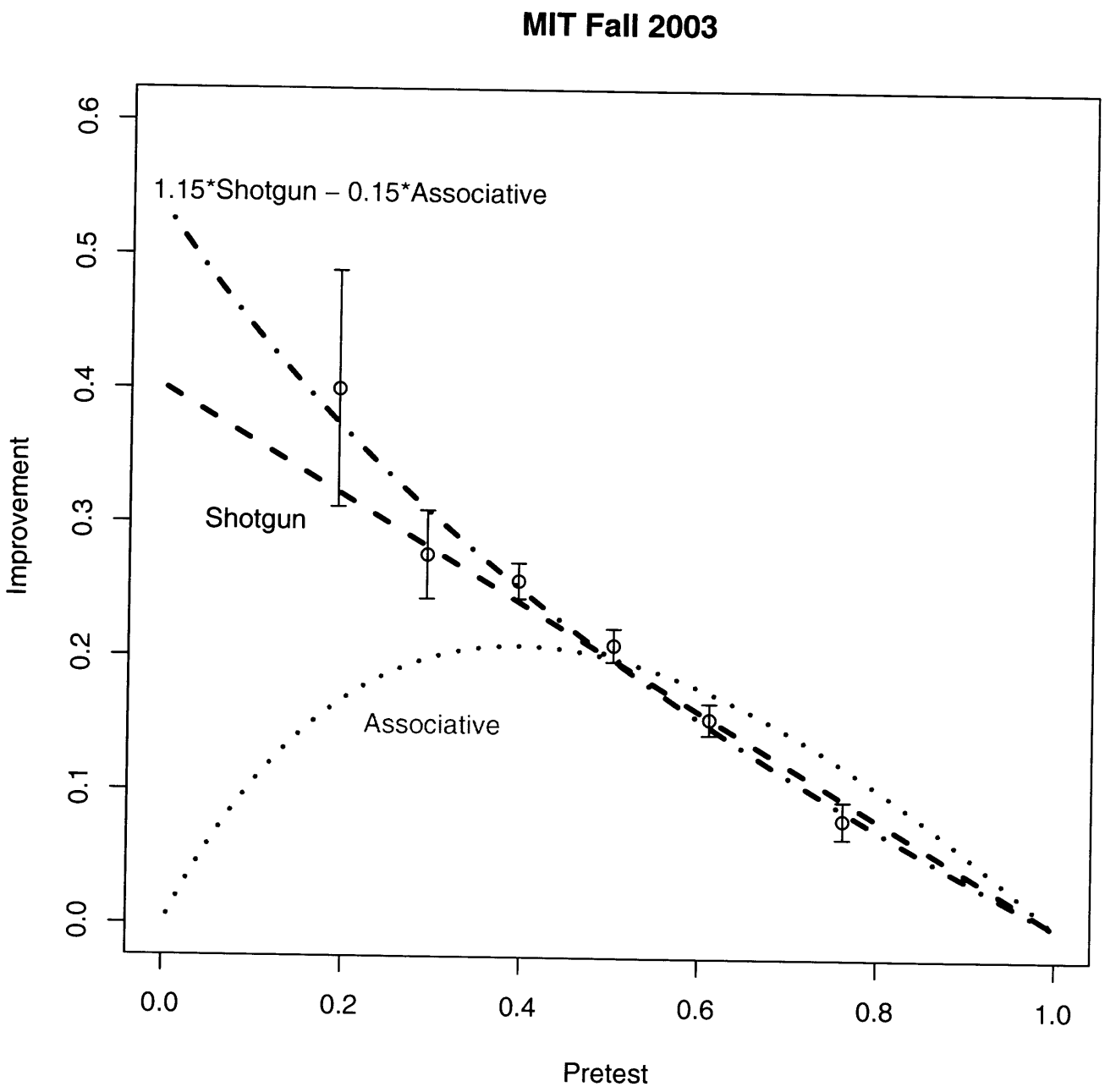
MIT Fall 2003
1.15*Shotgun – 0.15*Associative
Shotgun
Associative
Improvement
Pretest
0.0
0.1
0.2
0.3
0.4
0.5
0.6
0.0
0.2
0.4
0.6
0.8
1.0